eman ta zabal zazu

Universidad del País Vasco
Euskal Herriko Unibertsitatea

TESIS DOCTORAL

Study of the distribution of nuclear basket-related nucleoporins after histone deacetylase inhibition.

Autor:
Miguel PÉREZ GARRASTACHU

Directores:
Dr. Juan M. ARECHAGA MARTÍNEZ
Dr. Jon ARLUZEA JAUREGIZAR

17 de Mayo de 2021

eman ta zabal zazu

Universidad del País Vasco
Euskal Herriko Unibertsitatea

UNIVERSITY OF THE BASQUE COUNTRY

DOCTORAL THESIS

Study of the distribution of nuclear basket-related nucleoporins after histone deacetylase inhibition.

Author:
Miguel PÉREZ GARRASTACHU

Supervisor:
Dr. Juan M. ARÉCHAGA MARTÍNEZ
Dr. Jon ARLUZEA JAUREGIZAR

A thesis submitted in fulfillment of the requirements for the degree of Doctor of Philosophy

in the

Stem Cells, Development and Cancer Research Laboratory
Department of Cell Biology and Histology

May 17, 2021

Resumen

Introducción

El núcleo es el orgánulo que define a los organismos eucariotas. Tal estructura contiene el genoma del individuo codificado en forma de ADN (Ácido Desoxirribonucleico) y organizado en cromosomas, que en conjunción a una variada cohorte de proteínas, conforma lo que se denomina como cromatina. Para que la información contenida en el ADN adquiera utilidad, la cromatina debe organizarse en el interior del núcleo de una manera coherente tanto espacial (dimensiones restringidas por el núcleo) como temporalmente (acorde a los estímulos externos). La evolución ha conseguido solventar ambas necesidades empleando dos mecanismos contrapuestos: la condensación y la relajación de la cromatina. En el primer estado, la cromatina adquiere una conformación inaccesible que impide la lectura de la información genética contenida en las regiones condensadas, mientras que cuando la cromatina se relaja, ésta puede ser editada por la maquinaria nuclear.

Existen varios mecanismos por los que la cromatina puede condensarse o relajarse, pero la acetilación de las histonas (proteínas que junto el ADN forman la mayoría de la cromatina) es uno de los mejor entendidos. Así, la acetilación de las histonas favorece la relajación de la cromatina, mientras que la desacetilación, asiste su condensación. Gracias a este y otros mecanismos, se pueden distinguir regiones en el núcleo cuya proporción entre cromatina condensada o relajada es variable o incluso excluyente. Teniendo en cuenta la inmensa dimensión del genoma humano y el reducido tamaño del núcleo, cabe preguntarse cómo es posible que la cromatina pueda organizarse en zonas bien segregadas y así mismo ser responsiva a estímulos externos.

Para responder a esta pregunta, se buscó inspiración en citoesqueleto, hipotetizándose la existencia de una estructura análoga en el núcleo a la que se refiere como nucleosqueleto. Aunque no se ha descrito como tal, sí que se acepta que existen varios elementos de soporte y regulación de la arquitectura nuclear como por ejemplo ocurre con la lámina nuclear, la actina nuclear así como las nucleoporinas.

Las nucleoporinas, son las proteínas que conforman los complejos del poro; estructuras gigantescas que se ubican en la envoltura nuclear y funcionan como portales entre el citoplasma y el núcleo. Inicialmente se aceptaba que estas proteínas únicamente existían con el propósito de mediar el transporte nucleocitoplasmático. Sin embargo, paulatinamente se

han descrito ciertas nucleoporinas en el interior nuclear en asociación con la cromatina, llegando incluso a regular la actividad de diversos mecanismos como la transcripción, replicación y la reparación del ADN por citar algunos. En algunos casos palmarios, como pueden ser los núcleos de los ovocitos de *Xenopus laevis*, se han llegado a observar genuinas redes poliédricas expandiéndose desde el complejo del poro hacia el interior del núcleo, llegando a establecer uniones con los nucléolos. De este modo, la creciente acumulación de evidencia favorece considerar las nucleoporinas como un constituyente más del nucleosqueleto.

En base a lo expuesto, el objeto de esta tesis doctoral es el de establecer en células humanas, un modelo de interacción funcional entre 946013061la cromatina y las nucleoporinas, con especial énfasis en aquellas orientadas al nucleoplasma, a saber: Nup153, Nup98 y Tpr. A este fin, nos valdremos de una amplia batería de drogas denominadas inhibidores de desacetilasas de histonas (iHDACs) para inducir experimentalmente la relajación de la cromatina. En este contexto, esperamos que la alteración experimental de la estructura nativa de la cromatina tenga un impacto sustancial en el comportamiento de las nucleoporinas mencionadas.

Metodología

El modelo experimental de esta tesis se circunscribe al trabajo con líneas celulares de origen humano de distintos linajes histológicos y embrionarios (pasando por carcinomas de cérvix, mamarios y melanoma, hasta fibroblastos asociados a cáncer de colon), pero primando el uso de la línea celular de neuroblastoma SMS-KCNR. Esta línea celular es especialmente adecuada para estudiar la arquitectura nuclear dado el gran volumen de su núcleo. Del mismo modo, la mencionada línea celular tiene como origen un tumor metastático postquimioterápico, lo que garantiza la supervivencia al tratamiento con los inhibidores de desacetilasas de histonas.

Para mayor robustez metodológica, se emplearon tres iHDACs diferentes: el butirato sódico (Na-But), la tricostatina A(TSA) y el ácido hidroxámico suberoilanílido (SAHA) también conocido como vorinostat por su designación comercial. Las tres drogas mencionadas se empelaron en un amplio espectro de concentraciones con el propósito de identificar dosis mínimas y máximas.

En el presente trabajo podemos describir tres líneas metodológicas. La primera se basó en la caracterización de los efectos de los inhibidores de desacetilasas de histonas (iHDACs) en la distribución de las nucleoporinas de la cestilla nuclear en las mencionadas líneas celulares. Si

bien, la primera aproximación experimental se realizó mediante microscopía óptica convencional, la segunda se desarrolló en microscopía de célula viva. Para ello se transfectaron células de neuroblastoma humano SMS-KCNR con el plásmido pEGFP-C3-hNup153, y se seleccionaron clones que expresaran cantidades bajas pero suficientes y de forma estable la proteína fusión Nup153-EGFP. Finalmente, se estudió en profundidad la perturbación ejercida por los iHDACs sobre la progresión del ciclo celular, mediante diversas técnicas, como son la citometría de flujo, patrones de expresión de Ki-67, diversos ensayos de proliferación, así como la monitorización en tiempo real de la progresión del ciclo celular mediante la sonda transgénica FUCCI (Fluorescence Ubiquitination Cell Cycle Indicator), por citar algunas.

El desarrollo e interpretación de la tesis pivota permanentemente entre estas tres metodologías, cuyos resultados son dependientes entre sí como se relata a continuación.

Resultados y Discusión

Los iHDACs provocan la aparición de condensados de nucleoporinas en el interior nuclear

Tras las primeras exposiciones de las varias líneas celulares a los tres iHDACs mencionados anteriormente, resultó evidente que las nucleoporinas Tpr, Nup153 y Nup98 eran capaces de desplazarse desde la envoltura hacia el interior nuclear, donde se condensaban intensamente, en detrimento de la señal procedente de la envoltura nuclear. Este efecto era contrastable tanto mediante microscopía óptica confocal en células fijadas, como mediante microscopía de célula viva en líneas celulares expresando establemente la nucleoporina Nup153 fusionada a EGFP, lo que descartaba la posibilidad de tratarse de un defecto de los procesos de fijación e inmunodetección de Nup153. A estos agregados intranucleares de nucleoporinas los denominamos como INCs por sus siglas en ingles: Intranuclear Nucleoporin Clusters.

Tales agregados, no eran distinguibles mediante microscopía electrónica de transmisión como podría esperarse si éstos conformaran un orgánulo nuclear fibroso o una región independiente del nucleoplasma, como ocurre por ejemplo en el caso del nucléolo o la heterocromatina. En cualquier caso, la inmunodetección de Nup153 en preparaciones de microscopía electrónica de transmisión reproducía los resultados obtenidos mediante microscopía óptica de fluorescencia confocal. El poder observar los mismos condensados nucleares de Nup153 mediante ambas técnicas microscópicas refuerzan la veracidad de estos agregados y es muy

improbable que éstos se deban por artefactos durante los procesos de fijación o manipulación de la muestra.

Los INCs resultan estar compuestos por la combinación de al menos tres nucleoporinas: Tpr, Nup153 y Nup98, tal como demuestran los experimentos de doble marcaje mediante microscopía confocal. Este dato cobra especial relevancia dado que en condiciones normales, estas tres nucleoporinas desempeñan funciones intranucleares similares o relacionadas entre sí independientemente de aquellas relacionadas con el transporte nucleocitoplasmático. De este modo podemos sugerir que la hiperacetilación de histonas potencia esta interacción haciéndola más evidente.

Este planteamiento resulta reforzado por la ausencia de P62 en los mencionados agregados. P62 es una nucleoporina del canal central del complejo del poro, eminentemente ajena a los eventos moleculares del interior del núcleo y centrada en el transporte entre el núcleo y el citoplasma. Este hecho cobra una importancia capital dado que P62 permanece impasible tras la inhibición de histonas tal como demuestran los recuentos de esta nucleoporina en la envoltura nuclear mediante microscopía de súper resolución. Por el contrario, el detrimento de Tpr en la envoltura nuclear resulta más que evidente una vez el cultivo celular se expone a los inhibidores de desacetilasas de histonas. Este resultado indica que no todas las nucleoporinas son sensibles a la hiperacetilación de la cromatina inducida por los iHDACs, y que solamente aquellas relacionadas con la cestilla nuclear pueden ubicarse en los INCs.

Por último, el análisis espacial de la ubicación de los INCs en el interior nuclear descarta que estas estructuras estén de algún modo asociados a la envoltura nuclear, siendo éstos estructuras eminentemente intranucleares e independientes de los complejos del poro.

Los INCs son independientes del nucleosqueleto y de las factorías de transcripción y replicación

Dada la estrecha relación entre las nucleoporinas y algunos elementos nucleosqueléticos como la lámina nuclear, nos pareció conveniente estudiar el comportamiento de ésta tras el tratamiento con iHDACs. Aunque tras la hiperacetilación de la cromatina, la lámina nuclear también sufrió un desplazamiento hacia el interior en detrimento de la envoltura nuclear, éste se mostraba mucho más vago y homogéneo que aquel ocurrido en los INCs. De hecho, no pudimos detectar ningún tipo de colocalización aparente que sugiriera una asociación entre ambos. Tal acontecimiento era esperable dada la estrecha interacción entre la heterocromatina perinuclear y la lámina nuclear. Ante el desvanecimiento de la heterocromatina causado por la

hiperacetilación de la cromatina, parece razonable que la lámina nuclear también se desvanezca parcialmente de la envoltura nuclear.

Entre las funciones asignadas al nucleosqueleto, estaría la de distribuir los diferentes orgánulos nucleares. Las factorías de replicación y transcripción sos de los más prominentes y en ciertos contextos las nucleoporinas de la cestilla son capaces de asociarse a éstos orgánulos y modular su actividad. Sin embargo, no detectamos ninguna coincidencia entre los INCs y los orgánulos mencionados, lo que a priori parecería demostrar que los INCs son estructuras independientes del nucelosqueleto. Sin embargo, también hemos demostrado que los los INCs son resistentes a la extracción con detergentes no iónicos, una característica de los elementos estructurales del núcleo.

Así mismo, en célula viva demuestran que los iHDACs reducen la movilidad de Nup153 tanto en los INCs como en la envoltura nuclear, lo que sugiere que la fracción soluble de Nup153 pierde importancia en favor de la fracción más nucleosquelética y estática probablemente representada por los INCs.

Los INCs aparecen en la fase G_1 del ciclo celular

Las imágenes de microscopía demostraban que los INCs estaban presentes en la mayoría de los núcleos celulares una vez el cultivo era expuesto a los inhibidores de HDACs. Sin embargo, una porción de núcleos mantenía un marcaje restringido exclusivamente a la envoltura nuclear. Curiosamente, esta proporción de núcleos sin INCs era mayor conforme se incrementaba la dosis de inhibidor. Tras explorar la evolución del ciclo celular en estos casos y recontar sistemáticamente las áreas de estos núcleos y relacionarlos con la presencia o ausencia de INCs, llegamos a la conclusión de que los INCs tan solo se ubicaban en los núcleos de menor tamaño propios a la fase G_1 del ciclo celular.

Para confirmar esta observación, se realizaron las pertinentes validaciones con marcadores de proliferación como Ki67, el cual mostraba ser una condición necesaria para la formación de INCs, es decir, las núcleos de células quiescentes en ningún caso mostraban condensados intranucleares de nucleoporinas. En vista a lo expuesto podría suponerse que cualquier droga inhibidora capaz de arrestar el ciclo celular en la fase G_1 pudiera ocasionar la aparición de INCs. Sin embargo, al repetir esta serie de experimentos con otros fármacos bloqueadores de la transición G_1/S se demostró que la hiperacetilación de la cromatina era, así mismo, otra condición necesaria para la formación de las estructuras descritas en este trabajo.

Por último un seguimiento temporal metódico desde el inicio de la adición del fármaco, demostró que las Nup153, Tpr y Nup98, pero no P62, sufren una gran sobreexpresión una vez transcurridas 12 horas tras el inicio del tratamiento. Tal sobreexpresión se reduce progresivamente hasta llegar a niveles normales a las 24 horas una vez el grueso de la población ha sufrido un proceso mitótico completo y ha pasado a estar arrestado en la transición G1/S del ciclo siguiente.

En vista a los resultados enumerados anteriormente, la aparición de los INCs podría explicarse por la coincidencia de varios procesos:

- La hiperacetilación de la cromatina estimula el reclutamiento de las nucleoporinas de la cestilla nuclear al interior nuclear en condensados moleculares.
- La fracción soluble de nucleoporinas queda secuestrada en los INCs una vez la cromatina es hiperacetilada por los iHDACs.
- La sobreexpresión momentánea de éstas nucleoporinas impide que los complejos del poro retornen una composición convencional quedando éstos vaciados de nucleoporinas de la cestilla. Este proceso podría explicarse mediante la disrupción del ensamblaje post-mitótico del complejo del poro.

Index of Contents

ABBREVIATIONS

ANC: Active Nuclear Compartment.

BCA: Bicinchoninic Acid.

DMEM: Dulbecco's Modified Eagle's Medium.

DNMT: DNA methyl transferase.

ChIP-Seq: Chromatin immunoprecipitation sequencing.

CR: Cytoplasmic Ring.

EGFP: Enhanced Green Fluorescent Protein.

FBS: Fetal Bovine Serum.

FRAP: Fluorescence Recovery After Photobleaching.

FRET: Förster resonance energy transfer

HAT: Histone Acetyl Transferase.

HDAC: Histone DeACetilase.

HDACi: Histone DeACetilase inhibitor.

INC: Intranuclear Nucleoporin Cluster.

INC: Inactive Nuclear Compartment.

INM: Inner Nuclear Membrane.

IR: Inner Ring.

MMP: Matrix Metaloproteinase.

MTT: 3-(4,5-Dimethylthiazol-2-yl)-2,5- diphenyltetrazolium bromide.

NE: Nuclear Envelope.

NEL: Nuclear Envelope Lattice

NL: Nuclear Lamina.

NPC: Nuclear Pore Complex.

NR: Nuclear Ring.

ONM: Outer Nuclear Membrane.

PBS: Phosphate Buffered Saline.

PBST: Phosphate Buffered Saline Tween.

PCNA: Proliferating Cell Nuclear Antigen.

PI: Propidium Iodide.

RCF: Radial Centrifugal Force.

RER: Rough Endoplasmic Reticulum.

RNA: Ribonucleic acid.

RNP: Ribonucleoprotein.

SAC: Spindle Assembly Checkpoint.

SAHA: Suberoylanilide Hydroxamic Acid.

TBS: Tris Buffered Saline.

TBST: Tris Buffered Saline Tween.

TEM: Transmission Electron Microscopy.

TSA: Trichostain A

1 INTRODUCTION

1.1 The eukaryotic chromosomes.

Eukaryotic genomes are several orders of magnitude larger than those of bacteria and archaea. This bigger size is not only relative to the coding sequences but especially in non-coding DNA. Among the non-coding sequences there are certain important ones that contain regulatory sequences that rule the expression of adjacent genes. It is precisely this regulatory complexity of the eukaryotic genome which is responsible for the formation of multicellular organisms and for the astonishing diversity of the eukaryotic branch in the tree of life.

By default, eukaryotic organisms hold their genetic content isolated from the rest of the cellular components inside their most prominent organelle: the nucleus. This compartment is delimited by the nuclear envelope (NE) and formed by two concentric lipid bilayer membranes: the outer nuclear membrane (ONM) and the inner nuclear membrane (INM). The ONM is directly connected to the rough endoplasmic reticulum (RER) and partake an obvious functional relationship, as both are punctuated by ribosomes and share their lumenal space, although the ONM integral membrane composition differs from the RER (Anderson & Hetzer, 2008). The INM of the NE is underlaid by a proteinaceous component called the nuclear lamina (NL). The NL is composed of intermediate filaments denominated as lamins that provide support to the NE (M. W. W. Goldberg et al., 2008). The NE is also seeded in multiple places by nuclear pore complexes (NPCs), which are large structures comprised of several copies of ~30 different subunits of nucleoporins (Cronshaw et al., 2002; Grossman et al., 2012). Inside the nucleus exist different sub-organelles, such as the nucleolus, that are specialized in the execution of specific tasks and are discussed in the sections below.

Chromosomes make up the inherited unit of organisms. They are composed of a unique and extremely long chain of DNA along with a series of associated proteins. The term chromatin, on the other hand, is more widespread and is not delimited to a single DNA molecule, but refers to a given set of DNA associated with two types of proteins: histones and non-histones. Histones are the proteins that make up the nucleosomes, the basic unit of chromosome compaction. Non-histone proteins comprise a wide range of proteins that bind to DNA and participate in transcription, repair, and replication, among other processes. Each nucleosome consists of a core of two copies of histones H2A, H2B, H3, and H4, around which it is wound the "central DNA." The DNA that separates each nucleosome is designated as “ligator DNA” and associates with ligation histone H1. When analyzing the protein sequence of the core histones, two regions can be identified in each one of them: the “histone fold” and the “N-terminal tail”. The histone fold is a very well conserved sequence that builds the inner part of

the nucleosome in a disk-like shape around which the core DNA is coiled, as stated above. On the contrary, the histone N-terminal tail is a sequence with a non-defined structure that protrudes eccentrically. Histones are covalently modified by post-translational modifications both in the histone fold and in the N-terminal tail, although this last one is much more extensively modified. Thus, the primary function of the N-terminal tail is to serve as the substrate for extensive post-translational modifications that are essential for the regulation of nucleosomal function. Indeed, the post-translational implications of histones have such profound connotations in the expression or repression of specific regulatory genes or regions that it has been proposed that they would form a biological code that can be written, read, and erased through auxiliary proteins; referred to as "histone-code." (Munshi et al., 2009; Prakash & Fournier, 2018; Strahl & Allis, 2000).

Thanks to the combined action of the N-terminal tails of core histones and the addition of histone H1, nucleosome collections can form more condensed structures known as the 30 nm fibers. Further condensation of chromatin leads finally to the formation of the mitotic chromosomes (Figure 1). The concept of chromatin compaction is essential for the accessibility of non-histone proteins to the DNA sequences. When chromatin is in a more condensed state, such as in the 30 nm fibers, the other DNA-binding proteins, such as transcription factors, lack the necessary space to bind strongly to their targeted sequences. In these terms, we can define two leading estates of the chromatin during the interphase: (I) active, relaxed chromatin; and (II) inactive, condensed chromatin.

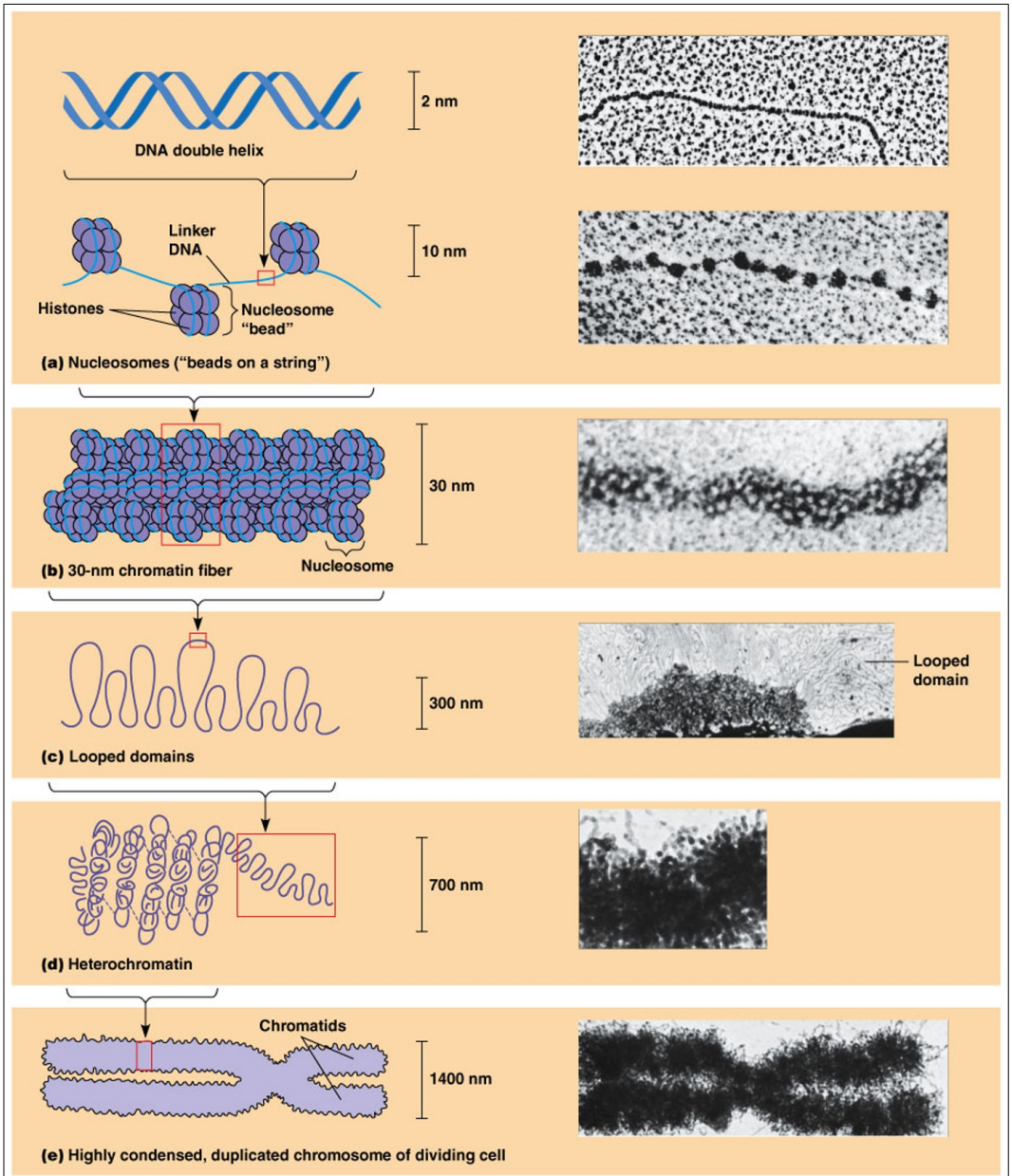

***Figure 1**: Chromosome condensation hierarchy scheme. The double DNA helix coils around the nucleosomes forming the 10 nm fiber (a). Histone H1 triggers the condensation of the nucleosomes, which causes the formation of the 30 nm fiber (b). Looped domains consist of chromatin loops of 30 nm fibers (c). The last condensation level in the interphase chromosomes is what traditionally has been denominated as heterochromatin (d). Finally, and once DNA has been duplicated, chromosomes are ultra-condensed into mitotic chromosomes, which possess the necessary structure to be properly segregated between daughter cells during mitosis (e). Illustration adapted from "Molecular biology of the Cell" by Bruce Alberts et al 6th edition.*

The chromatin condensation degree impacts in a compelling manner in the overall genome structure. Histone modifications rule the transition between the chromatin states by means of adapter proteins such as epigenetic regulators, transcription factors, chromatin remodeling complexes, and others. These chromatin states build different interdependent realities depending on the scale of the magnitude of the observed system (Prakash & Fournier, 2018).

Nucleosomes as beads-on-a-string constitute the active conformation at a small scale, and the 30 nm fiber is considered to be its opposite (Figure 1). On an intermediate scale, depending on the net balance of histone modifications, chromatin domains can be either active, reversely inactive, or entirely inactive. Finally, the highest organization order explains the existence of the bimodal euchromatin/heterochromatin model (active/repressed, respectively) and the distribution of the chromosome territories.

As said, histone modifications are the input code of the described systems above and, in many ways, their final rulers. To date, researchers have described at least twelve types of histone modifications (Figure 2) (Barnes et al., 2019), most of which operate through the disruption of the net charge between histone proteins and the DNA. For example, histone acetylation neutralizes the positively charged lysine residues and consequently impairs the association with the negatively charged DNA (Hong et al., 1993). The reduction of the interaction strength between DNA and histones favors the histone mobility along the DNA and the accessibility of transcription factors (Cosgrove et al., 2004).

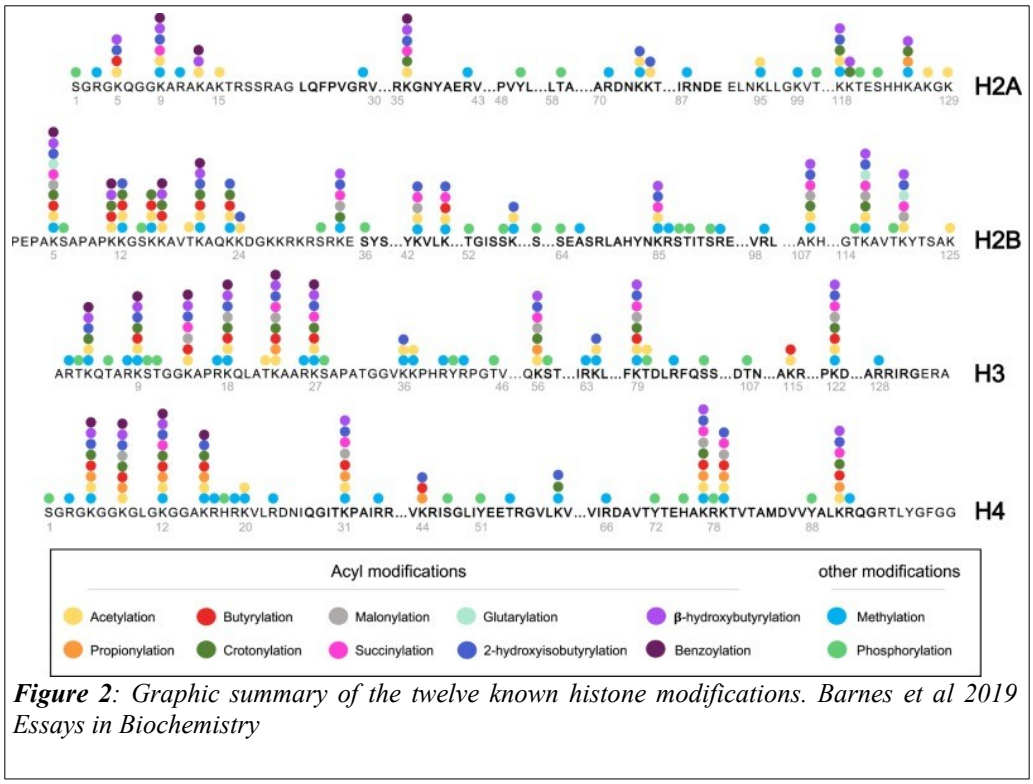

***Figure 2**: Graphic summary of the twelve known histone modifications. Barnes et al 2019 Essays in Biochemistry*

The different classes of histone modifications can coexist inside the same nucleosome. Many modifications work synergistically between them in order to amplify their readout within the nucleosome (Figure 3A). Nevertheless, these modifications do not need to be in the same histone protein to feedback with each other. In fact, the amplification can affect neighboring nucleosomes and even reach other chromosomal regions through protruding loops of

chromatin (Fraser & Bickmore, 2007). The amplification process implies that the histone code would be redundant in its nature in order to gain robustness in its reading so that no biological process is unintentionally started, such as the expression of pluripotency genes during terminal differentiation (Hawkins et al., 2010).

The amplification property of histone modifications creates small chromatin domains of relative homogeneity (Figure 3B). We can consider these domains as the functional structures of chromatin, as they tend to gather together sharing similar histone marks while repelling others of different composition; and consequently, this drives the formation of coherent functional regions inside the nucleus ranging from 0.5 Mb to 1 Mb (Rao et al., 2014). Current experimental data obtained through ChIP-Seq demonstrate that depending on their condensation, chromatin domains can be enriched in subsets of several histone modifications. In mammals, for instance, active open domains are rich in H3K4me3 and acetylated histones, whereas the H3K27me3 and H3K9me2 modifications are abundant in reversely repressed domains. Inactive chromatin instead, remains structurally ultra-condensed and strongly associated to the H3K9me3 and H4K20me3 modifications (Ernst & Kellis, 2010; Rao et al., 2014). The enrichment of certain histone marks in discrete genomic regions has also been demonstrated through single molecule super-resolution microscopy (Prakash, 2017; Smeets et al., 2014). In brief, histone modifications determine chromatin structure and function through the association and repulsion of active or silent chromatin domains (Figure 3C).

Histone modification is not the only referee in the chromatin remodeling process. DNA methylation impedes the expression of a DNA sequence. It usually takes place at genomic regions denominated as CpG sites, where cytosines are methylated through DNA methyltransferases (DNMT). DNMT activity is co-regulated by the histone methyltransferase HP1 which associates with H3K9me3, and is very abundant in silenced and compact chromatin domains (Smallwood et al., 2007). HP1 is the acronym for Heterochromatin Protein 1 which helps to understand the implication of these modifications in the nuclear ultra-structure.

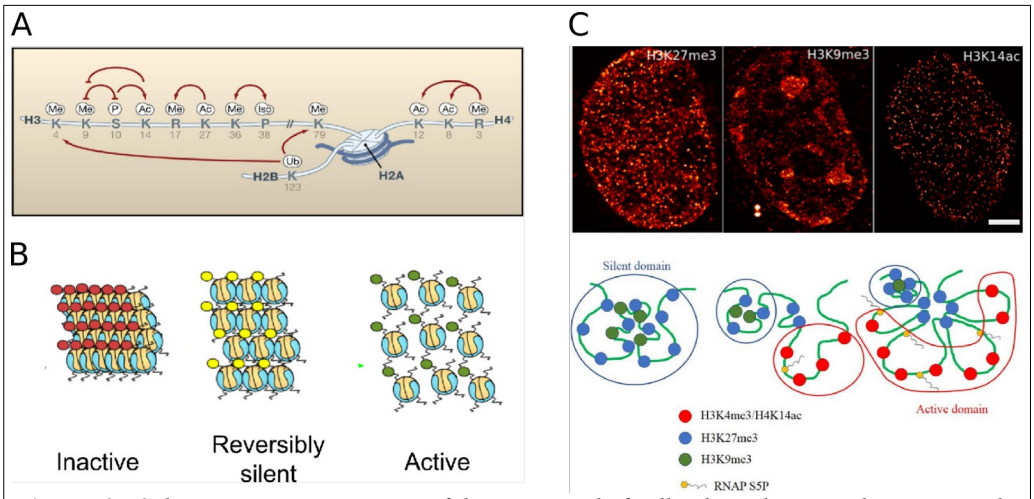

Figure 3: *Schematic representation of histone mark feedback and its implication in the structure of genetic domains. (A) Examples of crosstalk between histone marks. (B) The resulting code from this feedback determines the conformational structure of a determined domain. Inactive chromatin is enriched with the mark H3K9me3, rich in heterochromatin regions. H3K27me3 is usually associated with reversely silenced domains. Active chromatin is usually enriched in acetylated lysines and H3K4me3. (C) Chromatin domains enriched with specific histone marks tend to associate together and repelling the marks with opposite meanings. Prakash and Fournier 2018.*

Chromosomes must be able to replicate in order to be inherited by daughter cells after mitosis. The replication process takes place along the cell cycle: a sum of sequential steps along which cells accumulate enough resources to replicate the chromosomes and provide daughter cells enough materials to carry on with their lives. The cell cycle is divided into two main phases: the interphase and the mitosis (M phase). Likewise, interphase subdivides itself into three consecutive subphases: G1, S, and G2. During the G1 phase, the cell evaluates if environmental signals favor replication; and if so, the cell grows by accumulating nutrients and duplicating organelles. After DNA replication in the S phase, the cell falls into another growth phase designated as G2 in order to provide enough nutrients for the daughter cells. While the G2 phase houses twice as much genetic material as in the G1 phase, the nuclear volume is also doubled to adapt to the additional chromatin content correctly. During mitosis, the duplicated chromosomes segregate effectively into the daughter cells. Chromosomes behave very differently between cell cycle phases: while the mitotic chromosomes are condensed at their maximum capability and individually visible, the interphasic chromosomes are spread, and much of their chromatin exists as long and tangled fibers throughout all the nuclear space and are individually indistinguishable through conventional microscopic means. As the only function of mitotic chromosomes is to be segregated effectively, gene expression only takes place in the interphasic chromosomes.

When the surrounding environment of the cell does not favor cell division due to a stress condition or whether the tissue does not need further cell divisions, the cell can exit from the

cell cycle and enter into a resting state denominated as G0. In this phase, chromosomes are also relaxed and are considered as interphasic chromosomes.

1.2 Nuclear architecture and nucleoskeleton.

During evolution, the appearance of the nucleus allowed separating the genetic content from the rest of the cellular components, and consequently, specializing in the management of larger and, above all, much more complicated genomes. Ultimately, the nucleus is the supreme example of compartmentalization, which is an essential concept in cell biology since it allows the isolation of biochemical environments. The higher concentration of both enzymes and substrates facilitates biochemical reactions, specialization of functions, and reduces the interference of enzymes between biochemical pathways. In this manner, the nucleus itself is subdivided into specialized subareas and nuclear bodies, which are discussed in the following paragraphs.

Following this idea, the genome is organized non-randomly in the nuclear space. Modern microscopy and sequencing methods have demonstrated that each chromosome occupies specific and separated spaces denominated as “chromosome territories” (A. Buchwalter et al., 2019; Cremer et al., 2015; Cremer & Cremer, 2010). Each territory, although distinguishable, is not entirely separated from its neighbors, and the chromatin loops from different chromosomes are usually intermingled in discrete areas where specific functions can be carried out, such as transcription, DNA repair, replication, and others (Branco & Pombo, 2006). In addition to the existence of the chromosome territories, chromatin looping events, and zonification of gene expression, DNA density stands as another architectural element of the nucleus (Markaki et al., 2010). DNA staining combined with new super-resolution microscopy approaches have determined that DNA density within the nucleus varies greatly (Smeets et al., 2014).

Electron microscopy, fluorescence microscopy, computational modeling and the 3D genome mapping through biochemical approaches comprise the main experimental formulations to study nuclear architecture (Bickmore & van Steensel, 2013; Ryabichk et al., 2017). The integrated results provided through the mentioned methods, favor the perspective that nuclear architecture relies on the dynamic interplay of two main compartments (Figure 4) within the nucleus: the Inactive Nuclear Compartment (INC) and the Active Nuclear Compartment (ANC) (Cremer et al., 2015). Given the inversely proportional relation (described in the previous section) between the DNA condensation and its related activity, chromatin remains condensed in the INC while relaxed in the ANC.

ANC is itself subdivided into the interchromatin compartment (IC) and the perichromatin region (PR) (Masiello et al., 2018). Mostly deprived of DNA, the IC extends from the nuclear pores at the nuclear envelope towards the nuclear inside creating a network of tunnels and caverns through the interior and around the chromosomal territories. In this way, the IC

would delimit sets of chromatin domains of a size between approximately 100 and 1000 kb each (Markaki et al., 2010; Rao et al., 2014). The PR makes up the periphery of these domains, which is constituted by relaxed active chromatin. The majority of DNA-related activity is placed between the PR and the IC. Coherently, ANC is enriched in histone modifications related to chromatin relaxation, such as acetylation and methylation of lysines at the histone H4.

On the contrary, INC represents the condensed inactive fraction of the chromatin contained in the insides of the chromatin domains. Corresponding with its condensed nature, histone tails of these domains are extensively modified in repressive marks such as H3K27me3 and H3K9me3 (Figure 3C). In the vast majority of the cells exist a specific INC region associated with the nuclear envelope by the nuclear lamina denominated as Lamin Associated Domains (LADs). Repetitive DNA sequences are abundant in the LADs and the genes contained within are rarely expressed. In mammals for example, those can contain up to one third of the genome but only the 10% of coding genes (Kind et al., 2015; Peric-Hupkes et al., 2010).

Although the active and inactive areas of chromatin can be clearly differentiated, this does not imply that they are entirely independent of each other or that they are immutable. Cross-talk between both active and inactive nuclear compartments is essential for cell life and stimuli-dependent gene expression. For example, when genes are not entirely silenced but only reversely repressed, these genes may be relocated by chromatin looping towards the PR, where they will be certainly transcribed in association with other genes with similar regulatory mechanisms and promoter sequences, such as what happens during differentiation events (See et al., 2019; Teif et al., 2017). Another clear example of chromatin dynamics is how chromatin domains behave during DNA repairing, since upon DNA damage chromatin regions undergo transient expand and contraction events in order to proper DNA damage response signaling (Burgess et al., 2014).

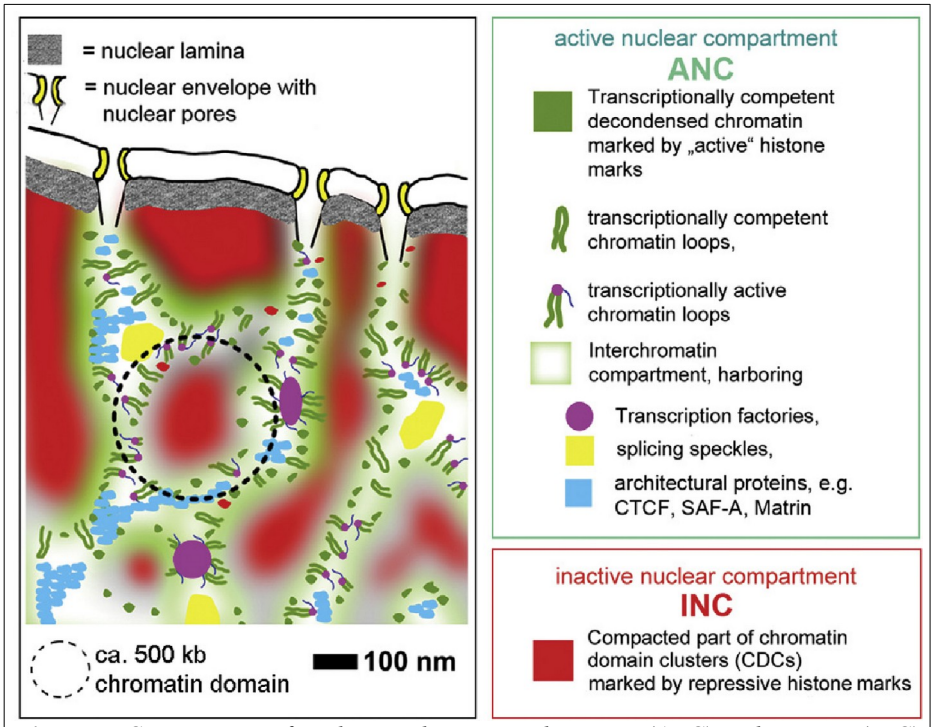

***Figure 4**: Current view of nuclear architecture. The active (ANC) and inactive (INC) nuclear compartments are the two main nuclear playgrounds. Interchromatin compartments dig through the ANC starting from the nuclear pore complexes; with low DNA content but rich in Non-histone proteins that interact with open chromatin, is the place where the majority of its metabolism takes place. INCs are mainly composed by silent condensed chromatin and frequently anchored to the nuclear lamina. Both compartments are usually composed of chromatin domains ranging from 100 to 1000 kb. Illustration modified from: T. Cremer et al. FEBS Letters 589 (2015) 29031-2943*

Soluble factors are especially abundant in the interchromatin channels, given their low chromatin density. The rapid flow of these factors favors the association with their target molecules, promoting the appearance of concentration gradients. The interactions between the different target molecules can form membrane-less compartments through a process called liquid–liquid phase separation (Strom & Brangwynne, 2019) (Albiez et al., 2006; Markaki et al., 2010). These membrane-less compartments inside the nucleus are denominated as nuclear bodies.

Nuclear bodies are dynamically regulated steady-state structures where specialized nuclear functions take place. Several Components of the different sub-organelles are present throughout all the nucleoplasm but concentrate in some highly permeable regions to other nucleoplasmic components. Up to date, researchers have not entirely determined how nuclear organelles are formed, but current data suggests that bodies can proceed from different pathways in a stochastic manner or by means of the so-called “seed model”. In the seed model, one specific RNA molecule or protein can trigger the formation of the body by recruiting the rest of the nuclear body components under certain situations. (Mao et al., 2011;

Staněk & Fox, 2017). These two approximations can be extrapolated to nuclear architecture as its whole and, whether the nuclear organization relies on deterministic, spontaneous self-organized, or a mix of both systems, is still unknown. In this regard, several researchers have proposed the existence of a fibrous structure denominated as nucleoskeleton, that would give physical support to the nuclear organization (Adam, 2017; P. R. Cook, 1989; Dahl & Kalinowski, 2011; Hozak et al., 1995; Simon & Wilson, 2011). The following lines collect a small preview of the most important nuclear bodies:

- *Nucleolus*: Being the most prominent organelle of the nucleus, it was the first to be studied and whose composition and function is best known. It plays a vital role in the manufacture of ribosomes by transcription (by RNA polymerase I activity) and processing of rRNA. Likewise, other RNAs and RNPs are also produced in the nucleolus, such as the U6 snRNA, necessary for pre-mRNA splicing. The transfer RNAs are also transcribed and matured in this important nuclear organelle. As the progression through the cell cycle is directly proportional to the ribosome number, it was thought that the nucleolus governed the cell cycle progression by crude ribosome production. However, recent investigations have demonstrated that the nucleolus is capable of sequestering and regulating the activity of essential cell cycle regulatory proteins, such as p53, which binds to the nucleostemin protein in the nucleolus suppressing its activity. (Kulikov et al., 2010; Weber et al., 1999). Thus, the relationship between cell cycle progression and nucleolar activity appears to be more deeply rooted than in a mere increase in ribosome demand. Through electron microscopy, several regions within the same nucleolus can be distinguished: the granular component, and the fibrillar centers surrounded by the dense fibrillar component. Each of these subzones is of different composition, varying the proportion between components rich in nucleic acids or proteins. However, the precise function of each of these components and their dependencies are still under discussion (Pederson, 2011).
- *Speckle*: Nuclear speckles, also known as interchromatin granule clusters, are domains specialized in the storage and post-translational modification of pre-mRNA splicing factors, such as snRNPs and serine/arginine-rich (SR) proteins. The splicing machinery stored in the speckles is accessed by nearby actively transcribed genes concentrated in hubs of gene activation denominated "transcription factories," consequently increasing the pre-mRNA metabolism's efficiency. (Spector & Lamond, 2011).
- *Paraspeckles*: Paraspeckles are composed of long non-coding RNAs (NEAT1 / Men ε/β) associated with members of the DBHS (Drosophila Behavior Human Splicing) protein family. They play a role in controlling gene expression by retaining RNAs in stress conditions and other cellular processes such as differentiation. Although similarly named, paraspeckles are independent of speckles. (Fox & Lamond, 2010)

- *Transcription factories*: RNA polymerases bind to the promoter sequences of genes, in conjunction with the rest of the transcription machinery, to start the synthesis of mRNAs. This whole process takes place in discrete areas within the nucleus denominated as transcription factories (Iborra et al., 1996; D.A. Jackson et al., 1993). These factories serve as a hub to store all the necessary components of the transcriptional machinery such as co-activators, transcription factors, RNA polymerases, histone modification enzymes, chromatin remodelers and DNA helicases among others (Rieder et al., 2012; Sutherland & Bickmore, 2009). Rather than assembling all the transcriptional machinery in each transcribed gene, data suggest that, upon activation, are the genes themselves that loop out of their chromosome territory towards pre-existing compartments specialized in transcription (Osborne et al., 2007). It is worth noting that these factories remain in the absence of transcription (Mitchell & Fraser, 2008).
- *Replication factories*: Genomic DNA is replicated during the S-phase of the cell cycle through the sequential activation of thousands of DNA replication origins which are distributed along the chromosomes. Due to the huge size of eukaryotic genomes, several replicons must work in parallel in order to complete the genome duplication in an acceptable period of time. It has been estimated that between 30000 – 50000 replicons are activated during the S-phase (Dean A. Jackson & Pombo, 1998). Microscopic observations of the replicon components such as the DNA polymerase, PCNA, or labeled newly synthesized DNA, state that replication takes place in discrete sites denominated as "replication foci" (Chagin et al., 2016). Taken these two observations together it is clear that the number of replication factories is much smaller than the predicted replication origin sites. Electron microscopy evidences suggest that replication foci are the result of the accumulation of the replication machinery in discrete sites of the nucleus containing several replicons (Hozák et al., 1994). Replication is a complex process submitted to epigenetic determinants and is still a mysterious topic.
- *Cajal body*: Is responsible for the assembly and modification of small nuclear ribonucleoproteins (snRNPs) necessary for the spliceosomal activity. Small nucleolar RNA (snoRNA) is also incorporated in this organelle for further maturation in its way to the nucleolus, but this process is not fully understood (Staněk, 2017).
- *PML body*: Promyelocytic leukemia protein (PML) posses tumor-suppressing activity, taking part in the regulation of apoptosis, cell cycle, and DNA damage responses (Hsu & Kao, 2018). PML bodies often appear in stress conditions such as senescence and viral infections. Both situations increase the number and size of these bodies. In particular, PML body proteins inhibit viral infection encapsulating the viral proteins (Reichelt et al., 2011). PML bodies are also rich in ATR kinase, needed for telomere maintenance (Flynn et al., 2015).

- *Polycomb group body*: polycomb group (PcG) proteins are epigenetic regulators that are found aggregated in these nuclear bodies. PcG bodies are associated with the silencing of developmental and cell fate genes such as *Hox (Pirrotta & Li, 2012)*. The silencing function is supported by the abundant presence of the polycomb repressive complex 1 (PRC1) and 2 (PRC2), responsible of the methyltransferase activity in the lysine 27 of the histone H3, which is strongly associated with repressed chromatin. Genes whose sequence contain PcG responsive elements (PREs) are clustered in this body by long-range chromosomal interactions (Tolhuis et al., 2011). Long-range chromosomal interactions were traditionally associated with gene activation until the study of this nuclear body (Dundr, 2012).
- *Histone locus body*: histone coding genes are placed in these specific sites where they are expressed. These bodies are enriched with specific histone mRNA processing factors such as FLASH. (Duronio & Marzluff, 2017; Tatomer et al., 2016).

With the term nuclear architecture, we refer to the spatio-temporal distribution of the chromatin and other associated elements necessary for proper nuclear operation. However, this definition does not cover the underlying mechanisms by which all these biochemical processes take place. Current biophysical models agree that nuclear architecture depends on the self-organizing properties of nuclear components. However, they differ in the level of dependence on the "concentration and interaction behavior of the molecules involved" in the construction of spatio-temporal chromatin units (Erdel & Rippe, 2018). It may be possible that the missing piece in this puzzle remains hidden in the components of the underlying nucleoskeleton. As previously mentioned, the nucleoskeleton is "a conceptual term that is analogous to the cytoskeleton and refers to all of the protein-based structures in the interphase nucleus, many of which also function during mitosis as the spindle matrix" (Simon & Wilson, 2011). Moreover, several of the nucleoskeletal proteins that we detail below (Figure 5) are definitively responsible, among other functions, for the anchoring and structural support of the nucleus, as well as for being the chain of transmission of mechanotransduction events (Wilson & Berk, 2010).

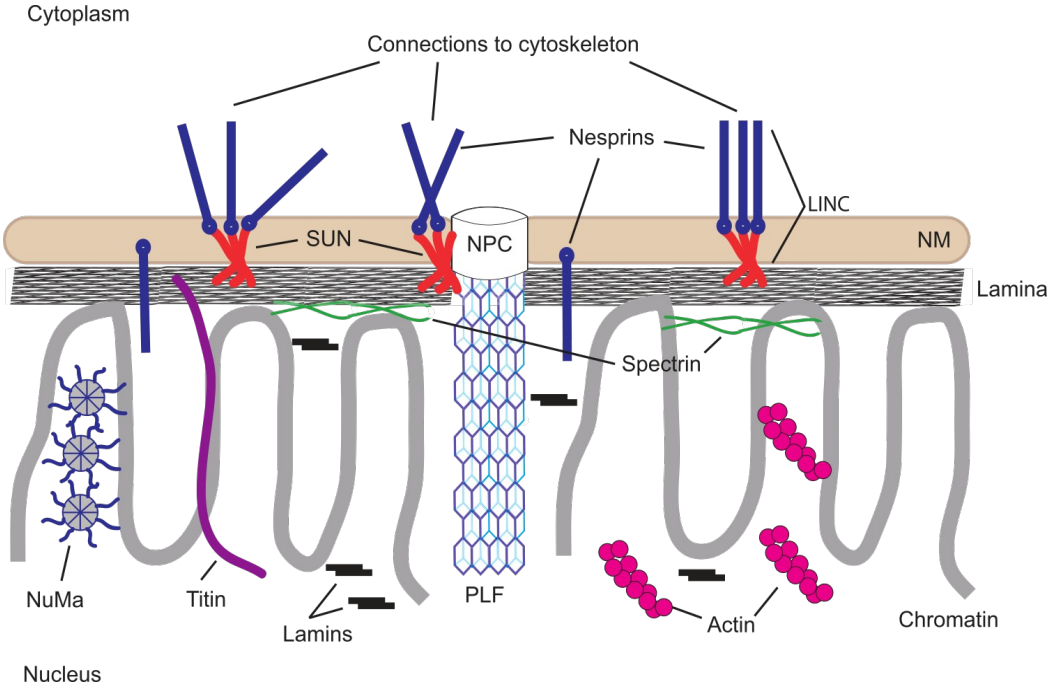

***Figure 5**: Schematic representation of the main nucleoskeletal players in the nuclear landscape. NM: Nuclear Membrane. NPC: Nuclear Pore Complex. PLF: Pore Linked Filament. SUN: Sad1 And UNC84 Domain Containing Complex. LINC: Linker of nucleoskeleton and cytoskeleton complex. NuMa: Nuclear mitotic apparatus protein 1. Adapted from s. Adams CSH Perspectives 2017*

In the same way that the cytoskeleton is responsible for the distribution of cellular organelles and, therefore, the cellular architecture, the nuclear skeleton organizes the distribution of nuclear organelles, with the particularity that they lack a membrane.

1.2.1 The Nuclear Lamina is the main ingredient of the nucleoskeleton.

There is the standard agreement that the nuclear envelope builds a uniform spherical cortex around the nucleus, except for specific cells such as polymorphonuclear leukocytes. Far from reality, this convention eludes the existence of many nuclear envelope irregularities, usually in the form of invaginations, in a large number of cell types (Fricker et al., 1997). The set of intrusions of the nuclear membrane constitute the so-called nucleoplasmic reticulum, and as happens with many other components that make up the nuclear architecture, we still do not understand its exact function. However, it is reliably suspected that it could be involved in improving nuclear transport, specifically with the transport of calcium ions. (R. K. Y. Lee et al., 2006; Lui et al., 1998; Malhas et al., 2011). In any case, it has been found that the nucleoplasmic reticulum arises from the combination of two simultaneous processes: the centripetal polymerization of F-actin filaments and the focal depression of the nuclear lamina (Clubb & Locke, 1998; Legartová et al., 2013; Schoen et al., 2017; Storch et al., 2007). The

existence of the nucleoplasmic reticulum perfectly exemplifies the connection between the nucleoskeleton and the cytoskeleton.

Several studies suggest that the nuclear lamin is the main component of the nucleoskeleton. The nuclear lamina is composed of lamins, which are type V intermediate filaments, the only ones found in the nucleus, and are only present in metazoans (M. W. W. Goldberg et al., 2008; Herrmann & Aebi, 2016; Stick & Peter, 2017). There are two types of lamins: type A and type B. Type A lamins are produced by alternative splicing of the LMNA gene, and in the case of mammals, there are two main isoforms: lamin A (LA) and lamin C (LC). In contrast, the two type B lamins that exist: lamina B1 (LB1) and B2 (LB2), come from the expression of two independent genes called LMNB1 and LMNB2, respectively. In most cases, cells express both lamin A and B, but the proportion in which they coexist is variable depending on the tissue and cell potentiality. Such is the case of the brain, where LC is abundantly expressed, but LA is anecdotal. As for embryonic stem cells, they express both lamin B1 and B2 but only begin to express type A lamins as they enter the differentiation processes (Adam & Goldman, 2012). The differential expression of these intermediate filaments and their close association with extensive chromatin regions lead to the idea that they largely orchestrate the genetic program of the cells. Generally, the interaction between the nuclear lamina and chromatin is repressive and rich in repetitive sequences, forming the Lamin Associated Domains (LADs) described in previous paragraphs. However, some chromatin zones linked to the A-lamins adopt more open conformations than in the LADs (which generally bind to the B1 lamina) and contain active genes (Lund et al., 2015). Interestingly, A-type lamins can be found inside the nuclear interior in association with LAP2α, an inner nuclear envelope transmembrane protein that binds to chromatin through its C-terminal domain (Dechat et al., 2010). Thus, it seems that the repressive or permissive nature in the lamina-chromatin association depends mainly on the spatial organization within the nucleus.

Type A and B sheets form functionally independent intermediate filament networks both in the nuclear envelope (where they compose the NL) and in the nuclear interior. Lamin filaments assist DNA replication in association with PCNA (Proliferating Cell Nuclear Antigen) (Shumaker et al., 2008), and also participate in transcription (Shimi et al., 2008); although in both cases, the molecular mechanisms governing these functions still remain unknown. Similarly, B1 lamin filaments form a framework around the nucleolus providing structural support (Martin et al., 2009).

As can be seen, the intermediate nuclear filaments actively participate in the organization of nuclear life as if they were a peripheral anchoring framework. However, it is known that they also participate in signaling pathways by binding directly with proteins such as protein kinase C (PKCα) and cyclin D3, for example. Likewise, in the nuclear envelope, there is a vast network of transmembrane proteins of the internal nuclear membrane (Emerin, MAN1, NET39, LAP1, or LAP2β, to name a few) that participates in other signaling mechanisms related to cell proliferation, development, and differentiation (Wilson & Berk, 2010). As the

main structural element of the NE, it can be affirmed that the nuclear lamina is co-protagonist in such signaling routes through direct or indirect participation. The signaling pathways that pass through the nuclear envelope are intimately related to the mechanotransduction events. When tissues are put under external mechanical forces, cells can transmit the tension through their cytoskeleton towards the nucleus affecting their gene expression. Inside the nuclear envelope, there is a protein complex spanning through the ONM and the INM denominated LINC that connect the cytoskeleton with the nuclear lamina (Figure 5). The combination of the nuclear envelope transmembrane proteins, LINC complex, and nuclear lamina generates a chain of transmission and information management system that profoundly affects cell life.

The importance of the nuclear lamina as in the mentioned system is evinced by mutations in the LMNA, LMNB1 and LMNB2 genes, which trigger a series of diseases known as laminopathies. These illnesses range from cardiomyopathies, muscular dystrophy (Emery-Dreifuss muscular dystrophy: EDMD) bone disorders and neuropathies to premature aging (progeria) (Dutta et al., 2018). Such terrible diseases are linked with alterations of the lamin filaments mechanotransduction capacity. For example, HGPS (Hutchinson-Gilford Progeria Syndrome) patients express an aberrant form of lamin A, denominated progerin, that causes the collapse of the nuclear lamin because it lacks the necessary strength to overcome any mechanical stress (Eriksson et al., 2003).

1.2.2 Other nucleoskeletal components.

As stated before, the only indubious and well-known nucleoskeletal components are lamin filaments. However, their participation in nuclear architecture remains mainly at the nuclear envelope, shaping the nuclear lamin. The composition of the internal nucleoskeleton is nowadays still unknown, but the presence of actin inside the nucleus brings some interesting suggestions in this regard (Belin et al., 2013; Xie & Percipalle, 2018). Nuclear actin does not behave like its cytoplasmic counterpart, where it forms long filaments, but rather forms unconventional short filaments of a transient nature that are not detectable by phalloidin staining in general conditions. Although its polymerization mechanism remains unknown, it has been proposed that a SUMO posttranslational modification is responsible to some extent. The actin concentration inside the nucleus is controlled by a fine-tuned import and export process through the protein complexes cofilin and profilin, respectively. Up to date, actin has been reported to participate in several processes in nuclear biology such as mRNA processing, export, nuclear envelope assembly, transcription mediated by RNA polymerases I, II, and III, chromatin remodeling, and DNA repair (Caridi et al., 2019; Cavellán et al., 2006; Percipalle et al., 2006).

Current data suggests that the short nuclear actin filaments interact with a viscoelastic mesh in the nucleoplasm, providing traction needed for chromosomal relocation. As one could imagine, a tractor scaffold only makes sense if it exists a driving force working alongside it. Accordingly, several motor proteins, six myosins, and four kinesins are present in the

nucleus, but only the myosin 1C (MYO1C) has been extensively studied (de Lanerolle & Serebryannyy, 2011). Indeed, MYO1C motor capacity has been observed in vivo working alongside nuclear actin in the repositioning of chromosomal loci (Dundr et al., 2007). The relocation capacity of MYO1C is not limited to local movements but reaches distances as far as 5 μm (C.-H. Chuang et al., 2006). The presence of nuclear motor proteins can explain the existence of nuclear traffic that has faster velocities than those achievable by simple diffusion dynamics (C. H. Chuang & Belmont, 2007); and thus, also may contribute to extensive nuclear architecture reshaping during differentiation processes (Mehta et al., 2008; Ranade et al., 2019).

Due to the labile nature of the nuclear actin filaments, it has been proposed that several other proteins also compose the internal nucleoskeleton. Nuclear mitotic apparatus protein 1 (NuMa) is a 238 KDa coiled-coil homodimer that organizes the spindle microtubules during mitosis. During interphase, NuMa is present throughout the nucleus, except for nucleoli. Despite being almost as abundant as lamins, its function in the interphasic nucleus is still under study. (Radulescu & Cleveland, 2010). In vitro experiments have demonstrated that NuMa can oligomerize and create a space-filling matrix. In the same way, the experimental alteration of its expression, causes the disorganization of nuclear architecture and the arrangement of chromatin. In addition to its great abundance in the nuclear interior, these properties suggest that this protein would work as a protein scaffold that would partially fill out interchromatin spaces. (Gueth-Hallonet et al., 1998; Razin et al., 2014).

In addition to actin, the internal nucleoskeleton may be composed of other candidates of cytoskeletal origin, such as spectrins. These are a family of proteins that add flexibility to the actin filaments and crosslink them with the protein 4.1, which connects actin threads to membrane proteins. Several isoforms of spectrin and protein 4.1 have been reported inside the nucleus of HeLa cells and resting lymphocytes and are supposed to work similarly to their cytoplasmic counterparts. (Dingová et al., 2009; Kristó et al., 2016; Oma & Harata, 2011). This statement is backed by the evidence of interaction between spectrins, actin, protein 4.1, lamin-A, emerin, MYO1C, and NuMa in co-immunoprecipitation experiments. (Mattagajasingh et al., 2009; Meyer et al., 2011; Sridharan et al., 2006). This protein mesh is supposed to exert some of the elastic properties of the nucleoskeleton and favors an interpretation of the nucleoskeleton as a highly dynamic and interdependent network of proteins interacting with chromatin or nuclear bodies (Holaska et al., 2004).

Finally, such protein mesh might be reinforced by the association with other giant elastic proteins known as titins. Titins are responsible for providing elasticity to the vertebrate striated muscle cells, where they work as molecular springs (Holaska et al., 2004). Almost all eukaryotic cell nuclei express a nuclear isoform of titin, and several results support the idea that it interacts with the nuclear lamina and chromosomes (Machado & Andrew, 2000; Zastrow et al., 2006).

Despite the abundant presence of cytoskeletal proteins inside the nucleus behaving like nuclear structural units, it is also possible that other elements such as the chromatin itself or long non-coding RNAs could complete the big picture of the nucleoskeleton as an architectural element. (Bergmann & Spector, 2014; Sun et al., 2018). If proven to be accurate, this idea would change our concept of nuclear architecture substantially.

1.2.3 The Nuclear Pore Complex.

Despite being separated from the cytoplasm by the nuclear membrane, the nucleus is not isolated from the rest of the cell. As the bearer of the genetic information, the nucleus must be well communicated with the cellular machinery in order to exert the instructions written within its genetic code. The flow of information between the nucleus and the cytoplasm is mediated by the nuclear pore complex (NPC). NPCs are immense macromolecular structures embedded in the nuclear envelope in circular openings where the inner and the outer nuclear membrane fuse.

1.2.3.1 NPC structure.

Direct observation through various electron microscopic techniques, have revealed an eightfold rotational symmetry; confirmed as well recently by super-resolution fluorescence microscopy (Akey & Radermacher, 1993; Hinshaw et al., 1992; Löschberger et al., 2014). Cryo-electron tomography from assembled human and *Xenopus laevis* NPC has allowed to resolve the heart of the NPC structure, achieving resolutions ranging from two to three nanometers (Bui et al., 2013; Eibauer et al., 2015; von Appen et al., 2015). According to these experiments, the NPC dimensions are estimated to be 50 nm thick and 80-120 nm of diameter and perforated by a central channel of 20 nm radius (Schwartz, 2016).

Each NPC is estimated to weight up to 120 MDa and assembled by 500 to 1000 individual proteins known as nucleoporins (Nups). Despite its impressive size, it is formed by the repetition of “just” 30 different Nups that can be classified in different groups depending on its mobility and biochemical affinity (Beck & Hurt, 2017; Schwartz, 2016). According to these parameters, we can define roughly two main groups: the static scaffold Nups, and the peripheral mobile Nups. (Figure 6). The first one is the best known from the structural point of view (Schwartz, 2016), and it seems to be formed by three rings: one in the middle of the NPC (Inner Ring: IR) and two facing the cytoplasmic and the nuclear faces respectively (Cytoplasmic Ring: CR; and Nuclear Ring: NR). The scaffold gives to the NPC its characteristic shape and is anchored to the nuclear envelope by the mediation of three transmembrane nucleoporins: NDC1, GP210, and POM121. In addition to the central scaffolding, the NPC is made up of highly mobile (both in conformational and turnover terms) peripheral elements that eccentrically expand towards the cytoplasmic and nuclear faces (Knockenhauer & Schwartz, 2016; Rabut et al., 2004). In consequence, we distinguish the so-called cytoplasmic "filaments" and the nuclear "basket," respectively. As both names

indicate, the data currently available suggests a consensus regarding its structure, which is not such, given that different details can be seen depending on the technique and the model organism used, especially in the case of the nuclear basket (Arlucea et al., 1998; Martin W. Goldberg & Allen, 1996; Kiseleva, Allen, et al., 2004). In the following paragraphs, these aspects will be further explored.

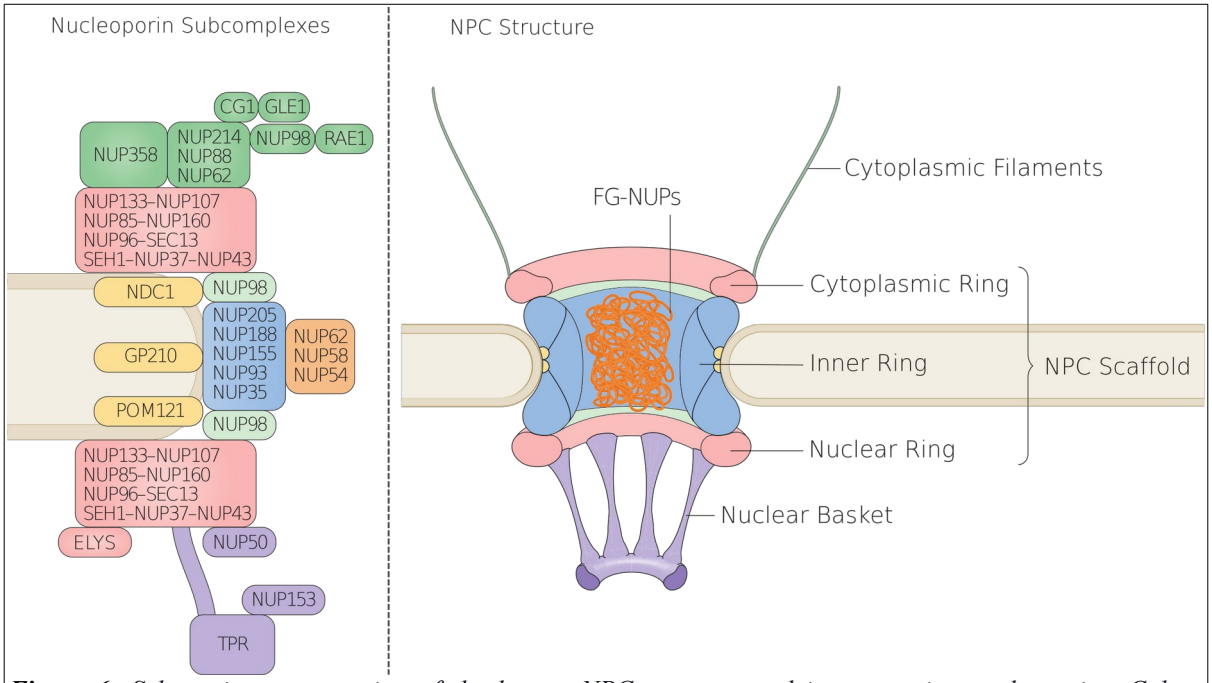

Figure 6: *Schematic representation of the human NPC structure and its composing nucleoporins. Colors schematize the approximated location of each nucleoporin subcomplex in the overall NPC structure. In red, Y-subcomplex mainly constitutes the cytoplasmic and inner rings. The Nup93 subcomplex (blue) completes the NPC scaffold in the inner ring, close to the Nup62 subcomplex (orange), whose FG repeats fill the central channel. The scaffold is anchored to the nuclear envelope by three different transmembrane Nups (Yellow). Pale green represents the presence of Nup98; an FG nucleoporin demonstrated to be placed throughout the channel and in close relation with the Nup214 subcomplex at the cytoplasmic filaments (dark green). The nuclear basket composed by Tpr, Nup153, and Nup50, is illustrated in purple projected towards the nucleoplasm. Illustration modified from M.Beck & E.Hurt, Nature Reviews Molecular Cell Biology 18 (2017) 73-89*

The construction of the previously cited elements relies on the modular composition of the 30 different nucleoporins, which, based on their biochemical affinity, constitute a few subcomplexes (Figure 6). The NPC scaffold is composed mainly of the Nup93-subcomplex, likely localized in the IR, and the Y-shaped subcomplex, which comprises the majority of the CR and NR (Kelley et al., 2015; Vollmer & Antonin, 2014). The unique biochemical properties of the Nup62 subcomplex, localized near the inner ring, set the central channel's permeability barrier. The nucleoporins of this special subcomplex are very rich in phenylalanine-glycine (FG) repeats extending towards the central channel (Hayama et al., 2017). Once is surpassed a minimal concentration, the FG repeats can form a permeable yet selective hydrogel, allowing free diffusion of small molecules and providing the required specificity for the directional movement of more convoluted molecules (Lemke, 2016;

Schmidt & Görlich, 2016). Among humans, we can find nine different Nups with FG repeats. Nup62, Nup54, and Nup58 constitute the central channel, but Nup62 is also present in the cytoplasmic filaments as part of the Nup214 subcomplex, where it coexists with the other two FG Nups (Nup214 itself and NupI2). Nup98 is another FG nucleoporin, characterized by its high mobility (Griffis et al., 2002). It is widely distributed through the NPC, as it interacts with Nup96 in the Y-subcomplex, Nup214 subcomplex in the cytoplasmic filaments, and with the nuclear basket nucleoporin Tpr (Fontoura et al., 2001; Griffis et al., 2003; Stuwe et al., 2012). Thus, Nup98 stands as the sole nucleoporin that can be found in the core and the periphery of the NPC. The transmembrane nucleoporin POM121 and the nuclear basket Nups Nup153 and Nup50 complete the list of human FG nucleoporins. As can be observed, FG-repeats are present in every NPC component, though more densely located at the central channel.

Nuclear basket, Nuclear Envelope Lattice (NEL) and Pore Linked Filaments (PLFs):

The nuclear basket is an NPC's substructure made up of eight filaments that emanate from the central scaffolding nuclear ring and converge in a distal ring. Three nucleoporins have been detected in this structure: Nup153, Nup50, and Tpr, the latter being its main component (Duheron et al., 2014; Krull et al., 2004). The Tpr sequence differs from the rest of the nucleoporins in that it has long coiled-coil domains that form homodimers, presumably forming the basket filaments (Hase et al., 2001). Tpr appears to expand nucleoplasmic inward, reaching distances of up to 350 nm and may also appear in isolation in the nuclear interior, suggesting that it forms long filaments projecting into the nuclear interior (Bangs et al., 1998; Volker C. Cordes et al., 1997; Frosst et al., 2002; Paddy, 1998). However, these data collide with the demonstrated Tpr inability to homopolymerize and build profound filaments (Hase et al., 2001; Grazyna Zimowska & Paddy, 2002).

Nup153 is another fundamental component of the nuclear basket, although its relationship with it is somewhat complicated, as demonstrated by domain-specific immunoelectron microscopy experiments. Moreover, this is because it is structured tripartitely between the N-terminal end in the nuclear ring, four zinc-finger domains in the basket's distal ring, and an FG domain in the C-terminal end, the location of which is highly variable, and can be located in the basket or the central channel FG soup (Ball & Ullman, 2005; Fahrenkrog et al., 2002). Various NPC elements converge in Nup153, such as the Y subcomplex, Tpr, and the soluble nucleoporin Nup50; the latter only related to the NPC through Nup153 in the distal ring of the basket (Duheron et al., 2014; Guan et al., 2000; Hase & Cordes, 2003; Makise et al., 2012).

From the structural perspective, despite extensive research, the nuclear basket is probably the less understood NPC substructure. Given its highly labile behavior, it has been excluded from cryo-ET studies due to technical impediments, and thus, our current knowledge arises from scanning electron microscopy. Most of the structural data stem from nuclear envelope spreads of amphibian oocytes (mostly *Xenopus laevis* and *Triturus cristatus*), as the massive size of

its nucleus allows its handling for scanning electron microscopy. First observations demonstrated the presence of the basket beneath the NPC at its nucleoplasmic size (Jarnik & Aebi, 1991). However, further experiments detected a regular mesh of fibrils of eight to ten nm in diameter bounded to the distal ring of the basket, referred as Nuclear Envelope Lattice (NEL). NEL was visible both in transmission and scanning electron microscopy, spreading horizontally and perpendicularly to the nuclear envelope axis with a regular pattern (V. C. Cordes et al., 1993; M. W. Goldberg & Allen, 1992). Accumulating evidence demonstrated that nuclear basket extended from the NPC towards the nuclear interior conforming which would be ultimately named as Pore Linked Filaments (PLFs) (Arlucea et al., 1998; Kiseleva, Drummond, et al., 2004; Ris, 1997; Simon & Wilson, 2011). At this point, available data backed that the repetitive pattern of NEL was occasioned by the interconnection of PLFs emanating from nearby NPCs. Arlucea and colleagues proposed that the nuclear basket elements were not aligned in a fish-trap-like structure as it is accepted today, but it rather was a part of an inwards projected network interacting with chromatin and other nuclear organelles such as nucleolus. So, the nuclear basket conceived as a fish-trap would be an artefactual structure due to the removal of the majority of the NEL during the NE spreading needed for scanning electron microscopy.

Ultrastructural aspects of both basket and NEL are subjected to great variability depending both on the preparation technique and the biological source. For example, in nuclear spreads of *Xenopus* germinal vesicle, bivalent ions such as calcium and magnesium seem to have a critical effect in the preservation of the NEL, as NEL and PLFs were better preserved in spreads exposed to concentrations higher than 3 mM Mg^{2+} (Arlucea et al., 1998; Kiseleva, Drummond, et al., 2004; Ris, 1997). On the contrary, the yeast nuclear basket seems to be less prominent than their vertebrates counterparts and there is no PLF nor NEL evidence (Kiseleva, Allen, et al., 2004).

The technical difficulty and the expertise required to observe these structures have complicated the direct and systematic study of PLFs. Nonetheless, it has been possible to verify a certain amount of its components, such as Tpr nucleoporin, which is detectable, especially in areas close to the NPC both in human cells and amphibian oocytes (Volker C. Cordes et al., 1997; Fontoura et al., 2001; Krull et al., 2010). Likewise, a very detailed study by Elena Kiseleva and collaborators in 2004, identified actin and protein 4.1 in the PLF network of *Xenopus laevis* oocytes (Kiseleva, Drummond, et al., 2004). In the same study, they also described the regular and spaced distribution of protein 4.1 epitopes throughout the filaments, whose structural integrity depended on actin polymerization. Furthermore, these filaments established a connection between the NPCs and some nuclear organelles such as nucleoli or Cajal bodies. The connection between nuclear organelles and pore complexes had been previously verified, and it was proposed that PLFs could facilitate communication between both nuclear components (Volker C. Cordes et al., 1997; Fontoura et al., 2001; Fricker et al., 1997; G Zimowska et al., 1997). This hypothesis is favored by the

demonstrated presence of motor and karyophilic proteins, such as nuclear myosin I and nucleoplasmin, throughout these filament networks, even interacting with NPCs and the nucleolus itself (Andrade et al., 2001; Obrdlik et al., 2010). Similarly, an experiment performed in human cells, demonstrated *in vivo* that a GFP-fused nucleolar phosphatase, CDC14B, was present in long actin-dependent filaments throughout the nucleus, connecting the nucleolus and the nuclear pores (Nalepa & Harper, 2004). The similarities between this report and the data gathered from amphibian oocytes are intriguing. Therefore, PLFs appear to be composed of actin, among other nucleoskeletal components, and would facilitate communication between nuclear organelles and pore complexes.

In summary, it is very tempting to extrapolate the architecture of the nuclear basket and the NEL to mammalian cells, especially given the similarity between their respective NPC scaffolds. However, it cannot be forgotten that amphibian oocytes are cells specialized in accumulating cellular elements that are subsequently inherited maternally during embryogenesis. Such is the case of NPCs, which populate the nuclear envelope more densely than in mammalian somatic nuclei. Thus, it is possible that the NEL, so prominent in the germinal vesicles, is limited to this cell type. It would be a reasonable explanation that the filaments projected from the NPCs were constituted in their proximity by the nucleoporins that populate the nuclear basket as we conceive it today (Tpr, Nup153, and Nup50), but that they were replaced or mixed with other nucleoskeletal elements (such as lamins, actin and protein 4.1) as they delved into the nucleus. Unfortunately, the experimental evidence is still insufficient to support such a claim.

1.2.3.2 Import and export cycles.

The most obvious and better-known purpose of the NPC is the regulation of the import and export of molecules from the nucleus. Metabolites, ions, small proteins, and molecules smaller than 40 kDa can diffuse freely through the insides of the NPC, whereas medium to big molecular weight proteins, ribonucleoproteins, and ribosome subunits, for example, must be transported actively through it. The transport mechanism varies depending on the molecule to be moved, but, in general terms, common mechanisms exist which are repeated on each transport event (Cautain et al., 2015; Katta et al., 2014; Sloan et al., 2016). The basic principle of active nuclear transport relies on the cyclic interactions between the cargo, Nuclear Transport Receptors (NTRs) (e.g., exportins, importins, and karyopherins) and the small GTPase Ran (Yoneda et al., 1999). Indeed the driving force of nuclear transport is carried out by the small GTPase Ran as explained in the following lines.

Thus, the energy needed for active transport is provided through a concentration gradient of Ran-GTP towards the cytoplasm. In the nucleoplasm, Ran GTP exchange factors (RanGEFs) transform RanGDP into RanGTP. The accumulation of RanGTP creates a stream towards the cytoplasm which will provide the necessary energy for NTR-mediated active transport. In order to preserve its high nuclear concentration, the innate GTPase activity of Ran is quite

low. Instead, the GTPase activity of Ran is boosted once it travels to the cytoplasm due to the presence of RanGTPase-activating proteins (RanGAPs). It is worth mentioning that RanGAPs are conveniently placed at the cytoplasmic filaments of the NPC by a strong association with Nup358 (Hutten et al., 2008). Once Ran hydrolyzes its GTP to GDP, the resulting RanGDP is recycled to the nucleus by the action of the nuclear transport factor 2 (NTF2) (Ribbeck, 1998; Smith et al., 1998; Yoneda et al., 1999).

Either synthesized in the cytoplasm or imported through cellular communication, proteins with a nuclear destination (e.g., histones or transcription factors) must bear a nuclear localization signal (NLS). Eventually, the NTRs importin α and importin β will sequentially recognize the NLS and form a trimeric import complex. NTRs are capable of establishing transient low-affinity interactions with the FG-repeats of the nucleoporins in the central channel, thereby causing the translocation of the cargo through the NPC (Aramburu & Lemke, 2017). Right after the trimeric import complex passes through the NPC, Ran-GTP binds to importin β, releasing the cargo to the nucleoplasm. Once the cargo is delivered, the importins are recycled towards the cytoplasm using the RanGTP gradient, well binding directly to RanGTP, as is the case for importin β, or using intermediating factors such as the exportin CAS (Kutay et al., 1997).

Nuclear export to the cytoplasm works analogously to import, but in a reversed manner, taking in advantage the direction of the RanGTP gradient. The export complex is composed of a karyopherin, RanGTP and the cargo itself. As said, the RanGTP gradient mediates the export, and once in the cytoplasm, the GTPase activity of Ran disassembles the export complex releasing the cargo.

As a final note, the processes defined above are rough approximations that exemplify the mechanics of soluble nucleo-cytoplasmic transport. Of course, each molecular family follows its own transport dynamics and usually relies on specific NTRs for appropriate transportation. For example, the transport of integral membrane proteins from the inner nuclear envelope is of particular interest. The synthesis of INM proteins begins at the endoplasmic reticulum, where it is co-transcriptionally integrated into its membrane thanks to the Sec61 translocon. If the nucleoplasmic portion of the transmembrane protein has a molecular mass of less than 40KDa or diameter less than 10nm, it will be able to freely diffuse through the curvature of the membrane in the pore complex until it reaches the INM. For bulkier dimensions, transport will require active intervention of importins and RanGTP mediated release. For an in-depth review, consult the review (Katta et al., 2014).

The export of mRNA is another transport mechanism of remarkable interest. The exportation of some RNA families has many similarities with the export of proteins. For example, karyopherins exportin-t and CRM1 export tRNAs and snRNAs respectively using the RanGTP gradient (A. G. Cook & Conti, 2010; Rodriguez et al., 2004). In contrast, the export of messenger RNA is radically different (Sloan et al., 2016). During transcription, nascent messenger RNA undergoes a wide range of modifications until it becomes transport

competent Transcription factories are nuclear organelles specialized in catalyzing transcription where the molecular machinery is accumulated for this purpose (Rieder et al., 2012). In these organelles, parallel to transcription, a series of modifications occur, which include the folding of the nascent RNA, cutting and splicing of the intronic sequences, capping of the 3 'end tail, polyadenylation of the 5' end, quality controls and the covering of transport factors (Björk & Wieslander, 2017). Once the nascent mRNA has been transformed into a transport-competent mRNP molecule, it begins its passage through interchromosomal channels possibly supported by nucleoskeletal elements such as PLFs, actin, and nuclear myosin. (Andrade et al., 2001; de Lanerolle & Serebryannyy, 2011; Obrdlik et al., 2010). The NXT1 / NXF1 heterodimer covers the bulk of the mRNP molecule and becomes crucial in the final stage of transport, that is, during translocation through the pore complex. Although the nature of the NXT1 heterodimer is different from that of the karyopherins, it is also highly soluble in the FG soup of the central channel. Release to the cytoplasm is mediated by the helicase protein family which, thanks to their ATPase activity, eliminate the NFT1 heterodimers as they appear on the cytoplasmic side; This ensures that the released part of the heterodimer cannot re-enter the NPC. Thus, sequentially, the mRNP passes from the NPC to the cytoplasm, where the translation machinery awaits it. The activity of RNA helicases is regulated by inositol6P and by the nucleoporin Gle1 of the cytoplasmic filaments. Rae 1, another cytoplasmic Nup, is responsible for Nup98-dependent mRNA export (Ren et al., 2010)

If the last steps of the export by the NPC are mediated in part by the cytoplasmic Nups, it is intuitive to associate the nucleoporins of the nuclear basket in facilitating the first steps of translocation to the NPC. Such is the case since both Nup153 and Tpr posses high-affinity binding domains for NFX1 heterodimer that stabilize its association with the basket. (Bachi et al., 2000; Coyle et al., 2011; Griffis et al., 2004). Mature mRNP joins the nuclear basket thanks to the THO and TREX2 complexes coordinated activity, which are responsible for synchronizing transcriptional activity to transport machinery (Jani et al., 2012). Moreover, TREX2 is stably tethered to the nuclear basket, thus supporting the idea that transcription and nucleoporin mediated transport are intimately related mechanisms (A. L. Buchwalter et al., 2014; Griffis et al., 2004; Umlauf et al., 2013). Once the mRNP molecule is bound to the basket, this last structurally reconfigures itself in order to accommodate the intake of the mRNP molecule to the central channel (Kiseleva et al., 1996; Soop et al., 2005). However, basket nucleoporins are not only necessary for NPC uptake of mRNAs, but they also impede the export of intron-containing mRNAs, revealing a vital role in the mRNA quality control regulatory machinery (Coyle et al., 2011; Rajanala & Nandicoori, 2012).

Additionally, Nup153 can also bind directly to RNA through an RNA binding domain in its N-terminal domain (Ball et al., 2004). Its central role in NPC transport is highlighted through its possession of a RanGTPase binding domain in its zinc-finger domain, the importin-β interaction through its FG domain and partnering with several karyopherins (Ball & Ullman,

2005). The implications of Nup153 in the nuclear import are co-regulated with Nup50 through importin-α association (Makise et al., 2012). Nup50, like Nup98, is also responsible in the export of molecules relying on the exportin CRM1 mediated route (Guan et al., 2000; Oka et al., 2010).

1.2.3.3 Assembly and Disassembly of the NPC.

The NPC is the largest non-polymeric protein complex in the eukaryotic cell. Given its gigantic size and sophisticated composition, it is not energy-efficient to have to deconstruct and rebuild it continuously throughout cell life. That is why eukaryotic cells have evolved to maximize their useful life. An example is the case of terminally differentiated cells, in which their NPCs do not change during the rest of their life cycle. Consequently, the gradual loss of nucleo-cytoplasmic permeability caused by the deterioration of the NPC (due to lack of turnover and oxidative damage) is one of the main aggravating factors of cellular aging events (D'Angelo et al., 2009). In contrast, in actively dividing cells, such as adult stem cells, the pore complex undergoes a cycle of construction and deconstruction parallel to cell cycle progression.

The NPC can be assembled in two ways: at the interface (*de novo* synthesis) during nuclear growth, or after mitosis by rebuilding the nucleus (Otsuka & Ellenberg, 2018). In higher eukaryotes, mitosis is open, that is, the nuclear envelope is deconstructed so that the microtubule organizing center (MTOC) can separate the mitotic chromosomes. On the contrary, in simpler organisms such as yeasts, mitosis is closed since the MTOC is located within the nucleus itself, which makes the disappearance of NE unnecessary. In this work, we will only address open mitosis. During the interface or after mitosis, the assembly mechanisms differ significantly from each other (Ungricht & Kutay, 2017; Weberruss & Antonin, 2016). At the end of mitosis, during the sealing of the nuclear envelope, a vast number of NPCs are formed in minutes, while during interface, the *de novo* synthesis of NPCs occurs sporadically, a process of approximately 1-hour duration that requires the fusion of the outer and inner nuclear membranes.

To explain how the NPC is reassembled (Figure 7), one must first understand how the NPC is disassembled and what happens to the Nups during mitosis. At the start of mitosis, the nuclear lamina, the INM membrane proteins, and the Nups undergo a series of extensive phosphorylations triggered by mitotic kinases (de Castro et al., 2018). The nucleoporin Nup98, which functions as a bridge between several subcomplexes of the NPC, leaves the NPC once phosphorylated, consequently weakening the interaction between TM-Nups, the Nup93 subcomplex, and Nup62 (Dultz et al., 2008; Laurell et al., 2011). Subsequent phosphorylations of the remaining nucleoporins complete disarmament of the NPC (Güttinger et al., 2009). Likewise, phosphorylation of the nuclear lamina and the INM proteins triggers the dissociation between the chromatin and nuclear envelope (Ungricht & Kutay, 2017). The mitotic spindle proliferation forces the NE to retract next to the

endoplasmic reticulum, leaving the necessary room for proper chromosome segregation (Schlaitz et al., 2013; Smyth et al., 2012). As the nuclear envelope disappears, the phosphorylated versions of the nucleoporins, intermediate filaments, and inner membrane proteins diffuse through the mitotic cytoplasm.

Some of the first released nucleoporins, such as Nup98, RAE1, or Y-subcomplexes, play an essential role in the microtubule organizing center, recruiting the nuclear mitotic apparatus protein (NuMA) during the spindle formation (Orjalo et al., 2006; Wong et al., 2006). At the same time, a considerable fraction of the soluble Y-subcomplex and Nup358 localize at the kinetochores, where they stabilize the binding of the spindle microtubules (Chatel & Fahrenkrog, 2011; Mishra et al., 2010). Before anaphase begins, a regulatory mechanism must be initiated that guarantees the correct union between the kinetochore of the chromosomes and the mitotic spindle; this is the so-called Spindle Assembly Checkpoint (SAC). MAD1 and MAD2 are two essential proteins that are needed in the kinetochores so that the rest of the checkpoint machinery can work. The nuclear basket nucleoporins Tpr and Nup153, turns out to be of vital importance mediating the unification of MAD1 and MAD2 at the kinetochores (S. H. Lee et al., 2008; López-Soop et al., 2017; Lussi et al., 2010; Schweizer et al., 2013). Once this checkpoint is passed, anaphase begins. As we can see, nucleoporins actively participate in mitosis, regulating the formation of the mitotic spindle, the anchorage of the kinetochores to it, and finally, verifying that this union is successful (Chatel & Fahrenkrog, 2011).

As explained, several nucleoporins regulate mitotic continuation, but leftover nucleoporins are sequestered in the cytoplasm by binding to nuclear transport factors (NTRs) such as importin β (Forbes et al., 2015). In this manner, NTRs prevent NE proteins and Nups from interacting with other proteins that would hinder subsequent reconstruction (Bernis et al., 2014). On the other hand, Ran-GFP is produced and accumulated in chromosomes due to the activity of RCC1, a chromatin-bound RanGEF protein. This zonal separation between the NTRs and the RanGTP will be essential for the restoration of the transport gradient and the nuclear envelope's assembly.

One of the functions of the mitotic spindle is to generate an exclusion zone in which only the activity of mitotic proteins, such as the components of the kinetochore, the SAC machinery, and motor proteins, are allowed. The capacity of such an exclusion zone is weakened as anaphase progresses, especially at the spindle poles, causing some allowance for the endoplasmic reticulum to approach until eventually the connection between the budding nuclear envelope and the chromosomes is established. However, the association of both elements cannot be accomplished without the parallel initiation of two other processes (Otsuka & Ellenberg, 2018): I) Ran-GTP, accumulated in the proximity of the chromosomes, binds to the neighboring NTRs. The binding between RanGTP and NTRs, like importin B, releases nucleoporins and other proteins from the nuclear envelope that were being sequestered. II) The activation of mitotic phosphatases triggers the dephosphorylation of

nucleoporins and other nuclear envelope proteins recently released into the cytoplasm. Once free and dephosphorylated, the elements of the nuclear envelope are reassembled and rejoin with the decompressing chromatin (Figure 7A). This event initiates the reconstruction of the nuclear envelope and the nuclear pores.

As discussed in the previous paragraph, the mitotic reconstruction of the NPC begins during the late anaphase when chromosomes begin to decompress. Although the exact sequence in which the entire pore is reestablished is subject to extensive research, most publications agree that it occurs in different phases (Bodoor et al., 1999; Weberruss & Antonin, 2016). The first of these consists of the union between chromatin and nucleoporin ELYS of the nuclear ring, which in turn recruits the Y subcomplex, an essential architectural element of the pore. Although the incorporation of Nup153 is not necessary for a successful reassembly, it does seem to favor the union of the budding pore with the transmembrane nucleoporins that inhabit the nuclear envelope (Smythe et al., 2000); this is the second crucial point of reassembly, but the arrangement of transmembrane nucleoporins at this point is not fully understood (Weberruss & Antonin, 2016). Some studies suggest that some transmembrane and inner ring nucleoporins constitute a kind of "pre-pores" in the retracted nuclear envelope, next to the reticulum that later will serve as the basis for reconstruction (Otsuka et al., 2018). Nevertheless, pre-pore presence does not seem to be a necessary condition for successful TM-Nups binding with the Y-subcomplex (Doucet et al., 2010; Rasala et al., 2008). Whether the presence of prepores is a must condition or not, both observations would favor a model where the progression of the nuclear envelope enclosure would fuse with the emerging pores planted in the chromatin (Otsuka et al., 2018). However, other scientists have reported that the complete enclosure of the nuclear envelope occurs previously to the pore reassembly, implying the necessity of INM/ONM fusion at the NPC afterwards (Fichtman et al., 2010; Lu et al., 2011). Whether or not they are parallel processes, it seems that the incorporation of the TM-Nups initiates the next phase of the reconstruction, which is characterized by recovering import competence thanks to the progressive incorporation of the nucleoporins of the inner ring and the FG-Nups of the central channel. In the last phase, and there seems to be consensus in this aspect, the cytoplasmic filaments and the nuclear basket are reestablished by incorporating Nup214 and Tpr, respectively (Bodoor et al., 1999; Dultz et al., 2008; Haraguchi et al., 2000; Hase & Cordes, 2003).

In sum, during late anaphase, chromosomes leave the exclusion zone of the mitotic spindle, allowing RanGTP to release nucleoporins and other NE-proteins, which can begin to rebuild the envelope and pore complex thanks to mitotic phosphatase activity.

After mitotic exit, the daughter cells can either continue actively dividing (such as the case of cancer cells and stem cells) or differentiate and exit from the cell cycle. In the last case, nuclear pore synthesis is virtually nonexistent, and the cell will continue its vital cycle with the inherited number of pores (Weberruss & Antonin, 2016). On the contrary, if the cell continues through the cell cycle, it enters interphase, divided into three subphases: G1, S, and

G2. During G1 and G2 phases, the cell is focused on accumulating energy, nutrients, and cellular machinery for the DNA duplication during the S phase and mitosis. From the beginning to the end of interphase, the nuclear envelope doubles its NPC number; this is required in order to proportionate enough NPCs to daughter cells after mitosis and is expected to couple its metabolic activity and nuclear growth (Dultz & Ellenberg, 2010; Maeshima et al., 2010; Maul et al., 1971).

In contrast with the fast mitotic reassembly, the new formation of NPCs during interphase is a long process that requires the gradual incorporation of nucleoporins to the INM and the fusion of the INM and the ONM. Similar to the mitotic case, RanGTP and importins are critical elements for *de novo* NPC formation since they orchestrate the import of cytoplasm synthesized nucleoporins towards the nuclear interior. Such is the case of the POM121 and Nup153 nucleoporins, which initiate the interphasic assembly (Figure 7B). Either solubly imported as Nup153 or diffused through the pore envelope's curvature as POM121, importins release their cargo in the nuclear interior by Ran-GTP mediated displacement. Once free, Pom121 and Nup153 associate in the nuclear envelope, serving as the basis for the Y subcomplex to bind. These initial steps are well described in the literature (Dultz & Ellenberg, 2010; Iino et al., 2010; Vollmer et al., 2015), yet not the following ones, which involve the curvature of the inner nuclear envelope until it merges with the outer nuclear membrane (Otsuka & Ellenberg, 2018; Weberruss & Antonin, 2016). Amphipathic helices of some nucleoporins such as POM121 and Nup155 are likely to favor the curvature of the INM (Funakoshi et al., 2011; Weberruss & Antonin, 2016). Besides, INM transmembrane proteins as SUN2 (belonging to LINC complex) have also been shown to facilitate the assembly of NPC and membrane fusion (Jahed et al., 2016). It also exists evidence of participation of reticulons, one type of membrane-shaping protein (Dawson et al., 2009). Thus, the molecular and cellular mechanisms that govern the intermediate and final phases of the interphase NPC assembly remain unknown, due in part to the technical difficulty of their study. After all, the interphasic assembly is sporadic, and it is often difficult to distinguish the emerging pores from those already formed.

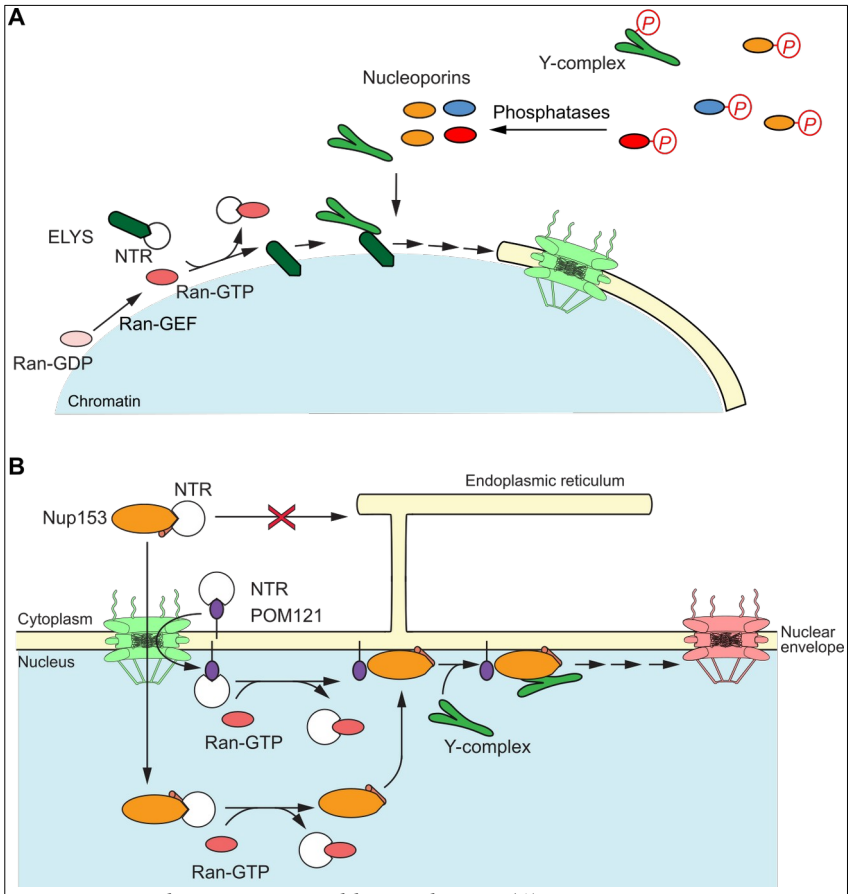

Figure 7: Nuclear pore assembly regulation. (A) Post-mitotic reconstruction of NPC is regulated by the Ran-GTP induced Nup release and dephosphorilation of nucleoporins. This process is coordinated with the nuclear envelope reconstruction. The nuceloporin ELYS and Y-subcomplex are responsible for the first phase of the NPC reconstruction. (B) Interphasic "de novo" NPC assembly into intact nuclear envelope imply the sequential nucleoporin incorporation. The firsts steps of the assembly imply the Ran-GTP mediated recruitment of nucleoporins Nup153 and Pom121. The incorporation of Y-subcomplex from its nucleoplasmic pool, triggers the consecutive recruitment of Nups towards the emerging NPC. Figure adapted from M.Weberrus & W.Antonin. Journal of Cell Science 129 (2016) 4439-4447

1.2.3.4 Nucleoporin dynamics.

As explained in the previous section, NPCs are exceptionally long-lived complexes. More specifically, scaffold nucleoporins are no longer expressed at significant levels once a cell is differentiated, persisting its entire lifespan (D'Angelo et al., 2009). As differentiated cells are no longer actively cycling, both interphase and mitotic NPC biogenesis are inhibited. Presumably, NPC's structural complexity impedes successful recycling of its scaffold elements, but this seems not true for its peripheral and dynamic constituents such as basket and FG-rich nucleoporins, as demonstrated by FRAP (Fluorescence Recovery After Photobleaching) data of EGFP-fused nucleoporins (Daigle et al., 2001; Rabut et al., 2004).

These investigations reported that each component of the Y-subcomplex and Nup93, an essential element of the central ring, were highly stable. In contrast, the dynamics of most FG-motif-containing Nups (except for the cytoplasmic nucleoporin Nup214) behaved closer to what would be expected for an adapter element. Surprisingly, the transmembrane nucleoporin Gp210, traditionally thought to be an anchoring element of the scaffold, in addition to basket Nups Nup153 and Nup50 conducted bi-exponential dissociation kinetics, which means that exist two populations of the cited Nups in the nucleus: one bound to the NPC, and another diffusive through the nucleoplasm or the nuclear envelope in the case of Gp210. The off-pore biology of the mobile Nups is closely related with gene regulation and export of RNAs as mobility of Nup153, Nup50 and also Nup98 is transcriptionally dependent (A. L. Buchwalter et al., 2014; Griffis et al., 2002, 2004). The implications of the shuttling properties of these nucleoporins root profoundly in nuclear biology, as seem to add an additional regulatory layer of genome architecture by controlling the spatiotemporal placement of specific genes in the NPC vicinity or deep in the nucleoplasm; especially for genes related to development. (A. L. Buchwalter et al., 2014; Jacinto et al., 2015; Kalverda et al., 2010; Liang et al., 2013).

Intriguingly, recent evidence suggests that bi-exponential dissociation kinetics are not an absolute requirement for the existence of an intranuclear pool of a determined nucleoporin, being this the case of the scaffold nucleoporin Nup107 (a major constituent of the Y-Subcomplex) and the transmembrane nucleoporin Pom121 (Franks et al., 2016; Morchoisne-Bolhy et al., 2015). However, the intranuclear presence of both Nups rely on the nucleoplasmic pool of Nup98. In some cell types, such as HeLa-C cell line, Nup98 is enriched in intranuclear aggregates denominated as GLFG bodies (so named because of its dependence of the GLFG repeats in the Nup98 sequence (Griffis et al., 2002). Nup98 is constantly moving between the NPC, nucleoplasm and GLFG bodies. However, additional nucleoporins reside in these nuclear bodies. Two of these are Nup107 and Pom121. However, contrarily to Nup98, intranuclear pools of Nup107 and Pom121 are independent from its NPC counterparts as there is no exchange between these populations; and shuttle only between the GLFG bodies and nucleoplasm, coinciding with previous FRAP experiments (Griffis et al., 2002; Rabut et al., 2004). In fact, intranuclear Pom121 is slightly different from its NPC counterpart as its sequence does not possess the transmembrane domain any longer. The transcripts of this soluble Pom121 isoform are only expressed in mammalian species and evolved independently, suggesting a convergent evolutionary solution that enlightens the rapid nucleoporin evolution as possible transcriptional regulators (Franks et al., 2016).

NPC dynamics are not restricted to a nucleoporin turn-over perspective. In this regard, NPCs are uniformly arranged through the nuclear envelope. The global concentrations of nuclear lamina is deeply responsible for even NPC distribution, as it is demonstrated that NPCs are tightly connected with lamins and share parallel movements as demonstrated by live microscopy tracking of EGFP-fused nucleoporins and lamins (Daigle et al., 2001; Guo et al.,

2014). This intimate union is established by tight association of A and B type lamins with the nuclear basket nucleoporins Nup153 and Tpr. (Al-Haboubi et al., 2011; Fišerová et al., 2019). Following this evidence, it is not casual that depletion of Nup153 impaired cell migration through the disruption of cytoskeleton (Zhou & Panté, 2010), as nuclear lamina is bound to the cytoskeleton via the LINC complexes spanning the INM and ONM. Sun1 is an inner nuclear membrane protein that interacts with lamin A and is responsible for evenly distributing the NPCs synthesized during interphase (Haque et al., 2006; Talamas & Hetzer, 2011). Again, not casually, Sun1 interacts with the NPC via Nup153 (Q. Liu et al., 2007), which is one the first nucleoporins to be recruited to *de novo* produced NPCs (Figure 7).

As we can see, the nuclear lamina, the main nucleoskeletal element is in close relationship with the NPC, and more specifically with the nuclear basket nucleoporins. Importantly, every nuclear basket related nucleoporin can also be found in the nuclear interior. When considered in parallel with the labile nature of the pore-linked-filaments, in opposition to the solid scaffold, one can suggest the possibility that basket nucleoporins are closely related to nucleoskeletal elements; even more when the presence of intranuclear fractions of lamin A is taken in consideration.

1.2.3.5 Nucleoporins as regulators of genome structure and function.

One of the attributed roles of the nucleoskeleton is the spatio-temporal support of nuclear activities. The presence of GLFG bodies, including the fact that various intranuclear Nups behave in a transcriptional dependent manner, strongly favor the idea of nucleoporins as overall nuclear architectural organizers. For example, Tpr is responsible for impeding heterochromatin's expansion, establishing pore associated heterochromatin exclusion zones. (Krull et al., 2010). According to this, NPCs could serve as higher-order chromatin organizers. Accumulating evidence favors this thought, as locus control regions or super-enhancers (these are the terms for referencing the clustering of several enhancers found in close genomic proximity) are bound to nuclear pore complexes in metazoan genomes (Pascual-Garcia & Capelson, 2019). Enhancers are responsible for recruiting transcription factors and coactivators such as mediator complex to favor transcription of a certain gene. Consequently, super-enhancers are very enriched in active-chromatin related histone modifications as H3K4me and H3K27ac; in addition to chromatin remodeling elements as is the case for the histone acetyltransferase P300/CBP (Calo & Wysocka, 2013).

In *Drosophila*, Nup98 mediates enhancer-promoter association at the nuclear pore, especially in the ones inducible by hormones helping to preserve the cellular transcriptional memory. This implies the stabilization of the gene location to the nuclear pores through architectural elements such as the insulator protein CTCF which physically interacts with Nup98 (Kalverda & Fornerod, 2010; Pascual-Garcia et al., 2017). The enhancer-NPC boundary is also extended to mammals as human Nup153, Nup98, and Nup93 recruit super-enhancers and

other regulatory elements to the nuclear pores. Notably, Nup153 and Nup98 resulted in being crucial for the activation of the detected enhancer-dependent genes which were usually related to cell identity (Ibarra et al., 2016; X. Liu et al., 2017).

The considerable distance between the enhancers and promoters forces the DNA sequence to loop over itself to trigger transcription. These looping events take place thanks to the mediator and cohesin complexes among others (Matharu & Ahituv, 2015). The studies cited in the preceding paragraph propose NPC-bound nucleoporins as additional chromatin looping and enhancer anchorage elements. However, these sets of nucleoporins can also be found in the nuclear interior interacting with active chromatin. Abundant data from *Drosophila* reveals that the nucleoporins Nup50, Nup62, Nup98, Sec13, Nup153, and mTor (the *Drosophila* ortholog of Tpr) interact extensively with active chromatin in the nuclear interior predominantly with developmental and cell cycle-related genes. Importantly, the activity of the identified genes was up or down-regulated through the overexpression or silencing of the interacting nucleoporins; being this tendency especially evident for Nup98 (Capelson et al., 2010; Kalverda et al., 2010; Pascual-Garcia et al., 2014; Vaquerizas et al., 2010).

It seems that data obtained from the *Drosophila* model is comparable and follows similar considerations about Nup-genome interactions in mammalian systems. Nup98 as an instance, dynamically associates with developmentally regulated genes during human embryonic stem cell differentiation at the NPC and in the nuclear interior, suggesting different regulation mechanisms (Liang et al., 2013). It seems that the zonification of Nup98-genome binding is related to the preservation of transcriptional memory of inducible genes through the binding and recruitment of epigenetic regulators at the transcription start sites (Franks et al., 2017; Light et al., 2013). Similarly, Nup153 is also involved in stem cell pluripotency maintenance through the inhibitory binding to the transcription starting sequence of developmental genes both at the NPC and the nuclear interior (Jacinto et al., 2015). In neural progenitor cells, Nup153 interacts with Sox2 in order to maintain adult neuronal stemness co-regulating large amounts of differentiation genes. This regulation is dependent on the binding of Nup153 with promoters or transcription ending sites up-regulating or inhibiting its expression respectively. Moreover, Nup153 silencing altered the open chromatin structure of the Sox2 depending genes causing its miss-regulation (Toda et al., 2017). Another basket nucleoporin, Nup50, has been reported to behave likewise to Nup153 as the mobility of the Nup50 nucleoplasmic pool is directly dependent on the activity of RNA PolymeraseII (A. L. Buchwalter et al., 2014). These authors also demonstrated that depletion of Nup50 inhibited myoblast differentiation, which in turn, proposes Nup50 and other nucleoplasmic nucleoporins as transcriptional coactivators.

Thereby, it seems that the genome-nucleoporin binding takes place both at the nuclear interior and at the NPC. This pivoting interaction is related to nuclear organization mechanisms as nucleoporins interact with chromatin remodeling complexes and recruit histone modifiers (Kuhn & Capelson, 2019); also, and importantly, the NPC-bound nucleoporin fractions are

preferentially associated with enhancers and insulator proteins contributing with chromatin clustering and arrangement of transcription associated domains. On the contrary, nucleoplasmic Nups are more linked to association with proximal promoters and the generation of active transcription, working closely with transcription factors as co-activators. Significantly, most nucleoporins interacting with chromatin are rich in FG-repeats, which could create selective permeable intranuclear aggregates rich in transcription factors and specific molecular machinery (Pascual-Garcia & Capelson, 2019). All in all, the molecular machinery involved in the nucleoporin-genome relation is still unknown but under intense study during the past decade (A. Buchwalter et al., 2019).

The findings enumerated along the present and previous sections, suggest that the nuclear basket is the last element of a long chain of a highly dynamic interaction network. The nucleoporins that compose it offer a platform where all these synergistic processes can be carried out successfully, ranging from RNA processing, transport, epigenetic regulation, cell cycle progression and nuclear organization.

1.3 Nucleoporins and histone modifications.

Chromatin structure and function is tightly regulated by several covalent modifications of core histone tails (Figures 2 and 3). Methylation and acetylation are the best known up to date. Both modifications can be reversely added or erased to the lysine residues of histones by the finely tuned activity of histone methyltransferases (HMTs), histone demethylases (HDMTs), histone acetyltransferases (HATs) and histone deacetylases (HDACs) respectively. Some methylation hallmarks are responsible for recruiting chromatin remodeling complexes and trigger the condensation or relaxation of certain chromatin domains. On the contrary, lysine acetylation can relax the chromatin structure by itself. Although up to twelve different covalent histone modifications have been reported, methylation and acetylation stand as the best comprehended as epigenetic regulators.

Transcriptional memory is one example of epigenetic regulation of gene expression; which can be defined as an enhanced transcription capacity of a determined subset of genes after previous stimulation (Brickner, 2009; Palozola et al., 2019). This phenomenon can only occur if the implied chromatin domains are open and active; thus, it is not surprising that promoters and enhancers at these domains are particularly enriched with histone acetylation and methylation of H3K4. Genome-interacting nucleoporins are commonly found in regulatory sequences enriched with the mentioned histone modifications and are responsible to some extent for their spatial organization, as they can interact directly with insulator proteins. Not only that, nucleoporins can be directly responsible mediators of preserving the transcriptional memory, as its association with the promoter and enhancer sequences is imperative for successive transcription of inducible genes. Nup98 as an instance is involved explicitly in transcriptional reactivation of IFN-γ inducible genes as methylation of its promoters relies on Nup98. (Light et al., 2013). The methylation events related to Nup98 are probably mediated

through its association with the Set1/COMPASS complex, known to exert a strong HMT activity especially in the promoters of actively expressed genes (Franks et al., 2017).

P300/CBP is a protein complex well known for its histone acetyltransferase activity in opened chromatin. Recent evidence has demonstrated that Nup153 interacts directly with this HAT complex, targeting a similar set of cardiac tissue genes. In addition, Nup153-p300/CBP interaction resulted in being interdependent for correct gene expression (Nanni et al., 2016). While Nup153-linked HAT activity has been demonstrated in cardiac tissue, this does not reproduce in other cell lineages, such as mouse embryonic stem cells, where Nup153 silences the expression of differentiation-related genes through the recruitment of the polycomb repressive complex 1 (PRC1) (Jacinto et al., 2015). PRC1-mediated repression is mediated by the recruitment of the polycomb repressive complex 2 (PRC2), a histone modifier known for its methyltransferase activity in H3K27, a classic repressive mark rich in reversibly condensed chromatin.

While Nup153 (in some conditions or tissues, as said) and Nup98 seem to enhance and facilitate transcription, others are usually related to repressive modifications present in chromatin under compaction processes. This is the case for Nup155 and Nup93; nucleoporins placed in the inner and nuclear rings of the NPC and characterized by its low turn-over and dynamics. For example, HDAC4, a histone deacetylase strongly implicated in chromatin condensation and gene repression, establishes direct contact with Nup155 in human cardiomyocytes; and significantly, Nup155 enhanced the deacetylase activity of HDAC4 at its target genes. (Kehat et al., 2011). Similarly, in HeLa cells, Nup93 is bound to regions of transcriptional repression copiously modified with H3K9me3 and H3K27me3, both heterochromatin-associated histone marks. Nonetheless, after treatment with the histone deacetylase inhibitor trichostatin A (TSA), Nup93-interacting sites switched towards active and open domains rich in H3K4me2 and strongly acetylated promoter regions (Brown et al., 2008).

It seems that the influence exerted by nucleoporins at epigenetic regulation roots so profoundly in cell fate determination that different types of nucleoporins can exert opposite reactions; when it is not that even the same nucleoporin can enhance or repress different genetic sets, as is the case of Nup153.

The acetylation PTM is regulated by the coordinated and balanced action of the acetyl transferases and deacetylases. Histone acetyl transferases (HATs) catalyze the acetylation reaction mainly in the lysine residues of the N-terminal tails of histones H3 and H4. On the contrary, histone deacetylases (HDACs) erase the acetyl modification.

As said, and like the rest of the other PTMs, refined tuning of histone acetylation is imperative for proper cellular functioning, and through extension, healthy microenvironment and tissular function.

1.4 HDAC inhibitors as antitumoral therapy.

As discussed in the previous section, the implications of histone modifications in gene expression and chromatin structure are so profound that new regulation layers, such as those related to nucleoporin-chromatin contacts, are being discovered.

While methylation can both open and enclose chromatin domains, histone acetylation is exclusively associated with chromatin opening. Histone acetylation is modulated by the opposing activity of histone acetyltransferases (HATs) and histone deacetylases (HDACs). During cancer development, disruption of acetylation and deacetylation balance causes alterations in gene expression, upregulating cell cycle progression, inhibiting apoptosis, and favoring metastatic events (Figure 8). For instance, during tumorigenesis, HDAC activation causes the deacetylation of H4K16, which is a shared event in most human cancers (Fraga et al., 2005).

In humans, the HDAC superfamily comprises up to eighteen known proteins and is classified into four classes (summed up in table 1) according to their structure, subcellular distribution, activity, and co-factor dependency. These classes can furtherly be summed up into two leading families: class I, II, and IV comprise the "classical HDACs", while those belonging to class III are referred to as "sirtuins." The two families differ significantly in the co-factors needed in its enzymatic center. The activity of classical HDACs is dependent on zinc ions, but sirtuins rely on the catalysis of NADH molecules.

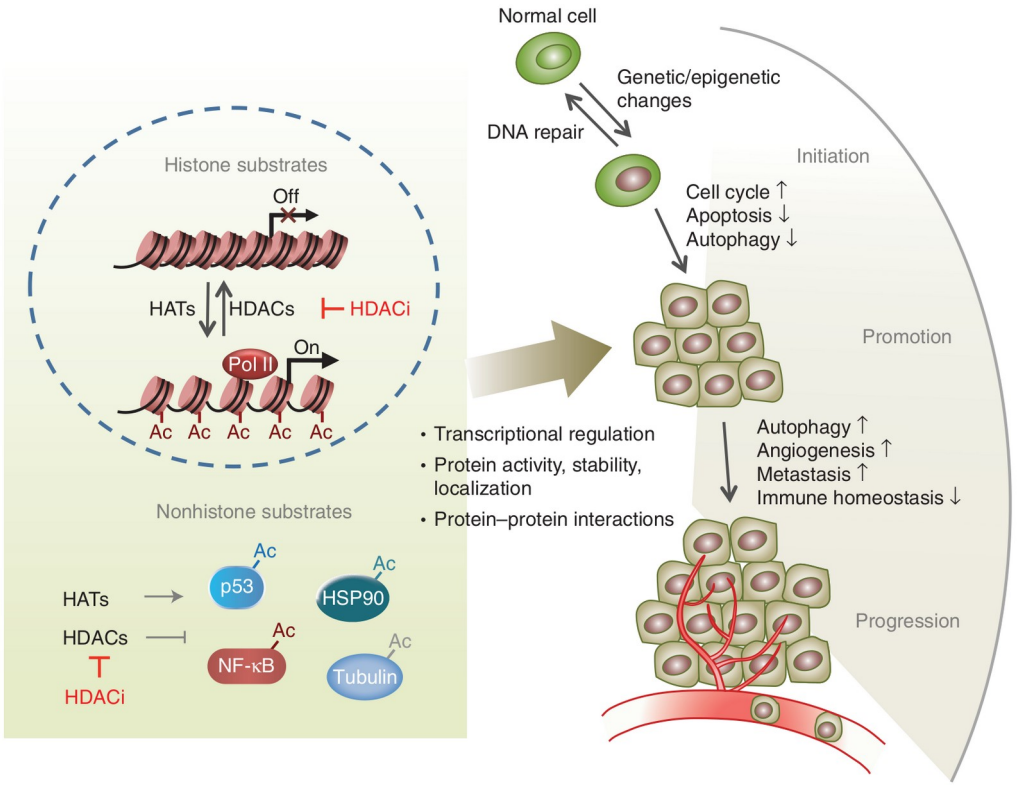

***Figure 8**: Overview of the impact of HDACs and their inhibitors on cancer progression. Histone Acetyl Transferases (HATs) mediate the acetylation of histones that favors the creation of open-chromatin domains. Histone Deacetylases (HDACs) mediate the opposite effect. Both enzyme groups also operate on other non-histone substrates. During tumorigenesis, HDAC activity is generally boosted, which, through complex mechanisms involving p53 deacetylation and CDK inhibitor suppression, it drives ultimately towards cell-cycle progression, apoptosis inhibition, and angiogenesis in later stages. Inhibitors of HDACs (HDACi) prevent the harmful action of HDACs in cancer cells by restoring the acetyl balance. (Li and Seto Cold Spring Harb Perspect Med2016;6:a026831)*

Both families also behave differently during cancer progression. Overall, classical HDACs are usually upregulated in many carcinomas, including lung, gastric, breast, colorectal, liver, and neuroblastoma (Li & Seto, 2016). On the contrary, sirtuins are usually described as cancer-protective enzymes, as their primary role is to promote cellular senescence under stressful conditions, avoiding mutation accumulation (Saunders & Verdin, 2007). Consequently, most of the currently used HDAC inhibitors employed in cancer therapy restrictively target classical HDACs by chelating zinc ions in its enzymatic center (Manal et al., 2016). For convenience, when talking about HDACs, we will refer only to classical HDACs, ignoring sirtuins from this point forward.

Superfamily	Family	Class	Subclass	Protein	Localization
Arginase / Deacetylase superfamily	Histone deacetylase family	I		HDAC1 HDAC2 HDAC3 HDAC8	Nuc Nuc Nuc Nuc/Cyt
		II	A	HDAC4 HDAC5 HDAC7 HDAC9	Nuc/Cyt Nuc/Cyt Nuc/Cyt/Mit Nuc/Cyt
			B	HDAC6 HDAC10	Cyt Cyt
		IV		HDAC11	Nuc/Cyt
Deoxyhypusine synthase like NAD / FAD binding domain superfamily	Sir2 regulator family	III	I	SIRT1 SIRT2 SIRT3	Nuc/Cyt Nuc/Cyt Nuc/Mit
			II	SIRT4	Mit
			III	SIRT5	Mit
			IV	SIRT6 SIRT7	Nuc Nuc

Table 1: HDAC Classification. Modified from Seto and Moshida (2014. Cold Spring Harbor Perspectives). Nuc: Nucleus. Cyt: Cytoplasm. Mit: Mitochondria.

In most cases, a high level of HDACs is directly associated with poor prognosis and favors cancer development at its different propagation stages. Notably, class I HDACs upregulation correlates with inferior patient survival (Delcuve et al., 2013). Although HDAC support in tumorigenesis is not restricted to a single mechanism, it is generally accepted that overexpression of HDACs could deacetylate the promoters and inhibit the expression of tumor suppressor genes. Nonetheless, as many HDACs are part of large molecular complexes, overexpression is not an urgent requirement, as an activity increase mediated through co-activators would prompt a similar outcome (Seto & Yoshida, 2014).

Lysine acetylation is a modification that is not restricted to histones. In fact, this post-translational modification is quite frequent among a multitude of proteins; And it has been raised that its importance rivals phosphorylation-mediated activity (Glozak et al., 2005; Spange et al., 2009). This broad-spectrum activity explains why an approximately equal number of genes are activated or repressed after HDAC inhibition and overall impairment of whole proteome acetylation in tumor cells (Parbin et al., 2014). According to this, HDACs could regulate tumor progression through the deacetylation of key signaling molecules, in addition to repression of promoters of tumor suppressor genes. The clinical hopes on HDAC inhibitors rely on the expectation of reestablishment of a correct HDAC homeostasis through hyperacetylation. Even though many of its mechanisms are pendant of elucidation, our

current knowledge points that inhibition of HDACs plays a vital role in impeding tumor progression.

HDAC repression has demonstrated to be an effective **proliferation inhibitor** of cancer cells, inducing cell-cycle arrest both at the G_1/S and the G_2/M transitions depending on the dose, cell lineage, and type of HDAC inhibitor (Cha et al., 2009; Wanczyk, 2011). This cell cycle progression blockage is exerted by the down-regulation of cyclins and cyclin-dependent kinases (CDK), and by up-regulation of CDK inhibitors (Chun, 2015). For instance, HDAC 1 and 2 are well known to deacetylate and repress the promoters of the CDK inhibitors p21, p27 and p57. Consequently, after HDAC1 or 2 inhibition, promoters of the three mentioned CDK inhibitors are no longer silenced, allowing its expression and finally causing cell cycle arrest.

Tumor suppressor p53 is responsible for triggering the **apoptotic reaction** and cell cycle blockade as it is a transcription factor of CDK inhibitors. HDAC inhibitors are able to regulate the activity of p53 as its lysine 320 is a substrate of acetylation. In particular, the acetylation of the mentioned residue increases the stability of p53, favoring its cancer-protective properties and avoiding its degradation through ubiquitination (Feng et al., 2005). On the contrary, HDAC1 is responsible for deacetylating p53, which favors its inactivation via MDM2 binding in tumor cells. Consequently, when malignant cells are exposed to HDAC inhibitors, p53 remains acetylated upregulating CDK inhibitors and apoptotic machinery (Ito et al., 2002; Kulikov et al., 2010). In addition to p53 mediated apoptosis, HDAC inhibitors can also activate both intrinsic and extrinsic apoptotic pathways as they upregulate death receptors and downregulate the prosurvival proteins Bcl-2 and Bcl-1 responsible for mitochondrial integrity (Rikiishi, 2011; Srivastava et al., 2010).

Angiogenesis is a crucial step for tumor spreading and growth. This process starts with the emergence of hypoxic conditions in cancer cells as tumors reach a critical mass. Hypoxia triggers the expression of Hypoxia-inducible factor-1α (HIF-1α) and the release of vascular endothelial growth factor (VEGF), both necessary for starting the angiogenic response in the tumoral microenvironment (Adams & Alitalo, 2007). In the cited context, class I and II HDACs inhibit the expression of p53, which have the downstream effect of HIF-1α and VEGF overexpression (M. S. Kim et al., 2001). Vorinostat and Trichostatin A (TSA), both broad-spectrum HDAC inhibitors, are reported to reverse the angiogenic response by inhibiting both HIF-1α and VEGF (Deroanne et al., 2002).

Currently, numerous clinical trials are studying the antitumor potential of HDACs inhibitors. Among these, the broad-spectrum inhibitors (Table 2) are those that have aroused the most significant interest to date, given that they are capable of inhibiting HDACs of various subclasses, which would help the reestablishment of acetyl residue homeostasis in cells tumorous. Some, such as Vorinostat, have even passed the trial phases and are used in treatment against Cutaneous T-Cell Lymphoma (CTCL). Vorinostat is a hydroxamic acid (Suberoylanilide Hydroxamic Acid: SAHA) capable of inhibiting the activity of class I, II,

and IV HDACs, that is, all the classic HDACs with a pharmacological potency in the micromolar range. Although by itself it is not effective in reducing solid tumors, it is capable of stopping the progression of the cell cycle, reduces the metastatic potential of tumor cells, in addition to sensitizing the tumor to other antitumor agents when these are administered as pharmacological combinations.

HDAC inhibitor	HDAC Class Specificity	Potency
Trichostatin A (TSA)	I, II, IV	nM
Vorinostat (suberoylanilide hydroxamic acid: SAHA)	I, II, IV	μM
Sodium Butyrate	I, II	mM

Table 2: List of broad-spectrum HDAC inhibitors tested in this work. Both TSA and SAHA are described as hydroxamic acids, while sodium butyrate is a short-chain fatty acid. These inhibitors target every classical HDAC, except for HDAC 11 (the unique class IV HDAC) in the case of sodium butyrate.

Another inhibitor from the hydroxamate family is trichostatin A (TSA). Like vorinostat, both mimic the lysine substrate and chelate essential Zinc ions in the enzymatic center of classical HDACs. Although both are similar inhibitors, TSA results to be more potent and exerts strong histone acetylation at nanomolar concentrations. As a downside of this high potency, TSA generally results in excessively cytotoxic for healthy cells, which significantly increases undesired side effects in patients. For this reason, TSA has been ruled out as an antitumor agent in the clinic sphere, although it is widely used in histone hyperacetylation models.

Lastly, sodium butyrate is another broad-spectrum inhibitor that belongs to the family of short-chain fatty acids. Unlike the other two inhibitors described above, sodium butyrate requires high concentrations to inhibit HDAC activity down to the millimolar scale. Except for HDAC11, sodium butyrate targets all classic HDACs.

2 HYPOTHESIS

Global histone acetylation and the consequent chromatin remodeling lead to global nuclear architecture reshaping. As nucleoskeletal components would be affected by such nuclear architectural changes, it is expected that, fundamentally, nucleoporin behavior should be perturbed due to their demonstrated association to chromatin.

3 OBJECTIVES

1. Observe any alteration in nucleoskeletal components after the epigenetic remodeling of chromatin by massive histone acetylation.
2. Study cell morphology, migration properties, and cell cycle alterations after global HDAC inhibition.
3. Explain the molecular mechanisms that govern nucleoskeletal remodeling episodes when observed, and relate them with other cellular processes such as those mentioned in objective number 2.

4 METHODOLOGY

4.1 Cell culture techniques.

SMS-KCNR, HeLa, MCF7/6, CT5.3hTERT and A375 cells were cultured in DMEM (Lonza BE12-733F) supplemented with 1%L-Glutamine (Sigma-Aldrich G7513), 1% Penicillin-Streptomycin (Sigma-Aldrich P0781) and 10%Fetal Bovine Serum (FBS) (HyClone SV30160.03). DEMEM supplemented with the mentioned elements was denominated as complete DMEM (DMEMc).

All the manipulation of cell cultures were carried out under sterile conditions in a class II biosafety vertical laminar flow hood. Cultures were maintained in incubators set at 37ºC, with an atmospheric condition of saturated humidity, ambient O_2 levels (21%) and 5% $CO_{2.}$. Standard mammalian cell culture protocols employed in this work are described below, although for full detailed protocol description bibliography reading is recommended (Phelan & May, 2017).

When raising up a cell line from a liquid nitrogen frozen stock, the cryovial containing the frozen cells was warmed up in a 37ºC water bath until it started to melt. Then, the thawing process was completed by adding and mixing 37ºC prewarmed DMEM and diluting the cell suspension to a final volume of 10 mL of DMEM. This process was done as quick as possible and then the cell suspension submitted to a 3 minutes 500 RCF centrifugation in a swinging bucket rotor. Once pelleted, cells were resuspended in 5 mL of DMEMc and transferred to a T25 culture flask.

Once the cell line was thawed, when cells covered around 70% of the flask surface, the culture was maintained by successive subculturing processes driven by trypsinization. In brief, DMEMc was removed, followed by two washes of prewarmed PBS and incubated with a solution containing 0,25% (w/v) trypsin and 0,2% (w/v) EDTA in the incubator in a proportion of 1 mL of trypsin mixture for each 25 cm^2 of vessel surface. After 2 minutes, cells acquired a rounded up appearance indicating that detachment was almost complete, and with gentle shacking, cells were finally separated from the bottom of the flask. As excessive trypsin digestion is toxic for cells, the protease was neutralized adding an equal volume of DMEMc. Next, cell suspension was collected in a polypropylene tube and centrifuged at 300 RCF 5 minutes in a swinging bucket rotor. After that, cells were resuspended in DMEMc (generally 1 mL for each flask). Cells were seeded again by diluting the initial cell concentration by a 1/3 dilution factor. Additionally to the dilution factor, when scaling up or down the culture, the surface of the new flask must be considered in the calculation. When a

specific number of cells is meant to be cultured, cells must be counted using a hemocytometer.

For long term storage, exponentially growing cells must be resuspended in freezing medium (pure FBS supplemented with 10% (v/v) DMSO) and distributed in 1 mL aliquots in cryovials. As a rule of thumb each 1 mL aliquot should represent subconfluent T25 of the specific cell line. Once labeled, cryovials were frozen in an isopropanol freezing container (Thermo Scientific 5100-0001) in a -80ºC freezer overnight. Next day cryovials were transferred to a liquid nitrogen cell bank.

4.1.1 Drug treatment.

For each experiment, SMS-KCNR were cultured at a density of 40000 cells/cm2 and after a resting period of 24 hours, the experimental treatment was started by replacing the culture media with fresh one containing the appropriate drug cocktail or DMSO alone as a negative control (DMSO is the vehicular substance for the drugs used in the present work).

All HDAC inhibitors (Trichostatin A: Sigma-Aldrich T1952, sodium butyrate: Sigma-Aldrich B5887 and suberoylanilide hydroxamic (SAHA, Vorinostat, Selleckchem S1047) were added to the culture medium at the appropriate concentration and mixed before addition to the cell culture. The HDAC inhibition was done during 24 hours using SAHA at a final concentration of 1,5 µM while not indicated otherwise.

4.2 Flow cytometry.

We employed a flow cytometric approach for study cell cycle alterations in SMS-KCNR cells under different drug treatments. Although described in the following lines, the protocols we used in the present work were based on standardized flow cytometry bibliography (Adan et al., 2017; K. H. Kim & Sederstrom, 2015; Macey, 2007).

Cells were analyzed in a Beckman Coulter Galios flow cytometer. Cell cytometry data was analyzed using the Flowing Software program (http://flowingsoftware.btk.fi/)

4.2.1 Conventional cell cycle analysis.

After HDACi treatment, control and treated cells were collected by trypsinization, resuspended in 0,2 µm filtered PBS and fixed with chilled EtOH at a final concentration of 70% (absolute ethanol added to cell suspension dropwise while gentle vortexing) during 2 h at -20ºC. Afterwards, fixed cells were pelleted (1000 RCF during 10 min in a swinging bucket rotor at 4ºC), washed with 0,2 µm filtered PBS, pelleted again (300 RCF during 5 min in a swinging bucket rotor) and finally resuspended to a final concentration of 10^6 cells/mL. Cell suspension was incubated with propidium iodide (PI) (10 µg/mL) and RNAse A (100 µg/mL) in 0,2 µm filtered PBS during 1 h at 4ºC in the dark.

4.2.2 Cell cycle status assisted by Ki-67 immunodetection.

For immunolabeling Ki-67 antigen, cells were collected by trypsinization and resuspended in 0,2 µm filtered PBS and fixed with chilled EtOH at a final concentration of 70% (absolute ethanol added to cell suspension dropwise while gentle vortexing) during 2 h at -20ºC. Subsequently, cells were submitted to centrifugation at 1000 RCF in a swinging bucket rotor during 10 min at 4ºC and resuspended in FACS Buffer (5% FBS in PBS) (1 mL of FACS buffer for each TC100 culture dish). After counting the total number of cells using a hemacytometer, 10^6 cells were separated in low retention 1,5 mL tubes for each experimental condition including their technical controls: a first tube containing cells only stained with propidium iodide (PI), and a second tube with cells incubated with a non specific IgG (IgG). Once splitted, cells were incubated for one hour under gentle agitation at room temperature, after which they were centrifuged (500 RCF, 5 min at room temperature in a swinging bucket rotor), and resuspended in 100 µL of FACS buffer containing the antibody against Ki-67 (in the IgG technical control it is substituted by a non specific IgG from the same host species as the antibody against Ki-67, and in the case of the PI control any IgG was added). Cells were incubated in mild rotation overnight at 4ºC. Afterwards, corresponding to a washing step, samples were diluted by adding FACS buffer up to 1 mL, incubated 5 minutes in rotation, centrifuged (500 RCF, 5 min at room temperature in a swinging bucket rotor), resuspended in 1 mL of FACS buffer, centrifuged (500 RCF, 5 min at room temperature in a swinging bucket rotor) and resuspended again in 100 µL of FACS buffer containing the corresponding secondary antibody coupled with a 488 fluorophore (with the exception of the PI technical control tube). After an incubation of 2 hours at room temperature in gentle rotation, cell suspensions were washed again. The following step consisted in an incubation with propidium iodide (PI) (10 µg/mL) and RNAse A (100 µg/mL) in 0,2 µm filtered PBS during 1 h at 4ºC in the dark. Once passed this final step tubes were introduced in the flow cytometer and submitted to analysis.

The immunofluorescence signal Ki-67 was proved to be above the background signal emitted by an equivalent nonspecific IgG. Noise in the 488 channel coming from PI was determined using the PI technical control tube and consequently compensated in the rest of the tubes.

4.3 Cell proliferation assay.

For testing cell viability we used the MTT tetrazolium reduction assay. MTT ((3-(4,5-Dimethylthiazol-2-yl)-2,5- diphenyltetrazolium bromide) is a positively charged tetrazole salt that penetrates rapidly into living cells, where it undergoes a reduction reaction in the mitochondria, transforming into formazan crystals. These crystals are purple colored and after redissolved with DMSO its absorbance can be measured in a plate reading spectrophotometer. The amount of 560 nm absorbance read is directly proportional to the viability of the cell culture in terms of metabolic activity.

The experimental procedure (Ehrich & Sharova, 2000) is explained below. SMS-KCNR cells were plated in a 96 flat-bottomed well culture plate (11000 cells per well in 200 µL of culture medium) and allowed to settle overnight. Next day drug treatment started by replacing old culture media with fresh one containing the HDAC inhibitor. In control cells culture medium was replaced by fresh one. It is important to include proper technical controls when designing well plate distribution such as: wells with medium without cells or test compound, medium without cells but with test compound and cells without HDAC inhibitor but with compound vehicle (DMSO). Once the incubation time was completed, 20 µL of MTT solution (MTT stock solution: 5 mg/mL dissolved in PBS and sterile filtered. This stock is stable at 4ºC protected from light from 2 to 3 weeks) were added to the 200 µL of culture medium on each well and incubated during 4 hours at 37ºC, 5%CO_2. During this incubation period the MTT is reduced to formazan crystals and once finished we proceeded to remove very carefully the MTT containing medium. To dissolve formazan crystals we added 200 µL of DMSO and mixed the plate until the formazan crystals were completely dissolved. Then the plate was placed in a plate reader spectrophotometer and measured its absorbance at 570 nm. Raw absorbance values were processed subtracting the background signal from the technical controls. Three technical replicates were analyzed on each experiment in a total of three biological tests.

4.4 Wound healing assay.

Wound healing assay stands among the simplest ways to study cell migration (Justus et al., 2014). This method is used to determine the migration ability of two cell masses. When these two masses of cells are separated between a known distance the investigators can record the time that it takes to the culture to enclose the gap. This assay acquires its name of “wound healing” because the gap, or wound, between the two cell groups is typically generated by scratching a cell monolayer with a pipette tip. Nevertheless, nowadays commercially available silicon inserts (Ibidi: 80209) make the process more reproducible as the gap remains unaltered between experiments.

To test if HDAC inhibition interferes with migration processes in SMS-KCNR cells, we cultured the cells on both sides of a sterile silicon insert and let them grow until they formed a homogeneous monolayer. Reaching this point the insert was removed with the help of sterile forceps and the old culture medium was renewed with fresh medium in the case of control cells or with culture medium containing the HDAC inhibitor in the tested group. Before putting the culture in the incubator, the gap was micrographed at different points. After 24 hours the gap was micrographed again. To analyze the data, we measured the surface of the gap at the start and at the end of the experiment and referred the results as gap area reduction % respect from its initial surface.

For immunolocalization fluorescence microscopy experiments, the wound-healing assay must be performed over glass-bottomed 35mm Petri dishes (Ibidi 81158) suited for confocal

microscopy. Once, the migration process was finished, cells were fixed in 4% paraformaldehyde and processed for conventional immunocytochemistry as explained in more detail later in this section (4.6 Immunocytochemistry.).

4.5 Gelatin zymography.

Zymography is a technique that allows the visualization of the proteolytic activity of a determined proteinase after its separation by electrophoresis from a complex mixture (Birkedal-Hansen et al., 2008; Hu & Beeton, 2010; Troeberg & Nagase, 2003). It is widely used with the purpose of studying the activity of secreted matrix metalloproteinases (MMPs) such as the gelatinases MMP-2 and MMP-9. When casting the SDS-polyacrylamide gels for zymography, the substrate of the studied proteinases (gelatin in this case) is included in the casting mix and thus, after polymerization, it is distributed uniformly throughout the gel as it is entrapped in the polymerized polyacrylamide. After non-reducing electrophoresis, the proteins can be renatured and recover enzymatic activity under appropriate conditions. After an incubation period, the gel is stained with Coomassie brilliant blue acquiring an intense blue color due to the uniform distribution of the gelatin within the gel. The gelatin degradation caused by proteolytic activity can be visualized as clear bands in the stained gel revealing the presence of an MMP.

<table>
<tr><th></th><th>Day 0</th><th>Day 1</th><th>Day 2</th><th>Day 3</th><th>Day 4</th><th>Day 5</th></tr>
<tr><td>0 h serum starvation</td><td>Seed</td><td>Allow to grow in DMEMc</td><td>Start drug treatment in DMEMc
Start drug treatment in DMEM (0,1%)</td><td>Store the conditioned medium</td><td></td><td></td></tr>
<tr><td>24 h serum starvation</td><td>Seed</td><td>Allow to grow in DMEMc</td><td>Replace DMEMc with DMEM (0,1%)</td><td>Start drug treatment in DMEMc
Start drug treatment in DMEM (0,1%)</td><td>Store the conditioned medium</td><td></td></tr>
<tr><td>48 h serum starvation</td><td>Seed</td><td>Allow to grow in DMEMc</td><td>Replace DMEMc with DMEM (0,1%)</td><td>Allow the culture rest</td><td>Start drug treatment in DMEMc
Start drug treatment in DMEM (0,1%)</td><td>Store the conditioned medium</td></tr>
</table>

Table 3: Schematic view of the workflow for obtaining conditioned media. DMEMc refers to DMEM supplemented with 10% FBS (usual FBS concentration). DMEM (0,1%) refers to DMEM supplemented with 0,1% FBS (negligible FBS content).

As explained, gelatin zymography is an adequate approach to study variations of MMPs in media conditioned by cells submitted to drug treatment. Table 3 shows in a schematic manner the workflow for obtaining the conditioned medium. It is important to note that each drug treatment was done in presence and absence of FBS in order to discard any activity of the gelatinases contained in the FBS of the culture medium. As well, we deprived cells from FBS during 0, 24 and 48 hours prior drug treatment with the intention of inducing a decelerated metabolic activity, and further discard any interference produced by the FBS.

Before storing (in a -80ºC freezer) the collected media, these must be filtered through a 0.2 µm filter in order to remove traces of cellular debris. As the phenol red contained in the culture media interfered with a precise quantification of the protein content of the media, samples inside each experiment were relativized to the final cell content. So, after media collection, cultured cells on each plate were trypsinized and counted using an hemocytometer. Once known the final number of cells, each conditioned media was diluted appropriately with 5X non-reducing loading buffer (10% (w/v) SDS; 0,25% (w/v) bromophenol blue; 50% (v/v) glycerol; 156,25 mM Tris·Cl pH6,8). Typically, 20 µL of media form control cells is taken as a reference for loading the wells of the gel. Table 4 shows the volumes of each constituent in order to make a gelatin-SDS-polyacrylamide gel. It is of extreme importance not boiling the samples as it would denature irreversibly the proteinases.

	4% Stacking Gel (mL)	**12% Resolving Gel (mL)**
MiliQ H2O	1,875	1,8
1 % Gelatin	-	0,6
30% Acrylamide	0,413	2
1,5M Tris pH8,8	-	1,5
0,5M Tris pH6,8	0,788	-
10% SDS	0,030	0,060
10% amonium persulfate	0,030	0,060
TEMED	0,006	0,003

Table 4: Recipe for casting one SDS-gelatin-polyacrylamide minigel of 1 mm thickness.

After loading the samples, electrophoresis was run in running buffer (25 mM Tris pH 8,3; 190 mM Glycine; 0,1% SDS) at 120 V until the migration front reached the bottom of the gel. The migrated gel, was washed twice during 30 minutes at room temperature with gentle agitation in washing buffer (2,5% TX100; 50 mM Tris·HCl pH7,5; 5 mM $CaCl_2$; 1 µM $ZnCl_2$). The washing steps remove the SDS and aid the renaturing process of the MMPs. After rinsing the gel with incubation buffer (1% TX100; 50 mM Tris·HCl pH7,5; 5 mM $CaCl_2$; 1 µM $ZnCl_2$) for 5-10 minutes, fresh incubation buffer was added and incubated at 37ºC during at least 12 hours with constant gentle agitation. The incubation buffer provides

the necessary conditions for the protease digestion to happen. Once this incubation time was finished the gel was stained with staining solution (0,1% (w/v) Coomassie brilliant blue R-250; 50% (v/v) methanol; 10% (v/v) glacial acetic acid; 40% dH_2O) during 30 minutes at room temperature and then destained using destaining solution (40% (v/v) methanol, 10% (v/v) glacial acetic acid, 40% dH_2O) until clear bands of MMP activity were visible against the blue background. Gels were photographed in the Syngene G box system using a deep-yellow to yellow-orange filter and discarded in an appropriate toxic drum.

4.6 Immunocytochemistry.

In the present work, we intensively analyze the location of nucleoporins and other cellular elements under different experimental conditions by means of fluorescence optical microscopy. To do this, we performed immunolocalization tests using indirect immunofluorescence. The method used is briefly described below, which is based on the conventional immunofluorescence protocol for cultured cells (immunocytochemistry) but with minor modifications (Donaldson, 2015).

A single sterile gelatin coated 12 mm glass coverslip was placed per well in a 24 well plate. Each of them 50000 cells were sown in 500 µL of culture medium. Cells settled overnight and the next day the culture media was changed by a fresh one containing the appropriate experimental treatment; except in the experimental controls where the culture medium was replaced by a fresh one. After treatment, culture medium was removed and cells washed with preheated PBS and then fixed in 4% paraformaldehyde (Diluted from a 37% stock (PanReac 141328.1211)) dissolved in PBS during 20 min at room temperature. After fixation, paraformaldehyde was removed and cells washed with PBS; then, permeabilized with 0.2% Triton-X100 (Diluted in PBS from a 10% Triton X-100 stock) during 10 min at room temperature. Once permeabilization was completed, specimens were submitted to a blocking step in 10% FBS (1 h at room temperature) and incubated with the appropriate antibodies dissolved in 5% FBS overnight at 4ºC in a wet chamber. After 3 washes with PBS of 5 min each, secondary antibodies were incubated during 2 h at room temperature in the dark. For DNA counter-staining, cells were incubated with Hoechst 33342 (BioRad#1351304) diluted in PBS at a final concentration of 1µg/mL for 10 min in the dark at room temperature. The excess of Hoechst staining was removed with two brief washes of PBS. Coverslips were mounted in Fluoromount G (Southern Biotech 0100-01) and sealed with nail polish.

The immunofluorescence signal for every tested antigens was proved to be above the background signal emitted by the corresponding nonspecific IgG.

As indicated for each image, confocal microscopy was performed using the following equipment: Zeiss Axio Observer fluorescence microscope with structured illumination (Zeiss Apotome 2) and Leica TCS SP2 AOBS (for live and FRAP analysis of Nup153-GFP expressing cells). Super-resolution imaging was performed with a Zeiss LSM880 Airyscan

(BioCruces Health Research Institute), an Olympus FV3000 OSR, a Leica TCS SP8 Hyvolution or a stimulated emission depletion microscope, Leica TCS STED CW SP8 (Achucarro Basque Center for Neuroscience). In all double labeling experiments, sequential acquisition was used in order to avoid signal crosstalk. Sampling was always set to fulfill Nyquist criterion and the best available optics (maximum numerical aperture and optical corrections) were used. Image processing and cell counting: fluorescence intensity profiles were constructed exporting raw fluorescence intensity data to a spreadsheet file. INC counting and nuclear area measurement was performed using ImageJ/FIJI software, applying the same threshold values in images taken under the same acquisition conditions.

4.7 Transmission Electron Microscopy (TEM).

Transmission electron microscopy is the technique to choose when in depth cellular details are pretended to be observed (Cortadellas et al., 2012; Graham & Orenstein, 2007). Although this microscopy approach follows the same rationale as conventional light microscopy they differ in crucial components. The illumination source is an electron beam generated by a tungsten filament submitted to a high voltage current. This beam is focused towards he sample by a system of magnetic lenses. Thus photons and glass lenses from conventional microscopy are replaced by an electron beam and magnetic lenses. Sample preparation is also different. As high energy electrons could destroy fixed samples, these must be post fixed with osmium tetroxide, and the samples are contrasted with heavy metals (such as depleted uranium from uranyl acetate, and lead from lead citrate) and included in a plastic resin in order to perform thin sectioning.

The detailed sample preparation protocol is described below. It is important to note that every step involving glutaraldehyde, osmium tetroxide, uranyl acetate and lead citrate manipulation must be done in a fume extraction hood.

After removing culture medium and washing the cell culture with previously warmed PBS, control and HDAC inhibited cells were fixed in previously warmed 2,5% glutaraldehyde in 0,1 M phosphate buffer. After 1 hour fixation at room temperature, the fixative was removed and cells were scrapped in the remaining fixative, transferred to a 1,5 mL tube and centrifuged at 2000 RCF during 10 min in a swinging bucket rotor. For better manipulation of the cell pellet an additional centrifugation step is included at 20000 RCF during 5 minutes in a fixed angle rotor. After this, the cell pellet is washed three times for 20 minutes each in an isosmolar phosphate-buffered 6% sucrose solution. In the next step samples are post fixed in a 1% osmium tetroxide buffered in 0,1M phosphate buffer during 2 hours at 4ºC protected from light. Once post fixation is completed samples are washed again three times during 20 minutes each in 0,1M phosphate buffer. At this point samples can be kept overnight at 4ºC. After post fixation, samples must be dehydrated and included in epoxy plastic resin. These processes are explained in the following table (Table 5). After overnight epoxy inclusion resin must be polymerized. To this end, samples were moved into the bottom of beem capsules,

filled with fresh epoxy resin and placed in an oven at 55ºC during 48 hours of polymerization.

Now that resin blocks with samples included have been made, ultramicrotomy is the next step to proceed. First, blocks are trimmed in order to orientate samples towards the edge of the knife. Slides of 1 µm are made and stained with toluidine blue in order to ensure the presence of the desired part of the sample. Afterwards 70 nm slides are cut over nickel grids and contrasted with 2% uranyl acetate dissolved in miliQ water during 10 minutes and with 0,2% lead citrate during another 5 minutes. Finally, micrographs were obtained using an EM208S Philips TEM microscope or a JEOL JEM 1400 Plus.

DEHYDRATION	
30% Acetone	30 min
50% Acetone	30 min
70% Acetone	30 min
90% Acetone	30 min
100% Acetone	2 x 30 min
RESIN INCLUSION	
2 vol acetone : 1 vol epoxy	60 min
1 vol acetone : 1 vol epoxy	60 min
1 vol acetone : 2 vol epoxy	60 min
100 % epoxy	Overnight (16 hours)

Table 5: Scheme that describes sample dehydration process and its inclusion in epoxy resin.

4.7.1 Immunoelectron Microscopy.

For immunolocalization of Nup153, a post-embedding approach was considered to be the most convenient (De Paul et al., 2012).

Cells were fixed in methanol free paraformaldehyde (Electron Microscopy Science 15710) at a final concentration of 4% diluted in PBS preheated at 37ºC. Fixation was done at ambient temperature for 1 hour. After fixation, in order to inactivate residual aldehyde groups, cells were incubated in 50mM NH_4Cl solution during 1 hour, then scrapped and pelleted by centrifugation at 9000 RCF during 20 min. The resulting pellet was fragmented into pieces of 1 mm^3 maximum and submitted to the dehydration process. To this end, samples were submerged in ethanol solutions of ascendent concentration during 15 min each as follows: 30%, 50%, 70%, 95%, 100% and 100%. Every ethanol incubation was done at -20ºC except the 30% one which was done at 0ºC. Once samples were completely dehydrated we proceeded to the inclusion of the samples in the acrylic resin Lowicryl K4M (Electron Microscopy Science 14330-14360). Every step involved in the handling of Lowicryl resin

was done in the fume hood. Lowicryl components were mixed according to the manufacturer's instructions following the next proportion: 2,7 g Crosslinker A, 17,3 g Monomer B and 0,1 g of Initiator C. Infiltration procedure of the resin with the samples was carried out according to table 6. The resin, ethanol and all the other components employed in the infiltration protocol were previously cooled at 4ºC in order to prevent air condensation during the infiltration process.

RESIN : ETHANOL	TIME	TEMPERATURE
Vol : Vol	minutes	-20 ºC
1 : 2	60	-20 ºC
1 : 1	60	-20 ºC
2 : 1	60	-20 ºC
100 % Resin	60	-20 ºC
100% Resin	Overnight (4-16 hours)	-40 ºC

Table 6: Scheme of Lowicryll K4M infiltration process.

All infiltration steps described in table 6 were done in 1,5 mL tubes except the last one which was carried out in 350 µL transparent gelatin capsules filled with pure resin. Samples were manipulated between infiltration steps using a pre-cooled Pasteur pipette. Once Samples were embedded in resin inside the gelatin capsules, they were placed in a capsule holder made of wire and moved to a freezer at -40ºC and incubated overnight as indicated in table 6. Next day, samples were transferred to a polymerization chamber. This chamber consisted in a freezer set at -40ºC which inside was covered in aluminum foil. An UV lamp situated on the inner side of the freezer lid provided the 360 nm wavelength light needed for polymerization. Between the UV lamp and the capsule holder a light deflector was placed in order to guarantee that samples were only irradiated with indirect UV light reflected from the aluminum foil. Ultraviolet polymerization was done during 24 hours at -40ºC and continued at room temperature from two to three days more under indirect UV light.

After resin polymerization, samples were ready for sectioning by ultramicrotomy. Sections (50 nm) were made and settled on formvar coated nickel grids (EMS G150Cu).

Further information and in depth described protocols about Lowikrill resin handling can be found at Electron Microscopy Science's website:

https://www.emsdiasum.com/microscopy/technical/datasheet/14330b.aspx

4.7.1.1 Immunostaining:

Once ultrathin sections were mounted on formvar coated nickel grids, non-specific binding of primary antibody was blocked with 10% normal goat serum in PBST (0,1% Tween 20 in PBS, pH 8,2) during 1 hour at room temperature. Incubation with monoclonal antibody

against Nup153 (Abcam ab96462, dilution 1:10) was performed (in PBST containing 1% normal goat serum) overnight at 4ºC in a humid chamber. After five washes of 5 minutes each in blocking solution, samples were incubated during 2 hours with 10 nm gold-conjugated antibody raised against the host species of the primary antibody (Sigma G7652, dilution 1:50). This incubation was followed by five washes of five minutes each in blocking solution. Next, specimens were contrasted with uranyl acetate and lead citrate as described previously.

Parallel to each experiment an additional sample section was incubated with non-specific IgG raised in the same host as the primary antibody in order to discard any background signal. These samples were considered as technical controls and were also examined in order to discard any gold aggregate of the secondary antibody.

Samples were visualized and electrographed in a 208 S Philips electron microscopy at 80 kV or a JEOL JEM 1400 Plus al 100kV.

4.8 Whole Cell Lysate Preparation.

When cells achieved a confluence about 70% culture medium (with or without drug treatment) was removed and followed by two washes with room temperature PBS. After removing the remaining PBS, cells were lysed by adding 12 µL/cm^2 of ice cold lysis buffer (40 mM HEPES pH 7,5; 150 mM NaCl; 1% NP-40; 0,5% Na-Deoxycholate; 2% SDS) and incubated at 4ºC during 10 minutes. Once the incubation was completed, the lysate (which at this point should have a mucous consistency) was collected using a cell scrapper (Corning Cell Lifter 3008) and transferred to a pre-cooled 1,5 mL tube for homogenization by ultrasonic means. Samples were submitted to ultrasonication at 4ºC applying three pulses of 20 seconds at 90% amplitude and resting 40 seconds between each pulse (Bandelin Sonoplus mini20 equipped with a MS1.5 probe). In order to avoid cross contamination, the probe was cleaned with 70% ethanol between samples. At the end of the sonication process the mucous consistency should have been completely gone and transformed into a homogeneous liquid phase. Afterwards, insoluble material was pelleted at 20000 RCF during 10 minutes in a pre-cooled centrifuge. Resultant supernatants were stored and its protein content was quantified using the BCA (Bicinchoninic acid) assay (Olson, 2016). Once determined its protein concentration, samples were diluted to a final concentration of 2 mg/mL with 4X loading buffer (250 mM Tris-HCl pH 6,8; 10% SDS; 20% β-Mercaptoethanol; 40% Glycerol) and molecular grade distilled water, then boiled at 95ºC during 10 minutes. Once boiled, samples were allowed to cool down at room temperature and then stored at -20ºC or loaded into an SDS polyacrylamide gel for electrophoresis.

4.9 SDS Polyacrylamide Gel Electrophoresis (SDS-PAGE).

One dimensional gel electrophoresis (Gallagher, 2012) allows to separate a complex protein mixture according to the size and molecular weight of its components. Moreover, is the

standard starting point prior to western blotting. Among all the electrophoretic separation techniques, we selected the denaturing (SDS) discontinuous method (also known as the Laemli method). When comparing SMS-KCNR cells under different treatments, equal amounts of protein (40 µg on each well) were loaded onto 12% SDS-polyacrylamide gels.

For casting the SDS polyacrylamide gels, we used the Mini-Protean casting stand (BioRad 1658050) and the 1 mm thick glass plates (BioRad 1653311 and 1653308). After mixing the gel components (summed in table 7) in polypropylene tubes, the resolving gel was loaded between the plates, covered with ethanol and allowed to polymerize during 40 minutes. Once the resolving gel was solidified, the top layer of ethanol was removed, washed with distilled water and substituted by stacking gel. Before the stacking gel polymerized, 1 mm combs containing the convenient number of wells were inserted and allowed to solidify during additional 40 minutes. After complete polymerization the gels were removed from the casting stands, wrapped in humidified paper cloth and stored in a closed container up to two weeks.

Electrophoresis was carried out in the BioRad's Mini Protean Tetra® ecosystem. After chamber assembly, the electrophoresis cell was filled up with SDS-Tris-Glycine electrophoresis buffer (25 mM Tris pH 8,3; 190 mM Glycine; 0,1% SDS) diluted with distilled water from a 10X concentrated stock. The electric field was set at 120 V until the migration front reached the bottom of the gel (which usually takes around 1 hour and 30 minutes). After electrophoresis, gels were stained with Coomassie blue or submitted to western blotting.

	4% Stacking Gel (mL)	12% Resolving Gel (mL)
MiliQ H2O	7,5	6,6
30% Acrylamide	1,65	8
1,5M Tris pH8,8	-	5
0,5M Tris pH6,8	3,15	-
10% SDS	0,125	0,2
10% ammonium persulfate	0,125	0,2
TEMED	0,025	0,01

Table 7: Solutions for preparing stacking and resolving gels for Tris-Glycine SDS-Polyacrylamide gel electrophoresis. The volumes indicated in this recipe are designed for casting four minigels of 1 mm thickness. The recipe is designed so that each minigel contains 4,5 mL of resolving gel.

4.10 Coomassie blue staining of SDS-Poliacrylamide gels.

Once completed the electrophoresis, gels were washed briefly with distilled water and fixed with fixing solution (50% (v/v) methanol, 10% (v/v) glacial acetic acid, 40% dH2O) for 1

hour to overnight in gentle agitation. Afterwards, proteins contained in the gel were stained with Coomassie staining solution (0,1% (w/v) Coomassie Brilliant Blue R-250; 50% (v/v) methanol; 10% (v/v) glacial acetic acid; 40% dH2O) during 20 minutes with gentle agitation. Once passed this staining period, the staining solution was poured out, and the gel was washed several times with destaining solution (40% (v/v) methanol, 10% (v/v) glacial acetic acid, 40% dH2O) until the background of the gel was fully destained. Gels were photographed in the Syngene G box system using a deep-yellow to yellow-orange filter and discarded in an appropriate toxic drum.

The process described above is the most usual method of staining proteins in polyacrylamide gels. Further insights in this field can be accessed in the bibliography section (Sasse & Gallagher, 2009).

4.11 Western Blotting.

Once proteins were separated along the polyacrylamide gel according to their molecular weight after electrophoresis, they were submitted to electroblotting towards a nitrocellulose membrane; a process also known as western blotting or immunoblotting (Ni et al., 2016). Among overall electroblotting existing approaches we elected the wet/tank transfer method using the Mini Trans-Blot® Cell system from Bio Rad.

Blotting conditions vary depending on the protein pretending to be detected afterwards. Although 12% SDS-polyacrylamide gels are not claimed to be suited for transfer proteins bigger than 150 KDa such as Nup153 and Tpr, we managed to transfer all proteins contained in the gel; as we did not detect any residual proteins in the post-transferred gels by Coomassie blue staining (Figure 9).

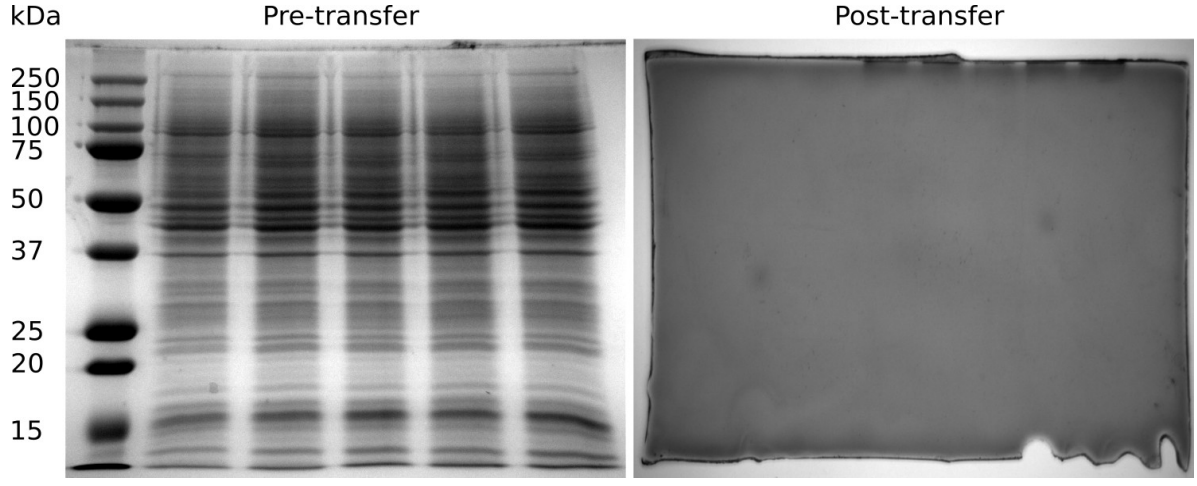

Figure 9: *Examples of Coomassie blue stained SDS-Polyacrylamide gels before and after transfer of SMS-KCNR lysates.*

Proteins were transferred to nitrocellulose membranes (Amersham Protram 10600001) in transfer buffer (25 mM Tris pH8.3; 192 mM glycine; 20% (v/v) methanol; 0,1% (w/v) SDS) during 4 h in a cold room at a constant current intensity of 400 mA and variable voltage (250V max) and power (600W max). Membrane blocking was done with 5% nonfat-dry milk dissolved in TBST (10 mM Tris-HCl pH8; 150 mM NaCl; 0.05% Tween20) or with 10% FBS dissolved in TBST for phosphorylated epitopes. Appropriate antibody incubation was done in blocking solution in a cold room with permanent agitation. Secondary antibodies were incubated in TBST during 2 h at room temperature in constant agitation, washed three times in TBST and developed using the Luminata Crescendo Western HRP Substrate (Millipore WBLUR0500). Western blotting images were acquired in a Syngene G box imaging system.

4.12 Antibodies.

4.12.1 Primary antibodies.

Antibody	Reference	Application		
		Western Blott	Immunocyto chemistry	ImmunoTEM
Tpr	Abcam ab84516	1:1000	1:500	
Nup153	Abcam ab96462	1:1000	1:1000	1:10
Nup98	Sigma N1038	1:1000	1:500	
P62	Transduction Laboratories N43620	1:100	1: 200	
Nup93	Santa Cruz sc-374400	1:500		
Acetyl Histone 3	Sigma N1038	1:2000		
PCNA	Chromotek 16D10	1:500	1:500	
Lamin A/C	Santa Cruz sc6215	1:500	1:500	
RNApol II CTDSer5P	Chromotek 3E8	1:1000	1:500	
Ki-67	Millipore MAB4190	1:500	1:1000	
Rabbit IgG isotype control	GeneTex GTX35035			
Normal mouse IgG	Santa Cruz sc-2025			

Table 8: Primary antibodies list.

4.12.2 Secondary antibodies.

Antibody	Reference	Application	Working Dilution
anti-mouse alexa555	Molecular Probes A31570	ICC	1:2000
anti-mouse alexa488		ICC, FC	1:2000
anti-rabbit alexa488	Molecular Probes A21206	ICC	1:2000
anti-rat alexa488	Molecular Probes A11006	ICC	1:2000
anti-mouse-Cy5	Jackson ImmunoResearch 715-176-151	ICC	1:500
M-IgGκ BP-HRP	Santa Cruz sc-516102	WB	1:4000
anti-rabbit-HRP	Santa Cruz sc-2357	WB	1:4000
anti-rat-HRP	Santa Cruz sc-2006	WB	1:4000

Table 9: Secondary antibodies list.

4.13 Plasmids and stable transfection.

Expression of an EGFP-Nup153 fusion protein in SMS-KCNR cells allowed live cell imaging of the nucleoskeleton-related nucleoporin Nup153, before and after HDAC inhibition. Any rearrangement in the nucleoskeleton mediated by Nup153 would be visible in vivo thanks to the fluorescence emanated from the EGFP (Enhanced Green Fluorescent Protein).

The plasmid pEGFP(C3)-Nup153 encodes a full length Nup153 fused with one copy of EGFP and was ideal for the aim of this work. pEGFP(C3)-Nup153 was a gift from Birthe Fahrenkrog (Duheron et al., 2014) (Addgene plasmid#64268).

The following sections contain descriptions of the overall workflow and procedures involved in the plasmid amplification, storage, quality tests, transfection of SMS-KCNR cells and generating stably transfected colonies.

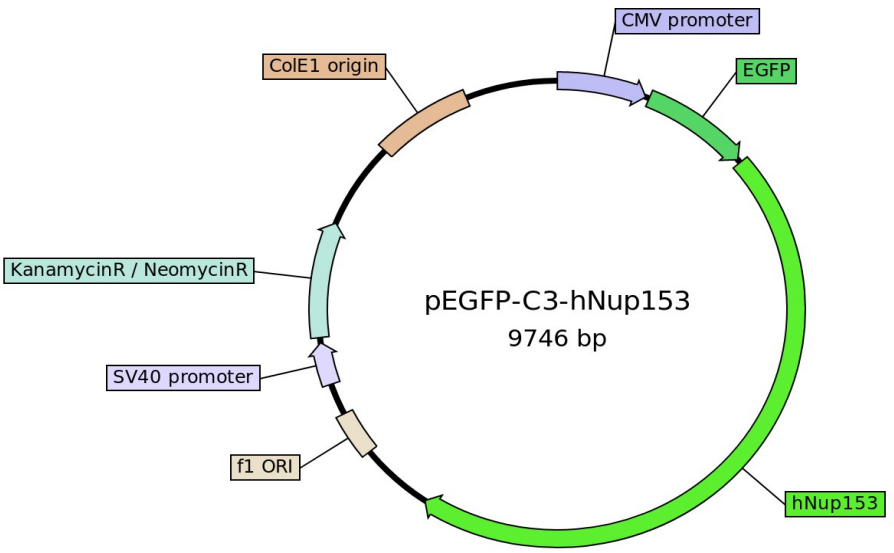

Figure 10: *Map of the plasmid pEGFP-C3-hNup153.*

4.13.1 Plasmid amplification.

The plasmid pEGFP(C3)-Nup153 arrived in the form of transformed bacteria inside of a stab culture. Plasmid must be amplified from the same bacterial colony so with that in mind, the stab culture was extended to an antibiotic selective LB agar plate with a sterile toothpick and incubated at 37ºC overnight. After incubation, single colonies were expanded to liquid cultures with two purposes in mind: isolate the plasmid (miniprep) and create a clonal bacteria stock frozen in glycerol for long term storage. The whole development of the described procedure was performed under sterile conditions. Full detailed information about plasmid handling, protocols and helpful tips are available at Addgene's website (https://www.addgene.org/recipient-instructions/myplasmid/).

4.13.1.1 Making LB agar plates.

Luria broth (LB) is a nutrient rich media used to culture bacteria in the lab. When agar is mixed with the LB medium, and once solidified, it provides to the bacteria of a solid surface where to grow on. Additionally, when an antibiotic is added to the LB medium of the plate, a substrate is being created where only the bacteria carrying the antibiotic resistance gene contained in the plasmid are allowed to grow. The following recipe allows to create about 25 LB agar plates: 5 g NaCl; 5 g tryptone; 2,5 g yeast extract; 7,5 g agar; distilled H_20 up to 500 mL. After partially mixing, the components were autoclaved and allowed to cool down at room temperature. The antibiotics were added to the sterilized mixture once it cooled down to hand-bearable temperature. As figure 10 shows, pEGFP(C3)-Nup153 contains the ampicillin resistance gene, so we added ampicillin at a final concentration of 100 µg/mL. Once mixed, liquid LB agar is poured into the Petri dishes in a sterile environment and allowed to solidify.

After solidification (usually takes up to an hour) plates where labeled, placed into sealed plastic bags and stored upside down at 4ºC. Plates should be used within 1 month after preparation.

4.13.1.2 Inoculating an overnight liquid culture.

Once single colonies are identified in the LB agar plate, the next step is to expand the colony at larger scale in a liquid LB culture. To make 400 mL of LB medium mix in 400 mL of distiled water: 4 g of NaCl; 4 g of tryptone and 2 g of yeast extract. Once mixed, autoclave the medium and store it at room temperature.

Using a sterile pipette tip or toothpick, touch the selected single colony and drop it into 2 mL of LB medium supplemented with the selection antibiotic (ampicillin at 100 µg/mL) contained in culture tubes (300807). Close the tube loosely and allow it to grow at 37ºC for 12-18 hour in a shaking incubator. After incubation the culture should be cloudy as it is indicative of bacterial growth. At this point, as explained above, the culture can be submitted to plasmid extraction (miniprep) or stored as a glycerol stock for long term storage.

4.13.1.3 Isolating plasmid DNA from bacteria (Miniprep).

The final objective of all these procedures is a successful transfection of SMS-KCNR cells with the plasmid pEGFP(C3)-Nup153. To do so, isolated pure and good quality plasmids from bacteria is a must. Convenient low scale (miniprep) plasmid isolation kits are commercially available for this purpose. In our case we used the GeneJET Plasmid Miniprep kit (Thermo Scientific K0502) and followed the instructions contained in the kit, which operation is based in the alkaline lysis of the bacteria and plasmid isolation by silica columns. From a 2 mL bacterial culture we achieved plasmid concentrations around 700 ng/µL in 50 µL of TE buffer (10 mM Tris·Cl pH 8; 1 mM EDTA pH 8). Plasmid DNA can be stored at -20ºC or at 4ºC if it is expected to be used in a short period of time.

4.13.1.4 Creating a plasmid glycerol stock.

Glycerol stocks are of vital importance as they allow to restart all the plasmid amplification process. Once a good culture of transformed bacteria is obtained, 500 µL of it are transferred to a 2 mL cryovial and mixed with an identical volume of 50% glycerol. The vial is stored at -80ºC as a long term plasmid repository.

To restore the culture, simply touch the stock with a sterile toothpick and streak the bacteria onto an LB agar plate (containing ampicillin). After the incubation period, select isolated colonies and start a liquid culture.

4.13.1.5 Diagnostic restriction digest.

After plasmid purification is convenient to check the integrity of the isolated DNA. Although sequencing is the best quality test, especially after intense cloning, most times plasmid digestion is enough when plasmids are coming from a trustworthy source as Addgene is.

The sequence of the pEGFP(C3)-Nup153 was analyzed with the program called Serial Cloner (http://serialbasics.free.fr/Serial_Cloner.html). Using its virtual cutting tool, the user can predict the length of the DNA fragments after nuclease digestion. The plasmid has target sequence for the nucleases EcoRV (Thermo Scientific ER0301), HindIII (Thermo Scientific ER0501) and NheI (Thermo Scientific ER0971) at unique sites: specifically at the base pairs 2389, 1348 and 1248 respectively (Figures 11 and 12).

Virtual cutter report:

- Restriction analysis of pEGFP-C3-Nup153human.txt.xdna [Circular]
  Incubated with NheI
  1 fragment generated.
  1: 9.224 bp - Linearized by NheI[591]

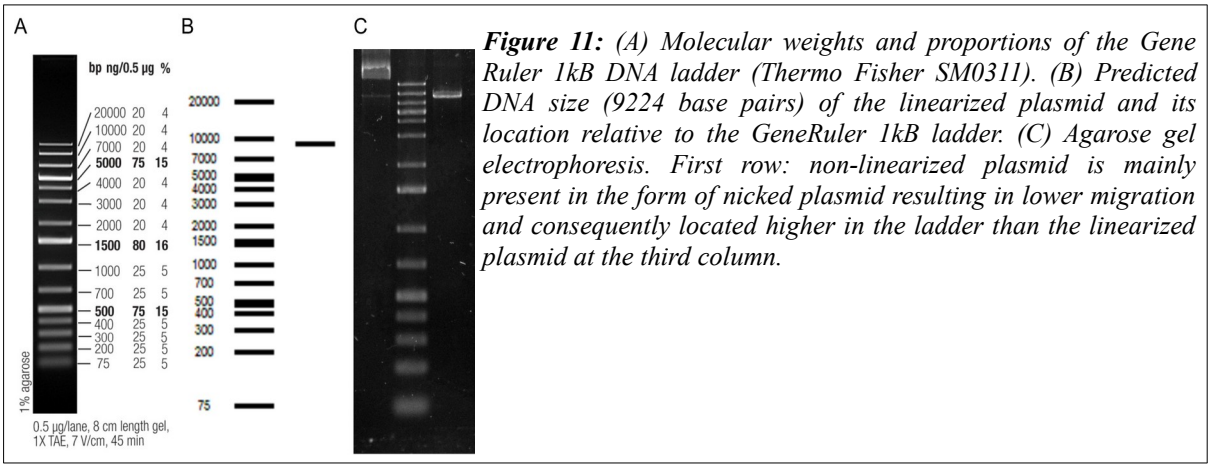

Figure 11: *(A) Molecular weights and proportions of the Gene Ruler 1kB DNA ladder (Thermo Fisher SM0311). (B) Predicted DNA size (9224 base pairs) of the linearized plasmid and its location relative to the GeneRuler 1kB ladder. (C) Agarose gel electrophoresis. First row: non-linearized plasmid is mainly present in the form of nicked plasmid resulting in lower migration and consequently located higher in the ladder than the linearized plasmid at the third column.*

- Restriction analysis of pEGFP-C3-Nup153human.txt.xdna [Circular]
  Incubated with EcoRV + HindIII
  2 fragments generated.
  1: 8.183 bp - From EcoRV[2389] To HindIII[1348]
  2: 1.041 bp - From HindIII[1348] To EcoRV[2389]

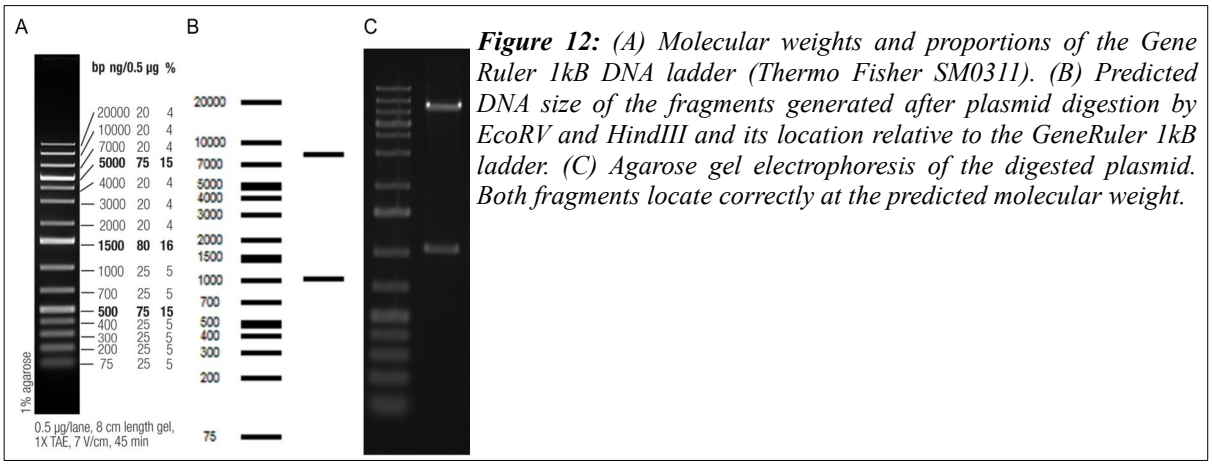

Figure 12: *(A) Molecular weights and proportions of the Gene Ruler 1kB DNA ladder (Thermo Fisher SM0311). (B) Predicted DNA size of the fragments generated after plasmid digestion by EcoRV and HindIII and its location relative to the GeneRuler 1kB ladder. (C) Agarose gel electrophoresis of the digested plasmid. Both fragments locate correctly at the predicted molecular weight.*

DNA plasmids were digested by incubation with the nucleases and digestion buffer according to the recipe described in table 10. The digestion was incubated at 37ºC for 1 hour. Although the plasmid DNA is dissolved in a buffer containing EDTA, a well-known nuclease inhibitor, this is diluted to inappreciable concentration in the final volume of the reaction and thus not affecting it. Digestion was stopped with a 20 minutes incubation at 80ºC. Once stopped, the digestion product was stored at 4ºC or mixed with the loading buffer for its analysis by agarose gel electrophoresis.

Double digestion	Linearization
500 ng of plasmid DNA	500 ng of plasmid DNA
1U of HindIII for 100 ng of plasmid DNA 1U of EcoRV for 100 ng of plasmid DNA	1U of NheI for 100 ng of plasmid DNA
2 µL of 10X Buffer R (Thermo Scientific BR5)	2 µL of 10X Buffer B (Thermo Scientific BB5)
MiliQ H_2O up to 20 µL	MiliQ H_2O up to 20 µL

Table 10: Nuclease digestion reaction for a double or single enzymatic digestion.

4.13.1.6 Agarose gel electrophoresis.

After plasmid digestion, the fragments were separated and visualized by agarose gel electrophoresis (P. Y. Lee et al., 2012). The full detailed protocol can be found in the cited literature although minor alterations were done for our convenience such as the substitution of the ethidium bromide by Gel Red (Biotium 41003) staining dye.

To make a 1% gel the agarose was measured in an Erlenmeyer flask and dissolved in TBE buffer (45 mM Tris-borate, 1 mM EDTA) using a microwave. Once fully dissolved, the liquid

agarose was poured into an appropriate mold located in a BioRad's gel caster (BioRad Mini-Gel Caster#1704422edu). Before solidification, a comb was placed inside the agarose in order to make the convenient number of wells. During the solidification process, samples and molecular weight marker (Gene Ruler 1kB DNA ladder Thermo Scientific SM0311) were diluted with 6X loading buffer (0.25% bromophenol blue, 0.25% xylene cyanol, 30% glycerol) (10 µL of digestion product and 1 µL of weight marker is usually more than enough). Once solidified, the gel was placed in the electrophoretic apparatus and after covering the gel with TBE buffer, the comb was removed and the samples loaded in the wells carefully. The electrophoresis was run at 90V until the migration front reached the bottom of the gel. In order to detect the DNA in the gel, it was placed in a polypropylene container and covered with distilled water containing GelRed nucleic acid stain diluted until working concentration. After 30 minutes of incubation in gentle agitation the DNA bands in the gel were visualized using UV-light provided by a transilluminator. Once photographed, the gel and the GelRed containing buffer were discarded in a toxic waste container.

4.13.1.7 DNA quantification.

After plasmid purification in TE buffer, we measured its DNA content by spectrophotometric means. Quantification was done using the Take3 micro-volume plate from Biotek in conjunction with the Synergy HT multi-mode microplate reader also from Biotek. Although the quantification process is briefly depicted in the following lines, the operator's manual of the mentioned equipment describes it in depth and its reading is recommended. The Take3 plate provides the capacity to read microliter volumes, thus, we used 2 µL of plasmid solution in one well and 2 µL of TE buffer in another one to read background absorbance. After inserting the Take 3 plate into the spectrophotometer, we read the absorbance at 280 nm, 260 nm and 230 nm. Nucleotides have a maximum absorbance at 260 nm meanwhile proteins and phenolic compounds have their absorbance peaks at 280 and 230 nm respectively. With the purpose of detecting any possible contamination during the plasmid purification process it is mandatory to compare the 260/280 nm absorbance ratio for protein contamination and 260/230 nm for phenolic contamination. As during the plasmid purification protocol an RNAse incubation step is included, all the 260 nm absorbance comes from plasmid DNA as all the RNA is completely digested. A plasmid preparation is considered to be pure when the 260/280 ratio ranges from 1,80-2,00 and the 260/230 ratio covers from 2,00-2,10. As said in the "Isolating plasmid DNA from bacteria" section, we obtained plasmid concentrations ranging from 500 ng/µL to 1000 ng/µL with 260/280 and 260/230 ratios inside their good purity ranges.

4.13.2 SMS-KCNR stable transfection.

Unlike transient transfection where introduced DNA (commonly plasmid DNA) is only present and expressed during a few days, stable transfection imply long term internalization

of DNA. Cells that are stably transfected can pass the introduced DNA to their progeny mainly because transfected DNA has been integrated into their genome.

In transient transfection, when the protein coded in exogenous DNA is also coded in the genome, both proteins are coexpressed, causing an excess of the protein of interest. Conversely, in long-term transfection, proteins from both origins coexist with a relative harmonious balance due to protein homeostasis regulation. This consideration is of vital importance as some proteins, when overexpressed, lead to severe phenotype modification. Several reports demonstrate that when overexpressed, EGFP-Nup153 leads to inner nuclear membrane proliferation and general nuclear architecture aberrations (Bastos et al., 1996). Therefore, we decided to use a stable transfection approach in order to avoid any incorrect localization of EGFP-Nup153. The process to make a stable transfection follows the next steps: First, plasmid DNA must be introduced in the cells by chemical (cationic lipids, viral infection) or physical (nucleofection or microinjection) ways, and after a period of rest given to allow the expression of the inserted DNA, the culture has to be submitted to a selection of positive cells, which is done by including antibiotic into the culture medium. After several weeks of antibiotic selection, only transfected cells will survive, as only they possess the antibiotic resistance gene contained in the foreign DNA. Once achieved a culture expressing the desired amounts of target protein, cell colonies are splitted and allowed to expand. In this way stably transfected clones are generated.

4.13.2.1 G418 dose-response curve.

Prior to the selection period that follows the transfection, knowing the selective antibiotic's killing dose in non resistant cells is a must. To find this out, it is necessary making a dose-response curve within a range of antibiotic concentration combined with different cell numbers.

The plasmid pEGFP(C3)-Nup153 contains the neomycin resistance gene that gives resistance to the antibiotic G418 (04727878001 Roche). In a 24 well plate, increasing cell numbers were seeded in rows: 20000, 30000, 40000, 50000 cells were the tested numbers. In columns, growing G418 concentration was included in the culture medium: 0, 50, 200, 500, 800 and 1200 µg/mL. After two weeks of selection, where G418 containing medium was replaced every 48 hours, cells were submitted to crystal-violet staining. To do so, cells were fixed in cold 100% methanol at -20ºC for 10 minutes after removing culture media and washing it with cold PBS. Following the fixation, cells were rewashed with cold PBS and stained with crystal violet staining solution for 20 minutes at room temperature. Passed this period, cells were washed gently with distilled water and allowed to desiccate.

As demonstrated in figure 13, 800 µg/mL caused complete death of the culture independently of cell number. Consequently, 800 µg/mL was an adequate concentration for selection of transfected cells.

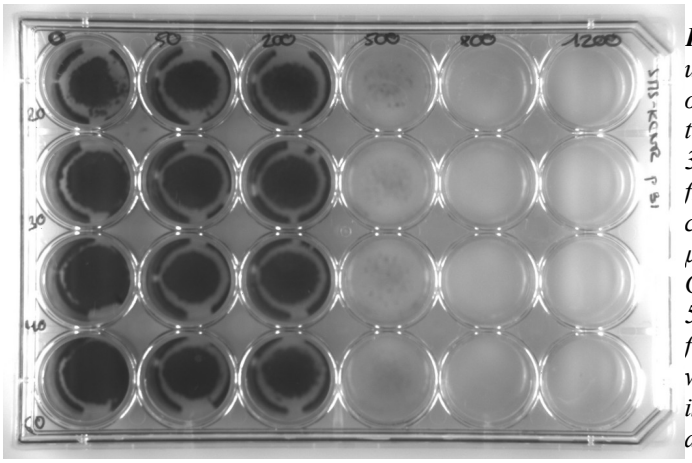

Figure 13: *Crystal-violet stained untransfected SMS-KCNR cells after 2 weeks of G418 selective treatment. In rows, from top to bottom: increasing cell numbers (20000, 30000, 40000 and 50000 cells). In columns, from left to right: increasing G481 concentration (0, 50, 200, 500, 800 and 1200 µg/mL). As can be observed, up to 200 µg/mL G418 had barely no effect on cell survival. At 500 µg/mL almost every cells were dead, and finally at 800 µg/mL any surviving colonies were appreciated. G418 effect on cell survival is independent from cell density as no differences between rows are observed.*

4.13.2.2 Transfection and selection of colonies.

SMS-KCNR cells were transfected using Lipofectamine 3000 (L3000-008 Invitrogen) following manufacturer's instructions. SMS-KCNR cells were seeded in a 6 well plate. Once they covered approximately 70% of the surface, the complete culture medium was substituted with 1,5 mL of serum free DMEM on each well. After preparing the transfection mixes illustrated in table 11, these were added dropwise to four out of the six seeded wells, as two of them must remain untreated in order to be compared with the transfected cultures and identify any possible effect of cytotoxicity exerted by the transfection reagent.

	Linearized DNA		Circular DNA	
Opti-MEM™	241,25 µL	237,5 µL	241,25 µL	237,5 µL
DNA	2,5 µg	2,5 µg	2,5 µg	2,5 µg
Lipofectamine 3000	3,75 µL	7,5 µL	3,75 µL	7,5 µL
P3000	5 µL	5 µL	5 µL	5 µL

Table 11: Four different transfection reactions. Circular and linear plasmids are delivered to the cultures mixed by 3,75 or 7,5 µL of Lipofectamine3000. The transfection components and DNA must be dissolved in serum free culture medium such as Opti-MEM™.

As indicated by the manufacturer, four transfection conditions were tested: 3,5 µL and 7,5 µL of Lipofectamine 3000 mixed with 2,5 µg of linearized and circular plasmid DNA. The linearized plasmid was obtained by its digestion with the NehI nuclease as indicated in the "diagnostic restriction digestion" section. After 48 hours of incubation cells were observed under fluorescence microscopy and only circular plasmid DNA achieved successful

transfection (Figure 14). Afterwards, cells were submitted to antibiotic selection by replacing the transfection medium by a complete culture medium supplemented with 800 µg/mL of G-418. After two weeks of antibiotic selection, colonies expressing medium to low amounts of plasmid (Figure 15) were isolated using cloning rings (Mathupala & Sloan, 2009). The colonies contained in the cloning rings were progressively expanded. At this point a nice looking polyclonal culture must be frozen in the cell bank as a stock reservoir.

To make a monoclonal culture (Yokoyama et al., 2013) (https://www.addgene.org/protocols/limiting-dilution/), the polyclonal population was seeded at a final concentration of 0,5 cells/well in a 96 well plate. In this way, the chances of seeding a single cell in one of the wells are increased. As localizing single cells in a 96 well plate is complicated, it is very helpful to seed 1000 cells in a corner well to facilitate the localization of the correct focal plane in the rest of the wells. After several days, the first colonies will be formed (Figure 16). At this point the colonies can be expanded and be prepared for experimentation. It is important to note that not all cell lines can form single colonies. In these cases it is helpful the usage of conditioned media from the same cell line previously stored.

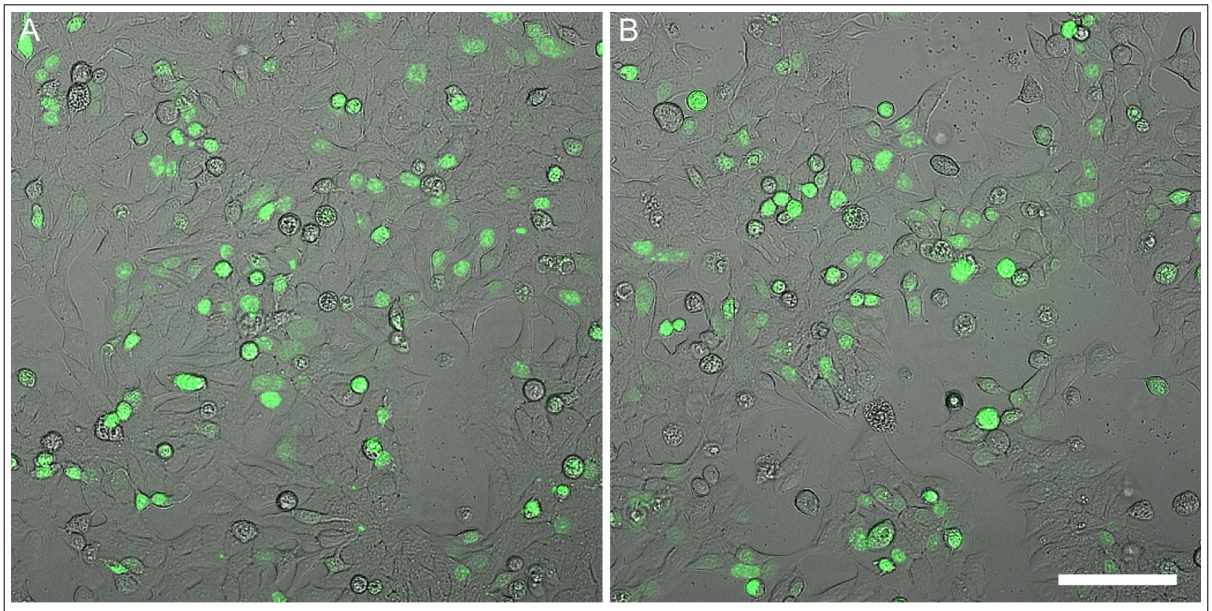

Figure 14: *SMS-KCNR cells 48h post-transfection. (A) 3,5 µL of Lipofectamine 3000. (B) 7,5 µL of Lipofectamine 3000. Scale bar: 100 µm*

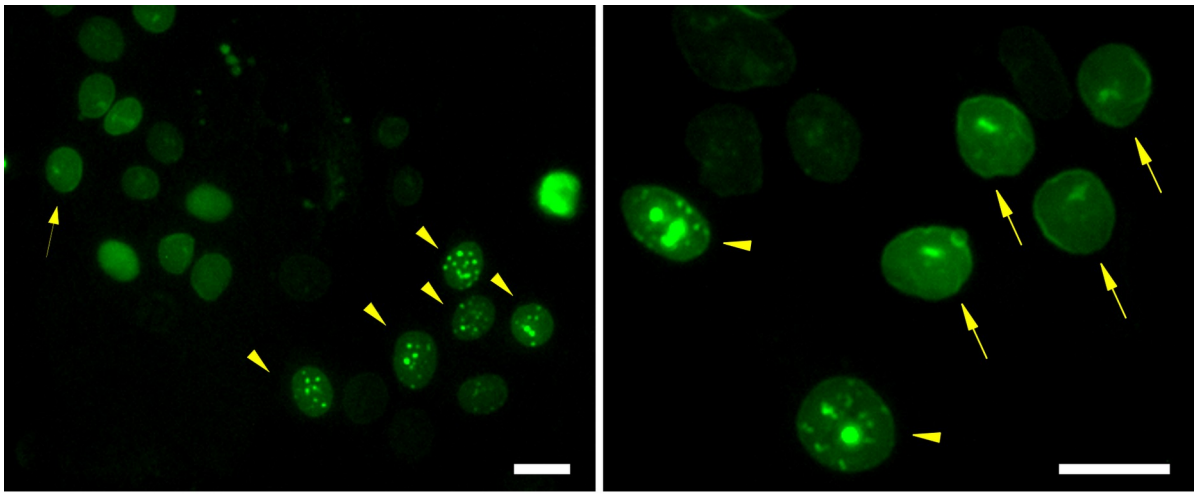

Figure 15: *During the selection process several cells expressed excessive amounts of Nup153-EGFP that resulted in the appearance of inclusion bodies (arrowheads). The selection process continued until the majority of the culture displayed low to medium expression levels of the construct (arrows). Scale bars: 20 µm.*

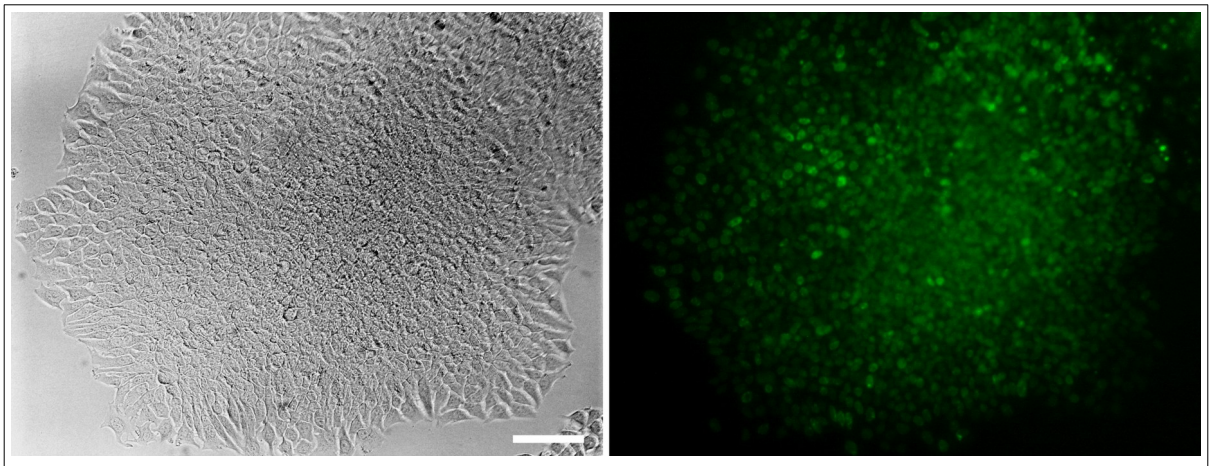

Figure 16: *Example of a colony expressing desired amounts of Nup153-EGFP. Phase contrast vision of the colony is illustrated in the left and the green fluorescence signal emanated from the EGFP-Nup153 is shown in the right. Scale bar: 100 µm*

4.14 Live time lapse imaging.

Cells were seeded on 35 mm glass bottom dishes (Ibidi 81158). Control and HDACi treated cells were recorded in a Nikon Biostation IMq time lapse imaging system.

4.15 Fluorescence Recovery After Photobleaching (FRAP).

Live SMS-KCNR-Nup153EGFP cells were seeded on 35 mm imaging glass bottom dishes (Ibidi 81158) and were observed in a Leica TCS SP2 AOBS confocal microscope using a 63x NA1.4 Plan Apochromatic lens. FRAP experiments were done using the Leica imaging

software assistant. FRAP data was analyzed using the Leica imaging software assistant and a LibreOffice Calc spreadsheet.

4.16 Fluorescence Ubiquitination Cell Cycle Indicator (FUCCI) and nuclear size analysis.

50000 SMS-KCNR cells were seeded on 12 mm glass coverslips coated with gelatin during 1 hour in a P24 plate. When cells settled over the coverslips, 40 particles per cell of FUCCI (Molecular probes P36238) were added in a final volume of 500 µL of complete culture medium and incubated overnight. HDAC inhibitors were added and after 24 hours cells were processed for immunochemistry. Nuclear size calculations were made measuring the DAPI signal using ImageJ/FIJI software, applying the same threshold values in images taken under the same acquisition conditions.

5 RESULTS

5.1 Intranuclear Nucleoporin Clusters (INCs) arise after HDAC inhibition.

HDAC inhibition leads to massive chromatin remodeling due to the hyperacetylation of histones. As mentioned during the introduction, NPCs are in a close relationship with the chromatin. In order to detect any alteration in the behavior of the NPC after chromatin hyperacetylation, we performed immunolocalization experiments of NPCs by means of optic fluorescence microscopy. We selected Nup153 as an NPC marker, and it unexpectedly revealed that after HDAC inhibition, Nup153 was accumulated inside the nucleus. This effect was not exclusive to a specific cell line. Instead, we were able to identify these accumulations inside the nuclei of several cell lines from different developmental origins. As demonstrated in 17, all control cells show the distinctive nuclear envelope signal of Nup153 and other nucleoporins, but no significant signal inside the nuclei could be observed. In contrast, when cells were exposed to trichostatin A, a potent HDAC inhibitor, several nuclei showed intranuclear accumulations of Nup153 with a rice grain-like shape. We coined the term Intranuclear Nup Clusters (INCs) to refer to these accumulations.

While all the cell lines tested presented intranuclear accumulations of Nup153 after the inhibition of histone acetylation, we could appreciate that these did not appear at the same frequency. For example, while in the case of HeLa and MCF7/6 cells, it was easy to find these accumulations, they were less frequent in A375 melanoma cells and very scarce in the case of the CT5.3-hTERT cell line. Therefore, it seemed to us that the frequency of these intranuclear accumulations was at least dependent on the cell lineage. Consequently, we decided to test another cell line, which needed to be undifferentiated, very proliferative, and resistant to pharmacological treatment. The neuroblastoma SMS-KCNR cell line full-filed these requirements.

Neuroblastoma is a developmental tumor that can be spontaneously reprogrammed and continue with its development and reverse its cancerous behavior. In addition, the cell line SMS-KCNR has an exciting feature from the point of view of nuclear architecture, which consists of an invagination of the nuclear envelope that frequently crosses the nucleus from one side to the other. This invagination is composed of double-membrane (Figure 18), possesses nuclear pore complexes, and is almost always associated with nucleoli (Figure 19). We found these two properties very convenient as a model to study nucleoskeleton reorganization after HDAC inhibition.

The SMS-KCNR cell line displayed a very reactive behavior to HDAC inhibition (Figure 20). As NPC markers, we decided to focus on the nuclear basket components Tpr and Nup153 in addition to Nup98, an FG nucleoporin that is related to the two mentioned ones. As expected, all of them showed the typical nuclear envelope associated staining in control cells. To induce HDAC inhibition, we tested three different drugs: Trichostatin A (TSA), Sodium butyrate, and Vorinostat (SAHA). Independently of the drug used, the three tested Nups manifested intranuclear accumulations (INCs) (Figure 20A). Conventional confocal microscopy showed that the nuclei containing INCs displayed a lower nucleoporin signal at the nuclear envelope than those that did not. To further support our findings, we observed the same preparations under super-resolution microscopy (Figure 20B) without any significant difference. In parallel to traditional immunocytochemistry, in order to discard that INCs were an artifact of the immunofluorescence preparations, we generated a stable cell line expressing low amounts of recombinant Nup153-EGFP. Again, after HDAC inhibition, live-cell imaging experiments demonstrated that INCs are capable of arising *in vivo* (Figure 20C).

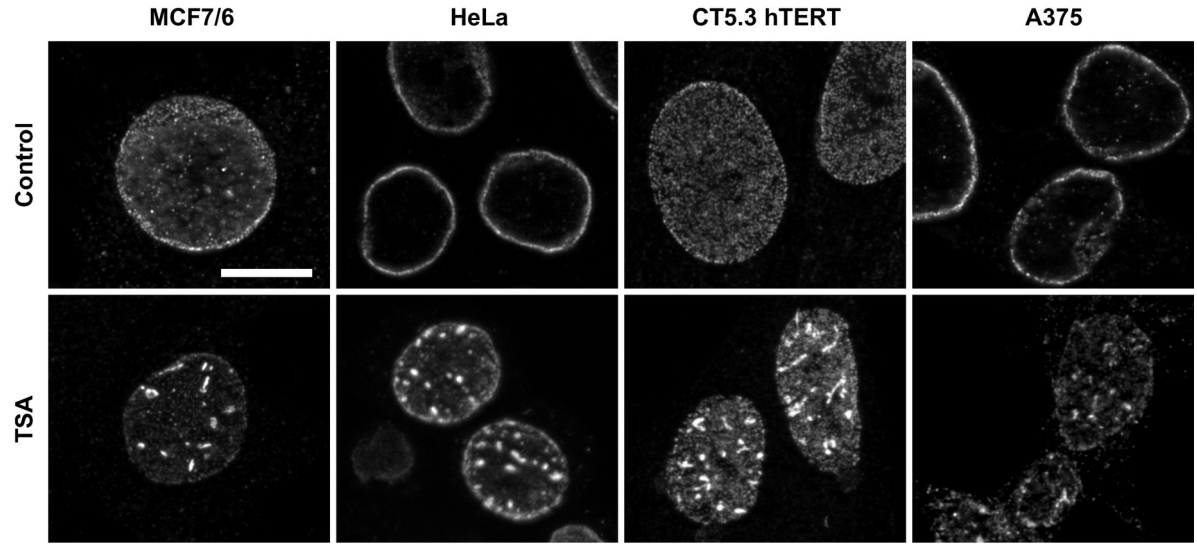

Figure 17: *Immunolocalization of Nup153 in several human cell lines in control cells and after treatment with 100 nM TSA during 24 h. From left to right: MCF7/6 human breast carcinoma, HeLa human cervix carcinoma, CT5.3 hTERT colon carcinoma-associated myofibroblasts, and A375 human melanoma. The Nup153 signal in the control CT5.3 hTERT cell has a punctuate pattern pointing out single NPCs as that micrography was acquired from the bottom of the cell in contact with the coverslip resulting in a completely flat slide. Scale bar: 10 µm.*

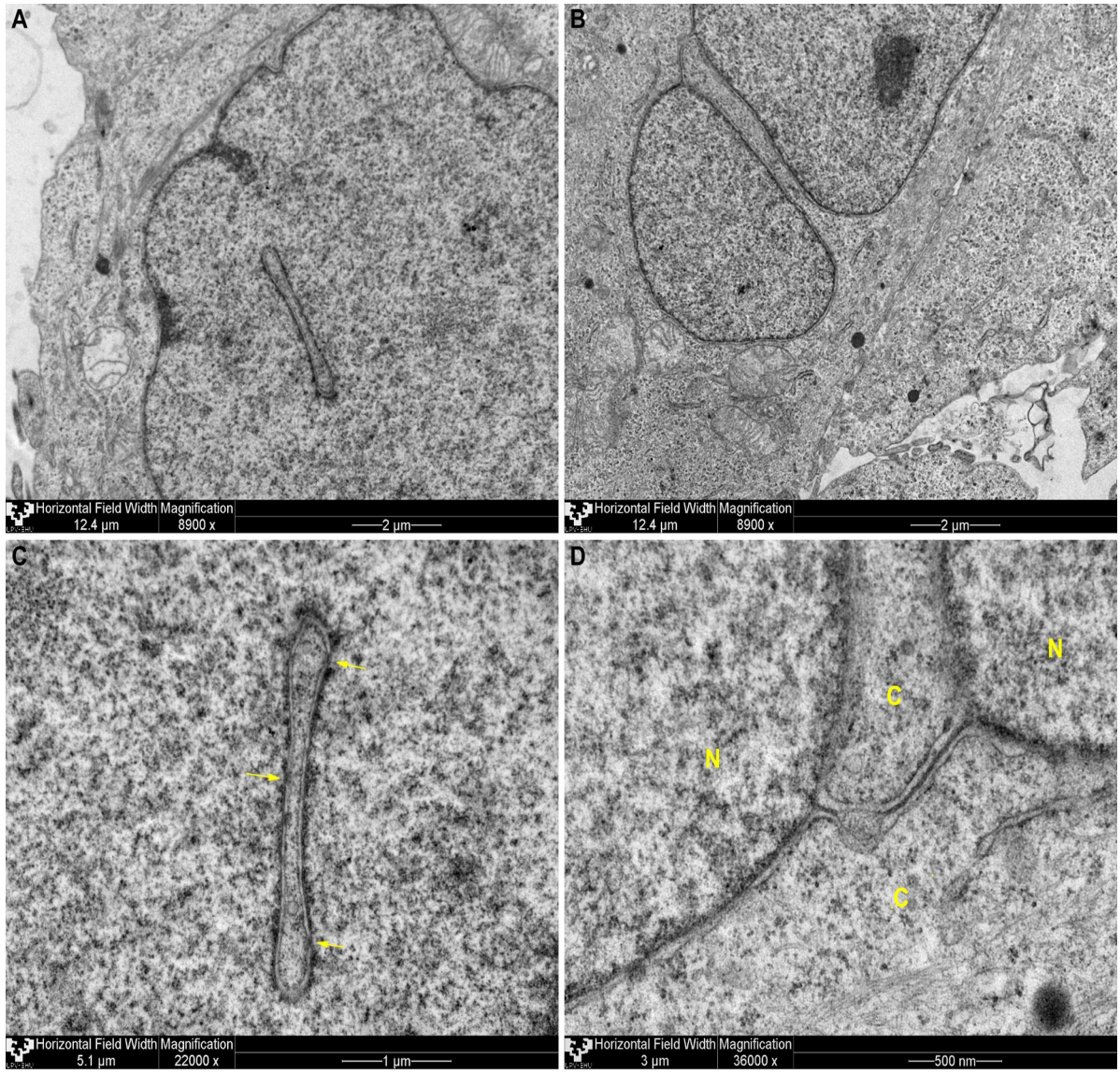

Figure 18: *SMS-KCNR nuclei visualized by Transmission Electron Microscopy (TEM). Panels A and C show a nuclear invagination cut transversely; while panels B and D exhibit longitudinal sections. The invagination is composed of double-membrane and contains NPCs within (Arrows in C). This structure goes through the whole nucleus from one side to the other until one of the nuclear membranes touches the one in the opposite side (B and D). N: nucleus. C: cytoplasm.*

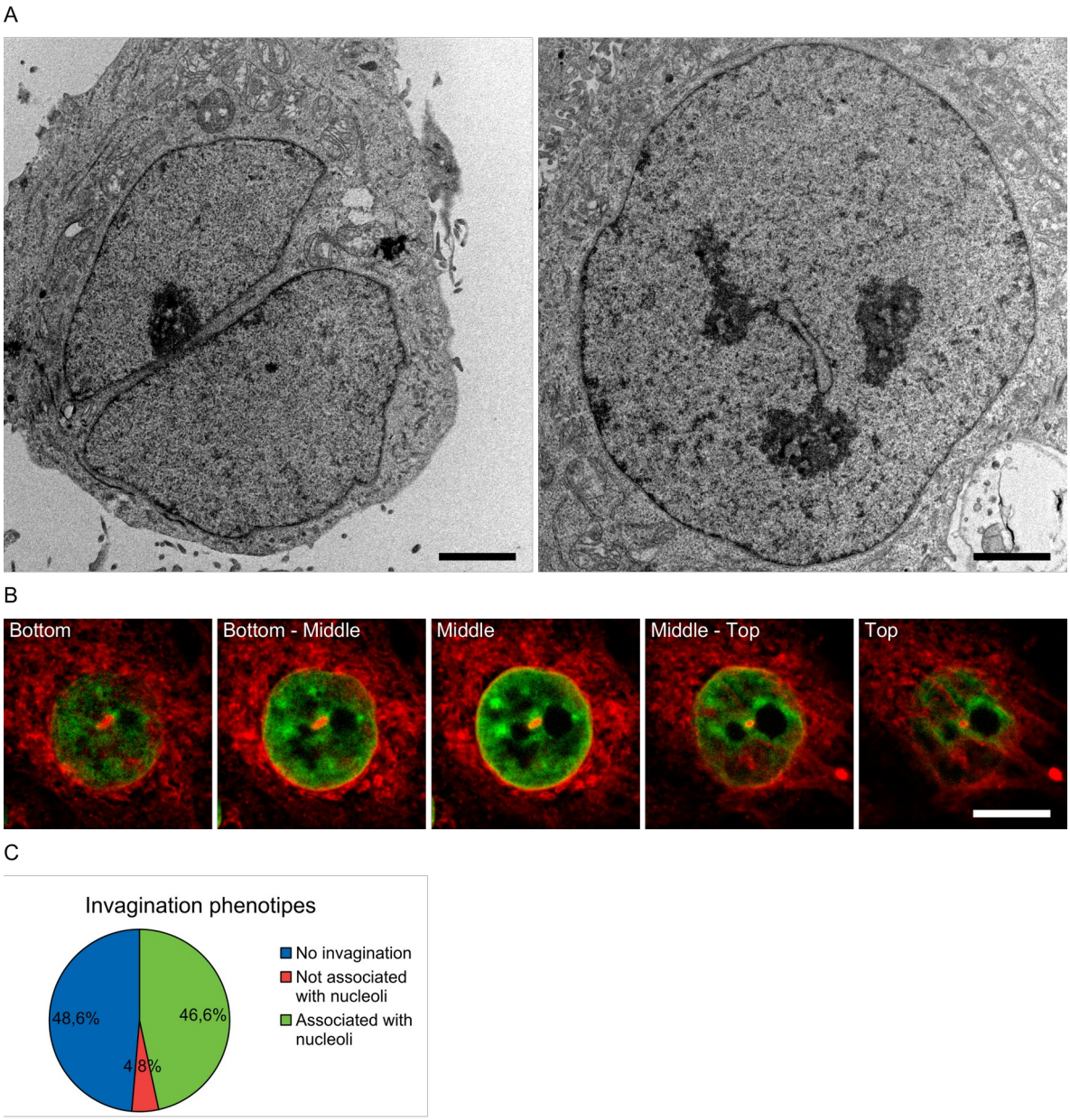

Figure 19: *Nuclear envelope invagination is in close contact with nucleoli in SMS-KCNR cells. (A) Transmission electron micrographs are illustrating the interaction between the nuclear invagination and the nucleolus longitudinally in the left image, and transversely in the right one. (B) Confocal sections of concanavalin-A-TRITC (red) and Hoechst (green) stained cells. The nuclear invagination, revealed by the concanavalin staining, goes all through the nucleus from the bottom to the top interacting with nucleoli, identified by the two big holes of absent Hoechst signal inside the nucleus. Scale bar: 10 um. (C) Proportions of the three different identified nuclear phenotypes according to the nuclear envelope shape: no invagination detected (48.6%), the nuclear invagination did not associate with any nucleoli (4.8%) and the nuclear invagination connected with at least one nucleolus (46.6%). N = 146*

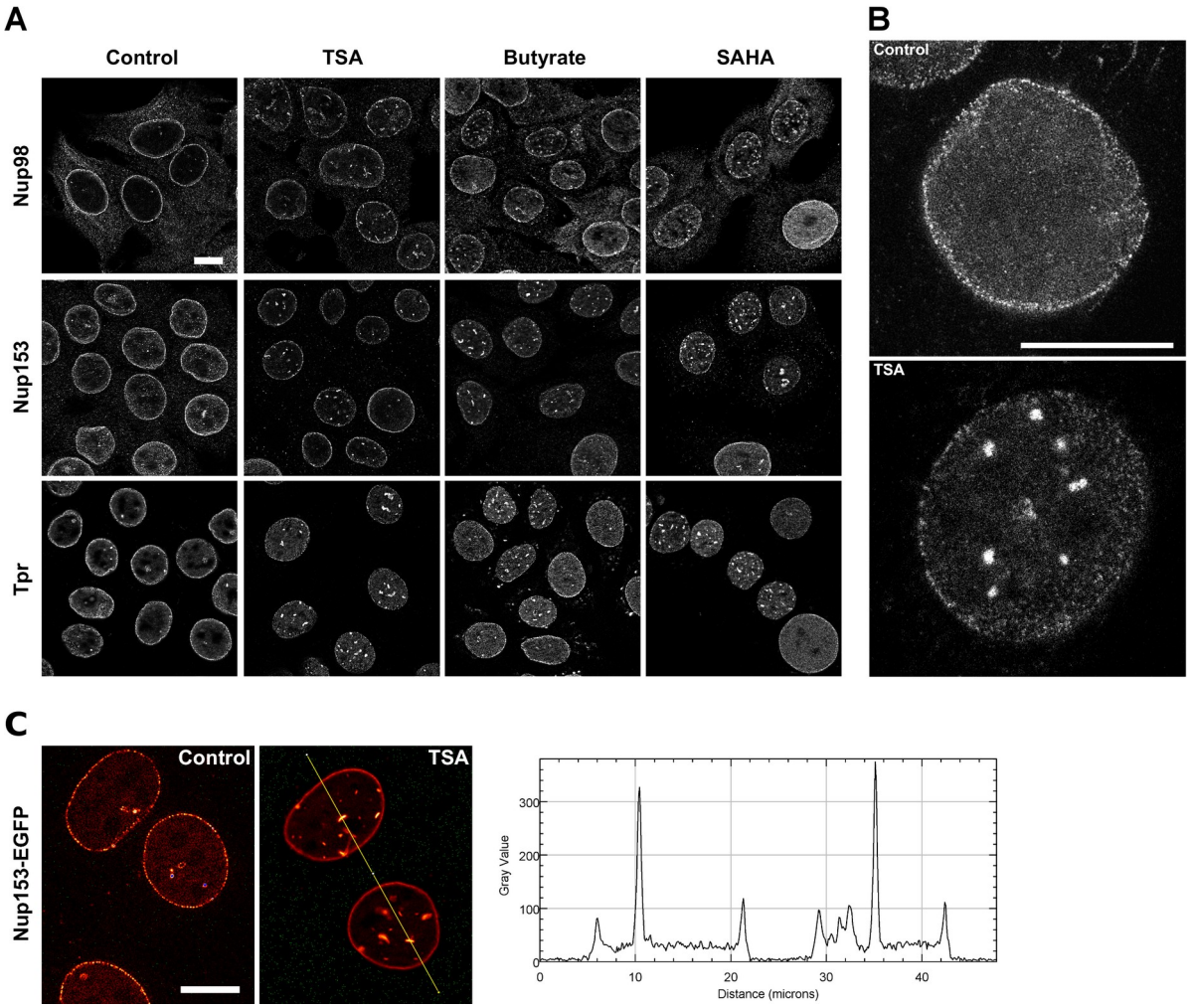

Figure 20: *Immunostaining of nuclear pore complex (NPC) basket-related nucleoporins (Nup98, Nup153, and Tpr) after HDACi treatment; visualized by confocal microscopy. (A) Control cultures and cells treated with three different HDACi are shown: TSA100 nM, sodium butyrate 3 mM, and SAHA 2 µM. In control cells, the three studied proteins situated at the nuclear envelope but after treatment, the location pattern in numerous cells changes towards the nuclear interior, appearing as intense clusters inside the nucleus, while reducing their nuclear envelope intensity. Scale bar: 10 µm. (B) STED super-resolution image detail of Tpr immunostaining. In control cells, Tpr was located in each NPC at the nuclear envelope. After TSA treatment, several Intranuclear Nucleoporin Clusters (INCs) arose accompanied by a lower-intensity nuclear envelope signal. Scale bar: 10 µm. (C) Confocal section from a live imaging experiment of Nup153-EGFP stably transfected cells before (Control) and after TSA100 nM treatment. The intensity plot profile of a TSA treated nucleus shows that the Nup153-EGFP signal is very intense at the INCs. Scale bar: 10 µm.*

5.2 Molecular characterization of INCs.

5.2.1 INCs are composed of nuclear basket related nucleoporins, and these are independent of the Nuclear Envelope (NE).

In Figure 20, we can see that Tpr, Nup153, and in a less precise manner, Nup98 have the capacity to form INCs. However, this does not imply that these remain together in the same INCs; therefore, we can not rule out the possibility that different nucleoporins accumulate in aggregates of varying compositions. Consequently, to clarify this possibility, double immunolocalization experiments were done (Figure 21). The three mentioned nucleoporins were stained by pairs in 100 nM TSA exposed SMS-KCNR cells, and all of them colocalized at the same INCs (Figure 21A). This result supports the idea that INC formation is not exclusive to a single nucleoporin and that they tend to associate in the same structure. Although Nup localization is firmly settled in the NPCs, we could not distinguish any kind of organized composition of Nups inside the INCs (Figure 21B). INC morphology and the nucleoporin distribution pattern within does not seem to be subordinated to an evident organization scheme such as it occurs at the NPC, where discrete differences in nucleoporin localization were perceptible (Figure 22) between the nuclear pore basket (Tpr) and the inner ring (P62). As expected, these observations were in harmony with the currently accepted structure of the NPC, as Tpr was located deeper inside the nucleus than P62, a protein that belongs to the inner core of the NPC (Figure 6).

In the same way, it is noticeable that P62 did not locate in the INCs of Tpr (Figure 22). Further experiments of P62 localization were done in order to corroborate this observation. The new P62-Tpr double-staining trials demonstrated that these two nucleoporins only colocalize at the nuclear envelope (Figures 23 and 24). Nevertheless, in numerous cases, P62 congregated intensely inside the nucleus, far away from the nuclear envelope. Orthogonal views of Z-stack images obtained by confocal microscopy clarify that P62 accumulations traverse vertically through the nucleus both in control and HDAC inhibited cells (Figure 24A). Distinctively, INCs of Tpr are located at specific planes, independently of P62, and do not span in depth all the nucleus (Figure 24B). These experiments support that HDAC inhibitors do not perturb the localization of P62, which is relegated mainly at the nuclear envelope, except in isolated solid points of the nucleus independently of the INCs composed of nuclear basket-related nucleoporins (Tpr, Nup153, and Nup98).

The absence of P62 in the INCs is indicative that the different subcategories of nucleoporins have a very different relationship with the nuclear envelope. It is possible that the redistribution of the nuclear basket nucleoporins towards the nuclear interior could be driven whether by a diffusion event, or by a nuclear envelope reconfiguration where the different nucleoporin categories would be organized independently. To answer this question, we

continued with the double-labeling confocal imaging experiments, but for this occasion, in addition to the antibodies against the nucleoporins, we needed a nuclear envelope marker coupled to a fluorochrome. The concanavalin A is a lectin isolated from *Canavalia ensiformis* that binds to α-D-mannosyl and α-D-glucosyl groups present at membranous structures such as the nuclear envelope. Figure 25 shows representative fields of concanavalin A fused to the fluorochrome TRITC accompanied by the immunolocalization of the nucleoporin Tpr. As expected, the concanavalin signal was excluded from the nuclear interior both in control and HDAC inhibited cells; the Tpr signal, as usual, came exclusively from the nuclear envelope in control cells, but also from the INCs in TSA treated ones. Importantly, concanavalin was able to detect the nuclear invagination, where it shared its location with Tpr. Nevertheless, the concanavalin signal was absent from the INCs of Tpr inside the nucleus.

Although concanavalin has a high affinity to the nuclear membrane (Fricker et al., 1997) and is resolved enough to discern membranous structures, transmission electron microscopy is a mandatory technique when studying cellular morphology. After examining control and HDAC inhibited cell micrographs (Figure 26), no significant nuclear envelope disarrangement was detected, in consonance with the previous fluorescence microscopy results. Taking advantage of the excellent resolution provided by transmission electron microscopy, we repeated the immunolocalization assays of INC components using the post-embedding approach (materials and methods: Immunoelectron Microscopy.). As figure 27 evinces, we could detect Nup153 both in control and SAHA treated cells. Nup153 was located at the nuclear envelope and inside the nucleus in an isolated manner (Arrowheads Figure 27) before HDAC inhibition, as expected. When SAHA was added to cells, we identified INCs by clear groups of Nup153 near the nuclear envelope or deep inside the nucleus (circles Figure 27). Some INCs appear just below NPCs at higher magnification, seemingly constituting what looks like a hypertrophied nuclear basket (Figure 27 right panel). If we look carefully at HDAC inhibited cells, electrodense zones of chromatin are associated with Nup153 present at INCs. Again, we did not observe any nuclear membrane malformations near INCs, corroborating that HDAC inhibition not only does not reorganize the nuclear envelope but also that INCs are not associated with it.

At this point, our results support that the nuclear envelope architecture is not disorganized after HDAC inhibition. Nonetheless, nuclear lamin is another essential component of the nuclear envelope that influences nuclear structure and function. Consequently, in order to finally assert if the nuclear envelope is affected by HDAC inhibition, another immunolocalization experiment was done using confocal fluorescence microscopy. Figure 28 sums representative images of double immunofluorescence assays of Nup153 and lamin A/C before and after SAHA treatment. Nup153 was placed at the nuclear periphery in control cells colocalizing with lamin A/C, a major component of the nuclear lamin, while after HDAC inhibition, it redistributes in the form of INCs. Lamin A/C instead was absent at the intranuclear accumulations of Nup153. Nevertheless, the intensity profiles of the fluorescence

signal (Figure 28B) indicate that lamin A/C is no longer concentrated only at the nuclear periphery but, on the contrary, spreads uniformly in the nuclear interior but not concentrating at any specific location, such as Nup153 does.

In conjunction with the previous ones, this final experiment prompts us to affirm that INCs are structured independently from the nuclear envelope and that the nucleoporins within are independent of the basic frame of the nuclear pore complex.

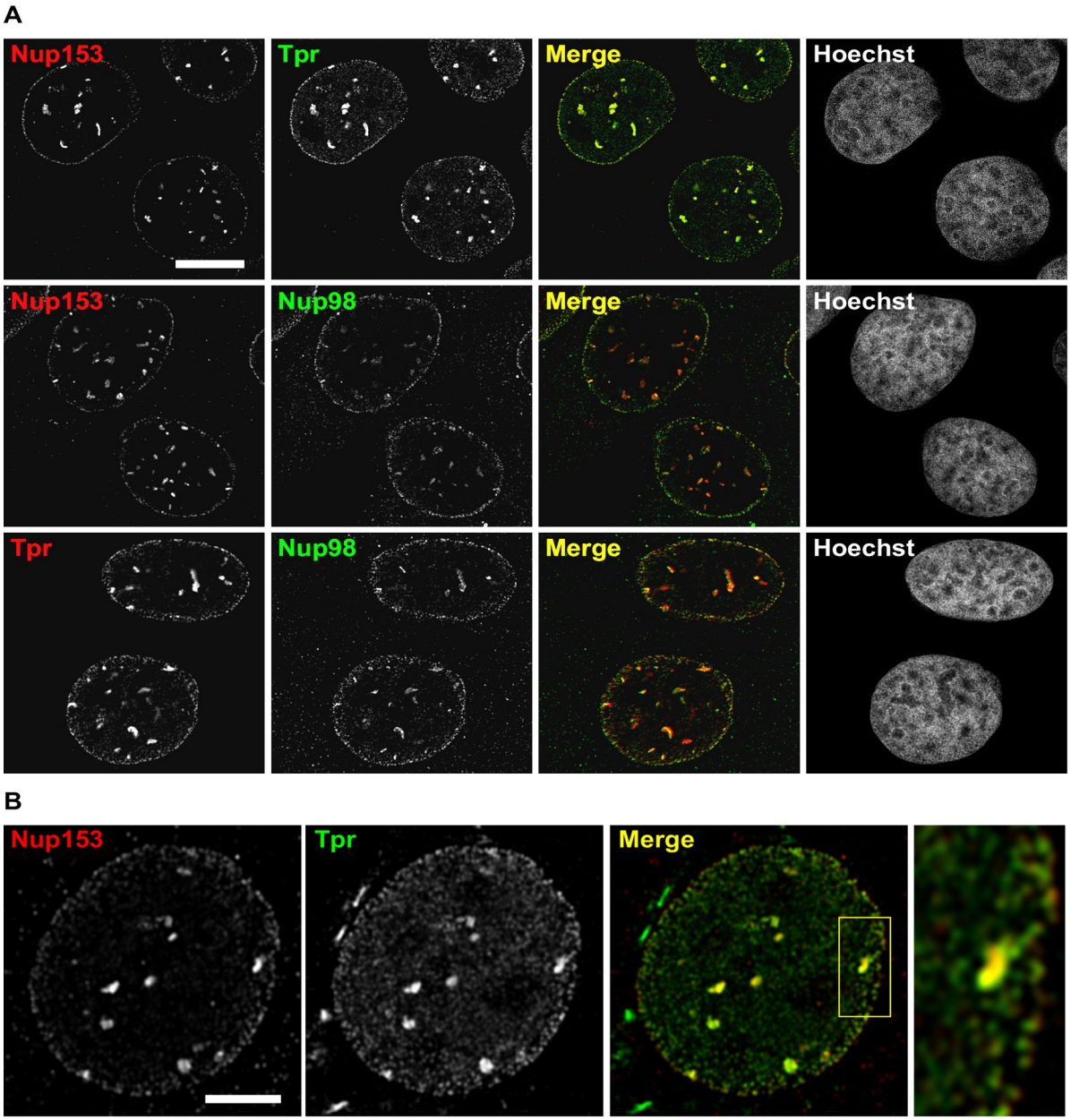

***Figure 21**: Colocalization experiments of Nup98, Nup153, and Tpr at the INCs of 100 nM TSA treated cells. (A) Deconvoluted images from structured illumination microscopy show that the three studied proteins colocalize at the INCs. Scale bar: 10 µm. (B) Super-resolution images of 100 nM TSA treated cells, double-labeled for Nup153 and Tpr show colocalization of both nucleoporins at INCs. As seen in the region of interest, Tpr placed deeper towards the nuclear interior than Nup153 in consonance with their relative positions in the nuclear pore. However, signals incoming from both proteins were not resolved enough to distinguish any structure at the INC. Scale bar: 4 µm.*

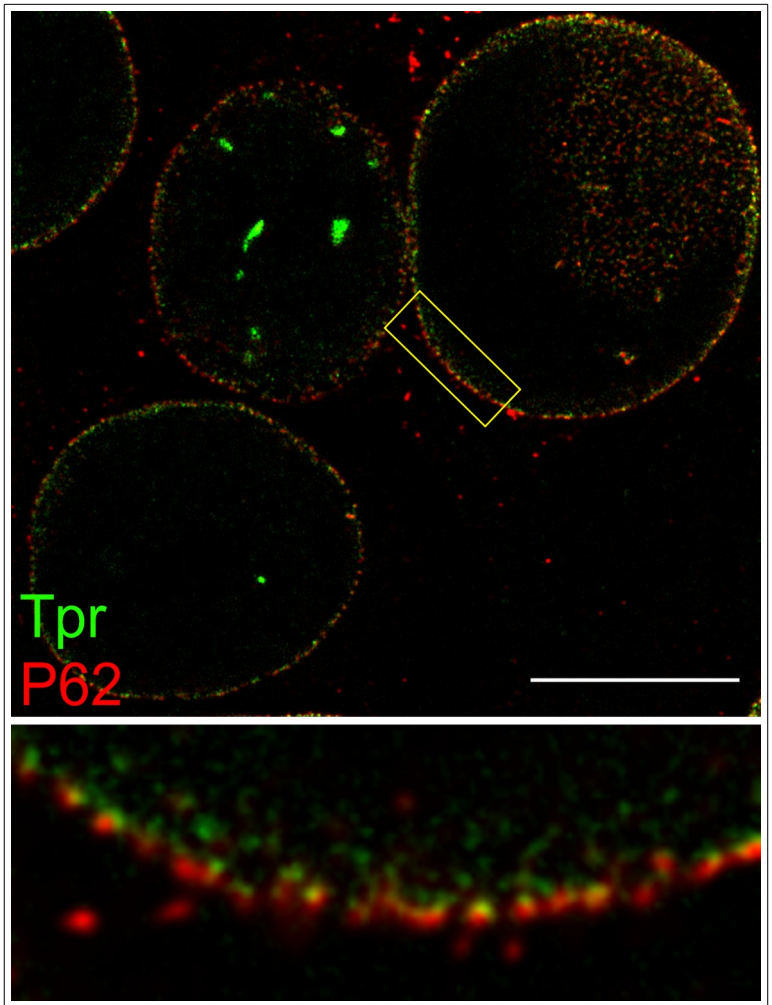

***Figure 22**: Tpr and P62 immunolocalization in nuclei of SMS-KCNR cells, after HDAC inhibition, by means of super-resolution confocal microscopy. The bottom image is an amplification of the yellow rectangle in the main illustration. Scale bar: 10 µm*

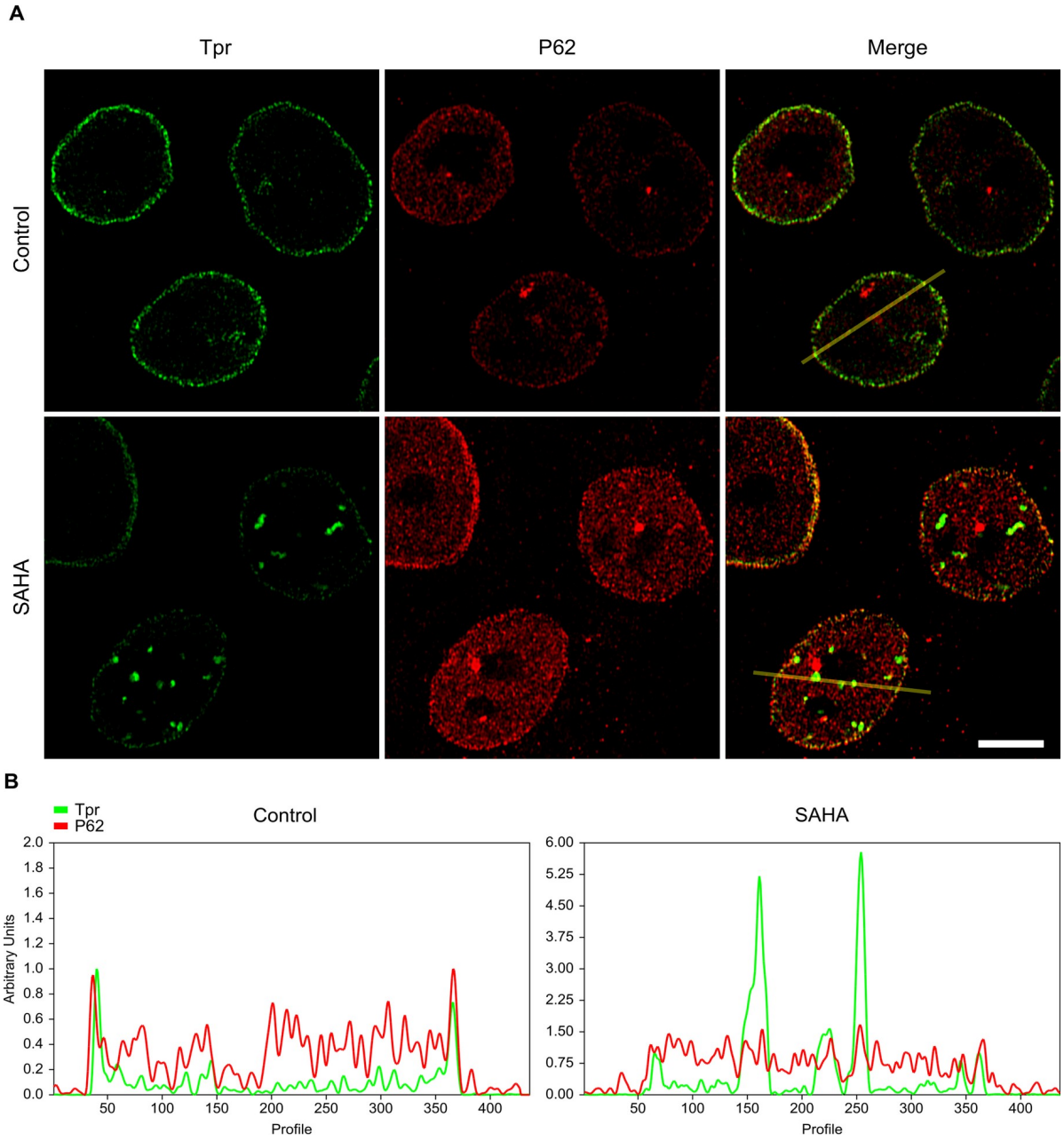

Figure 23: *P62 does not form INCs after HDAC inhibition. (A) In control cells, Tpr and P62 placed at the nuclear envelope. P62 as well is located within the nuclear interior but not forming any INC like structure. After SAHA 1,5 µM exposure, Tpr appeared in the form of INCs not colocalizing with P62. (B) Normalized intensity of fluorescence signal recorded along the yellow lines y the merged panels in A. Fluorescence signal at the nuclear envelope of both Tpr and P62 was used as a reference and assigned a value of 1. The intensity profile of SAHA treated cells demonstrates that, while Tpr is very concentrated at the INCs, P62 does not. Scale bar: 5 µm*

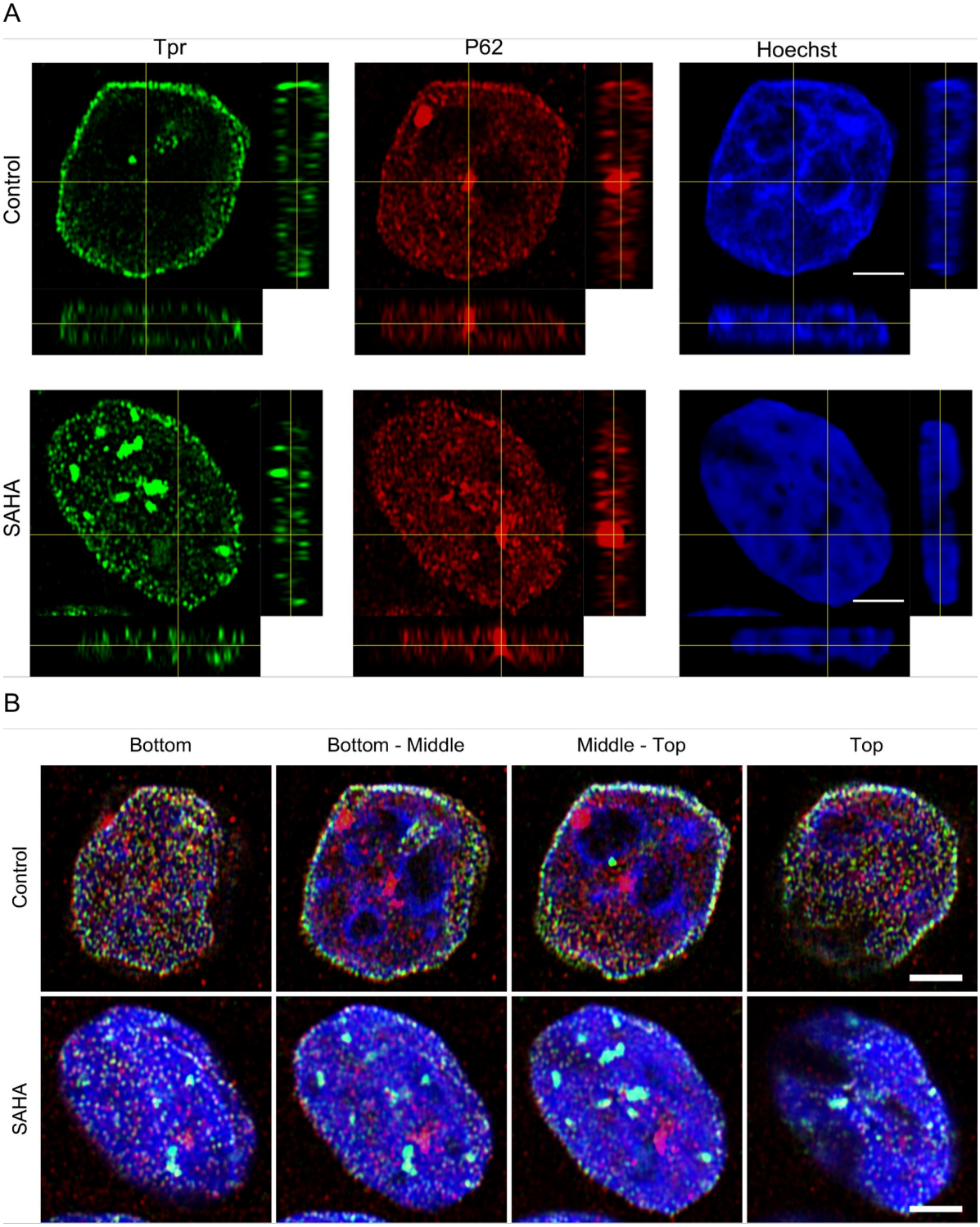

Figure 24: *P62 (red) accumulates independently from Tpr (green) alongside the nuclear interior, near the nucleolus (perceivable by the absence of Hoechst signal). (A) Orthogonal views of P62 concentrated areas. (B) Four representative planes of P62 (red), Tpr (green) and Hoechst (blue) merged signals ranging from the bottom to the top of the cell. Scale bar: 10 µm*

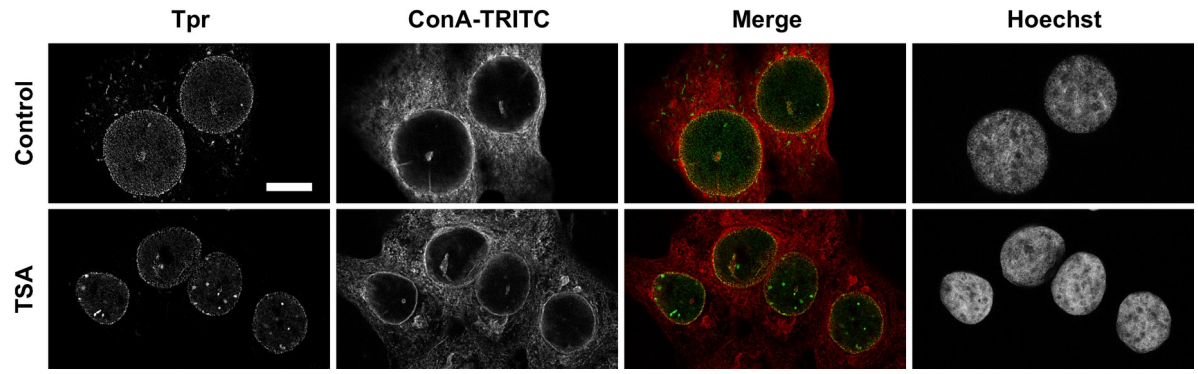

Figure 25: *Tpr immunolocalization and ConA-TRITC staining in control and 100 nM TSA treated cells. In control cells, concanavalin A stains the nuclear envelope in a continuous pattern in which nuclear invaginations are visible, but it is absent from the nuclear interior. When TSA is added to the culture, Tpr accumulates at Intranuclear Nucleoporin Clusters (INCs), but the concanavalin A lectin is absent from these structures. Scale bar: 10 µm*

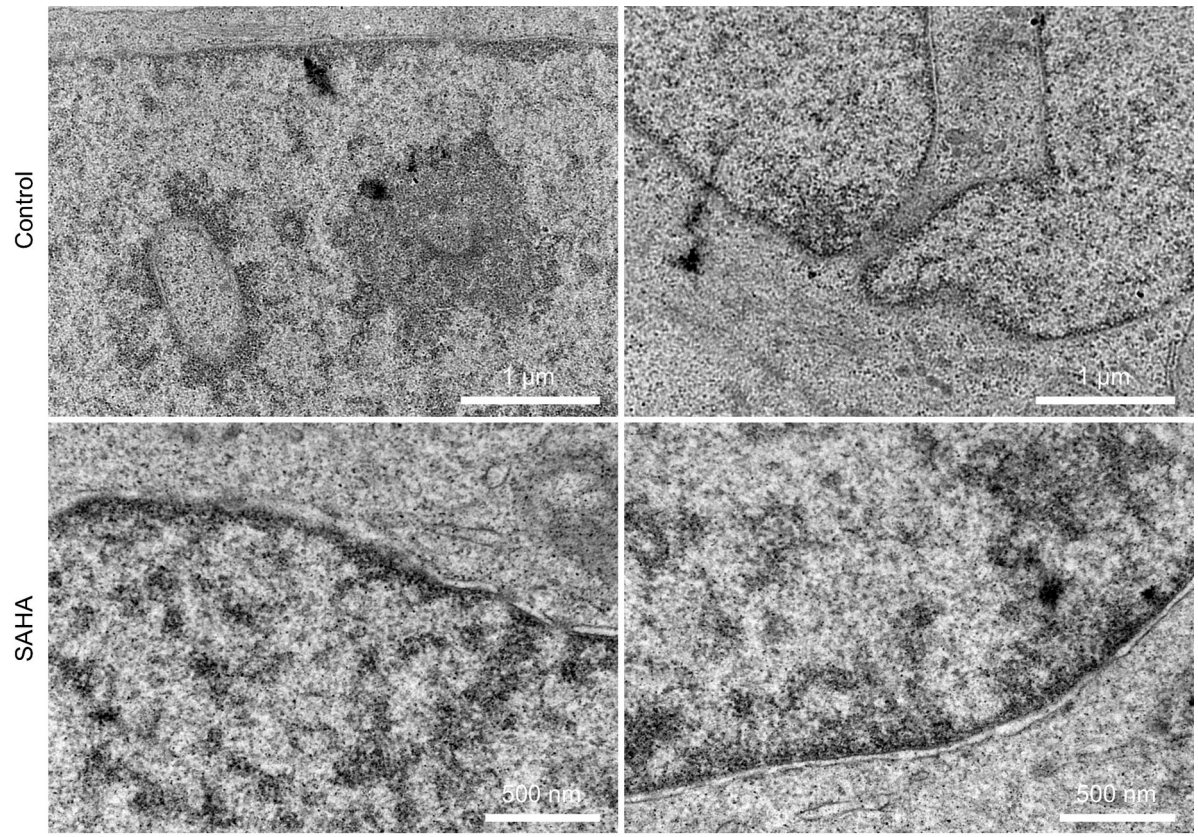

Figure 26: *Representative nuclear envelopes visualized using Transmission Electron Microscopy, of SMS-KCNR cells before (control) and after 1,5 µM SAHA treatment. Control cells displayed nuclear invaginations in cross (left) and longitudinal (right) sections. NPCs can be observed clearly at a nuclear envelope forming heterochromatin exclusion zones beneath them. On HDAC inhibited cells, no structural differences can be observed compared to the controls.*

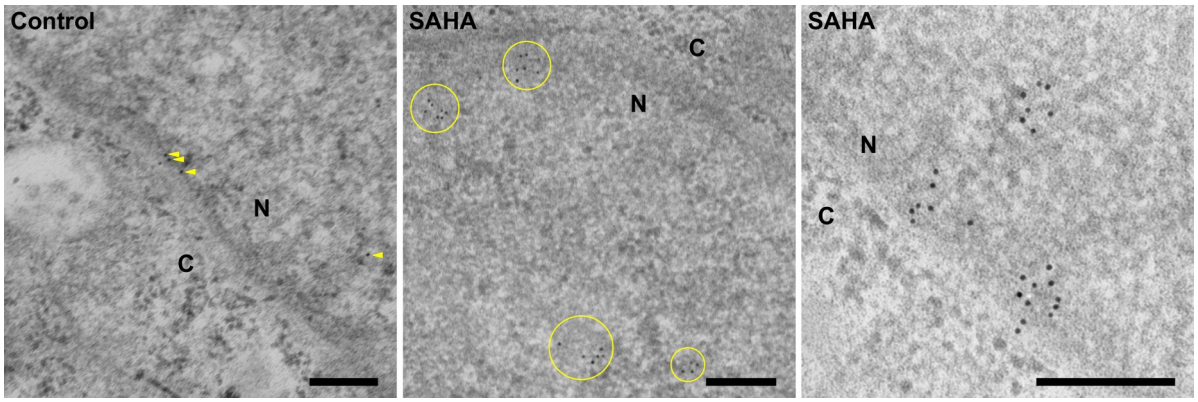

Figure 27: *Immunodetection of Nup153 using transmission electron microscopy. On control cells, Nup153 (arrowheads) is present individually at the nuclear envelope and, to a lesser extent, at the nuclear interior. After 1,5 µM SAHA 24 hours exposure, Nup153 formed aggregates at the nuclear envelope and deep inside the nucleus (circles). At higher magnification, Nup153 looks to be associated with electron dense zones of chromatin. Scale bar: 200 nm.*

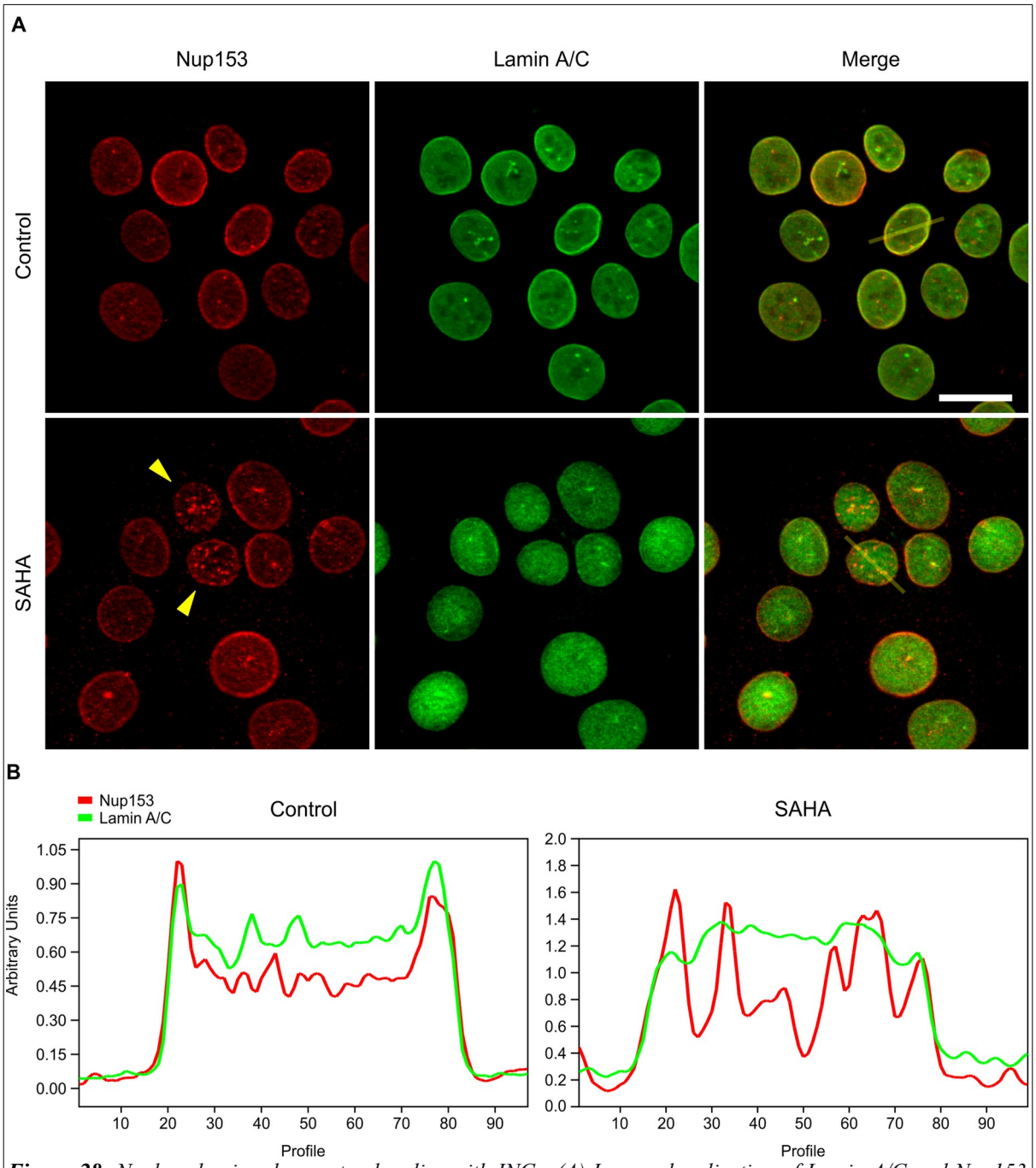

Figure 28: *Nuclear lamina does not colocalize with INCs. (A) Immunolocalization of Lamin A/C and Nup153 demonstrated that Lamin A/C does not form intranuclear accumulations, neither by itself nor by association with Nup153 (arrowheads). (B) Normalized intensity of fluorescence signal recorded along the yellow lines in the merged panels in A. Fluorescence signal at the nuclear envelope of both Nup153 and Lamin A/C was used as a reference and assigned a value of 1. Control cells display standard signals of both Lamin A/C and Nup153, relegating them only to the nuclear envelope. On the other hand, when cells were exposed for 24 hours to SAHA 1,5 µM, Nup153 showed up inside the nucleus placed at INCs, but this was not the case for Lamin A/C which was evenly distributed throughout the nucleus.*

5.2.2 INCs are not associated with transcription or replication factories.

DNA transcription and replication are highly regulated processes and take place at specialized microenvironments, denominated as transcription and replication factories (Chagin et al., 2016; Rieder et al., 2012). Several studies have related nucleoskeletal structures such as nucleoporins to these nuclear organelles (Di Nunzio et al., 2013; Iborra et al., 1996). As both these processes are strongly regulated at an epigenetic level, we wondered if HDAC inhibition led nucleoskeleton-related nucleoporins to accumulate with the other components of the replication and transcription machinery, ultimately causing the formation of INCs. In fact, as figure 27 illustrates, Nup153 seems to be associated with electron-dense zones of chromatin, suggesting that INCs could be forming part of the transcription or replication machinery.

Consequently, we performed double immunofluorescence experiments of Nup153 with PCNA or RNApol II CTDSer5P in control and TSA100 nM treated cells. By confocal microscopy, PCNA label in TSA treated cells exhibited a diffuse pattern, typical for G_0/G_1 cells (Chagin et al., 2016). As expected, Nup153 formed INCs, but they did not colocalize with any appreciable structure of PCNA. Similar results were obtained after double staining of Nup153 with RNApol II Ser5P. In both control and treated cells, transcription foci could be observed as small and intense dots, but we did not observe any colocalization with Nup153 INCs. In HDAC inhibited cells, it can be appreciated that RNApol II ser5P distribution is more uniform throughout the nucleus when compared with controls, indicative of open and actively transcribed chromatin, plausibly due to hyperacetylation (Figure 29).

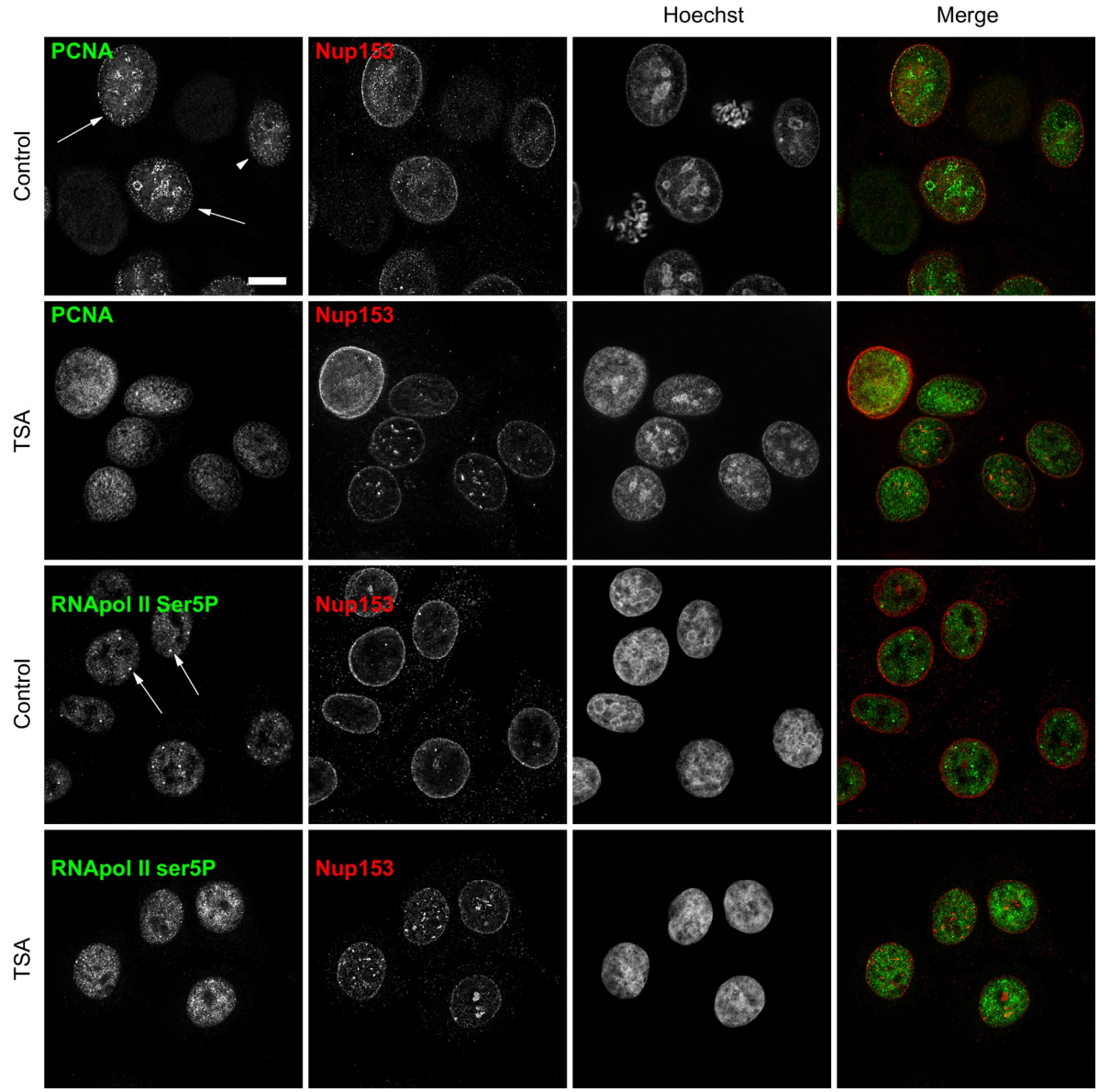

Figure 29: *Double immunolocalization of Nup153-PCNA and Nup153-RNApolII Ser5P. PCNA accumulates in replication foci in S cells (arrows) or diffused in G_1 cells (arrowhead), but it is not present at Nup153 intranuclear clusters after 100 nM TSA. Likewise, active RNA polymerase II (RNApolII Ser5P) is located in transcription factories in control cultures (arrows) and diffuses throughout the nucleus after 100 nM TSA incubation. Scale bar: 10µm*

5.2.3 Nucleoporins form stable structures inside the nucleus.

As seen in previous images, nucleoporins usually are located at the nuclear envelope, forming a characteristic nuclear rim when observed under fluorescence microscopy. Nevertheless, this distribution changed after HDAC inhibition, which drove many cells to the appearance of very intense nucleoporin accumulations inside the nuclei, usually accompanied by a reduction of the fluorescence intensity coming from the nuclear rim. This rim signal loss in cells containing INCs stands out, especially when compared to the INC-absent nuclei after HDAC inhibition, where the nuclear rim seemed much more intense. In order to fine-tune this appreciation, we extracted densitometric data from confocal immunofluorescence microscopy in control and HDAC inhibited cells (Figure 30). The densitometry was carried out by measuring the raw fluorescence intensity from double immunolocalization of Tpr and P62 at the nuclear rim in equatorial sections of the analyzed nuclei. Control nuclei were compared to the HDAC inhibited ones, both, INC-positive and INC-negative nuclei. In every case, Tpr signal was also compared to the signal emanating from P62, which is not present at the INCs (Figures 15 and 24). As expected, in HDAC treated cells, Tpr signal was less intense at the nuclear envelopes of the INC-positive nuclei while it increased in the INC-absent ones. P62 values, on the contrary, remained constant in INC-positive nuclei; but increased, in the same manner as Tpr, in those absent of INCs.

Although not statistically significant (Figure 30C), data indicated a tendency of Tpr signal loss at the nuclear envelope at INC-positive nuclei compared to controls. To overcome the technical limitations of densitometry when comparing fluorescence signals, we extended the examination to super-resolution microscopy, in order to identify single Tpr and P62 molecules at the nuclear envelope. Consequently, we systematically counted the number of Tpr and P62 particles at the nuclear envelope in sections of 6 μm^2 and was only carried out on INC-positive nuclei after HDAC inhibition (Figure 31). These super-resolution studies allowed us to resolve the molecular localization of both nucleoporins with greater detail and demonstrated that, although the NPC number (represented by P62 molecules) remained unperturbed after HDAC inhibition, the amount of Tpr placed alongside the NPCs suffered a noticeable down-regulation.

The results obtained by densitometry and super-resolution quantitation indicate that nucleoporins accumulated in the nuclear interior lose presence in the pore complexes at the nuclear envelope. It seems that the presence inside or at the nuclear periphery is mutually exclusive in the context of histone hyperacetylation. This circumstance could be due to a pivotal displacement between both locations as long as both are relatively stable locations. If so, INCs should be resistant to soft biochemical extraction using mild non-ionic detergents such as Triton X-100, as is the case with NPCs and other nuclear organelles such as the nucleolus. (Melan & Sluder, 1992) .

To clarify this issue, we set out to conduct an immunolocalization study of Nup153, which, in addition to being a nucleoporin present in the INCs, has been described as having a mobile subpopulation between the interior and the nuclear envelope (Rabut et al., 2004). was performed after subjecting the cells to digestion with triton X-100 before being fixed and processed. Permeabilization caused by triton X-100 provokes all soluble intracellular contents to go outside and be removed by the different washes during preparation, leaving only the most robust structures inside the cell. The images demonstrate that Nup153 INCs are resistant to permeabilization and retain their shape and number in cells treated with the HDAC inhibitor. Regardless of the order in which the fixation and permeabilization were performed, Nup153 remained in its usual location, in the nuclear envelope of the controls, and the INCs of the cells treated with SAHA.

As we have seen, the nucleoporins that makeup the INCs lose presence in the nuclear envelope in favor of their new location in the nuclear interior, where they accumulate intensely (Figures 20 and 23). Likewise, the permeabilization results show that Nup153 has similar biochemical properties in the nuclear envelope and the INCs, indicating that these structures might be as stable as NPCs. It remains to be known whether these nucleoporins behave in the same way in intranuclear aggregates as in NPCs. To clarify this matter, we organized a FRAP experiment in living cells stably expressing Nup153-GFP, both for control cells and after treatment with 100 nM TSA for 24 hours. In control cells, only a region of the nuclear envelope was bleached (Figure 33). In TSA treated cells, a region of the nuclear envelope (NE) was bleached and, right afterward, an INC inside the very same cell was bleached so that the mobility of Nup153 in both compartments could be compared. Inverting the bleaching order (first an INC and then the NE) did not affect the dynamics of Nup153 (data not shown). Our results show that Nup153 in control cells recovered rapidly after bleaching (Figure 33B), as has been previously described (Griffis et al., 2004; Rabut et al., 2004). However, the recovery dynamics of Nup153 after TSA treatment were significantly slower than in control cells, taking longer to stabilize than in control cells. The reduction in the mobility of Nup153 was independent of the bleached region, as the recovery curves for INCs and NE were indistinguishable. These results suggest that treatment with TSA induces a change in the mobility of Nup153 by its interaction with non-soluble components inside the nucleus.

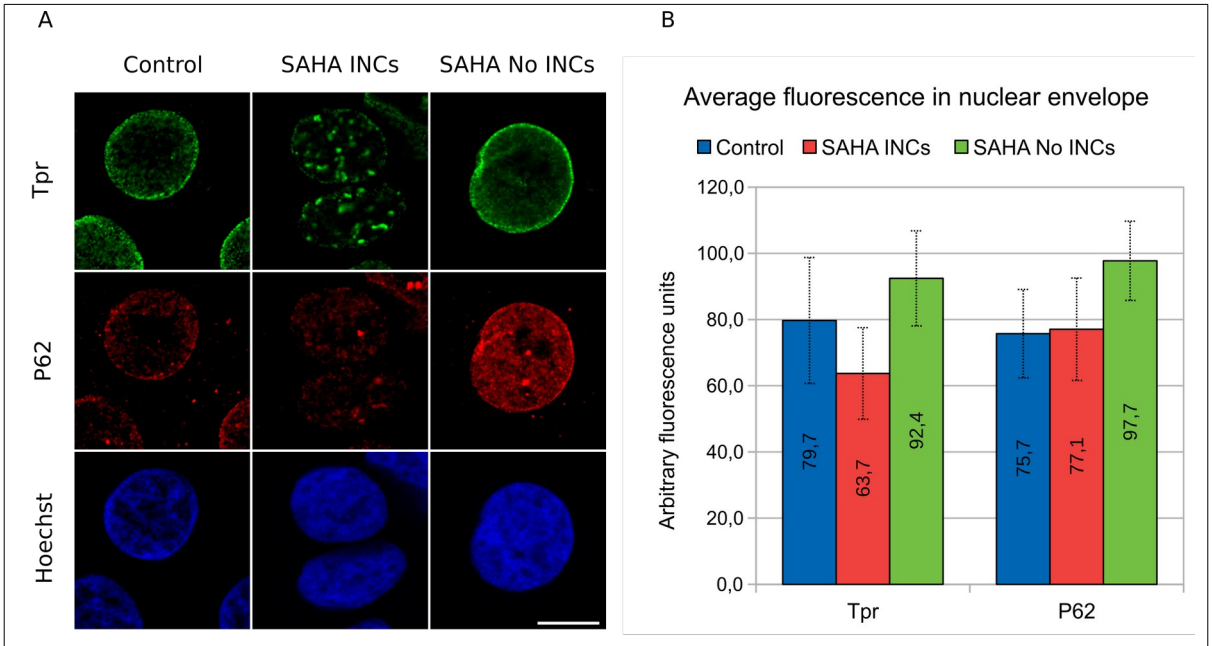

C

Bonferroni test		Tpr			P62		
		CNT	SAHA INC	SAHA NO INC	CNT	SAHA INC	SAHA NO INC
Tpr	CNT		0,64380	1,00000	1,00000	1,00000	0,30080
	SAHA INC	0,64380		0,00663	1,00000	1,00000	0,00047
	SAHA NO INC	1,00000	0,00663		0,61310	0,81120	1,00000
P62	CNT	1,00000	1,00000	0,61310		1,00000	0,10820
	SAHA INC	1,00000	1,00000	0,81120	1,00000		0,14890
	SAHA NO INC	0,30080	0,00047	1,00000	0,10820	0,14890	

Figure 30: *Densitometric analysis of the nuclear envelope fluorescence signals from the nucleoporins Tpr and P62. Images were acquired under equal exposure times and identical microscope configuration in samples processed in the same experiment. (A) Representative sections of nuclei immunostained against Tpr and P62. In SAHA treated cells, we measured the nuclear envelope signal in nuclei that presented INCs (SAHA INCs) and in nuclei that did not (SAHA no INCs). Scale bar: 10 µm. (B) graphical representation of densitometric data measured in arbitrary fluorescence units (n = 12). Dunn's post hoc Bonferroni corrected p-values.*

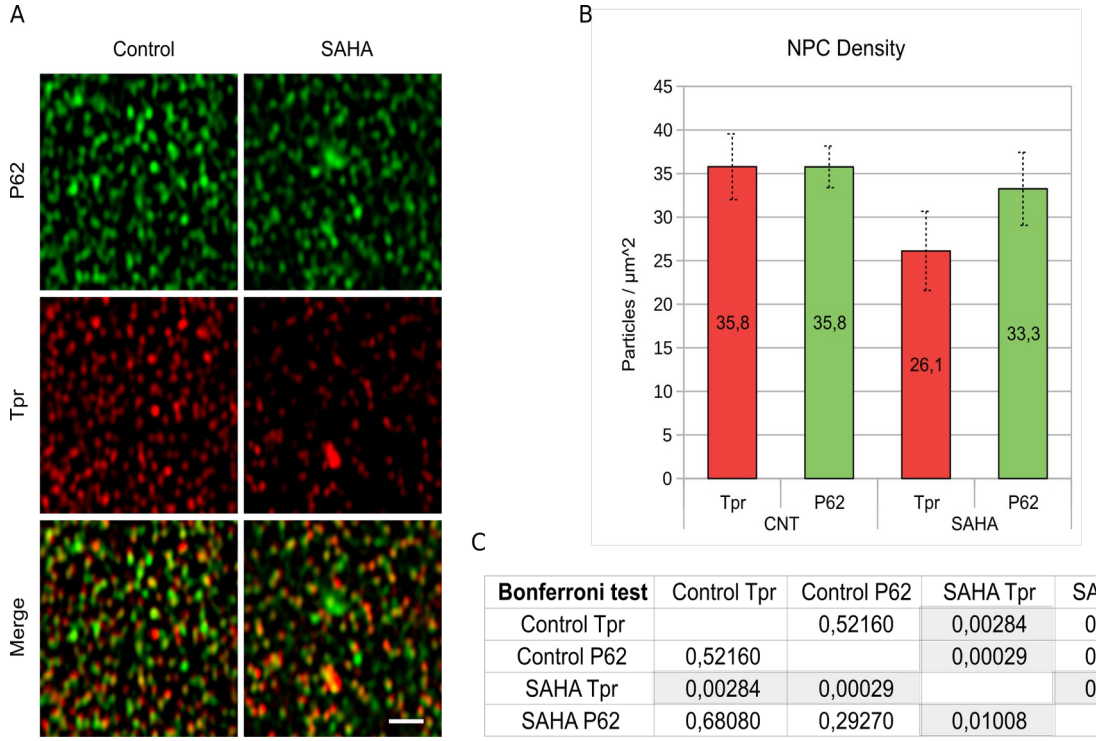

C

Bonferroni test	Control Tpr	Control P62	SAHA Tpr	SAHA P62
Control Tpr		0,52160	0,00284	0,68080
Control P62	0,52160		0,00029	0,29270
SAHA Tpr	0,00284	0,00029		0,01008
SAHA P62	0,68080	0,29270	0,01008	

Figure 31: *Each particle of P62 and Tpr was considered to represent a single NPC. In cells treated with SAHA, we only measured particles in those nuclei that contained INCs inside. (A) Representative tangential sections of 6 µm² in which the particles were counted. These were acquired by double immunodetection super-resolution fluorescence microscopy at the baseline of the nuclear envelope of 10 independent nuclei. (B) Graphical representation of the density of NPCs (NPC / µm²) according to the particles accounted for Tpr and P62. (c) The density of Tpr particles decreases in a statistically significant way (ANOVA: Dunn's post hoc Bonferroni corrected p-values) compared to all other conditions (Grey darkened grids p-values < 0,05).*

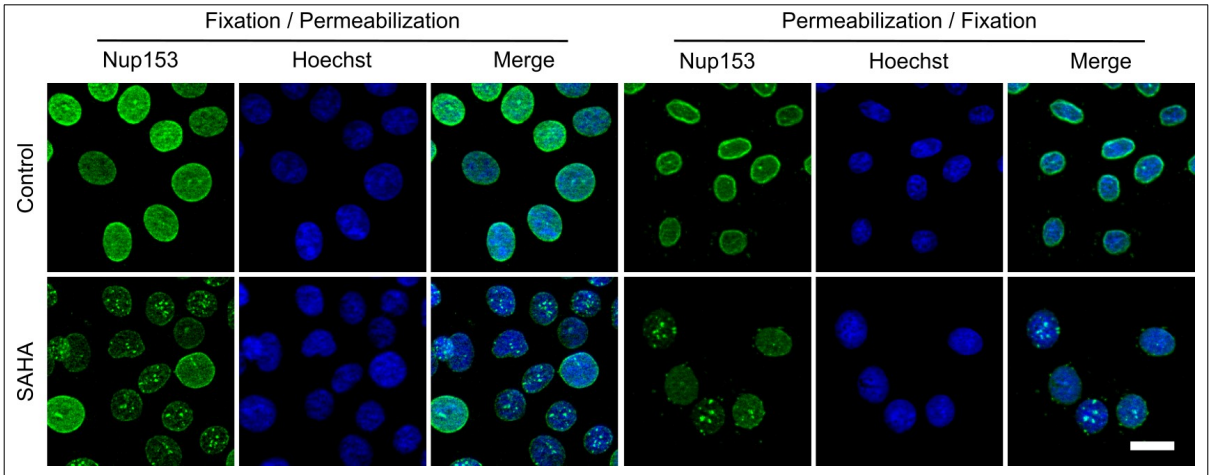

Figure 32: *INCs are structures resistant to mild detergent extraction. After permeabilization by 0,1% TX-100 (Permeabilization / Fixation), INCs of Nup153 remained inside SAHA treated cells' nuclear interior. Scale bar: 20 µm.*

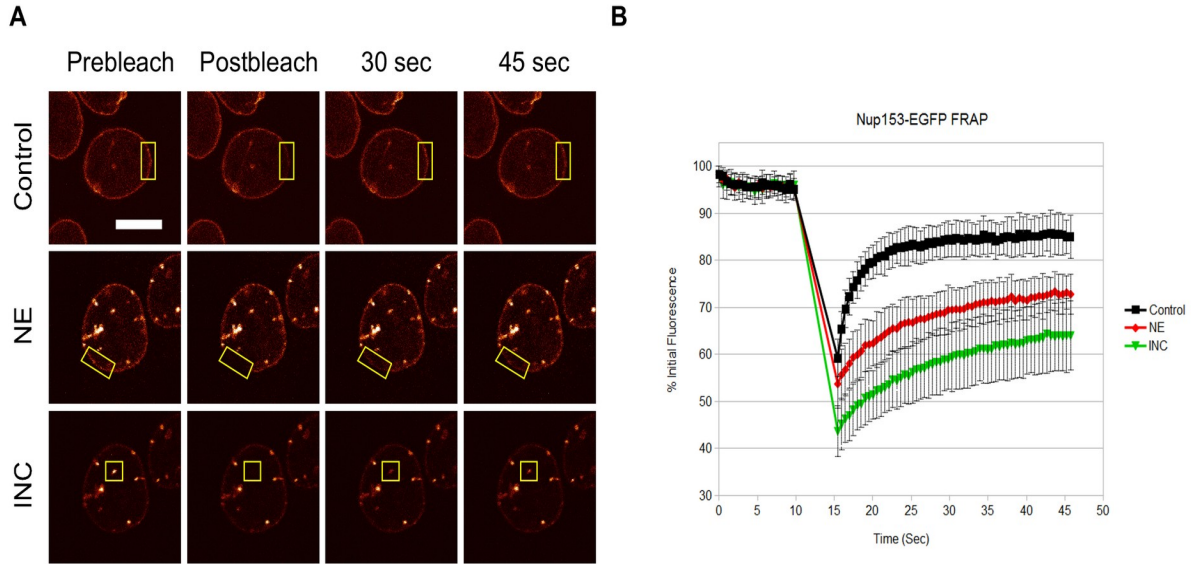

***Figure 33**: Quantitative FRAP analysis of Nup153-EGFP in stably transfected SMS-KCNR cells (A) Representative samples of control and 100 nM TSA treated cells are shown. In cells exposed to TSA, both the nuclear envelope (NE) and an Intranuclear Nup Cluster (INC) of the same cell were consecutively bleached. A rectangle indicates the bleached area. Scale bar: 10 mm. (B) Average normalized fluorescence signals with their corresponding standard deviations of control nuclear envelopes (n = 34) compared with the nuclear envelopes and INCs of 100 nM TSA treated cells (n = 32)*

5.3 INC formation is not related to migration processes.

The nucleoskeleton is connected to the cytoskeleton through the nuclear envelope by means of a trans-membranous protein complex denominated as LINC complex. This system mediates the binding between microtubules, intermediate, and actin filaments with the nuclear lamin and through it with the rest of the nucleoskeletal components (Dahl & Kalinowski, 2011).

Previous investigations (Díaz-Núñez et al., 2016) have described HDAC inhibitors as causers of pro-apoptotic effects and promoters of cell migration. As the cytoskeleton is the fundamental machinery carrying out cell motility and is connected to the nuclear lamina and NPCs (Martin W. Goldberg, 2017), the alterations caused by HDAC inhibition in the cytoskeleton might be reflected in the behavior of the nucleoskeletal constituents located at the INCs.

Thus, we designed a series of experiments with the aim to clarify if the nucleoskeletal rearrangement driven by HDAC inhibition (Figure 20) is led by cytoskeletal changes that would imply modifications on cellular migratory conduct.

Wound healing assays are an easy and straightforward approach to study cell migration between different experimental conditions. These are based on measuring the time it takes for a monolayer of cells to cover a known distance between two migration fronts. As described in

materials and methods, we grew SMS-KCNR cells in the chambers of Ibidi® silicon constructs until cells formed a monolayer. At that point, we removed the silicon insert and added complete fresh media to control cells and complete media containing the HDAC inhibitor SAHA to another culture. We measured the surface of the gap between the two migration fronts right after insert removal (0 hours) and after 24 hours (Figure 34). In untreated complete culture media, SMS-KCNR cells covered 28% of the initial gap, whereas when treated with SAHA, the gap reduction ascended to 39%. Consequently, this result asserts that SAHA treatment promotes the gap enclosure.

Nevertheless, when we observed the cell culture under the phase-contrast microscope, we could not ignore that cell morphology suffered a significant alteration when submitted to HDAC inhibition. For this reason, we decided to carry out a cell morphology analysis by visualizing the microtubule network of the cytoskeleton (Figure 35). Tubulin immunodetection in control cells illustrated that the SMS-KCNR cell line possesses a natural tendency to form groups or small colonies. The intimate connections between cells were lost when they were submitted to HDAC inhibition, acquiring a morphology more typical of a mesenchymal phenotype. This change was even more notorious when we relativized the tubulin-covered surface to the number of cells (counted by nuclei number) present in the image. In control cells, that ratio had a value of 0,35; but after SAHA treatment, it ascended to 0,58, indicating significant growth of cellular surface.

However, these approaches do not show nucleoporin distribution disturbances during cell migration. In order to clear this matter, we decided to immunolocalize Nup153 at the end of a wound-healing assay performed over a glass-bottomed Ibidi 35mm plate (compatible for posterior confocal immunofluorescence microscopy). Fluorescence signal coming from Nup153 mainly located at the nuclear envelope both in control and HDAC inhibited cells (Figure 36). Nuclei containing INCs of Nup153 were very scarce (arrowheads in Figure 36). Additionally, the few cells that showed INCs at their nuclei did not locate apparently at any particular place, neither in the migration front nor in the overall culture.

The secretion of matrix metalloproteinases to the medium is an event that takes place in parallel to migratory processes. Consequently, and complementary to the wound healing assays, conditioned media of cells cultured in the presence and absence of HDAC inhibitor were recollected. Parallel to each condition, additional cells were exposed only to DMSO, which is the vehicular substance of the HDAC inhibitor. Gelatin zymography was the chosen technique to check for the presence of metalloproteases in the collected conditioned media. The two main gelatinases (metalloproteases that digest gelatin) are the MMP-2 (72 kDa) and the MMP-9 (92 kDa). As both gelatinases are present in the FBS that supplements DMEM, zymographies were also done with DMEM conditioned media not supplemented with FBS.

In the same way, to discard any interference of the FBS in the secretion properties of the cells, experiments were repeated by submitting the culture to FBS deprivation during 24 and 48 hours before HDAC inhibition. As figure 37 reveals, no significant differences are

observable in the enzymatic activities of MMP-2, and MMP-9 between control and HDAC inhibited cells. Furthermore, the zymographies reveal that, independently of the FBS deprivation period (0, 24, and 48 hours) previous to the drug treatment, the MMP-9 activity is exclusively caused by the presence of FBS in the media. In summary, HDAC inhibition does not alter gelatin metalloprotease secretion, either in serum-deprived or non-deprived SMS-KCNR cultures.

The results in this section allow us to assert that there is not a straightforward relationship between the intranuclear nucleoporin accumulation caused by HDAC inhibition and the migration capabilities of SMS-KCNR cells: first, neither HDAC inhibition favors nor impedes migration, and second, the presence of INCs in the HDAC inhibited nuclei was negligible in the wound healing assays.

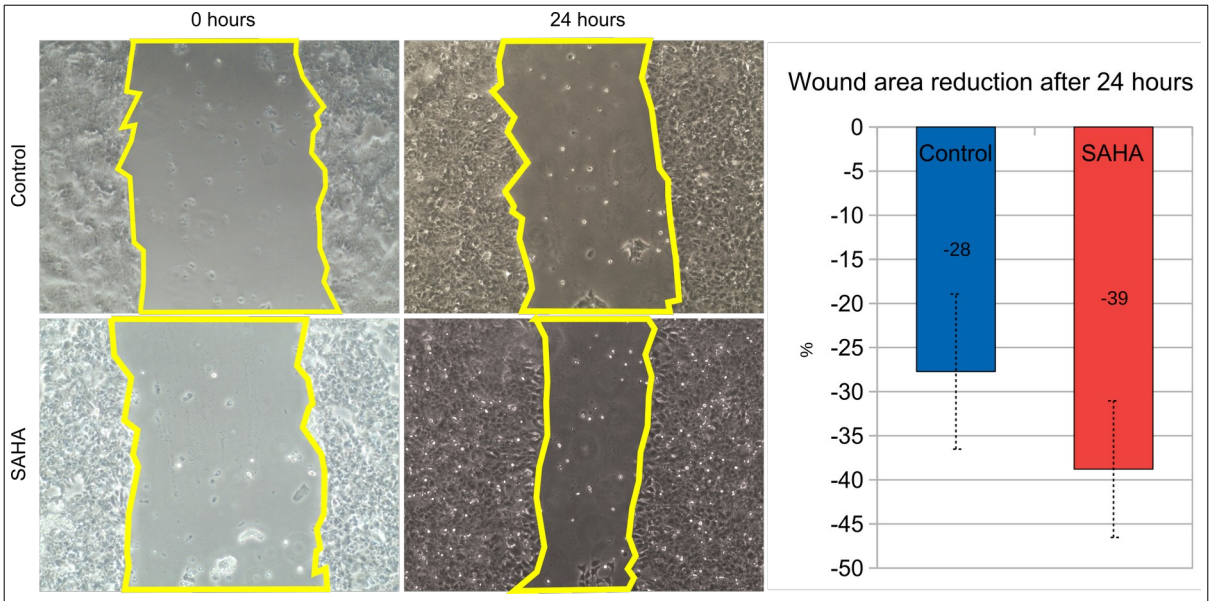

Figure 34: *Wound healing assay on HDAC inhibited (SAHA) and not inhibited (Control) cells. Bruised area (yellow selection) was quantified at the beginning (0 hours) and the end (24 hours) of the experiment. The right graphic illustrates the reduction % of the initial wound area, both in control and treated cells. (Control: n = 26; SAHA: n = 29) (p-value < 0,01)*

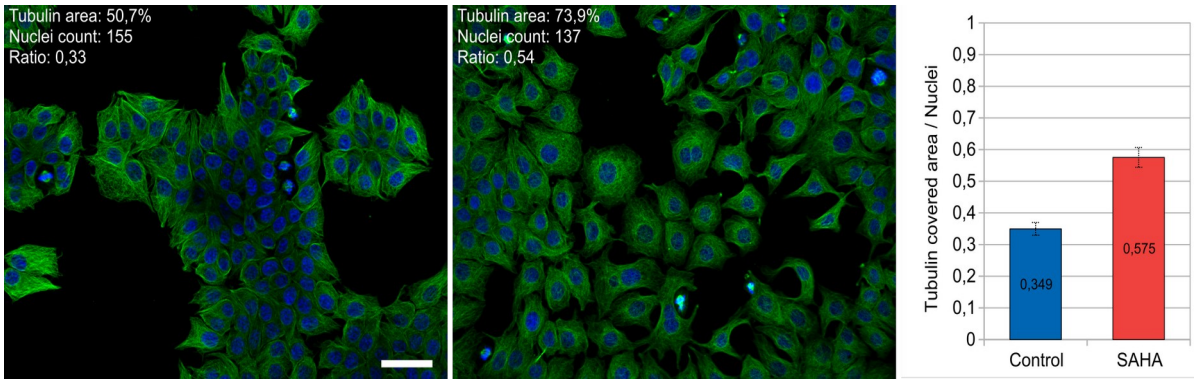

Figure 35: *Tubulin immunostaining in control versus HDAC inhibited cells (SAHA). Control cells tend to form small colonies, whereas, after SAHA treatment, they deform due to tubulin rearrangement. The graphic on the right displays the ratio between the tubulin covered area on the captured field against the number of nuclei contained within. This proportion is interpreted as a cellular size calculation where control cells have a ratio of 0,35 and HDAC inhibited ones of 0,58. Student's t-test demonstrated that SAHA treated cells were significantly bigger than control ones (p-value 0,00045 < 0,05) (control fields n = 3; SAHA fields n = 3). Scale bar: 50 µm*

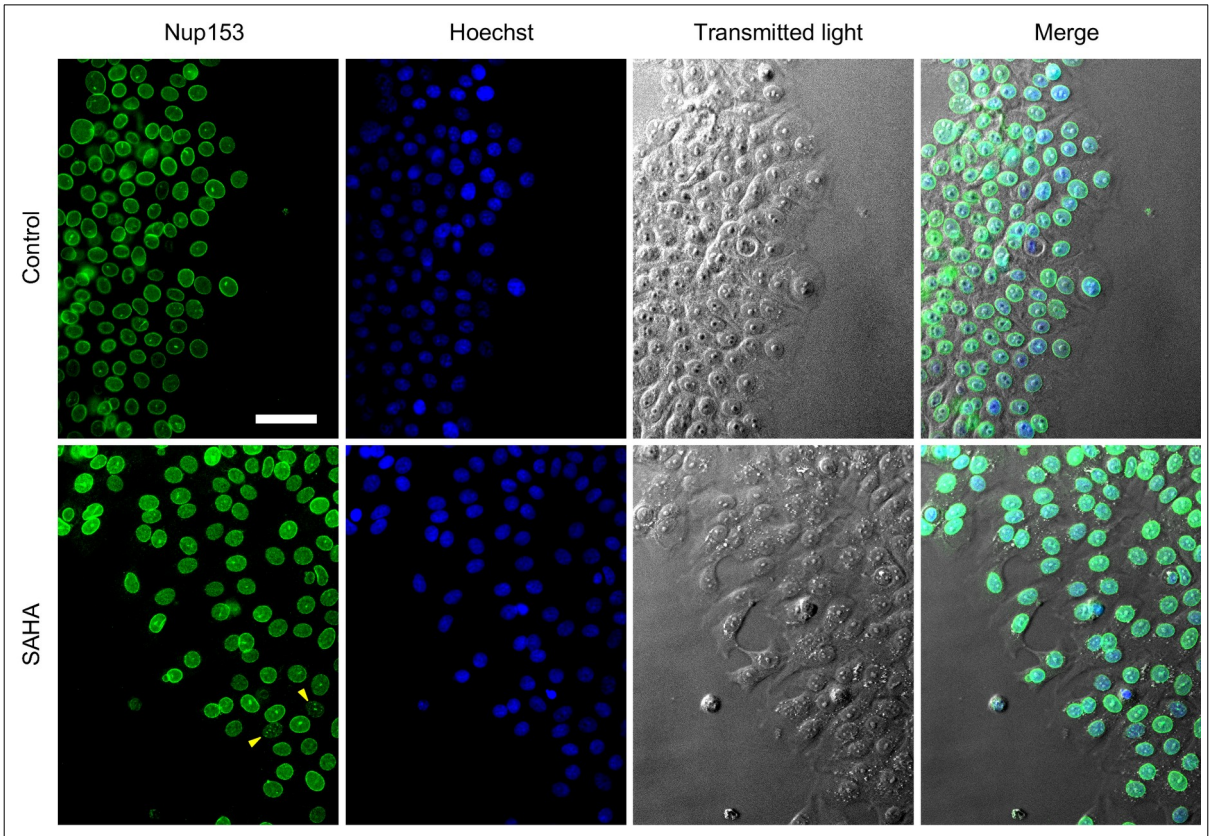

Figure 36: *Immunolocalization of nup153 in a finished wound-healing assay after 24-hour incubation. The panel shows representative fields of the migration-front of control and SAHA treated cells. In control cells, nup153 locates at the nuclear envelope as usual. Meanwhile, in HDAC inhibited, very few of these cells show INCs (arrowheads). DNA (Hoechst) and bright-field images are also displayed. (scale bar: 50 µm)*

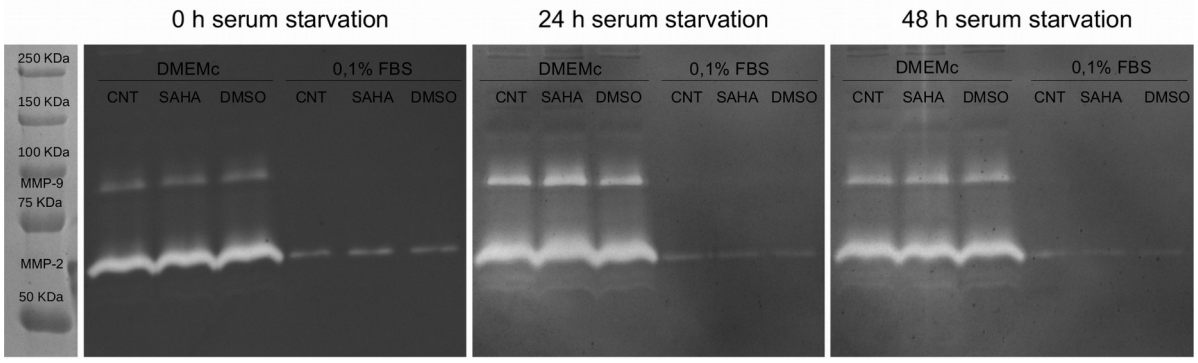

Figure 37: *Zymograms of SMS-KCNR cells conditioned DMEM media supplemented with 10% FBS (DMEMc) or FBS deprived (0,1% FBS). Before SAHA exerted the HDAC inhibition, different cultures were subjected to serum deprivation for 24 and 48 hours. The media of non-treated cells (CNT) and treated with the SAHA solvent (DMSO) were also analyzed. MMP-9 digestion bands located between the 75 and 100 KDa molecular weight marker bands and only appeared in 10% FBS complemented DMEM (DMEMc). On the contrary, MMP-2 presented metabolic activity in both complete (DMEMc) and serum-deprived media (0,1% FBS)*

5.4 INCs are present only at G_1 arrested cells.

As mentioned in the introduction, HDAC inhibitors exert several alterations both in cell migration and proliferation. The impact of the inhibitors over these two cellular properties relies mainly upon the cell lineage. After an initial approach, our results suggest that the migration capabilities of the SMS-KCNR cells are not affected by HDAC inhibition; Moreover, we have not observed any relationship between INC formation and migrant cells. In order to deepen into the mechanisms generating INCs after exposure to HDAC inhibitors, we set a series of experiments to investigate if they are related to cell proliferation and cell cycle processes.

MTT proliferation assay was the first approximation we made in order to know the effect of the HDAC inhibitor SAHA on SMS-KCNR cells. The experiment was designed with the aim to discard any FBS interference, so HDAC inhibition was carried out in the presence (10%) and absence (0,1%) of FBS in the culture medium. Accordingly, prior to any drug treatment, cells were submitted to 0, 24, or 48 hours of FBS deprivation (0,1%) to discard any metabolic inertia that the serum could be causing over the culture. After normalizing the raw absorbance with respect to each group's controls, the data (Figure 38) indicate that the main differences depend significantly on the presence or the absence of FBS in the medium where the HDAC inhibitor was delivered. This fact became particularly evident after submitting cells to 24 and 48-hour deprivation of serum before HDAC inhibition, where, as expected, the absorbance readings were much lower.

Contrary to what was suspected, SAHA did not cause any noticeable alteration over the proliferative capabilities of SMS-KCNR cells. A tiny absorbance increase was detected, though, when cells were exposed to SAHA in complete culture media without being

previously serum deprived. Nonetheless, since this increase was so minuscule and not repeated in the other tested scenarios, we can not associate that gain to the SAHA treatment but to an inherent imprecision of the MTT assay.

As the results of MTT seemed to be in contradiction with the existing literature, we decided to complement them by means of cell cycle analyses by flow cytometry. Accordingly, we treated SMS-KCNR cells with a wide range of HDAC inhibitor concentrations during 24 hours in complete culture media (Figure 39). We decided to exclude the serum interference variable in view of the previous results, as it did not exert any synergy with SAHA in the cell proliferation assays. Flow cytometric results showed that both TSA and SAHA exerted a cell cycle blockade at the G_1/S and G_2/M checkpoints, and this effect was subjected to the amount of inhibitor employed. Once a minimal dose was overcome, low concentrations of TSA (100 nM) and SAHA (2 μM) arrested the cell population at the G_0/G_1 phase of the cell cycle (87% and 67% respectively), drastically reducing the G_2/M population and virtually eliminating the S phase group. However, this scenery was gradually inverted while exposing cells to higher doses of both inhibitors, until the point where at 600 nM TSA and 10 μM SAHA, the G_2/M arrested cells became the main population (72% for TSA and 67% for SAHA).

HDAC inhibition seemed to generate two well-differentiated cell populations, as the S phase is completely collapsed. As we have previously observed in nucleoporin immunolocalization experiments, not every cell manifested intranuclear accumulations of nucleoporins. Indeed, analogously to cell cytometry data, two very different groups could be observed: one comprised of small nuclei with INCs and another composed of large nuclei with an intense nucleoporin signal relegated exclusively to the nuclear envelope (Figure 20 and Figure 30). Both observations prompted us to hypothesize that the presence or absence of INCs inside the nuclei was determined by the phase of the cell cycle where the cells were arrested.

To assess this question, Nup153 (INC marker) distribution and nuclear area were carefully analyzed on each nucleus in equatorial sections of images obtained by confocal fluorescence microscopy (A panels of figures 40 and 41). Figure 40 collects the HDAC inhibitor TSA results, while figure 41 sums the SAHA inhibitor data. These counts were realized with low (TSA 100 nM and SAHA 2 μM) and high (TSA 250 nM and SAHA 4 μM) doses of each inhibitor, where the population percentages according to the cell cycle phase were significantly different (B panels of figures 40 and 41). Nuclei were classified according to their nuclear size and the presence or absence of INCs. The analysis (C panels of figures 40 and 41), showed that there were two entirely distinct populations. The first one was characterized by small nuclei with intranuclear accumulations of Nup153 (INCs), and the second one, distinguishable by large nuclei where Nup153 was exclusively located at the nuclear envelope.

Moreover, there was also a noticeable and clear correlation between the INC presence-absence frequencies and the percentage of each phase of the cell cycle; and importantly, these percentages were dependent on the HDAC inhibitor concentration. At low drug doses (TSA

100 nM and SAHA 2 μM), the presence of INCs was dominant alongside the G_0/G_1 phase; while, at higher doses (TSA 250 nM and SAHA 4 μM), the opposite effect was detected. Consequently, this correlation allows us to assert that INCs are linked to the G_0/G_1 phase. The fact that the small nuclei are the ones that present the intranuclear accumulations of nucleoporins favors this assessment since G_0/G_1 nuclei are always smaller than the ones in the G_2 phase (Maeshima et al., 2011).

In order to confirm the linkage between the INCs and the G_0/G_1 phase, we repeated the same experiment as before, but this time the FUCCI (Fluorescence Ubiquitination Cell Cycle Indicator) system was included in the test. FUCCI is a genetically encoded two-color (red and green) indicator that reveals the cell cycle phase by expressing two recombinant proteins: Cdt1-RFP, expressed solely in the G_1 phase, and the Geminin-GFP, which is present during the S and G_2 phases. After the FUCCI transfection, SMS-KCNR cells were treated with low (2 μM) and high concentrations (4 μM) of SAHA (Figure 42).

The combination of FUCCI, DNA staining by Hoechst, and Nup153 immunolocalization allowed us to extract all the needed information directly in a single fluorescence microscopy image (Figure 42A). We divided this data into three categories: INC presence or absence (according to Nup153 distribution), nuclear surface (measured by Hoechst covered area), and phase of the cell cycle (colorless: G_0 or early G_1; red: G_1; green: S or G_2).

First, the different frequencies of INC apparition and cell cycle phases were plotted against nuclear area intervals (figure 42B: upper graphics). As stated before (Figure 41C), the graphics demonstrate that INC containing nuclei are smaller than nuclei without them. Again, like in the previous experiments, the population groups inverted depending on the delivered SAHA concentration: at 2 μM, the main population was the one that presented INCs, while at 4 μM the opposite effect could be observed (figure 42B and C). Next, after plotting the cell cycle phases against nuclear area intervals (figure 42B: lower graphics), it was verified that the prominent nuclei (240 – 400 μm^2) were indeed those arrested in the G_2 phase (revealed by Geminin-GFP expression). Although they were predominantly smaller (80 – 240 μm^2), some of the nuclei in the other phases of the cycle (colorless and expressing Cdt-1-RFP) showed nuclear surfaces close to those of G_2. Altogether, these data demonstrate that the INC containing nuclei are arrested in the G_0/G_1 phase and are predominantly smaller than the G_2 INC absent ones.

If we focus only on the INC frequencies on each phase of the cell cycle (Figure 42C), it remains clear that INCs are more intimately related to the early G_1 or G_0 phase (both colorless) instead of the main G_1 (Cdt1-RFP) or late G_1 (yellow: Cdt1-RFP and Geminin-GFP). Although the frequencies of the main and late G1 phases were similar to those of Early G1 and G0, they showed a much greater variability (large standard deviations in G1, G1/S graphics in Figure 42C). Additionally, these frequency graphics finally verify that G2 arrested cells are undoubtedly devoided of INCs.

To sum up this set of experiments, we were able to classify four main groups of cells, which are described in table 12.

	Nuclear size	Nup153 location	FUCCI
Class 1	Big nuclei	NE	S and G_2
Class 2	Small and big nuclei	INCs and NE	G_1
Class 3	Small nuclei	INCs	Colorless (Early G_1 or G_0)
Class 4	Big nuclei	NE	Colorless (Early G_1 or G_0)

Table 12: Summary of the four nuclear phenotypes after HDAC inhibition according to the nuclear surface, Nup153 location, and FUCCI indicator signal. Although geminin-GFP is also expressed during the S phase, it must be reminded that this phase vanished after HDAC inhibition (Figure 39).

Class 3 cells were the only ones that undoubtedly present INCs. Unfortunately, this group of cells did not express FUCCI. As Cdt1-RFP is absent both in the early G1 and in the G0 phase, it is not possible to specify if these are arrested in the early G1 or expelled from cell cycle progression to the G0 phase. Instead, it remains clear that G2 cells do not present INCs inside their nuclei. In order to distinguish between early G1 and G0 cells, we decided to test for the presence or absence of Ki-67, a proliferation marker expressed in all dividing cells and consequently absent in G0 cells, which are quiescent or differentiating.

Taking advantage of this property of Ki-67, we immunolocalized this marker alongside the nucleoporin Tpr, both in control and 2 µM SAHA treated cells (Figure 43A). Images clearly showed that only Ki-67 positive nuclei presented INCs; meanwhile, Tpr remained located exclusively at the nuclear envelope in Ki-67 negative nuclei. This observation means that INCs are exclusively related to the G_1 phase, and especially at its early stages; on the other hand, it also indicates that the class 4 nuclei corresponded to cells arrested in the G_0 phase.

After observing several images, it seemed that Ki-67 negative cells were hard to find in control cells; instead, in SAHA treated ones, Ki-67 negative nuclei were more abundant. To confirm this tendency, we studied by cell cytometry the cell cycle of control, and HDAC inhibited cells. As conventional propidium iodide assisted cytometry does not allow to distinguish between G_0 and G_1 cells, we also immunodetected Ki-67 in the cell cytometry preparations. Every cell above the Ki-67 antibody background signal was considered to be in the G_1 phase (Figure 43B). Results demonstrate an increase of around 20% in the G_0 phase after SAHA treatment. This outcome could explain why the proportion of cells arrested in G_0/G_1 (around 65% assessed by conventional flow cytometry: Figure 41B) was barely higher than the INC positive nuclei population (around 50% in Figure 41C).

In the light of the presented data, INC formation is heavily dependent on cell cycle progression alteration caused by global HDAC inhibition. Accordingly, it is reasonable to question whether the cell cycle detention causes the formation of INCs by itself or if the HDAC inhibition is a needed condition. To answer this question, cells were exposed to

several well-known drugs to induce cell cycle arrest at different phases through different mechanisms.

L-Mimosine is a compound that stops cell cycle progression at the G_0/G_1 checkpoint after starting the DNA repair machinery as it is a DNA chelator. We also used mitomycin C to stop cell proliferation. Results summed at figure 44 demonstrate that, satisfyingly, none of the cell cultures exposed to these drugs presented INCs at their nuclei and none advisable nucleoporin distribution differences respect to controls could be observed. Remarkably, despite the shared similarities between G_0/G_1 arrested population percentages on SAHA and L-mimosine treated cells, INCs only showed up in the first case.

Therefore, independently of its relation to the G_1 phase, INCs are only visible after global HDAC inhibition.

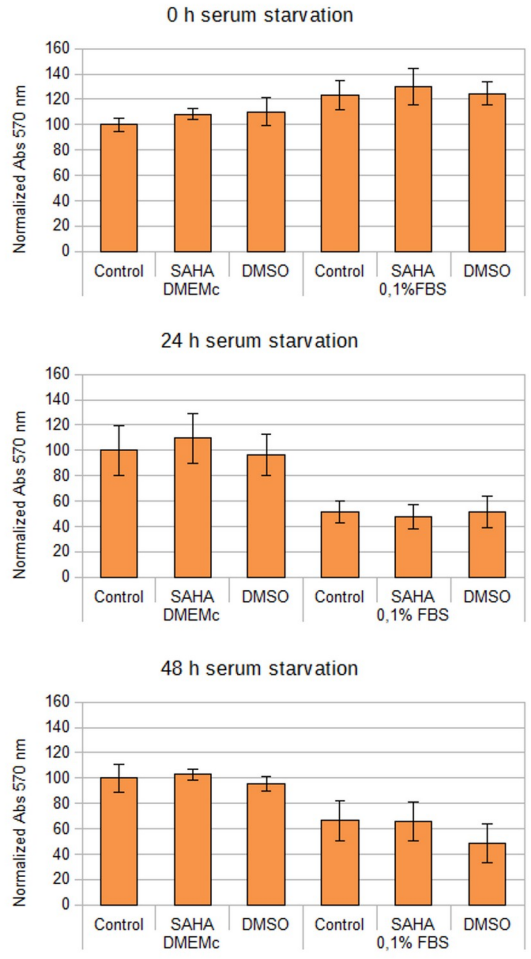

0 h serum starvation		DMEMc			0,1% FBS		
Tamhane test		Control	SAHA	DMSO	Control	SAHA	DMSO
DMEMc	Control		0,046	0,394	1,000	0,005	0,002
	SAHA	0,046		1,000	1,000	0,044	0,035
	DMSO	0,394	1,000		1,000	0,102	0,191
0,1% FBS	Control	1,000	1,000	1,000		0,977	0,998
	SAHA	0,005	0,044	0,102	0,977		0,999
	DMSO	0,002	0,035	0,191	0,998	0,999	

24 h serum starvation		DMEMc			0,1% FBS		
Tamhane test		Control	SAHA	DMSO	Control	SAHA	DMSO
DMEMc	Control		0,998	1,000	0,001	0,000	0,000
	SAHA	0,998		0,942	0,000	0,000	0,000
	DMSO	1,000	0,942		0,000	0,000	0,000
0,1% FBS	Control	0,001	0,000	0,000		0,830	1,000
	SAHA	0,000	0,000	0,000	0,830		0,931
	DMSO	0,000	0,000	0,000	1,000	0,931	

48 h serum starvation		DMEMc			0,1% FBS		
Bonferroni test		Control	SAHA	DMSO	Control	SAHA	DMSO
DMEMc	Control		1,000	1,000	0,000	0,000	0,000
	SAHA	1,000		1,000	0,000	0,000	0,000
	DMSO	1,000	1,000		0,000	0,000	0,000
0,1% FBS	Control	0,000	0,000	0,000		1,000	0,000
	SAHA	0,000	0,000	0,000	1,000		0,001
	DMSO	0,000	0,000	0,000	0,000	0,001	

Figure 38: *Effect of the SAHA inhibitor (1,5 μM) on cell proliferation measured by MTT assays. On the left, the graphics show the normalized absorbance at 570 nm with the corresponding standard errors on each treatment. On the right, results of Tamhane (equal variances not assumed) and Bonferroni (equal variances assumed) ANOVA posthoc test between the compared treatments. Shadowed numbers indicate statistical significance ($\alpha \leq 0,05$)*

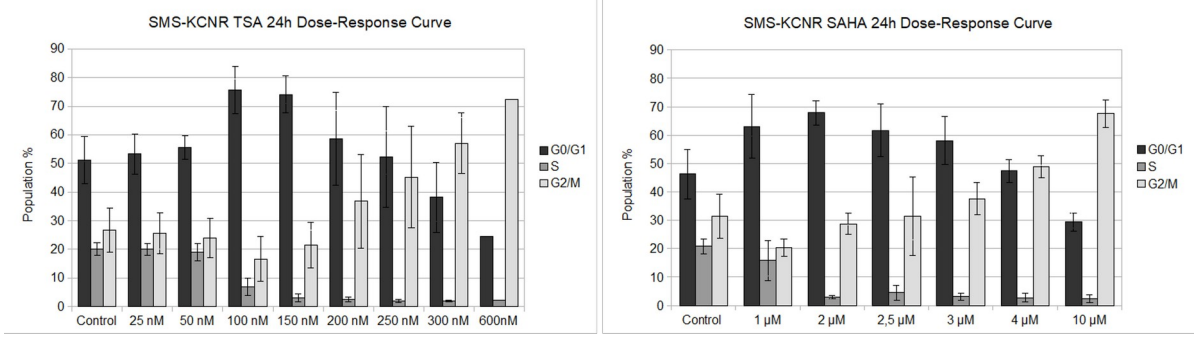

Figure 39: *Dose-response curves in cell cycle analysis by flow cytometry of the HDAC inhibitors TSA and SAHA. Both inhibitors have a similar behavior: once a minimum concentration is overcome, both drugs exerted a blockade of the cell cycle progression in the G_0/G_1 phase when delivered at low doses (TSA 100 nM and SAHA 2 µM). When cells were exposed to higher concentrations, they were progressively arrested in the phase G_2/M. In all cases, the S phase remains virtually missed.*

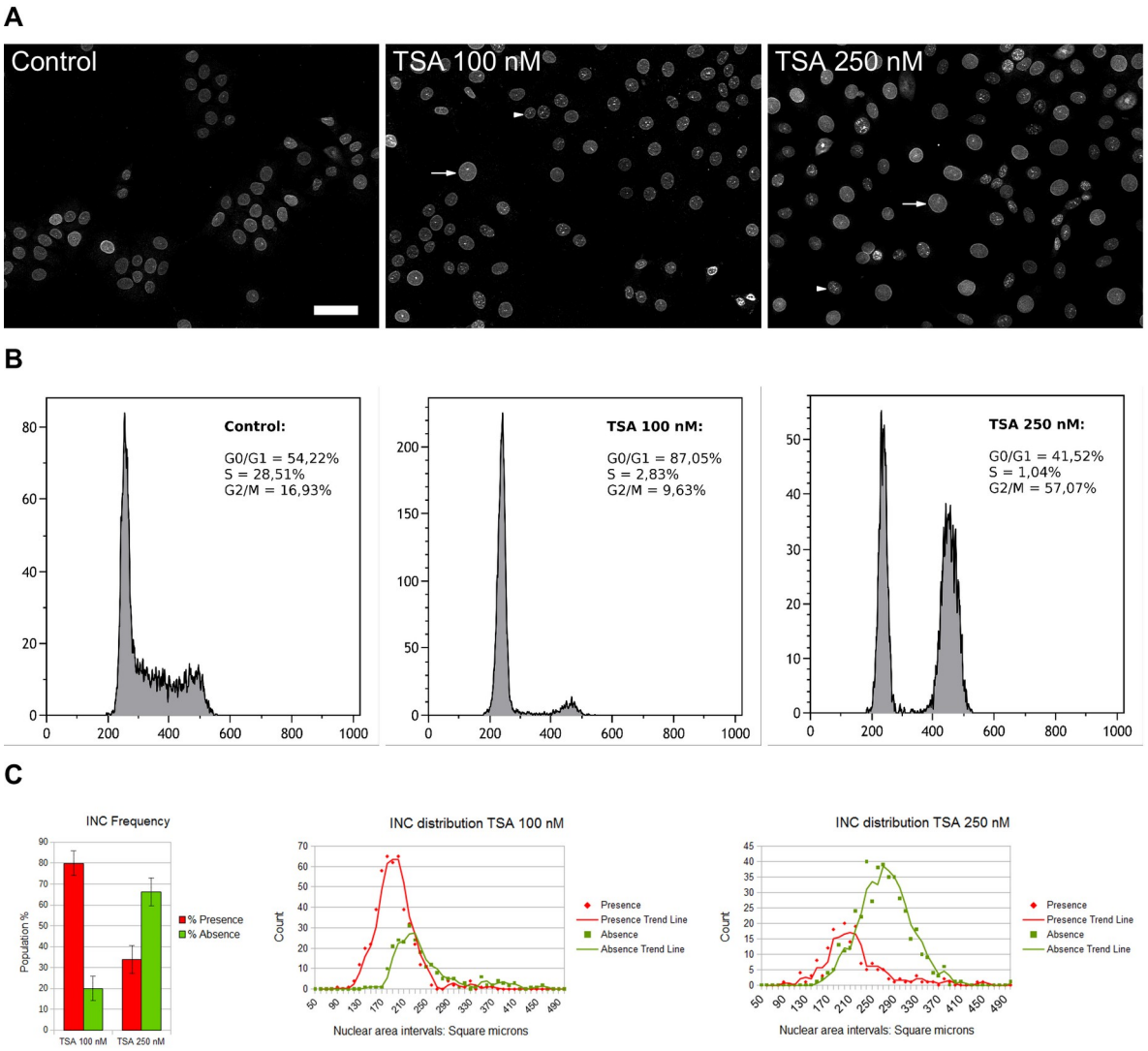

Figure 40: *Quantification of cells showing INCs and their association with cell cycle status and nuclear size. TSA treatment, 24 hours. (A) Representative images of confocal microscopy in which two types of nuclei can be seen: small ones in which Nup153 accumulates in the INCs (arrowheads), and a second larger population where Nup153 was only in the nuclear envelope (arrows). Scale bar: 50 µm. (B) Cell cycle analysis by flow cytometry shows that 100 nM TSA for 24 h blocks cells at the G0/G1 phase, whereas a higher concentration (250 nM) additionally blocks cells at the G2/M phase. Y-axis: cell count. X-axis: propidium iodide fluorescence intensity. (C) Calculation of the percentage of nuclei showing INCs after exposure to 100 nM or 250 nM TSA. Frequency histograms showing the distribution of nuclear size for each individual cell in relation to the presence or absence of INCs after TSA exposure for 24 h (n = 717 nuclei for 100 nM TSA; n = 595 nuclei for 250 nM TSA).*

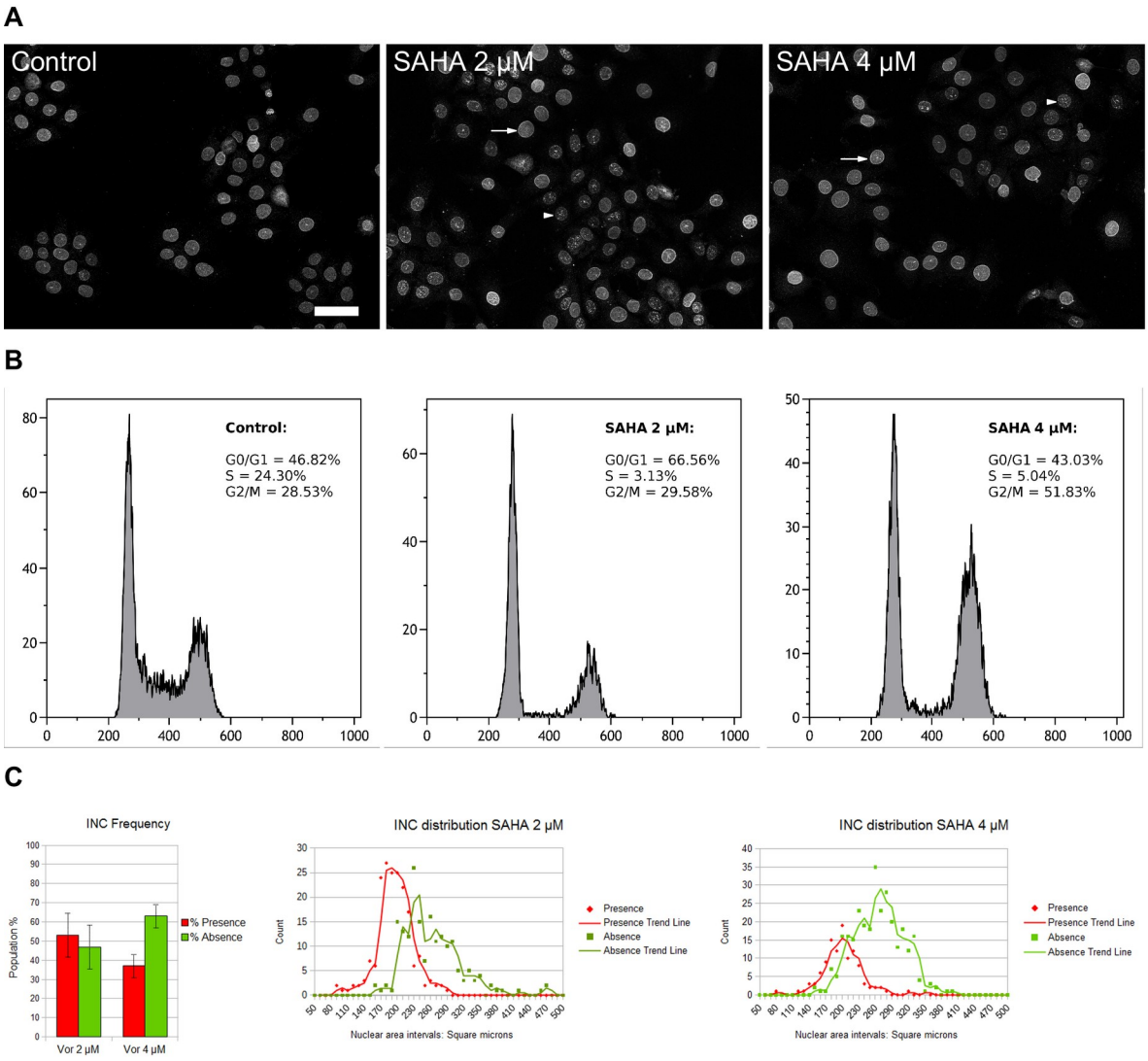

Figure 41: *Quantification of cells showing INCs and their association with cell cycle status and nuclear size. SAHA treatment, 24 hours. (A) Representative images of confocal microscopy in which two types of nuclei can be seen: small ones in which Nup153 accumulates in the INCs (arrowheads), and a second larger population where Nup153 was only in the nuclear envelope (arrows). Scale bar: 50 µm. (B) Cell cycle analysis by flow cytometry shows that 2 µM SAHA for 24 h blocks cells at the G_0/G_1 phase, whereas a higher concentration (4 µM) additionally blocks cells at the G_2/M phase. Y-axis: cell count. X-axis: propidium iodide fluorescence intensity. (C) Calculation of the percentage of nuclei showing INCs after exposure to 2 µM or 4 µM SAHA. Frequency histograms showing the distribution of nuclear size for each individual cell in relation to the presence or absence of INCs after SAHA exposure for 24 h (n = 815 nuclei for 2 µM SAHA; n = 882 nuclei for 4 µM SAHA).*

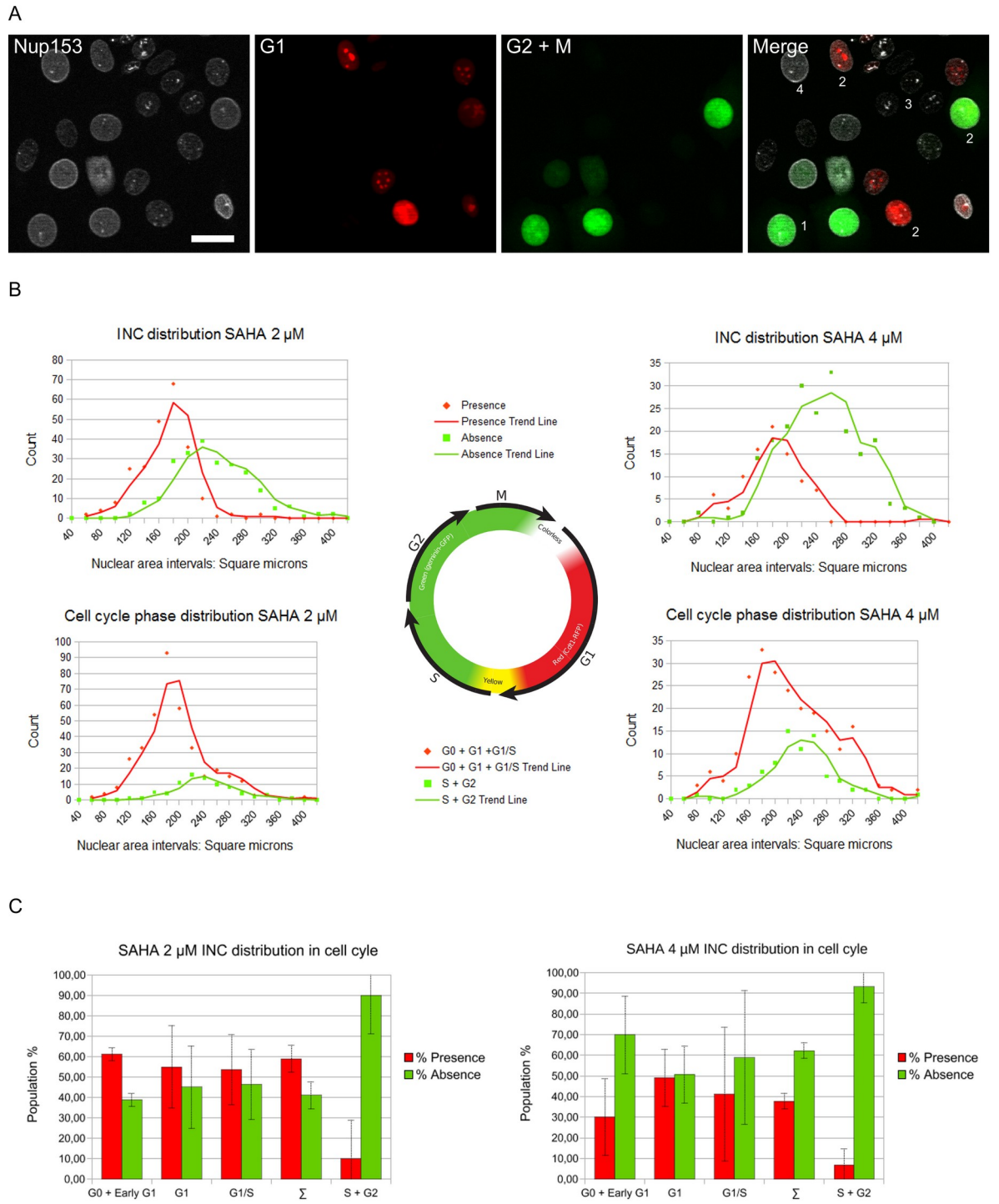

Figure 42: *Presence or absence of INCs in relation to the nuclear size and the phase of the cell cycle after treatment with an HDAC inhibitor. FUCCI transfected cells were treated with a low (2 µM) or high (4 µM) concentration of SAHA and immunostained for Nup153. The red construct (Cdt1-RFP) is expressed only in cells in the and G_1 phase of the cell cycle, whereas the green construct (Geminin-EGFP) is present during the S, G_2 and M phases of the cell cycle. Colorless nuclei correspond to cells in early G_1, which are starting to synthesize Cdt1-RFP; and also to G_0 where none of both constructs are expressed. Yellow nuclei belong to cells at the G_1/S transition, when Cdt1-RFP is starting to be degraded while Geminin-EGFP is being synthesized (A). Representative field of FUCCI transfected cells after fixation and immunodetection of Nup153 with Cy5 fluorescence. The numbers inside the merged image correspond to the cell class according to the classification in table 12. Scale bar: 25 µm. (B) Frequency histograms displaying the proportion of cells containing INCs in relation to their nuclear size or their phase of the cell cycle. (C) Percentage of cells at each phase of the cell cycle and presence or absence of INCs after exposure to a low or high concentration of SAHA. Σ refers to the combination of early G_1, G_0+G_1, and G_1/S FUCCI indicators*

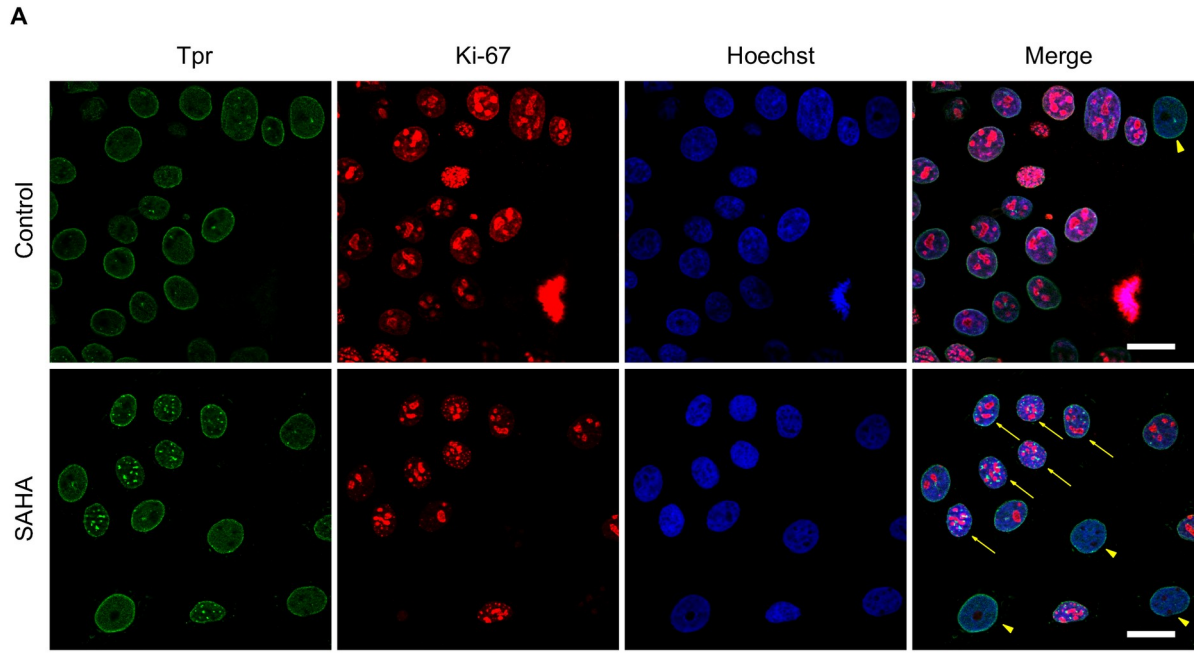

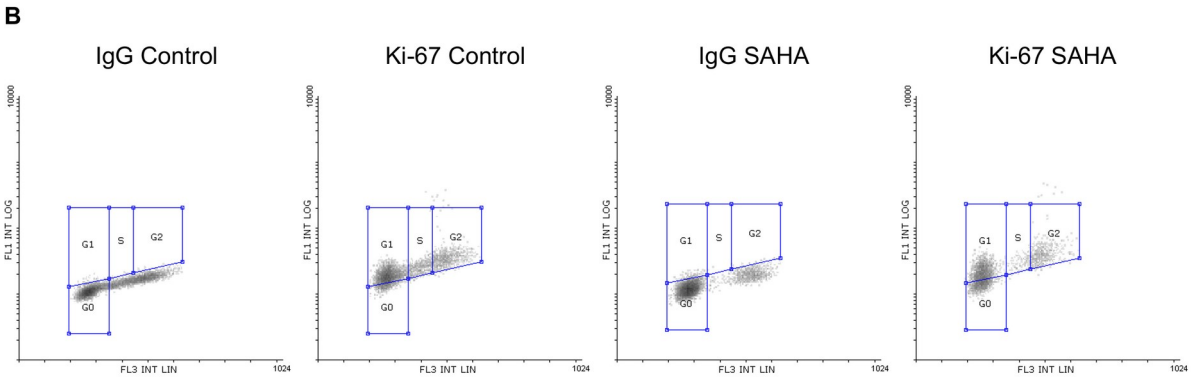

C

Control	% of Vis	Desvest (n=3)
G0	11,29	8,56
G1	49,00	9,76
S	12,18	3,22
G2/M	23,51	1,34

SAHA	% of Vis	Desvest (n=3)
G0	32,03	7,88
G1	44,94	6,35
S	3,38	1,56
G2/M	16,19	3,15

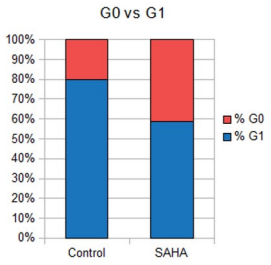

Figure 43: *SAHA partially promotes a quiescent state in some cells whose nuclei are absent of INCs. INCs are excluded from quiescent cells (Ki-67 negative cells). (A) Representative fields of double immunolocalization experiments of Tpr and Ki-67 on control and HDAC inhibited cells (24 hours SAHA 1,5 µM). After HDAC inhibition, INCs are formed in a subset of nuclei which always co-express Ki-67. By the other side, when Ki-67 was absent, (arrowheads) we never were able to detect INC formations, and Tpr signal was excluded from the nuclear envelope. Scale bar: 20 µm. (B) Ki-67 expression addressed through flow cytometry. Y-Axis: logarithmic fluorescence signal coming from Ki-67. X-Axis: Linear fluorescence intensity proceeding from DNA staining through propidium iodide. Fluorescence signal incoming from non-specific IgGs was considered as a negative Ki-67 signal, and thus, every cell gated inside, classified as G_0. Every cell above the non-specific IgG signal will be considered as positive for Ki-67 and thus present in the cell cycle. (C) Mean population percentages from 3 independent Cell cycle analysis. SAHA increases the proportion of G_0 arrested cells by 20%. The graphic in the right illustrates the G_0 increase when gating only G_0 and G_1.*

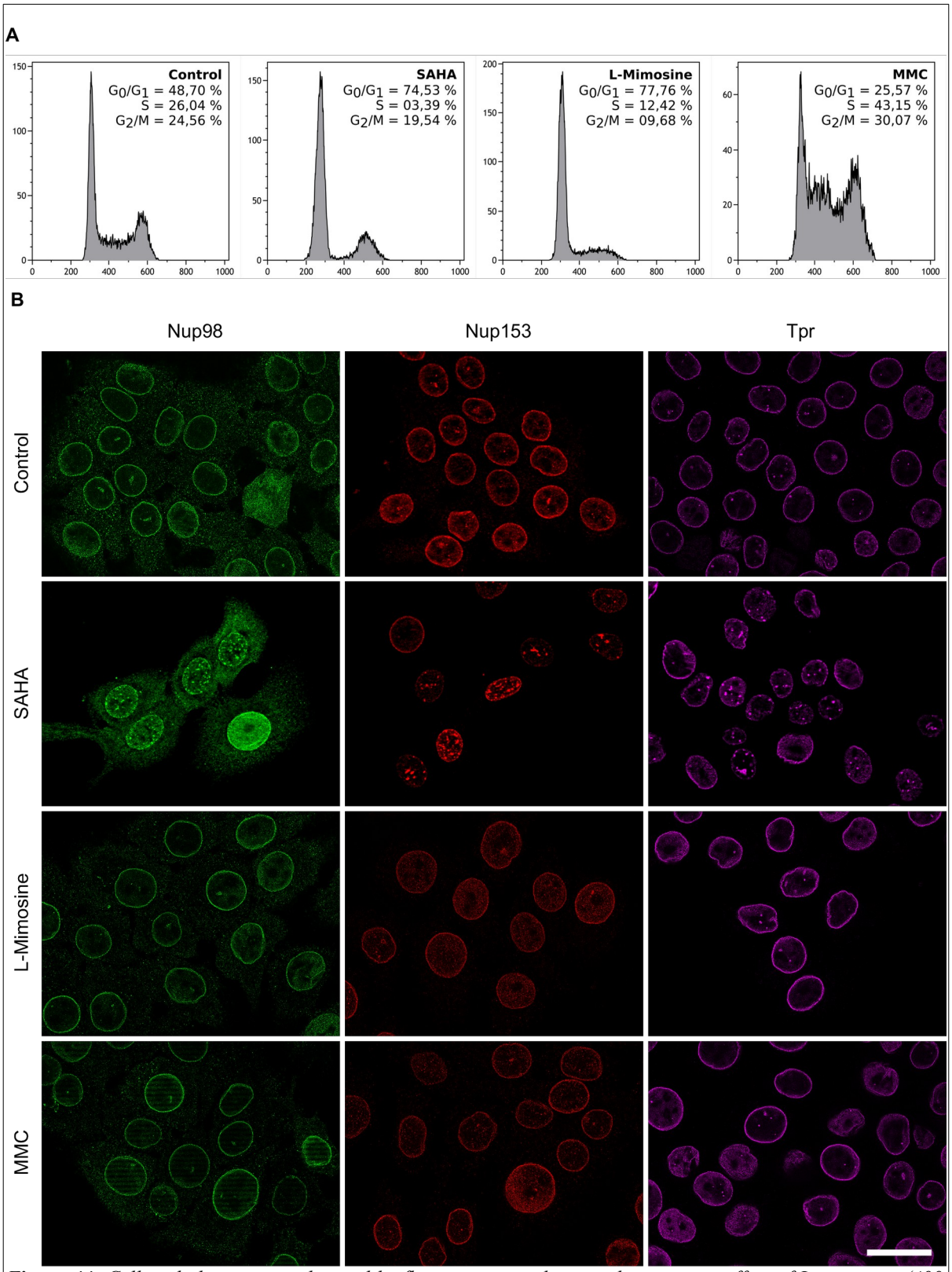

***Figure 44**: Cell cycle histograms obtained by flow cytometry showing the arresting effect of L-mimosine (400 µM) and mitomycin C (MMC; 10 µg/mL) when compared to control and SAHA (1,5 µM) treated cells. The population percentages are shown framed in each histogram. Y-axis: cell frequency. X-axis: propidium iodide fluorescence intensity. (B) Immunolocalization of Nup98, Nup153 and Tpr demonstrated that these set of nucleoporins only accumulated at the nuclear interior after SAHA treatment. Scale bar 30 µm.*

5.5 Nuclear basket proteins are accumulated after 12 hours of HDAC inhibition.

As demonstrated in the previous chapter, INCs are only present at the G_1 phase; and more precisely, in its early stages. Furthermore, all our studies were made after 24 hours of incubation with the HDAC inhibitors. For a better insight into cell cycle progression and its impact on INC formation, we decided to study the events that took place before the 24 hours of HDAC inhibitor incubation (Figure 45).

First, we analyzed the cell cycle progression several times: 1 hour after treatment, after 8 hours, 12, 16, and 24 hours. After cell cytometry-assisted cell cycle analysis (Figure 45A), we managed to unravel how the different phases progressed until the 24 hours scenario. Control and SAHA treated cells were seeded at the same time and were obtained from the same culture. First, control cells demonstrate that the population passing through the S phase is constant, while the G0/G1 and G2/M ones were inverse to each other, suggesting that the replication rate of the SMS-KCNR cells is around 16 hours.

In the first events of HDAC inhibition (after 1 hour), no distinguishable cell cycle alterations were detected. Likewise, we were not able to detect any difference in the nucleoporin levels between the control and SAHA treated cells right after the start of the treatment, although HDAC inhibition was effective, as acetyl histone 3 (AcH3) was overexpressed (Figure 45B). In the same way, all the Tpr signal proceeded from the nuclear envelope, and we were unable to detect any INCs (Figure 45C).

After the progression of 8 hours, the SAHA treatment broke the normal cell cycle progression, evinced by a slowdown of the mitosis and the G_2 phase, which caused a deficit of around 10% at the G_0/G_1 phase in respect to the control counterpart. Also, cells that were progressing through the G_1 phase at the beginning of the HDAC inhibition managed to pass through the S phase and consequently causing a slight increase.

The slowdown of the G_2 phase and the mitosis was especially acute after 12 hours, overcoming the rest of the phases. As there are not so many dividing cells, the cell income to the G_0/G_1 phase decreases and its population drops, which is contributed as well because some cells in the G_1 managed to pass to the S phase; because otherwise, the S phase would have suffered a considerable decrease. It is of special interest that in this context, there is an excess of the nuclear basket nucleoporins Tpr and Nup153 (Figure 45B). Nup93 and Nup98 were also slightly overexpressed, while P62 remained undaunted. At the same time, the first INCs of Tpr arose inside the nucleus (arrowheads Figure 45C).

Once completed the 16 hours, it became clear the collapse of the S phase, caused by the interruption of the cell income from the G_1 phase, anticipating the sharp G_1 arrest observed after 24 hours. Regarding the G_2 population, these kept slowly overcoming its delay, completing the mitosis while progressing until 24 hours when the majority of the culture was stuck at the G_0/G_1 phase. As expected, elapsed 24 hours, numerous nuclei presented

intranuclear accumulations of Tpr (Figure 45C). It is worthy of mention that the nucleoporins Tpr and Nup153, overexpressed during 12 hours of SAHA treatment, returned to levels equal to the control, even though the chromatin hyperacetylation exerted by SAHA persisted (Figure 45B).

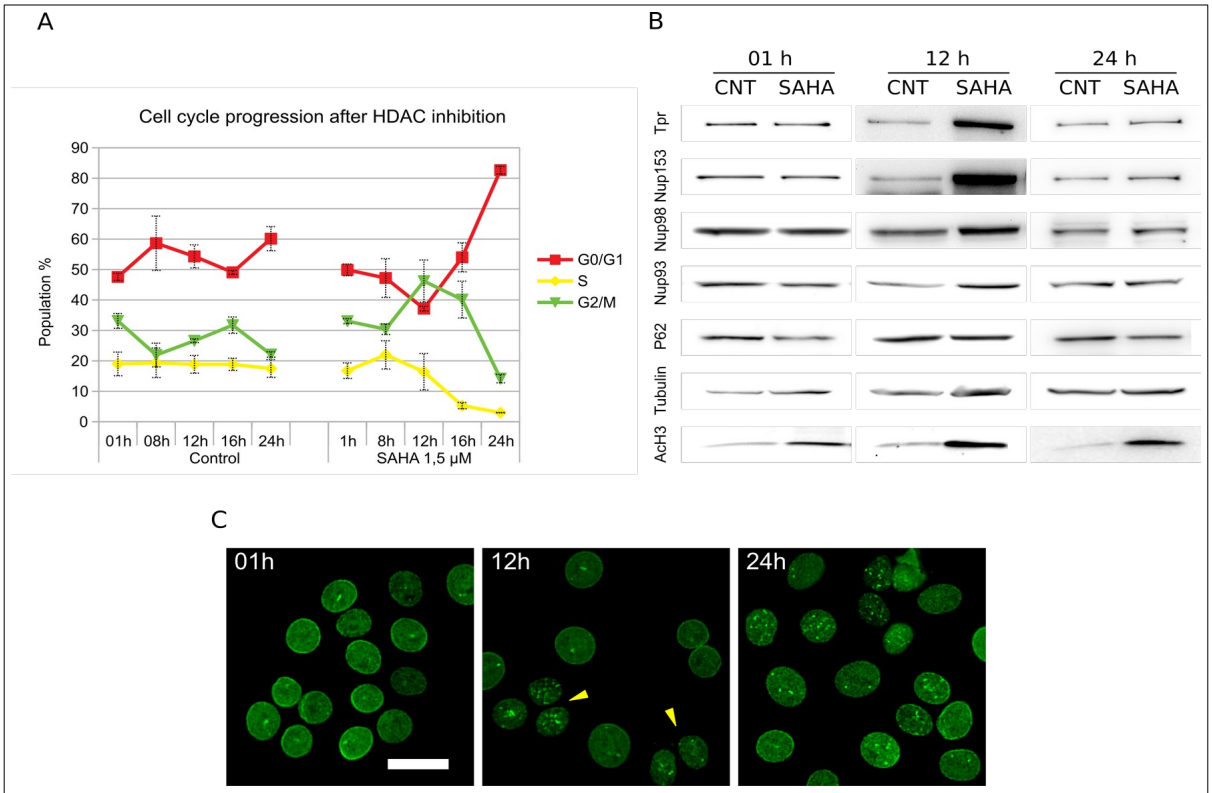

Figure 45: *INC formation and nucleoporin expression variate along cell cycle progression after HDAC inhibition. (A) Distribution of the cell culture according to its cell cycle phase studied at 1; 8; 12; 16; and 24 hours after the start of the experiment, in control and 1.5 µM SAHA treated cells. It is worth noting the sharp fall of the S phase after 8 hours of treatment and the accumulation of cells in G_2 at 12 hours, after which, disappears together with the S phase. (B) Analysis of the expression of nucleoporins by western blot after 1; 12 and 24 hours of the experiment. In all times studied, the acetyl histone 3 (AcH3) epigenetic hallmark suffers an overexpression, proving the effectiveness of the SAHA treatment, causing chromatin hyperacetylation by inhibiting the HDACs. (C) Immunolocalization of Tpr in cells exposed to 1.5 µM SAHA for 1; 12 and 24 hours. The arrowheads indicate the presence of INCs after 12 hours of treatment. Scale bar: 20 µm*

6 DISCUSSION

In this work, we have described the appearance of intranuclear accumulations of nucleoporins related to the nuclear basket after the inhibition of histone deacetylases. These groupings, which we have referred to as Intranuclear Nup Clusters (INCs), do not bear similarity to other nuclear substructures described in the current scientific literature, and they behave in a cell cycle-dependent manner. Specifically, they are closely associated with the G1 phase after mitosis. This chapter will contextualize these findings in relation to the current knowledge available on nucleus biology.

6.1 About INC composition.

First, INCs appear to be preferentially made up of nuclear basket-related nucleoporins. Tpr and Nup153 are the main components of this region of the NPC, in conjunction with the soluble nucleoporin Nup50. The third nucleoporin present in the aggregates, Nup98, on the contrary, is located halfway between the inner ring and the nuclear and cytoplasmic rings of the NPC.

These three nucleoporins share an architectural vocation within the nucleus independent of transport, establishing extensive chromatin contacts. However, these connections are pretty diverse. Nup153 and Nup98 recognize the regulatory regions of a various set of genes, preferentially related to embryonic development, as mentioned in the introduction (Sections 1.2.3.4, and 1.2.3.5). Tpr also sustains nuclear architecture by establishing heterochromatin-free channels in the pore complex vicinity. All this nucleoporin-chromatin play is, of course, naturally dependent on histone modifications. Chromatin unfolding caused by experimentally induced hyperacetylation after HDAC inhibition would surely disrupt the current Nup-chromatin connection; We will briefly discuss the implications of the mentioned alterations.

After HDAC inhibition, additional accessible promoters and enhancers would significantly increase their affinity for the nuclear basket nucleoporins. However, due to spatial restrictions, not all of them could be relocated towards the pore, so the intended interaction would necessarily occur in the nuclear interior far away from the nuclear envelope. Thus, the high demand for Nup153, Nup98, or Tpr in the newly opened regions could imply the sequestration of these at the mentioned genomic domains, causing the INC formation. Some of our results, such as the notable decrease in the soluble portion of Nup153-EGFP both in the nuclear envelope and in the INCs (Figure 33) in favor of its stable subpopulation (supposedly linked to hyperacetylated enhancers), would favor this interpretation. Likewise, the reduction of the density of Tpr in the nuclear envelope, but not of the number of nuclear

pore complexes (Figure 30 and 31), would support the nuclear interior sequestration hypothesis to the detriment of the NPC-bound population.

Other researchers have already verified that the hyperacetylation of chromatin induced by HDACis indeed triggers chromatin decompression and promoter outcrops (Brown et al., 2008). In the aforementioned study, Brown and collaborators studied the central ring nucleoporin Nup93-bound domains through chromatin immunoprecipitation. Exposing HeLa cells to the HDACs inhibitor trichostatin A showed that newly acetylated histones were relocated towards the nuclear pore complex by binding to Nup93. Hence, they described a reorganization of acetylated regions to the NPCs. In future experiments, it would be exciting to carry out the same test by substituting Nup93 for any of the Nups detected in the INCs: Nup153, Nup98, or Tpr.

Additionally, in this study, the authors did not report the appearance of any intranuclear accumulation of Nup93; and it is that, in the light of the data that we have been able to collect at the present work, it seems that **only peripheral dynamic nucleoporins can aggregate at the nuclear interior after HDAC inhibition.** As Brown and cols demonstrate, Nup93 does not appear at INCs after TSA treatment. Nup93 is an inner ring nucleoporin with slow dissociation dynamics, so it is not surprising that it remained at the NPC after TSA treatment. Similarly, in our immunofluorescence studies, P62 was absent at INCs and stayed at NPC after HDAC inhibition (Figures 22, 23, and 24). P62, just like Nup93, cannot be considered a dynamic nucleoporin despite its slightly faster kinetics (Rabut et al., 2004). In this way, it seems that only true nucleoplasmic nucleoporins can relocate within the nuclear interior at the described aggregates.

These deductions are mainly based on high-resolution immunocytochemistry confocal microscopy. While it is possible that INCs could be the outcome of any fixation artifact or antibody nonspecificity, we do not think that to be the case for several reasons:

- The direct observation in live-cell microscopy of Nup153-EGFP clustering in the nuclear interior after HDAC inhibition (Figure 20 C) demonstrated that INCs are not fixation artifacts. Reversely, immunocytochemistry confocal microscopy discarded the possibility of an overexpression-driven inclusion body.
- The preservation of the localization of these Nups in microscopy samples was confirmed by analyzing the discrete distribution differences of several NPCs components via super-resolution microscopy (Figure 22). Through this means, we detected that the nuclear basket nucleoporin Tpr was located at a more profound distance beneath the central channel than the nucleoporin P62, as expected.

In contrast to its NPC counterparts (Figure 22), the nucleoporins contained within the INCs do not appear to be organized through a defined distribution or based on any observable pattern (Figure 21B). In any case, based on what we know regarding the interaction between the nucleoporins in the basket, we cannot expect to see large differences by confocal

microscopy as Tpr and Nup153 are directly associated (Hase & Cordes, 2003). Likewise, Nup98, although apparently less abundant in the INCs than its other two partners, is also a close associate of Tpr (Fontoura et al., 2001), which mirrors the problem of insufficient resolution needed to discern the architecture of the INCs. In order to deepen into their possible interaction at the INCs, It would be interesting to perform future studies by using FRET (Fröster Resonance Energy Transfer) or double immunoelectron microscopy experiments.

6.1.1 Nucleoskeletal nature of INCs.

Previous experiments performed in germinal vesicles of *Xenopus laevis* demonstrated how the nucleoli maintained remarkable contacts with the pore complexes through the pore-linked filaments (Andrade et al., 2001; Arlucea et al., 1998; Kiseleva, Drummond, et al., 2004). These pore-linked filaments could be partially composed of nucleoporins and other nucleoskeletal molecules such as nuclear actin and protein 4.1. Although such structures have not yet been observed in mammalian cells, we hoped to unravel PLF-like structures between the nucleoli of SMS-KCNR cells and its characteristic nuclear invagination, given the tight junction witnessed between both (Figure 19). Unfortunately, this seemed not to be the case, as we did not discern any appreciable difference in nuclear morphology after HDAC inhibition (Figure 26 and 27).

The INCs were related neither to the nuclear envelope nor to the invagination itself; and in fact, with special independence of the latter. As one can understand from figure 24, the invaginations are richly populated with pore complexes, as revealed by the P62 labeling. However, Tpr is depleted at this invagination in control and SAHA treated cells. Moreover, in the opposite trend, P62 is absent from the INCs. It should be noted that the densely P62 populated invagination remains very close to the nucleoli, attested by the exclusion of the DNA probe Hoechst 33342, and as stated by previous investigators (Fricker et al., 1997; Legartová et al., 2013). Such an interpretation is coherent considering a publication reporting basket-absent NPCs embedded within the nucleoli-associated invaginations (Galy et al., 2004). This last nuance would be an interesting appreciation, considering that NPCs of nucleoli independent invaginations are populated with Tpr (Figure 23A), conforming a functional heterochromatin exclusion zone beneath the pore, as illustrated in the pore of the nucleoli independent invagination from figure 26 (top left). From a functional perspective, this makes perfect sense, as Tpr is considered a docking protein for the transport machinery as the Tpr lattice supports its guidance and enhances its affinity for central channel nucleoporins (Coyle et al., 2011; Rajanala & Nandicoori, 2012; Umlauf et al., 2013). Opposingly, the invagination would promote direct interaction between the inner pore complex and the exported material coming from nucleoli, where the long filaments composed by Tpr could result as an unnecessary topological disturbance or barrier. This latter

suggestion is in accordance with previous reports from wild-type yeast cells, where Tpr's ortholog Mlp1/2 was absent from NPCs placed near the nucleolus (Galy et al., 2004).

In order to be able to assert with certain guarantees the independence between the INCs and the nuclear envelope, we carried out a series of additional experiments. Figure 25 sums that nuclear membranes, unraveled by concanavalin A reactivity, are utterly absent at INCs. Transmembrane nucleoporin Gp210 is the only nucleoporin reactive to concanavalin A as it is thoroughly post-translationally modified with high-mannose type oligosaccharides. Taking into account this characteristic from Gp210 nucleoporin, we can assert that INCs are independent of membrane-bound NPCs as we could not observe any concanavalin-A staining at the INCs.

Transmission electron microscopy did not reveal any unusual intranuclear organelle nor any nuclear membrane deformation. This fact surprised us greatly, as the strong flaring fluorescence signal coming from nucleoporins placed at INCs (Figure 20C, 23) led us to speculate that they would shape an observable TEM structure. However, Nup153 immunodetection on TEM sections revealed discrete intranuclear accumulations of this nucleoporin placed both near and far away from the nuclear envelope (Figure 27). Although immuno-TEM preparations may not be best suited for structural observations, we did not detect any remarkable organelle-like disposition at the INCs, but anti-Nup153 gold conjugated antibodies were usually placed between the electron-dense chromatin zones.

Despite the fact that the aforementioned results favor that the nuclear envelope architecture is mostly unaffected by HDAC inhibition, endogenous lamin A/C staining (Figure 28) suggests the contrary. Thus, SAHA treatment triggered the redistribution of lamin A/C signal from the nuclear rim towards the nuclear interior, in what seemed as a homogeneous intranuclear pattern. This Lamin A/C redistribution is not surprising, as HDAC inhibition is known to disarrange the lamin associated chromatin domains, which could trigger nuclear envelope modifications (Schoen et al., 2017). Accordingly, previous observations have described that the HDAC inhibitor TSA disbanded heterochromatin associated with the nuclear envelope and promoted the A-type lamin invaginations towards the nuclear interior (Galiová et al., 2008; Legartová et al., 2013). On the contrary, in our experience, lamin A/C staining did not appear to unravel further nuclear invaginations but, instead, was redistributed uniformly throughout the nuclear interior. Significantly, lamin A/C did not accumulate near Nup153 intranuclear aggregates, despite its known interaction at the NPC in normal conditions (Al-Haboubi et al., 2011). Both lamin A and lamin B are close partners to Nup153 and Tpr, up to the point where the nuclear lamin meshwork is responsible for evenly distributing NPCs throughout the nuclear envelope (Fišerová et al., 2019; Fiserova & Goldberg, 2010; Guo & Zheng, 2015). Given the interdependence of the nuclear lamina and the two major constituents of the nuclear basket, we are surprised about the nuclear envelope's integrity after such an obvious redistribution of both Nup153 and Tpr towards the intranuclear INCs. This imbalance is probably corrected by other INM integral proteins, which are also

responsible for maintaining nuclear envelope integrity (Galiová et al., 2008). However, we must take into consideration that the intranuclear diffusion of lamin A/C is not in conflict with the persistence of a considerable portion of this intermediate filament at the nuclear envelope. In the same manner, we missed how HDAC inhibition would affect lamin B, though likely to be also disordered.

During immunolocalization experiments, we realized that the presence of Nup98, Nup153, and Tpr at the nuclear envelope was vastly diminished after INC formation in favor of the latter ones (Figures 20, 23, and 30). Oppositely, P62 seemed unscathed to this phenomenon, and, as our nuclear envelope-associated Tpr and P62 spot counting reveals, a significant proportion of NPCs are basket-depleted after INC formation (Figure 31). According to this, the NPC number is not significantly reduced, nor are they randomly arranged throughout the nuclear envelope, which is surprising, due to NPC dependency on basket nucleoporins for its anchorage to the nuclear lamina, despite the mentioned lamin A/C mesh disorganization.

The lack of a considerable portion of nuclear basket elements at the NPCs after INC formation could explain at some degree the observed lamin A/C intranuclear homogeneous distribution, as Nup153 effect on the nuclear envelope architecture is well reported (Mészáros et al., 2015). For example, Nup153 silencing by RNA interference RNA technology caused severe alteration of lamin localization (Zhou & Panté, 2010). We are well aware that our results are not comparable to a complete Nup153 silencing, despite its severe depletion at the NPCs followed by INC arousal. Thus, we suggest that the preservation of a minimal number of basket-positive NPCs could be enough to some degree for the sustainment of the nuclear envelope's architecture.

The homogeneous distribution of the pore complexes is dependent on the balanced distribution of Lamina A and B by the nuclear envelope. This dependency has been demonstrated by the so-called pore-free-islands, broad areas of the envelope that do not have NPCs. These areas are predominantly populated by lamin A and emerin, while lamin B and LBR are practically non-existent (Imamoto & Funakoshi, 2012). Our immunolocalization results demonstrated the homogeneous distribution of p62 and proved that the NPCs were equitably distributed through the nuclear envelope before and after HDAC inhibition. This observation, combined with the fact that lamin A/C was also evenly distributed at the nuclear envelope (Figures 28 and 31), prompts us to speculate that although NPCs are mostly basket depleted, some of these still preserve a minimum but enough amounts of Tpr or Nup153 in order to avoid the formation of pore-free-islands.

Paradoxically, overexpression of full-length Nup153 constructs mirrors the altered nuclear envelope architecture seen after Nup153 silencing. Among the most prominent modifications, we can notice intranuclear projections of membrane foldings and the formation of inclusion bodies (Bastos et al., 1996). To avoid the overexpression drawbacks, we took great care in our live-imaging experiments to not confound inclusion bodies and membrane folding with INCs. We are reasonably confident that INCs do not correspond with such aberrancies as

INCs are usually rice-shaped and are not correlated with increased endogenous nucleoporin levels (Figure 45), while inclusion bodies are rounded structures caused by undoubted upregulation. Furthermore, concanavalin-A staining, electron microscopy images, and P62 vs INC and lamin A/C vs INC colocalization experiments (Figures 23, 24, 25, 26, 27, and 28), strongly suggest that intranuclear nucleoporin clusters are independent of both the nuclear envelope and nuclear lamina.

At this point, the evidence we handle on INCs suggests that the nucleoporins that compose them are independent of their counterparts bound in the pore complex. As nucleoporins are formerly supposed components of the nucleoskeleton, we intended to study these structures from a dynamic and structural perspective. Accordingly, we tested the structural integrity of the INCs submitting cells to mild non-ionic detergent extraction prior to immunolocalization of Nup153. In this matter, results clearly showed that INCs were detergent-resistant, which reveals that INC-associated nucleoporins are, to some degree, stable structures, or at least, as stable as their NPC counterparts (Figure 32). Initially, we tried to replicate nuclear matrix-like preparations, but technical difficulties impeded us from replicating the high-salt extractions, numerous washes, and DNAse incubation without significant sample loss. Furthermore, we dismissed this course as results obtained from these techniques are often prone to artifactual formations (Razin et al., 2014).

Fluorescence Recovery After Photobleaching (FRAP) is considered a gold standard for the study of the dynamics of a particular protein. Accordingly, we performed FRAP experiments in SMS-KCNR cells stably transfected with the full-length Nup153-EGFP fusion protein. Great care was taken during the cloning steps in order to select cells expressing low quantities of the construct and avoid the aforementioned drawbacks of Nup153 ectopic expression (Bastos et al., 1996). In control cells (Figure 33), recovery rates followed biexponential dynamics and fast recovery rates in concordance with previous studies suggesting two Nup153 populations: one nucleoplasmic and another bound to the NPC; the latter surely needed for Tpr anchorage to the NPC (Daigle et al., 2001; Griffis et al., 2004; Hase & Cordes, 2003; Rabut et al., 2004). However, after HDAC inhibition, the recovery of Nup153 was significantly reduced both at the nuclear envelope and at the INCs, which favored the idea of Nup153 soluble fraction sequestration and suggesting an indistinctive relationship between Nup153 at the INC and at the NPC. This observation deserves special attention precisely during the first five seconds after bleaching when the characteristically fast Nup153 recovery is completely absent after HDACi treatment. Although we did not perform FRAP experiments with a Nup98-EGFP construct, we adventure to hypothesize that the dynamics of Nup98 would also be reduced as it shares similar diffusion rates and transcription dependency with Nup153 (Griffis et al., 2002, 2004). On the contrary, Tpr, the third detected nucleoporin at the INCs, is a very stable nucleoporin with not known nucleoplasmic soluble fraction. We suggest that Tpr would display similar recovery rates at

the NPC and the INCs, similar to Nup153 but with lower recovery rates (Griffis et al., 2004; Souquet et al., 2018).

The mentioned diffusion slowdown has been previously observed, with more severe outcomes, both in Nup98 and Nup153 FRAP experiments after transcription inhibition using actinomycin D, a well-known RNA polymerase I and II disruptor (Griffis et al., 2004). We wondered whether the global transcriptional activity was perturbed by any means after HDAC inhibition and the consequential chromatin opening. As Figure 29 illustrates, active transcription sites revealed by serine-5 phosphorylated RNA polymerase II are not apparently related to Nup153 unraveled INCs. We are well aware that this does not mean any implications regarding transcription related functions for Nup98 or Nup153, as many additional experiments would be needed for such a claim. However, we considered it worth the effort to check if INC arose after Nup153 accumulation at transcription factories, especially after HDACi-induced chromatin hyperacetylation. Similar to what happened with transcription factories, we could not report any relation between INCs and replication foci unraveled by PCNA (Chagin et al., 2016).

Nucleoporin clustering at the nuclear interior could be a consequence of the concentration of strongly Nup-binding regions that emerged after chromatin unfolding exerted by HDAC inhibitors. FG domains of Nup153 and Nup98 could create a different phase favoring the nucleoporin clustering generating a new intranuclear organelle (Schmidt & Görlich, 2016). However, if this would be the case, other FG-Nups such as P62 could also be present at the INCs, which did not occur, despite being topologically near Nups at the NPCs. On the contrary, Tpr, a non-FG nucleoporin and very different from a structural perspective, is significantly enriched within these organelles.

Nup153 and Nup98 are nucleoporins that are known to be associated with enhancer regions of genes, areas especially rich in acetyl labels. The relationship with these areas is dynamic, occurs on numerous occasions within the nuclear interior, and is dependent on the soluble fractions of the nucleoporins. After HDAC inhibition, previously repressed regions become active due to acetylation, which supposedly would increase the transcriptional activity and the trafficking of soluble nucleoporins. However, after the use of HDAC inhibitors, the opposite effect is observed. It may be that the generalized disorder of the chromatin structure affects other cofactors mediating in the interplay between the Nups and chromatin, thus impeding their traffic. Using an analogy with the real world and saving the distances, we would imagine the hyperacetylated nucleus as a stalled engine awaiting in standby mode.

6.2 Proliferation and migration.

As we have seen, the inhibition of histone deacetylases triggers a moderate mismatch of the distribution of lamin A/C and the nucleoporins Tpr and Nup153, both components of pore-linked-filaments, a secondary element of the nucleoskeleton. As mentioned previously, the

cytoskeleton and the nucleoskeleton constitute a single mechanical entity, where the nuclear lamina would be its medullary component. Thus, it is worth asking and evaluating the possible implications of these modifications in one of the cytoskeleton's primary functions, migration, even more so, when HDACis have been repeatedly referred to as modulators of migration in tumor cells. Perhaps the INCs may be indirectly related to the mechanical properties of the cytoskeleton.

In this sense, a study published in 2010 (Zhou & Panté, 2010) referenced that Nup153 is necessary to preserve the migratory capacities of tumor cells and that such disruption was mediated by destabilization of the cytoskeleton. Thus, the disappearance of Nup153 from the pore complex caused the collapse of the cytoskeleton. This study shows similarities with our finding that many nuclear pore complexes of cells treated with HDAC inhibitors were devoid of the main nuclear basket components. Although this is indeed extracted from figure 31, where Tpr particles were identified and not Nup153, we can safely assume that Nup153 would not be present either, given the evident specular behavior between both nucleoporins after the inhibition of HDACs (Figure 21). In any case, although the wound healing results show a more remarkable advance of the migration front after treatment with HDAC inhibitors, we have already shown that it can be explained by an increase in cell size, as illustrated in figure 35. In any event, immunodetection of Nup153 on migration fronts (Figure 36) showed that the frequency of INCs was critically low, so in no case could we hold Nup153 responsible for a supposed, although nonexistent, migratory response. The MMP2 and MMP9 zymograms did not provide information on a migratory stimulation since we did not observe any additional secretion of metalloproteases to the culture medium after treatment with HDAC inhibitors. We believe that it is interesting to highlight the significant increase in cell size, provided that we establish a correlation between size and the extension of the tubulin cytoskeleton. Although we have solely employed tubulin as a cytoskeletal marker in our experiments, we do not expect to observe significant differences in using other markers such as actin or vimentin, since they all join the nucleoskeleton via nesprins in the LINC complexes in the nuclear envelope. We cannot rule out that the expansion of the cytoskeleton is partly responsible for reorganizing the nuclear lamina. However, we consider it unlikely, and we are more inclined to think that the destabilization of peripheral heterochromatin due to its hyperacetylation is the main responsible for the aforementioned relocation (Galiová et al., 2008).

6.3 INC formation and its relation to the cell cycle.

HDAC inhibitors are more than well-known disruptors of cell proliferation and, as mentioned in the introduction (Section 1.4), this is one of the characteristics that support them as antitumor agents. Consequently, our results showed a marked arrest of cell cycle progression across a broad spectrum of concentrations (Figure 39). Cell cycle arrest occurred at both the G_{1i}/S and G_2/M transition, the former being the protagonist when low concentrations were

used, while the second stop was gaining presence as the dose of inhibitor used increased. This effect occurred in both the TSA inhibitor and the SAHA inhibitor, which is not surprising, given that both inhibitors belong to the hydroxamate family and inhibit the same substrates of HDAC classes I, II, and IV (Seto & Yoshida, 2014).

It should be noted that although a priori the results obtained with TSA were compelling, the results varied too much depending on the batch used (as can be seen by the large deviations in figure 39), while SAHA offered more "modest results" but more consistent. Perhaps this is one of the reasons why TSA has been discontinued as a possible antitumor agent in clinical trials, while SAHA is even used to combat T-cell lymphoma (CTCL) (Marks, 2007).

Although the results obtained by flow cytometry were clear-sighted, the cell proliferation assays by MTT were not so. As shown in Figure 38, we could not observe significant differences between control cells and cells exposed to 1,5 µM SAHA. This apparent passivity remained even after removing the serum from the culture medium in order to eliminate any interference. However, this result should not be interpreted as that the SAHA inhibitor does not stop proliferation, but rather due to the intrinsic performance of the MTT assays (Ehrich & Sharova, 2000). In this sense, MTT crystals are formed as a function of mitochondrial activity, which is expected to be proportional to the total cell population. Although the cell cycle did stop, the effects on the total number of cells may not be significant, or the MTT may not have sufficient resolution to observe them. It should not be forgotten that after all, the exposure to SAHA only took place for 24 hours, and perhaps if the exposure had been prolonged, we would have observed more significant differences.

When we started exposing cells to treatment with inhibitors, we were amazed at how well our cells endured the treatment. Although cell cycle arrest indeed occurred, if the medium was renewed with a fresh one or by prolonging the incubation period, the effect progressively disappeared, and the cells continued with their conventional growth. We have not observed any apoptotic effect during any of the drug treatments. Although they suffer a strong arrest of the cell cycle as might be expected, in no case did we observe signs of cellular debris due to apoptosis, autophagy, or necrosis at any dose. The SMS-KCNR cell line is an established line of a post-chemotherapy metastatic childhood tumor, which gives us an idea of the terrible malignant potential of this neuroblastoma cell lineage and, likely, it is already refractory to a wide variety of antitumor treatments such as HDAC inhibitors (Reynolds et al., 1986). Previous studies in our research group observed a similar effect in melanoma cell lines. In these studies, the HDAC inhibitors initially induced apoptosis and cell culture remission but, after overcoming the initial shock, the cells recovered to become relatively immune to the inhibitors and promoted invasive behavior (Díaz-Núñez et al., 2016). Thus, a positive discrimination of the population with more significant malignant potential was produced. Hence, antitumor agents must be used with great care and well-integrated in a multispectral treatment of varied surgery, radiotherapy, or pharmacological combination strategies.

In any case, our primary objective was to use the inhibitors as a tool to make visible the intranuclear accumulations of nucleoporins and not to study the antitumor effects of the HDAC inhibitors themselves.

At this point, we have to stop and reflect on the relationship between the formation of INCs and the distribution of the cell cycle phase. First, we have indirectly associated them with the G0/G1 phase through exhaustive interrelated counts of nuclear size, the presence-absence of INCs, and the cell cycle phase (Figures 40 and 41). Second, the evidence has been confirmed using the FUCCI probe and the Ki-67 proliferation marker (Figures 42 and 43). These latest experiments provide evidence that INCs are associated with the G1 phase, especially during its early progression. In this way, after the inhibition of HDACs, we can describe four well-defined nuclear phenotypes that would complete Table 12:

	Cell Cycle Phase	Nuclear Surface	Nucleoporin Position
Class 1	G_2	Big Nuclei	Nuclear Envelope
Class 2	G_1	Big and small nuclei	Mostly at INCs
Class 3	Early G_1	Small Nuclei	INCs
Class 4	G_0	Big Nuclei	Nuclear Envelope

Table 13: Actualization of nuclei classification in table 12 after merging data extracted from FUCCI and Ki-67 experiments (Figures 42 and 43). Big and small nuclei correspond to 180 ± 40 µm² and 240 ± 40 µm² respectively according to the distribution histograms illustrated in figure 42B.

Although we have managed to charactherize the phenotype of INC-containing nuclei, we can ask about their causality. In the first place, it would be expected that, given the close association between chromatin and nucleoporins, the hyperacetylation of the former would impact their distribution, generating the INCs. The fact that other cell cycle-arresting drugs such as L-mimosine or mitomycin C do not cause the formation of INCs suggests that hyperacetylation of chromatin is a necessary condition for this to occur. This requirement could partially explain the formation of these clusters; however, it does not explain why not all nuclei exhibit these nucleoporin accumulations, although all of them have undergone hyperacetylation of their chromatin. Therefore, the key must lie not only in the hyperacetylation of chromatin, but also in the role of the alteration of the cell cycle resulting from the inhibition of HDACs.

We know that HDAC inhibitors stop cell proliferation by promoting the expression of CDK inhibitors such as p21, p27 or, p57, after hyperacetylation of the promoters of the genes that encode them (Falkenberg & Johnstone, 2014; Y. B. Kim et al., 2000; Xu et al., 2007). Similarly, roscovitine is a very potent inhibitor of CDKs unrelated to chromatin hyperacetylation. Surprisingly, after using roscovitine, we could detect some intranuclear accumulations of nucleoporins which were extremely similar to the INCs described after the inhibition of HDACs. Although their frequency was substantially lower than when TSA or

SAHA was used, probably due to the different impact on cell cycle progression, the mere appearance of these accumulations cleared up many unknowns about the molecular mechanism that governs the formation of these clusters. According to this, not observing INCs after using L-mimosine or MMC is somehow expected since both drugs stop the cell cycle's progression independently of the inhibition of CDKs (Kubota et al., 2014) (PubChem 440473 and 5746). So it seems that this would be genuinely a necessary condition for the appearance of the INCs.

This fact is of central importance, since it is precisely during the G_1 phase, and specifically in the early G_1 phase, closely linked to the appearance of INCs, that the reconstruction of the pore complex takes place, a phenomenon governed strictly by CDKs (Maeshima et al., 2010). Therefore, everything seems to point out that the inhibition of CDKs, consequent to the inhibition of HDACs, could prevent the pore complex reconstruction after mitosis. Such interpretation is reinforced by analyzing the temporal progression of the different phases of the cell cycle, collected in Figure 45. In the mentioned figure, it can be seen that a typical asynchronous culture takes approximately 16 hours to complete an entire progression between two mitoses. However, once treated with the HDACs inhibitor, we see how the synthesis phase is progressively reduced until almost disappearing after 24 hours. On the other hand, the progression of the G_2 phase offers a more interesting perspective, from being the dominant population 12 hours after the start of treatment, to becoming a minority after 24 hours. Precisely, once 12 hours elapsed, we can observe the first INCs in few nuclei (Figure 45 C), probably originating from the first nuclei to complete mitosis.

The proportion of nucleoporins relativized to the whole protein content show no differences either at the beginning or at the end of the treatment but in its equator, Tpr, Nup153, and to a lesser extent, Nup98 and Nup93, are significantly more abundant in the cultures treated with HDAC inhibitors. It is especially significant that p62, the only nucleoporin absent in the aggregates, is not overexpressed, as with the rest of the tested nucleoporins. Nup93, like p62, is another nucleoporin from the central pore complex that, unlike the latter, is slightly overexpressed. Unfortunately, we were unable to perform immunolocalization experiments on Nup93. Although previous data report that this nucleoporin remains exclusively in the nuclear envelope after inhibition of HDACs by TSA (Brown et al., 2008), given our western-blot results, we venture to say that it would co-localize in our INCs. The results obtained by Brown et al. were performed at doses (132 nM) and exposure periods (12 hours) different from ours, both factors being of vital importance for the clear visualization of the INCs, as we have previously demonstrated (Figures 39 and 45).

We are surprised by the marked overexpression of Nup153 and Tpr after 12 hours. As mentioned, they reach their peak at G_2 phase, characteristic of having a higher density of NPCs. However, the overexpression of these two nucleoporins contrasts with the constant levels of P62, or the modest increase of Nup98 or Nup93.

Thus, this result suggests that the homeostasis of nucleoporins detected at the INCs may be misregulated. Accordingly, the inhibition of HDACs may alter the balance of posttranslational modifications for each nucleoporin. These include SUMO modifications, phosphorylation, which governs the localization of Tpr, or acetylation itself (Rajanala et al., 2014). As a matter of fact, the nucleoporin Tpr (Uniprot P12270) has several domains sensitive to acetylation, so we can not exclude the possibility that the inhibition of HDACs alters the natural balance of these acetylated domains, perhaps slowing down the turnover rate of Tpr and its most intimate interactors, like Nup153. Moreover, the relationship between the postranslational modifications of specific nuclear components and the regulation of gene expression would be the ultimate goal of our future research. It is interesting to mention the pioneer hypothesis of the "Gene Gating", a short note published in 1985 by the Nobel Laureate Günter Blobel (Blobel, 1985). He stated that nucleocytoplasmic transport would be linked to the activation of gene expression, creating intranuclear channels through which the components of the transcription machinery would travel from the nucleus to the cytoplasm through specific NPCs. Although it may sound as a simple and straight forward hypothesis, the understanding of the functional organization of the nucleus is probably one of the most elusive areas of research for the last decades (Burns & Wente, 2014).

Regarding the relationship between the cell cycle and the effect of HDAC inhibition, the CDKs themselves are the main components that govern the biogenesis of the pore complex after mitosis (de Castro et al., 2018; Güttinger et al., 2009; Maeshima et al., 2011; Weberruss & Antonin, 2016). Thus, it is not surprising that their inhibition through HDAC inhibitors prevents new NPC formation after mitosis. The excess of some nucleoporins accumulated during the G_2 phase, the global hyperacetylation, and the inhibition of the CDKs would prevent the construction of complete pore complexes, reducing them to its intermediates of earlier incorporation, such as the Y subcomplexes, the transmembrane Nups, and some elements of the central ring. Although there is no direct evidence on this, peripheral Nups such as Tpr and Nup153 would be excluded from these NPCs in reconstruction, which would cause their accumulation in the nuclear interior.

Finally, there is a proportion of cells arrested in G_0 (Figure 43B and C) that do not exhibit INCs. This population corresponds to the portion of nuclei that were not sufficiently advanced in the cycle after being exposed to the inhibitor, having sufficient margin to enter quiescence before entering the synthesis phase. Since these nuclei have not undergone any mitotic events, they would not have to rebuild their pore complexes, which explains why we did not observe INCs in these nuclei.

To recapitulate and conclude this section, we propose the following explanation for the formation of INCs and the different nuclear phenotypes found after the inhibition of HDACs with low drug concentrations:

1. After the immediate addition of the inhibitor, many of the cells in the early stages of the cycle would exit cell cycle to remain quiescent until drug degradation. These nuclei would retain a "normal" phenotype in terms of nucleoporin distribution.
2. Some nuclei would manage to ignore the early still weak signals of newly synthesized CDK inhibitors, such as p21. Thus, these cells would pass to the synthesis phase. Similarly, the nuclei in the G2 phase would manage to skip the G2/M checkpoint and begin mitosis, after which the first daughter nuclei with INCs would appear.
3. After 12 hours from the start of inhibition, nuclei with INCs would stop their progression at the G1/S checkpoint. The bulk of the population would manage to overstep the G2/M checkpoint (it would not happen when using high drug concentrations) to divide and form more daughter nuclei with INCs. Those cells that cannot overcome G2/M would remain in the G2 phase and would compose the INC absent nuclei along with the quiescent nuclei.

7 CONCLUSIONS

1. HDAC inhibitors exert Tpr, Nup153, and Nup98 accumulation at the nuclear interior in discrete foci referred to as Intranuclear Nup Cluster (INC).
2. INCs are only observable in G1 arrested cells, mainly in their early stages after mitosis.
3. INCs arise at the nuclear interior and are independent of the nuclear envelope nucleoskeletal elements such as NPC or nuclear lamin.
4. INCs do not relate to other nuclear bodies such as nucleoli, nucleoplasmic reticulum, transcription factories, and replication foci.

BIBLIOGRAPHY

Adam, S. A. (2017). The Nucleoskeleton. *Cold Spring Harbor Perspectives in Biology*, *9*(a023556), 1–12. https://doi.org/10.1007/7089

Adam, S. A., & Goldman, R. D. (2012). Insights into the differences between the A- and B-type nuclear lamins. *Advances in Biological Regulation*, *52*(1), 108–113. https://doi.org/10.1016/j.advenzreg.2011.11.001

Adams, R. H., & Alitalo, K. (2007). Molecular regulation of angiogenesis and lymphangiogenesis. *Nature Reviews Molecular Cell Biology*, *8*(6), 464–478. https://doi.org/10.1038/nrm2183

Adan, A., Alizada, G., Kiraz, Y., Baran, Y., & Nalbant, A. (2017). Flow cytometry: basic principles and applications. *Critical Reviews in Biotechnology*, *37*(2), 163–176. https://doi.org/10.3109/07388551.2015.1128876

Akey, C., & Radermacher, M. (1993). Architecture of the Xenopus nuclear pore complex revealed by three-dimensional cryo-electron microscopy. *The Journal of Cell Biology*, *122*(1), 1–19. https://doi.org/10.1083/jcb.122.1.1

Al-Haboubi, T., Shumaker, D. K., Köser, J., Wehnert, M., & Fahrenkrog, B. (2011). Distinct association of the nuclear pore protein Nup153 with A- and B-type lamins. *Nucleus*, *2*(5), 500–509. https://doi.org/10.4161/nucl.2.5.17913

Albiez, H., Cremer, M., Tiberi, C., Vecchio, L., Schermelleh, L., Dittrich, S., Küpper, K., Joffe, B., Thormeyer, T., Von Hase, J., Yang, S., Rohr, K., Leonhardt, H., Solovei, I., Cremer, C., Fakan, S., & Cremer, T. (2006). Chromatin domains and the interchromatin compartment form structurally defined and functionally interacting nuclear networks. *Chromosome Research*, *14*(7), 707–733. https://doi.org/10.1007/s10577-006-1086-x

Anderson, D. J., & Hetzer, M. W. (2008). Shaping the endoplasmic reticulum into the nuclear envelope. *Journal of Cell Science*, *121*(2), 137–142. https://doi.org/10.1242/jcs.005777

Andrade, R., Arlucea, J., Alonso, R., & Aréchaga, J. (2001). Nucleoplasmin binds to nuclear pore filaments and accumulates in specific regions of the nucleolar cortex. *Chromosoma*, *109*(8), 545–550. https://doi.org/10.1007/s004120000121

Aramburu, I. V., & Lemke, E. A. (2017). Floppy but not sloppy: Interaction mechanism of FG-nucleoporins and nuclear transport receptors. *Seminars in Cell & Developmental Biology*, *68*, 34–41. https://doi.org/10.1016/j.semcdb.2017.06.026

Arlucea, J., Andrade, R., Alonso, R., & Aréchaga, J. (1998). The Nuclear Basket of the Nuclear Pore Complex Is Part of a Higher-Order Filamentous Network That Is Related to Chromatin. *Journal of Structural Biology*, *124*(1), 51–58. https://doi.org/10.1006/jsbi.1998.4054

Bachi, A., Braun, I. C., Rodrigues, J. P., Panté, N., Ribbeck, K., von Kobbe, C., Kutay, U., Wilm, M., Görlich, D., Carmo-Fonseca, M., & Izaurralde, E. (2000). The C-terminal domain of TAP interacts with the nuclear pore complex and promotes export of specific CTE-bearing RNA substrates. *RNA*, *6*(1), 136–158. https://doi.org/10.1017/S1355838200991994

Ball, J. R., Dimaano, C., & Ullman, K. S. (2004). The RNA binding domain within the nucleoporin Nup153 associates preferentially with single-stranded RNA. *RNA*, *10*(1), 19–27. https://doi.org/10.1261/rna.5109104

Ball, J. R., & Ullman, K. S. (2005). Versatility at the nuclear pore complex: lessons learned from the nucleoporin Nup153. *Chromosoma*, *114*(5), 319–330. https://doi.org/10.1007/s00412-005-0019-3

Bangs, P., Burke, B., Powers, C., Craig, R., Purohit, A., & Doxsey, S. (1998). Functional Analysis of Tpr: Identification of Nuclear Pore Complex Association and Nuclear Localization Domains and a Role in mRNA Export. *Journal of Cell Biology*, *143*(7), 1801–1812. https://doi.org/10.1083/jcb.143.7.1801

Barnes, C. E., English, D. M., & Cowley, S. M. (2019). Acetylation and Co: An expanding repertoire of histone acylations regulates chromatin and transcription. *Essays in Biochemistry*, *63*(1), 97–107. https://doi.org/10.1042/EBC20180061

Bastos, R., Lin, A., Enarson, M., & Burke, B. (1996). Targeting and function in mRNA export of nuclear pore complex protein Nup153. *Journal of Cell Biology*, *134*(5), 1141–1156. https://doi.org/10.1083/jcb.134.5.1141

Beck, M., & Hurt, E. (2017). The nuclear pore complex: understanding its function through structural insight. *Nature Reviews Molecular Cell Biology*, *18*(2), 73–89. https://doi.org/10.1038/nrm.2016.147

Belin, B. J., Cimini, B. a, Blackburn, E. H., & Mullins, R. D. (2013). Visualization of actin filaments and monomers in somatic cell nuclei. *Molecular Biology of the Cell*, *24*(7), 982–994. https://doi.org/10.1091/mbc.E12-09-0685

Bergmann, J. H., & Spector, D. L. (2014). Long non-coding RNAs: Modulators of nuclear structure and function. *Current Opinion in Cell Biology*, *26*(1), 10–18. https://doi.org/10.1016/j.ceb.2013.08.005

Bernis, C., Swift-Taylor, B., Nord, M., Carmona, S., Chook, Y. M., & Forbes, D. J. (2014). Transportin acts to regulate mitotic assembly events by target binding rather than Ran

sequestration. *Molecular Biology of the Cell*, *25*(7), 992–1009. https://doi.org/10.1091/mbc.e13-08-0506

Bickmore, W. A., & van Steensel, B. (2013). Genome Architecture: Domain Organization of Interphase Chromosomes. *Cell*, *152*(6), 1270–1284. https://doi.org/10.1016/j.cell.2013.02.001

Birkedal-Hansen, H., Yamada, S., Windsor, J., Pollard, A. H., Lyons, G., Stetler-Stevenson, W., & Birkedal-Hansen, B. (2008). Matrix Metalloproteinases. *Current Protocols in Cell Biology*, *40*(September), 10.8.1-10.8.23. https://doi.org/10.1002/0471143030.cb1008s40

Björk, P., & Wieslander, L. (2017). Integration of mRNP formation and export. *Cellular and Molecular Life Sciences*, *74*(16), 2875–2897. https://doi.org/10.1007/s00018-017-2503-3

Blobel, G. (1985). Gene gating: a hypothesis. *Proceedings of the National Academy of Sciences*, *82*(24), 8527–8529. https://doi.org/10.1073/pnas.82.24.8527

Bodoor, K., Shaikh, S., Salina, D., Raharjo, W. H., Bastos, R., Lohka, M., & Burke, B. (1999). Sequential recruitment of NPC proteins to the nuclear periphery at the end of mitosis. *Journal of Cell Science*, *112*(13), 2253–2264.

Branco, M. R., & Pombo, A. (2006). Intermingling of chromosome territories in interphase suggests role in translocations and transcription-dependent associations. *PLoS Biology*, *4*, 780–788. https://doi.org/10.1371/journal.pbio.0040138

Brickner, J. H. (2009). Transcriptional memory at the nuclear periphery. *Current Opinion in Cell Biology*, *21*(1), 127–133. https://doi.org/10.1016/j.ceb.2009.01.007

Brown, C. R., Kennedy, C. J., Delmar, V. A., Forbes, D. J., & Silver, P. A. (2008). Global histone acetylation induces functional genomic reorganization at mammalian nuclear pore complexes. *Genes & Development*, *22*(5), 627–639. https://doi.org/10.1101/gad.1632708

Buchwalter, A., Kaneshiro, J. M., & Hetzer, M. W. (2019). Coaching from the sidelines: the nuclear periphery in genome regulation. *Nature Reviews Genetics*, *20*(1), 39–50. https://doi.org/10.1038/s41576-018-0063-5

Buchwalter, A. L., Liang, Y., & Hetzer, M. W. (2014). Nup50 is required for cell differentiation and exhibits transcription-dependent dynamics. *Molecular Biology of the Cell*, *25*(16), 2472–2484. https://doi.org/10.1091/mbc.E14-04-0865

Bui, K. H., von Appen, A., DiGuilio, A. L., Ori, A., Sparks, L., Mackmull, M.-T., Bock, T., Hagen, W., Andrés-Pons, A., Glavy, J. S., & Beck, M. (2013). Integrated Structural Analysis of the Human Nuclear Pore Complex Scaffold. *Cell*, *155*(6), 1233–1243. https://doi.org/10.1016/j.cell.2013.10.055

Burgess, R. C., Burman, B., Kruhlak, M. J., & Misteli, T. (2014). Activation of DNA Damage Response Signaling by Condensed Chromatin. *Cell Reports*, *9*(5), 1703–1717. https://doi.org/10.1016/j.celrep.2014.10.060

Burns, L. T., & Wente, S. R. (2014). From hypothesis to mechanism: uncovering nuclear pore complex links to gene expression. *Molecular and Cellular Biology*, *34*(12), 2114–2120. https://doi.org/10.1128/MCB.01730-13

Calo, E., & Wysocka, J. (2013). Modification of Enhancer Chromatin: What, How, and Why? *Molecular Cell*, *49*(5), 825–837. https://doi.org/10.1016/j.molcel.2013.01.038

Capelson, M., Liang, Y., Schulte, R., Mair, W., Wagner, U., & Hetzer, M. W. (2010). Chromatin-Bound Nuclear Pore Components Regulate Gene Expression in Higher Eukaryotes. *Cell*, *140*(3), 372–383. https://doi.org/10.1016/j.cell.2009.12.054

Caridi, C. P., Plessner, M., Grosse, R., & Chiolo, I. (2019). Nuclear actin filaments in DNA repair dynamics. *Nature Cell Biology*, *21*(9), 1068–1077. https://doi.org/10.1038/s41556-019-0379-1

Cautain, B., Hill, R., de Pedro, N., & Link, W. (2015). Components and regulation of nuclear transport processes. *FEBS Journal*, *282*(3), 445–462. https://doi.org/10.1111/febs.13163

Cavellán, E., Asp, P., Percipalle, P., & Farrants, A. K. Ö. (2006). The WSTF-SNF2h chromatin remodeling complex interacts with several nuclear proteins in transcription. *Journal of Biological Chemistry*, *281*(24), 16264–16271. https://doi.org/10.1074/jbc.M600233200

Cha, T.-L., Chuang, M.-J., Wu, S.-T., Sun, G.-H., Chang, S.-Y., Yu, D.-S., Huang, S.-M., Huan, S. K.-H., Cheng, T.-C., Chen, T.-T., Fan, P.-L., & Hsiao, P.-W. (2009). Dual Degradation of Aurora A and B Kinases by the Histone Deacetylase Inhibitor LBH589 Induces G2-M Arrest and Apoptosis of Renal Cancer Cells. *Clinical Cancer Research*, *15*(3), 840–850. https://doi.org/10.1158/1078-0432.CCR-08-1918

Chagin, V. O., Casas-Delucchi, C. S., Reinhart, M., Schermelleh, L., Markaki, Y., Maiser, A., Bolius, J. J., Bensimon, A., Fillies, M., Domaing, P., Rozanov, Y. M., Leonhardt, H., & Cardoso, M. C. (2016). 4D Visualization of replication foci in mammalian cells corresponding to individual replicons. *Nature Communications*, *7*(11231), 1–12. https://doi.org/10.1038/ncomms11231

Chatel, G., & Fahrenkrog, B. (2011). Nucleoporins: Leaving the nuclear pore complex for a successful mitosis. *Cellular Signalling*, *23*(10), 1555–1562. https://doi.org/10.1016/j.cellsig.2011.05.023

Chuang, C.-H., Carpenter, A. E., Fuchsova, B., Johnson, T., de Lanerolle, P., & Belmont, A. S. (2006). Long-range directional movement of an interphase chromosome site. *Current Biology : CB*, *16*(8), 825–831. https://doi.org/10.1016/j.cub.2006.03.059

Chuang, C. H., & Belmont, A. S. (2007). Moving chromatin within the interphase nucleus-controlled transitions? *Seminars in Cell and Developmental Biology*, *18*(5), 698–706. https://doi.org/10.1016/j.semcdb.2007.08.012

Chun, P. (2015). Histone deacetylase inhibitors in hematological malignancies and solid tumors. *Archives of Pharmacal Research*, *38*(6), 933–949. https://doi.org/10.1007/s12272-015-0571-1

Clubb, B. H., & Locke, M. (1998). 3T3 cells have nuclear invaginations containing F-actin. *Tissue & Cell*, *30*(6), 684–691. http://www.ncbi.nlm.nih.gov/pubmed/10189322

Cook, A. G., & Conti, E. (2010). Nuclear export complexes in the frame. *Current Opinion in Structural Biology*, *20*(2), 247–252. https://doi.org/10.1016/j.sbi.2010.01.012

Cook, P. R. (1989). The nucleoskeleton and the topology of transcription. *European Journal of Biochemistry*, *185*(3), 487–501. https://doi.org/10.1111/j.1432-1033.1989.tb15141.x

Cordes, V. C., Reidenbach, S., Kohler, A., Stuurman, N., Van Driel, R., & Franke, W. W. (1993). Intranuclear filaments containing a nuclear pore complex protein. *Journal of Cell Biology*, *123*(6 I), 1333–1344. https://doi.org/10.1083/jcb.123.6.1333

Cordes, Volker C., Reidenbach, S., Rackwitz, H.-R., & Franke, W. W. (1997). Identification of Protein p270/Tpr as a Constitutive Component of the Nuclear Pore Complex–attached Intranuclear Filaments. *Journal of Cell Biology*, *136*(3), 515–529. https://doi.org/10.1083/jcb.136.3.515

Cortadellas, N., Garcia, A., & Fernández, E. (2012). Transmission Electron Microscopy in Cell Biology: sample preparation techniques and image information. *Handbook of Instrumental Techniques for Materials, Chemical and Biosciences Research*, *3*(2), 12. https://doi.org/http://dx.doi.org/10.1007/s00268-009-0046-y

Cosgrove, M. S., Boeke, J. D., & Wolberger, C. (2004). Regulated nucleosome mobility and the histone code. *Nature Structural & Molecular Biology*, *11*(11), 1037–1043. https://doi.org/10.1038/nsmb851

Coyle, J. H., Bor, Y.-C., Rekosh, D., & Hammarskjold, M.-L. (2011). The Tpr protein regulates export of mRNAs with retained introns that traffic through the Nxf1 pathway. *RNA*, *17*(7), 1344–1356. https://doi.org/10.1261/rna.2616111

Cremer, T., & Cremer, M. (2010). Chromosome territories. *Cold Spring Harbor Perspectives in Biology*, *2*(3), a003889. https://doi.org/10.1101/cshperspect.a003889

Cremer, T., Cremer, M., Hübner, B., Strickfaden, H., Smeets, D., Popken, J., Sterr, M., Markaki, Y., Rippe, K., & Cremer, C. (2015). The 4D nucleome: Evidence for a dynamic nuclear landscape based on co-aligned active and inactive nuclear compartments. *FEBS Letters*, *589*(20 Pt A), 2931–2943. https://doi.org/10.1016/j.febslet.2015.05.037

Cronshaw, J. M., Krutchinsky, A. N., Zhang, W., Chait, B. T., & Matunis, M. J. (2002). Proteomic analysis of the mammalian nuclear pore complex. *The Journal of Cell Biology*, *158*(5), 915–927. https://doi.org/10.1083/jcb.200206106

D'Angelo, M. A., Raices, M., Panowski, S. H., & Hetzer, M. W. (2009). Age-Dependent Deterioration of Nuclear Pore Complexes Causes a Loss of Nuclear Integrity in Postmitotic Cells. *Cell*, *136*(2), 284–295. https://doi.org/10.1016/j.cell.2008.11.037

Dahl, K. N., & Kalinowski, A. (2011). Nucleoskeleton mechanics at a glance. *Journal of Cell Science*, *124*(5), 675–678. https://doi.org/10.1242/jcs.069096

Daigle, N., Beaudouin, J., Hartnell, L., Imreh, G., Hallberg, E., Lippincott-Schwartz, J., & Ellenberg, J. (2001). Nuclear pore complexes form immobile networks and have a very low turnover in live mammalian cells. *Journal of Cell Biology*, *154*(1), 71–84. https://doi.org/10.1083/jcb.200101089

Dawson, T. R., Lazarus, M. D., Hetzer, M. W., & Wente, S. R. (2009). ER membrane–bending proteins are necessary for de novo nuclear pore formation. *Journal of Cell Biology*, *184*(5), 659–675. https://doi.org/10.1083/jcb.200806174

de Castro, I. J., Gil, R. S., Ligammari, L., Di Giacinto, M. L., & Vagnarelli, P. (2018). CDK1 and PLK1 coordinate the disassembly and reassembly of the nuclear envelope in vertebrate mitosis. *Oncotarget*, *9*(8), 7763–7773. https://doi.org/10.18632/oncotarget.23666

de Lanerolle, P., & Serebryannyy, L. (2011). Nuclear actin and myosins: Life without filaments. *Nature Cell Biology*, *13*(11), 1282–1288. https://doi.org/10.1038/ncb2364

De Paul, A. L., H., J., P., J., Gutirrez, S., A., A., A., C., & I., A. (2012). Immunoelectron Microscopy: A Reliable Tool for the Analysis of Cellular Processes. In H. Dehghani (Ed.), *Applications of Immunocytochemistry* (pp. 65–96). InTech. https://doi.org/10.5772/33108

Dechat, T., Gesson, K., & Foisner, R. (2010). Lamina-independent lamins in the nuclear interior serve important functions. *Cold Spring Harbor Symposia on Quantitative Biology*, *75*, 533–543. https://doi.org/10.1101/sqb.2010.75.018

Delcuve, G. P., Khan, D. H., & Davie, J. R. (2013). Targeting class I histone deacetylases in cancer therapy. *Expert Opinion on Therapeutic Targets*, *17*(1), 29–41. https://doi.org/10.1517/14728222.2013.729042

Deroanne, C. F., Bonjean, K., Servotte, S., Devy, L., Colige, A., Clausse, N., Blacher, S., Verdin, E., Foidart, J.-M., Nusgens, B. V., & Castronovo, V. (2002). Histone deacetylases inhibitors as anti-angiogenic agents altering vascular endothelial growth factor signaling. *Oncogene*, *21*(3), 427–436. https://doi.org/10.1038/sj.onc.1205108

Di Nunzio, F., Fricke, T., Miccio, A., Valle-Casuso, J. C., Perez, P., Souque, P., Rizzi, E., Severgnini, M., Mavilio, F., Charneau, P., & Diaz-Griffero, F. (2013). Nup153 and Nup98 bind the HIV-1 core and contribute to the early steps of HIV-1 replication. *Virology*, *440*(1), 8–18. https://doi.org/10.1016/j.virol.2013.02.008

Díaz-Núñez, M., Díez-Torre, A., De Wever, O., Andrade, R., Arluzea, J., Silió, M., & Aréchaga, J. (2016). Histone deacetylase inhibitors induce invasion of human melanoma cells in vitro via differential regulation of N-cadherin expression and RhoA activity. *BMC Cancer*, *16*(1), 667. https://doi.org/10.1186/s12885-016-2693-3

Dingová, H., Fukalová, J., Maninová, M., Philimonenko, V. V., & Hozák, P. (2009). Ultrastructural localization of actin and actin-binding proteins in the nucleus. *Histochemistry and Cell Biology*, *131*(3), 425–434. https://doi.org/10.1007/s00418-008-0539-z

Donaldson, J. G. (2015). Immunofluorescence Staining. *Current Protocols in Cell Biology*, *69*(1), 4.3.1-4.3.7. https://doi.org/10.1002/0471143030.cb0403s69

Doucet, C. M., Talamas, J. A., & Hetzer, M. W. (2010). Cell Cycle-Dependent Differences in Nuclear Pore Complex Assembly in Metazoa. *Cell*, *141*(6), 1030–1041. https://doi.org/10.1016/j.cell.2010.04.036

Duheron, V., Chatel, G., Sauder, U., Oliveri, V., & Fahrenkrog, B. (2014). Structural characterization of altered nucleoporin Nup153 expression in human cells by thin-section electron microscopy. *Nucleus*, *5*(6), 601–612. https://doi.org/10.4161/19491034.2014.990853

Dultz, E., & Ellenberg, J. (2010). Live imaging of single nuclear pores reveals unique assembly kinetics and mechanism in interphase. *The Journal of Cell Biology*, *191*(1), 15–22. https://doi.org/10.1083/jcb.201007076

Dultz, E., Zanin, E., Wurzenberger, C., Braun, M., Rabut, G., Sironi, L., & Ellenberg, J. (2008). Systematic kinetic analysis of mitotic dis- and reassembly of the nuclear pore in living cells. *Journal of Cell Biology*, *180*(5), 857–865. https://doi.org/10.1083/jcb.200707026

Dundr, M. (2012). Nuclear bodies: Multifunctional companions of the genome. *Current Opinion in Cell Biology*, *24*(3), 415–422. https://doi.org/10.1016/j.ceb.2012.03.010

Dundr, M., Ospina, J. K., Sung, M.-H., John, S., Upender, M., Ried, T., Hager, G. L., & Matera, a G. (2007). Actin-dependent intranuclear repositioning of an active gene locus in vivo. *The Journal of Cell Biology*, *179*(6), 1095–1103. https://doi.org/10.1083/jcb.200710058

Duronio, R. J., & Marzluff, W. F. (2017). Coordinating cell cycle-regulated histone gene expression through assembly and function of the Histone Locus Body. In *RNA Biology* (Vol. 14, Issue 6, pp. 726–738). https://doi.org/10.1080/15476286.2016.1265198

Dutta, S., Bhattacharyya, M., & Sengupta, K. (2018). Changes in the nuclear envelope in laminopathies. *Advances in Experimental Medicine and Biology*, *1112*, 31–38. https://doi.org/10.1007/978-981-13-3065-0_3

Ehrich, M., & Sharova, L. (2000). In Vitro Methods for Detecting Cytotoxicity. *Current Protocols in Toxicology*, *3*(1), 2.6.1-2.6.27. https://doi.org/10.1002/0471140856.tx0206s03

Eibauer, M., Pellanda, M., Turgay, Y., Dubrovsky, A., Wild, A., & Medalia, O. (2015). Structure and gating of the nuclear pore complex. *Nature Communications*, *6*(May), 1–9. https://doi.org/10.1038/ncomms8532

Erdel, F., & Rippe, K. (2018). Formation of Chromatin Subcompartments by Phase Separation. *Biophysical Journal*, *114*(10), 2262–2270. https://doi.org/10.1016/j.bpj.2018.03.011

Eriksson, M., Brown, W. T., Gordon, L. B., Glynn, M. W., Singer, J., Scott, L., Erdos, M. R., Robbins, C. M., Moses, T. Y., Berglund, P., Dutra, A., Pak, E., Durkin, S., Csoka, A. B., Boehnke, M., Glover, T. W., & Collins, F. S. (2003). Recurrent de novo point mutations in lamin A cause Hutchinson-Gilford progeria syndrome. *Nature*, *423*(6937), 293–298. https://doi.org/10.1038/nature01629

Ernst, J., & Kellis, M. (2010). Discovery and characterization of chromatin states for systematic annotation of the human genome. *Nature Biotechnology*, *28*(8), 817–825. https://doi.org/10.1038/nbt.1662

Fahrenkrog, B., Maco, B., Fager, A. M., Köser, J., Sauder, U., Ullman, K. S., & Aebi, U. (2002). Domain-specific antibodies reveal multiple-site topology of Nup153 within the nuclear pore complex. *Journal of Structural Biology*, *140*(1–3), 254–267. https://doi.org/10.1016/s1047-8477(02)00524-5

Falkenberg, K. J., & Johnstone, R. W. (2014). Histone deacetylases and their inhibitors in cancer, neurological diseases and immune disorders. *Nature Reviews Drug Discovery*, *13*(9), 673–691. https://doi.org/10.1038/nrd4360

Feng, L., Lin, T., Uranishi, H., Gu, W., & Xu, Y. (2005). Functional Analysis of the Roles of Posttranslational Modifications at the p53 C Terminus in Regulating p53 Stability and Activity. *Molecular and Cellular Biology*, *25*(13), 5389–5395. https://doi.org/10.1128/MCB.25.13.5389-5395.2005

Fichtman, B., Ramos, C., Rasala, B., Harel, A., & Forbes, D. J. (2010). Inner/Outer Nuclear Membrane Fusion in Nuclear Pore Assembly. *Molecular Biology of the Cell*, *21*(23), 4197–4211. https://doi.org/10.1091/mbc.e10-04-0309

Fiserova, J., & Goldberg, M. W. (2010). Relationships at the nuclear envelope: lamins and nuclear pore complexes in animals and plants. *Biochemical Society Transactions*, *38*(3), 829–831. https://doi.org/10.1042/BST0380829

Fišerová, J., Maninová, M., Sieger, T., Uhlířová, J., Šebestová, L., Efenberková, M., Čapek, M., Fišer, K., & Hozák, P. (2019). Nuclear pore protein TPR associates with lamin B1 and affects nuclear lamina organization and nuclear pore distribution. *Cellular and Molecular Life Sciences*, *76*(11), 2199–2216. https://doi.org/10.1007/s00018-019-03037-0

Flynn, R. L., Cox, K. E., Jeitany, M., Wakimoto, H., Bryll, A. R., Ganem, N. J., Bersani, F., Pineda, J. R., Suvà, M. L., Benes, C. H., Haber, D. A., Boussin, F. D., & Zou, L. (2015). Alternative lengthening of telomeres renders cancer cells hypersensitive to ATR inhibitors. *Science*, *347*(6219), 273–277. https://doi.org/10.1126/science.1257216

Fontoura, B. M. A., Dales, S., Blobel, G., & Zhong, H. (2001). The nucleoporin Nup98 associates with the intranuclear filamentous protein network of TPR. *Proceedings of the National Academy of Sciences of the United States of America*, *98*(6), 3208–3213. https://doi.org/10.1073/pnas.061014698

Forbes, D. J., Travesa, A., Nord, M. S., & Bernis, C. (2015). Nuclear transport factors: global regulation of mitosis. *Current Opinion in Cell Biology*, *35*, 78–90. https://doi.org/10.1016/j.ceb.2015.04.012

Fox, A. H., & Lamond, A. I. (2010). Paraspeckles. *Cold Spring Harbor Perspectives in Biology*, *2*(7), a000687--a000687. https://doi.org/10.1101/cshperspect.a000687

Fraga, M. F., Ballestar, E., Villar-Garea, A., Boix-Chornet, M., Espada, J., Schotta, G., Bonaldi, T., Haydon, C., Ropero, S., Petrie, K., Iyer, N. G., Pérez-Rosado, A., Calvo, E., Lopez, J. A., Cano, A., Calasanz, M. J., Colomer, D., Piris, M. Á., Ahn, N., … Esteller, M. (2005). Loss of acetylation at Lys16 and trimethylation at Lys20 of histone H4 is a common hallmark of human cancer. *Nature Genetics*, *37*(4), 391–400. https://doi.org/10.1038/ng1531

Franks, T. M., Benner, C., Narvaiza, I., Marchetto, M. C. N., Young, J. M., Malik, H. S., Gage, F. H., & Hetzer, M. W. (2016). Evolution of a transcriptional regulator from a transmembrane nucleoporin. *Genes & Development*, *30*(10), 1155–1171. https://doi.org/10.1101/gad.280941.116

Franks, T. M., McCloskey, A., Shokirev, M., Benner, C., Rathore, A., & Hetzer, M. W. (2017). Nup98 recruits the Wdr82-Set1A/COMPASS complex to promoters to regulate

H3K4 trimethylation in hematopoietic progenitor cells. *Genes and Development*, *31*(22), 2222–2234. https://doi.org/10.1101/gad.306753.117

Fraser, P., & Bickmore, W. (2007). Nuclear organization of the genome and the potential for gene regulation. *Nature*, *447*(7143), 413–417. https://doi.org/10.1038/nature05916

Fricker, M., Hollinshead, M., White, N., & Vaux, D. (1997). Interphase nuclei of many mammalian cell types contain deep, dynamic, tubular membrane-bound invaginations of the nuclear envelope. *The Journal of Cell Biology*, *136*(3), 531–544. https://doi.org/10.1083/jcb.136.3.531

Frosst, P., Guan, T., Subauste, C., Hahn, K., & Gerace, L. (2002). Tpr is localized within the nuclear basket of the pore complex and has a role in nuclear protein export. *Journal of Cell Biology*, *156*(4), 617–630. https://doi.org/10.1083/jcb.200106046

Funakoshi, T., Clever, M., Watanabe, A., & Imamoto, N. (2011). Localization of Pom121 to the inner nuclear membrane is required for an early step of interphase nuclear pore complex assembly. *Molecular Biology of the Cell*, *22*(7), 1058–1069. https://doi.org/10.1091/mbc.e10-07-0641

Galiová, G., Bártová, E., Raška, I., Krejčí, J., & Kozubek, S. (2008). Chromatin changes induced by lamin A/C deficiency and the histone deacetylase inhibitor trichostatin A. *European Journal of Cell Biology*, *87*(5), 291–303. https://doi.org/10.1016/j.ejcb.2008.01.013

Gallagher, S. R. (2012). One-Dimensional SDS Gel Electrophoresis of Proteins. *Current Protocols in Molecular Biology*, *97*(1), 10.2A.1-10.2A.44. https://doi.org/10.1002/0471142727.mb1002as97

Galy, V., Gadal, O., Fromont-Racine, M., Romano, A., Jacquier, A., & Nehrbass, U. (2004). Nuclear Retention of Unspliced mRNAs in Yeast Is Mediated by Perinuclear Mlp1. *Cell*, *116*(1), 63–73. https://doi.org/10.1016/S0092-8674(03)01026-2

Glozak, M. A., Sengupta, N., Zhang, X., & Seto, E. (2005). Acetylation and deacetylation of non-histone proteins. *Gene*, *363*, 15–23. https://doi.org/10.1016/j.gene.2005.09.010

Goldberg, M. W., & Allen, T. D. (1992). High resolution scanning electron microscopy of the nuclear envelope: demonstration of a new, regular, fibrous lattice attached to the baskets of the nucleoplasmic face of the nuclear pores. *The Journal of Cell Biology*, *119*(6), 1429–1440. https://doi.org/10.1083/jcb.119.6.1429

Goldberg, M. W. W., Fiserova, J., Huttenlauch, I., & Stick, R. (2008). A new model for nuclear lamina organization. *Biochemical Society Transactions*, *36*(Pt 6), 1339–1343. https://doi.org/10.1042/BST0361339

Goldberg, Martin W. (2017). Nuclear pore complex tethers to the cytoskeleton. *Seminars in Cell & Developmental Biology*, *68*, 52–58. https://doi.org/10.1016/j.semcdb.2017.06.017

Goldberg, Martin W., & Allen, T. D. (1996). The Nuclear Pore Complex and Lamina: Three-dimensional Structures and Interactions Determined by Field Emission In-lens Scanning Electron Microscopy. *Journal of Molecular Biology*, *257*(4), 848–865. https://doi.org/10.1006/jmbi.1996.0206

Graham, L., & Orenstein, J. M. (2007). Processing tissue and cells for transmission electron microscopy in diagnostic pathology and research. *Nature Protocols*, *2*(10), 2439–2450. https://doi.org/10.1038/nprot.2007.304

Griffis, E. R., Altan, N., Lippincott-Schwartz, J., & Powers, M. A. (2002). Nup98 Is a Mobile Nucleoporin with Transcription-dependent Dynamics. *Molecular Biology of the Cell*, *13*(4), 1282–1297. https://doi.org/10.1091/mbc.01-11-0538

Griffis, E. R., Craige, B., Dimaano, C., Ullman, K. S., & Powers, M. A. (2004). Distinct functional domains within nucleoporins Nup153 and Nup98 mediate transcription-dependent mobility. *Molecular Biology of the Cell*, *15*(4), 1991–2002. https://doi.org/10.1091/mbc.E03-10-0743

Griffis, E. R., Xu, S., & Powers, M. A. (2003). Nup98 Localizes to Both Nuclear and Cytoplasmic Sides of the Nuclear Pore and Binds to Two Distinct Nucleoporin Subcomplexes. *Molecular Biology of the Cell*, *14*(2), 600–610. https://doi.org/10.1091/mbc.e02-09-0582

Grossman, E., Medalia, O., & Zwerger, M. (2012). Functional Architecture of the Nuclear Pore Complex. *Annual Review of Biophysics*, *41*(1), 557–584. https://doi.org/10.1146/annurev-biophys-050511-102328

Guan, T., Kehlenbach, R. H., Schirmer, E. C., Kehlenbach, A., Fan, F., Clurman, B. E., Arnheim, N., & Gerace, L. (2000). Nup50, a nucleoplasmically oriented nucleoporin with a role in nuclear protein export. *Mol Cell Biol*, *20*(15), 5619–5630. https://doi.org/10.1128/mcb.20.15.5619-5630.2000

Gueth-Hallonet, C., Wang, J., Harborth, J., Weber, K., & Osborn, M. (1998). Induction of a regular nuclear lattice by overexpression of NuMA. *Experimental Cell Research*, *243*(2), 434–452. https://doi.org/10.1006/excr.1998.4178

Guo, Y., Kim, Y., Shimi, T., Goldman, R. D., & Zheng, Y. (2014). Concentration-dependent lamin assembly and its roles in the localization of other nuclear proteins. *Molecular Biology of the Cell*, *25*(8), 1287–1297. https://doi.org/10.1091/mbc.E13-11-0644

Guo, Y., & Zheng, Y. (2015). Lamins position the nuclear pores and centrosomes by modulating dynein. *Molecular Biology of the Cell*, *26*(19), 3379–3389. https://doi.org/10.1091/mbc.E15-07-0482

Güttinger, S., Laurell, E., & Kutay, U. (2009). Orchestrating nuclear envelope disassembly and reassembly during mitosis. *Nature Reviews Molecular Cell Biology*, *10*(3), 178–191. https://doi.org/10.1038/nrm2641

Haque, F., Lloyd, D. J., Smallwood, D. T., Dent, C. L., Shanahan, C. M., Fry, A. M., Trembath, R. C., & Shackleton, S. (2006). SUN1 Interacts with Nuclear Lamin A and Cytoplasmic Nesprins To Provide a Physical Connection between the Nuclear Lamina and the Cytoskeleton. *Molecular and Cellular Biology*, *26*(10), 3738–3751. https://doi.org/10.1128/MCB.26.10.3738-3751.2006

Haraguchi, T., Koujin, T., Hayakawa, T., Kaneda, T., Tsutsumi, C., Imamoto, N., Akazawa, C., Sukegawa, J., Yoneda, Y., & Hiraoka, Y. (2000). Live fluorescence imaging reveals early recruitment of emerin, LBR, RanBP2, and Nup153 to reforming functional nuclear envelopes. *Journal of Cell Science*, *113*(5), 779–794. https://jcs.biologists.org/content/113/5/779

Hase, M. E., & Cordes, V. C. (2003). Direct Interaction with Nup153 Mediates Binding of Tpr to the Periphery of the Nuclear Pore Complex. *Molecular Biology of the Cell*, *14*(5), 1923–1940. https://doi.org/10.1091/mbc.e02-09-0620

Hase, M. E., Kuznetsov, N. V, & Cordes, V. C. (2001). Amino Acid Substitutions of Coiled-Coil Protein Tpr Abrogate Anchorage to the Nuclear Pore Complex but Not Parallel, In-Register Homodimerization. *Molecular Biology of the Cell*, *12*(8), 2433–2452. https://doi.org/10.1091/mbc.12.8.2433

Hawkins, R. D., Hon, G. C., Lee, L. K., Ngo, Q., Lister, R., Pelizzola, M., Edsall, L. E., Kuan, S., Luu, Y., Klugman, S., Antosiewicz-Bourget, J., Ye, Z., Espinoza, C., Agarwahl, S., Shen, L., Ruotti, V., Wang, W., Stewart, R., Thomson, J. A., … Ren, B. (2010). Distinct epigenomic landscapes of pluripotent and lineage-committed human cells. *Cell Stem Cell*, *6*(5), 479–491. https://doi.org/10.1016/j.stem.2010.03.018

Hayama, R., Rout, M. P., & Fernandez-Martinez, J. (2017). The nuclear pore complex core scaffold and permeability barrier: variations of a common theme. *Current Opinion in Cell Biology*, *46*, 110–118. https://doi.org/10.1016/j.ceb.2017.05.003

Herrmann, H., & Aebi, U. (2016). Intermediate filaments: Structure and assembly. *Cold Spring Harbor Perspectives in Biology*, *8*(11). https://doi.org/10.1101/cshperspect.a018242

Hinshaw, J. E., Carragher, B. O., & Milligan, R. A. (1992). Architecture and design of the nuclear pore complex. *Cell*, *69*(7), 1133–1141. https://doi.org/10.1016/0092-8674(92)90635-P

Holaska, J. M., Kowalski, A. K., & Wilson, K. L. (2004). Emerin Caps the Pointed End of Actin Filaments: Evidence for an Actin Cortical Network at the Nuclear Inner Membrane. *PLoS Biology*, *2*(9), e231. https://doi.org/10.1371/journal.pbio.0020231

Holmes, K., Lantz, L. M., Fowlkes, B. J., Schmid, I., & Giorgi, J. V. (2001). Preparation of Cells and Reagents for Flow Cytometry. *Current Protocols in Immunology*, 1–24. https://doi.org/10.1002/0471142735.im0503s44

Hong, L., Schroth, G. P., Matthews, H. R., Yau, P., & Bradbury, E. M. (1993). Studies of the DNA binding properties of histone H4 amino terminus. Thermal denaturation studies reveal that acetylation markedly reduces the binding constant of the H4 "tail" to DNA. *Journal of Biological Chemistry*, *268*(1), 305–314.

Hozák, P., Jackson, D. A., & Cook, P. R. (1994). Replication factories and nuclear bodies: The ultrastructural characterization of replication sites during the cell cycle. *Journal of Cell Science*, *107*(8), 2191–2202. https://jcs.biologists.org/content/107/8/2191.article-info

Hozak, P., Sasseville, A. M. J., Raymond, Y., & Cook, P. R. (1995). Lamin proteins form an internal nucleoskeleton as well as a peripheral lamina in human cells. *Journal of Cell Science*, *108*(2), 635–644.

Hsu, K.-S. S., & Kao, H.-Y. Y. (2018). PML: Regulation and multifaceted function beyond tumor suppression. *Cell and Bioscience*, *8*(1), 5. https://doi.org/10.1186/s13578-018-0204-8

Hu, X., & Beeton, C. (2010). Detection of Functional Matrix Metalloproteinases by Zymography. *Journal of Visualized Experiments*, *45*, 1–5. https://doi.org/10.3791/2445

Hutten, S., Flotho, A., Melchior, F., & Kehlenbach, R. H. (2008). The Nup358-RanGAP Complex Is Required for Efficient Importin α/β-dependent Nuclear Import. *Molecular Biology of the Cell*, *19*(5), 2300–2310. https://doi.org/10.1091/mbc.e07-12-1279

Ibarra, A., Benner, C., Tyagi, S., Cool, J., & Hetzer, M. W. (2016). Nucleoporin-mediated regulation of cell identity genes. *Genes & Development*, *30*(20), 2253–2258. https://doi.org/10.1101/gad.287417.116

Iborra, F. J., Pombo, A., Jackson, D. A., & Cook, P. R. (1996). Active RNA polymerases are localized within discrete transcription "factories" in human nuclei." *Journal of Cell Science*, *109 (Pt 6*(6), 1427–1436. http://jcs.biologists.org/content/109/6/1427.abstract

Iino, H., Maeshima, K., Nakatomi, R., Kose, S., Hashikawa, T., Tachibana, T., & Imamoto, N. (2010). Live imaging system for visualizing nuclear pore complex (NPC) formation during interphase in mammalian cells. *Genes to Cells*, *15*(6), 647–660. https://doi.org/10.1111/j.1365-2443.2010.01406.x

Imamoto, N., & Funakoshi, T. (2012). Nuclear pore dynamics during the cell cycle. *Current Opinion in Cell Biology*, *24*(4), 453–459. https://doi.org/10.1016/j.ceb.2012.06.004

Ito, A., Kawaguchi, Y., Lai, C.-H., Kovacs, J. J., Higashimoto, Y., Appella, E., & Yao, T.-P. (2002). MDM2–HDAC1-mediated deacetylation of p53 is required for its degradation. *The EMBO Journal*, *21*(22), 6236–6245. https://doi.org/10.1093/emboj/cdf616

Jacinto, F. V, Benner, C., & Hetzer, M. W. (2015). The nucleoporin Nup153 regulates embryonic stem cell pluripotency through gene silencing. *Genes & Development*, *29*(12), 1224–1238. https://doi.org/10.1101/gad.260919.115

Jackson, D.A., Hassan, A. B., Errington, R. J., & Cook, P. R. (1993). Visualization of focal sites of transcription within human nuclei. *The EMBO Journal*, *12*(3), 1059–1065. https://doi.org/10.1002/j.1460-2075.1993.tb05747.x

Jackson, Dean A., & Pombo, A. (1998). Replicon clusters are stable units of chromosome structure: Evidence that nuclear organization contributes to the efficient activation and propagation of S phase in human cells. *Journal of Cell Biology*, *140*(6), 1285–1295. https://doi.org/10.1083/jcb.140.6.1285

Jahed, Z., Soheilypour, M., Peyro, M., & Mofrad, M. R. K. (2016). The LINC and NPC relationship - it's complicated! *Journal of Cell Science*, *129*(17), 3219–3229. https://doi.org/10.1242/jcs.184184

Jani, D., Lutz, S., Hurt, E., Laskey, R. A., Stewart, M., & Wickramasinghe, V. O. (2012). Functional and structural characterization of the mammalian TREX-2 complex that links transcription with nuclear messenger RNA export. *Nucleic Acids Research*, *40*(10), 4562–4573. https://doi.org/10.1093/nar/gks059

Jarnik, M., & Aebi, U. (1991). Toward a more complete 3-D structure of the nuclear pore complex. *Journal of Structural Biology*, *107*(3), 291–308. https://doi.org/10.1016/1047-8477(91)90054-Z

Justus, C. R., Leffler, N., Ruiz-Echevarria, M., & Yang, L. V. (2014). In vitro cell migration and invasion assays. *Journal of Visualized Experiments*, *88*(88), 1–8. https://doi.org/10.3791/51046

Kalverda, B., & Fornerod, M. (2010). Characterization of genome-nucleoporin interactions in Drosophila links chromatin insulators to the nuclear pore complex. *Cell Cycle*, *9*(24), 4812–4817. https://doi.org/10.4161/cc.9.24.14328

Kalverda, B., Pickersgill, H., Shloma, V. V, & Fornerod, M. (2010). Nucleoporins directly stimulate expression of developmental and cell-cycle genes inside the nucleoplasm. *Cell*, *140*(3), 360–371. https://doi.org/10.1016/j.cell.2010.01.011

Katta, S. S., Smoyer, C. J., & Jaspersen, S. L. (2014). Destination: Inner nuclear membrane. *Trends in Cell Biology*, *24*(4), 221–229. https://doi.org/10.1016/j.tcb.2013.10.006

Kehat, I., Accornero, F., Aronow, B. J., & Molkentin, J. D. (2011). Modulation of chromatin position and gene expression by HDAC4 interaction with nucleoporins. *The Journal of Cell Biology*, *193*(1), 21–29. https://doi.org/10.1083/jcb.201101046

Kelley, K., Knockenhauer, K. E., Kabachinski, G., & Schwartz, T. U. (2015). Atomic structure of the Y complex of the nuclear pore. *Nature Structural & Molecular Biology*, *22*(5), 425–431. https://doi.org/10.1038/nsmb.2998

Kim, K. H., & Sederstrom, J. M. (2015). Assaying Cell Cycle Status Using Flow Cytometry. *Current Protocols in Molecular Biology*, *111*(1), 28.6.1-28.6.11. https://doi.org/10.1002/0471142727.mb2806s111

Kim, M. S., Kwon, H. J., Lee, Y. M., Baek, J. H., Jang, J.-E., Lee, S.-W., Moon, E.-J., Kim, H.-S., Lee, S.-K., Chung, H. Y., Kim, C. W., & Kim, K.-W. (2001). Histone deacetylases induce angiogenesis by negative regulation of tumor suppressor genes. *Nature Medicine*, *7*(4), 437–443. https://doi.org/10.1038/86507

Kim, Y. B., Ki, S. W., Yoshida, M., & Horinouchi, S. (2000). Mechanism of cell cycle arrest caused by histone deacetylase inhibitors in human carcinoma cells. *The Journal of Antibiotics*, *53*(10), 1191–1200. http://www.ncbi.nlm.nih.gov/pubmed/11132966

Kind, J., Pagie, L., de Vries, S. S., Nahidiazar, L., Dey, S. S., Bienko, M., Zhan, Y., Lajoie, B., de Graaf, C. A., Amendola, M., Fudenberg, G., Imakaev, M., Mirny, L. A., Jalink, K., Dekker, J., van Oudenaarden, A., & van Steensel, B. (2015). Genome-wide Maps of Nuclear Lamina Interactions in Single Human Cells. *Cell*, *163*(1), 134–147. https://doi.org/10.1016/j.cell.2015.08.040

Kiseleva, E., Allen, T. D., Rutherford, S., Bucci, M., Wente, S. R., & Goldberg, M. W. (2004). Yeast nuclear pore complexes have a cytoplasmic ring and internal filaments. *Journal of Structural Biology*, *145*(3), 272–288. https://doi.org/10.1016/j.jsb.2003.11.010

Kiseleva, E., Drummond, S. P., Goldberg, M. W., Rutherford, S. a, Allen, T. D., & Wilson, K. L. (2004). Actin- and protein-4.1-containing filaments link nuclear pore complexes to subnuclear organelles in Xenopus oocyte nuclei. *Journal of Cell Science*, *117*(Pt 12), 2481–2490. https://doi.org/10.1242/jcs.01098

Kiseleva, E., Goldberg, M. W., Daneholt, B., & Allen, T. D. (1996). RNP Export is Mediated by Structural Reorganization of the Nuclear Pore Basket. *Journal of Molecular Biology*, *260*(3), 304–311. https://doi.org/10.1006/jmbi.1996.0401

Knockenhauer, K. E., & Schwartz, T. U. (2016). The Nuclear Pore Complex as a Flexible and Dynamic Gate. *Cell*, *164*(6), 1162–1171. https://doi.org/10.1016/j.cell.2016.01.034

Kristó, I., Bajusz, I., Bajusz, C., Borkúti, P., & Vilmos, P. (2016). Actin, actin-binding proteins, and actin-related proteins in the nucleus. *Histochemistry and Cell Biology*, *145*(4), 373–388. https://doi.org/10.1007/s00418-015-1400-9

Krull, S., Dörries, J., Boysen, B., Reidenbach, S., Magnius, L., Norder, H., Thyberg, J., & Cordes, V. C. (2010). Protein Tpr is required for establishing nuclear pore-associated zones of heterochromatin exclusion. *The EMBO Journal*, *29*(10), 1659–1673. https://doi.org/10.1038/emboj.2010.54

Krull, S., Thyberg, J., Björkroth, B., Rackwitz, H., & Cordes, V. C. (2004). Nucleoporins as Components of the Nuclear Pore Complex Core Structure and Tpr as the Architectural Element of the Nuclear Basket. *Molecular Biology of the Cell*, *15*(9), 4261–4277. https://doi.org/10.1091/mbc.e04-03-0165

Kubota, S., Fukumoto, Y., Ishibashi, K., Soeda, S., Kubota, S., Yuki, R., Nakayama, Y., Aoyama, K., Yamaguchi, N. N., & Yamaguchi, N. N. (2014). Activation of the prereplication complex is blocked by mimosine through reactive oxygen species-activated ataxia telangiectasia mutated (ATM) protein without DNA damage. *The Journal of Biological Chemistry*, *289*(9), 5730–5746. https://doi.org/10.1074/jbc.M113.546655

Kuhn, T. M., & Capelson, M. (2019). Nuclear Pore Proteins in Regulation of Chromatin State. *Cells*, *8*(11), 1414. https://doi.org/10.3390/cells8111414

Kulikov, R., Letienne, J., Kaur, M., Grossman, S. R., Arts, J., & Blattner, C. (2010). Mdm2 facilitates the association of p53 with the proteasome. *Proceedings of the National Academy of Sciences of the United States of America*, *107*(22), 10038–10043. https://doi.org/10.1073/pnas.0911716107

Kutay, U., Bischoff, F. R., Kostka, S., Kraft, R., & Görlich, D. (1997). Export of Importin α from the Nucleus Is Mediated by a Specific Nuclear Transport Factor. *Cell*, *90*(6), 1061–1071. https://doi.org/10.1016/S0092-8674(00)80372-4

Laurell, E., Beck, K., Krupina, K., Theerthagiri, G., Bodenmiller, B., Horvath, P., Aebersold, R., Antonin, W., & Kutay, U. (2011). Phosphorylation of Nup98 by multiple kinases is crucial for NPC disassembly during mitotic entry. *Cell*, *144*(4), 539–550. https://doi.org/10.1016/j.cell.2011.01.012

Lee, P. Y., Costumbrado, J., Hsu, C.-Y., & Kim, Y. H. (2012). Agarose Gel Electrophoresis for the Separation of DNA Fragments. *Journal of Visualized Experiments*, *62*(62), 1–5. https://doi.org/10.3791/3923

Lee, R. K. Y., Lui, P. P. Y., Ngan, E. K. S., Lui, J. C. K., Suen, Y. K., Chan, F., & Kong, S. K. (2006). The nuclear tubular invaginations are dynamic structures inside the nucleus of HeLa cells 1. *Canadian Journal of Physiology and Pharmacology*, *84*(3–4), 477–486. https://doi.org/10.1139/Y05-110

Lee, S. H., Sterling, H., Burlingame, A., & McCormick, F. (2008). Tpr directly binds to Mad1 and Mad2 and is important for the Mad1-Mad2-mediated mitotic spindle checkpoint. *Genes & Development*, *22*(21), 2926–2931. https://doi.org/10.1101/gad.1677208

Legartová, S., Stixová, L., Laur, O., Kozubek, S., Sehnalová, P., & Bártová, E. (2013). Nuclear structures surrounding internal lamin invaginations. *Journal of Cellular Biochemistry*, *487*(October 2013), 476–487. https://doi.org/10.1002/jcb.24681

Lemke, E. A. (2016). The Multiple Faces of Disordered Nucleoporins. *Journal of Molecular Biology*, *428*(10), 2011–2024. https://doi.org/10.1016/j.jmb.2016.01.002

Li, Y., & Seto, E. (2016). HDACs and HDAC Inhibitors in Cancer Development and Therapy. *Cold Spring Harbor Perspectives in Medicine*, *6*(10), a026831. https://doi.org/10.1101/cshperspect.a026831

Liang, Y., Franks, T. M., Marchetto, M. C., Gage, F. H., & Hetzer, M. W. (2013). Dynamic Association of NUP98 with the Human Genome. *PLoS Genetics*, *9*(2), e1003308. https://doi.org/10.1371/journal.pgen.1003308

Light, W. H., Freaney, J., Sood, V., Thompson, A., D'Urso, A., Horvath, C. M., & Brickner, J. H. (2013). A Conserved Role for Human Nup98 in Altering Chromatin Structure and Promoting Epigenetic Transcriptional Memory. *PLoS Biology*, *11*(3), e1001524. https://doi.org/10.1371/journal.pbio.1001524

Liu, Q., Pante, N., Misteli, T., Elsagga, M., Crisp, M., Hodzic, D., Burke, B., & Roux, K. J. (2007). Functional association of Sun1 with nuclear pore complexes. *Journal of Cell Biology*, *178*(5), 785–798. https://doi.org/10.1083/jcb.200704108

Liu, X., Zhang, Y., Chen, Y., Li, M., Zhou, F., Li, K., Cao, H., Ni, M., Liu, Y., Gu, Z., Dickerson, K. E., Xie, S., Hon, G. C., Xuan, Z., Zhang, M. Q., Shao, Z., & Xu, J. (2017). In Situ Capture of Chromatin Interactions by Biotinylated dCas9. *Cell*, *170*(5), 1028-1043.e19. https://doi.org/10.1016/j.cell.2017.08.003

López-Soop, G., Rønningen, T., Rogala, A., Richartz, N., Blomhoff, H. K., Thiede, B., Collas, P., & Küntziger, T. (2017). AKAP95 interacts with nucleoporin TPR in mitosis and is important for the spindle assembly checkpoint. *Cell Cycle*, *16*(10), 947–956. https://doi.org/10.1080/15384101.2017.1310350

Löschberger, A., Franke, C., Krohne, G., van de Linde, S., & Sauer, M. (2014). Correlative super-resolution fluorescence and electron microscopy of the nuclear pore complex with

molecular resolution. *Journal of Cell Science*, *127*(20), 4351–4355. https://doi.org/10.1242/jcs.156620

Lu, L., Ladinsky, M. S., & Kirchhausen, T. (2011). Formation of the postmitotic nuclear envelope from extended ER cisternae precedes nuclear pore assembly. *The Journal of Cell Biology*, *194*(3), 425–440. https://doi.org/10.1083/jcb.201012063

Lui, P. P., Lee, C. Y., Tsang, D., & Kong, S. K. (1998). Ca2+ is released from the nuclear tubular structure into nucleoplasm in C6 glioma cells after stimulation with phorbol ester. *FEBS Letters*, *432*(1–2), 82–87. http://www.ncbi.nlm.nih.gov/pubmed/9710256

Lund, E. G., Duband-Goulet, I., Oldenburg, A., Buendia, B., & Collas, P. (2015). Distinct features of lamin A-interacting chromatin domains mapped by Chip-sequencing from sonicated or micrococcal nuclease-digested chromatin. *Nucleus*, *6*(1), 30–39. https://doi.org/10.4161/19491034.2014.990855

Lussi, Y. C., Shumaker, D. K., Shimi, T., & Fahrenkrog, B. (2010). The nucleoporin Nup153 affects spindle checkpoint activity due to an association with Mad1. *Nucleus*, *1*(1), 71–84. https://doi.org/10.4161/nucl.1.1.10244

Macey, M. G. (2007). *Flow cytometry: Principles and Applications* (M. G. Macey (ed.)). Humana Press. https://doi.org/10.1007/978-1-59745-451-3

Machado, C., & Andrew, D. J. (2000). D-Titin: A giant protein with dual roles in chromosomes and muscles. *Journal of Cell Biology*, *151*(3), 639–651. https://doi.org/10.1083/jcb.151.3.639

Maeshima, K., Iino, H., Hihara, S., Funakoshi, T., Watanabe, A., Nishimura, M., Nakatomi, R., Yahata, K., Imamoto, F., Hashikawa, T., Yokota, H., & Imamoto, N. (2010). Nuclear pore formation but not nuclear growth is governed by cyclin-dependent kinases (Cdks) during interphase. *Nature Structural & Molecular Biology*, *17*(9), 1065–1071. https://doi.org/10.1038/nsmb.1878

Maeshima, K., Iino, H., Hihara, S., & Imamoto, N. (2011). Nuclear size, nuclear pore number and cell cycle. *Nucleus*, *2*(2), 113–118. https://doi.org/10.4161/nucl.2.2.15446

Makise, M., Mackay, D. R., Elgort, S., Shankaran, S. S., Adam, S. a., & Ullman, K. S. (2012). The Nup153-Nup50 protein interface and its role in nuclear import. *Journal of Biological Chemistry*, *287*(46), 38515–38522. https://doi.org/10.1074/jbc.M112.378893

Malhas, A., Goulbourne, C., & Vaux, D. J. (2011). The nucleoplasmic reticulum: form and function. *Trends in Cell Biology*, *21*(6), 362–373. https://doi.org/10.1016/j.tcb.2011.03.008

Manal, M., Chandrasekar, M. J. N., Gomathi Priya, J., & Nanjan, M. J. (2016). Inhibitors of histone deacetylase as antitumor agents: A critical review. *Bioorganic Chemistry*, *67*, 18–42. https://doi.org/10.1016/j.bioorg.2016.05.005

Mao, Y. S., Zhang, B., & Spector, D. L. (2011). Biogenesis and function of nuclear bodies. *Trends in Genetics*, *27*(8), 295–306. https://doi.org/10.1016/j.tig.2011.05.006

Markaki, Y., Gunkel, M., Schermelleh, L., Beichmanis, S., Neumann, J., Heidemann, M., Leonhardt, H., Eick, D., Cremer, C., & Cremer, T. (2010). Functional nuclear organization of transcription and DNA replication: A topographical marriage between chromatin domains and the interchromatin compartment. *Cold Spring Harbor Symposia on Quantitative Biology*, *75*, 475–492. https://doi.org/10.1101/sqb.2010.75.042

Marks, P. A. (2007). Discovery and development of SAHA as an anticancer agent. *Oncogene*, *26*(9), 1351–1356. https://doi.org/10.1038/sj.onc.1210204

Martin, C., Chen, S., Maya-Mendoza, A., Lovric, J., Sims, P. F. G., & Jackson, D. A. (2009). Lamin B1 maintains the functional plasticity of nucleoli. *Journal of Cell Science*, *122*(Pt 10), 1551–1562. https://doi.org/10.1242/jcs.046284

Masiello, I., Siciliani, S., & Biggiogera, M. (2018). Perichromatin region: a moveable feast. *Histochemistry and Cell Biology*, *150*(3), 227–233. https://doi.org/10.1007/s00418-018-1703-8

Matharu, N., & Ahituv, N. (2015). Minor Loops in Major Folds: Enhancer–Promoter Looping, Chromatin Restructuring, and Their Association with Transcriptional Regulation and Disease. *PLOS Genetics*, *11*(12), e1005640. https://doi.org/10.1371/journal.pgen.1005640

Mathupala, S. P., & Sloan, A. E. (2009). An agarose-based cloning-ring anchoring method for isolation of viable cell clones. *BioTechniques*, *46*(4), 305–307. https://doi.org/10.2144/000113079

Mattagajasingh, S. N., Huang, S. C., & Benz, E. J. (2009). Inhibition of Protein 4.1 R and NuMA interaction by mutagenization of their binding-sites abrogates nuclear localization of 4.1 R. *Clinical and Translational Science*, *2*(2), 102–111. https://doi.org/10.1111/j.1752-8062.2008.00087.x

Maul, G. G., Price, J. W., & Lieberman, M. W. (1971). Formation and distribution of nuclear pore complexes in interphase. *The Journal of Cell Biology*, *51*(2), 405–418. https://doi.org/10.1083/jcb.51.2.405

Mehta, I. S., Elcock, L. S., Amira, M., Kill, I. R., & Bridger, J. M. (2008). Nuclear motors and nuclear structures containing A-type lamins and emerin: Is there a functional link? *Biochemical Society Transactions*, *36*(6), 1384–1388. https://doi.org/10.1042/BST0361384

Melan, M. A., & Sluder, G. (1992). Redistribution and differential extraction of soluble proteins in permeabilized cultured cells. Implications for immunofluorescence microscopy. *Journal of Cell Science*, *101*(4), 731–743.

Mészáros, N., Cibulka, J., Mendiburo, M. J., Romanauska, A., Schneider, M., & Köhler, A. (2015). Nuclear Pore Basket Proteins Are Tethered to the Nuclear Envelope and Can Regulate Membrane Curvature. *Developmental Cell*, *33*(3), 285–298. https://doi.org/10.1016/j.devcel.2015.02.017

Meyer, A. J., Almendrala, D. K., Go, M. M., & Krauss, S. W. (2011). Structural protein 4.1R is integrally involved in nuclear envelope protein localization, centrosome-nucleus association and transcriptional signaling. *Journal of Cell Science*, *124*(Pt 9), 1433–1444. https://doi.org/10.1242/jcs.077883

Mishra, R. K., Chakraborty, P., Arnaoutov, A., Fontoura, B. M. A., & Dasso, M. (2010). The Nup107-160 complex and γ-TuRC regulate microtubule polymerization at kinetochores. *Nature Cell Biology*, *12*(2), 164–169. https://doi.org/10.1038/ncb2016

Mitchell, J. A., & Fraser, P. (2008). Transcription factories are nuclear subcompartments that remain in the absence of transcription. *Genes & Development*, *22*(1), 20–25. https://doi.org/10.1101/gad.454008

Morchoisne-Bolhy, S., Geoffroy, M.-C., Bouhlel, I. B., Alves, A., Audugé, N., Baudin, X., Van Bortle, K., Powers, M. A., & Doye, V. (2015). Intranuclear dynamics of the Nup107-160 complex. *Molecular Biology of the Cell*, *26*(12), 2343–2356. https://doi.org/10.1091/mbc.E15-02-0060

Munshi, A., Shafi, G., Aliya, N., & Jyothy, A. (2009). Histone modifications dictate specific biological readouts. *Journal of Genetics and Genomics*, *36*(2), 75–88. https://doi.org/10.1016/S1673-8527(08)60094-6

Nalepa, G., & Harper, J. W. (2004). Visualization of a highly organized intranuclear network of filaments in living mammalian cells. *Cell Motility and the Cytoskeleton*, *59*(2), 94–108. https://doi.org/10.1002/cm.20023

Nanni, S., Re, A., Ripoli, C., Gowran, A., Nigro, P., D'Amario, D., Amodeo, A., Crea, F., Grassi, C., Pontecorvi, A., Farsetti, A., & Colussi, C. (2016). The nuclear pore protein Nup153 associates with chromatin and regulates cardiac gene expression in dystrophic mdx hearts. *Cardiovascular Research*, *112*(2), 555–567. https://doi.org/10.1093/cvr/cvw204

Ni, D., Xu, P., & Gallagher, S. (2016). Immunoblotting and Immunodetection. *Current Protocols in Molecular Biology*, *114*(1), 10.8.1-10.8.37. https://doi.org/10.1002/0471142727.mb1008s114

Obrdlik, A., Louvet, E., Kukalev, A., Naschekin, D., Kiseleva, E., Fahrenkrog, B., & Percipalle, P. (2010). Nuclear myosin 1 is in complex with mature rRNA transcripts and associates with the nuclear pore basket. *The FASEB Journal*, *24*(1), 146–157. https://doi.org/10.1096/fj.09-135863

Oka, M., Asally, M., Yasuda, Y., Ogawa, Y., Tachibana, T., & Yoneda, Y. (2010). The Mobile FG Nucleoporin Nup98 Is a Cofactor for Crm1-dependent Protein Export. *Molecular Biology of the Cell*, *21*(11), 1885–1896. https://doi.org/10.1091/mbc.e09-12-1041

Olson, B. J. S. C. (2016). Assays for Determination of Protein Concentration. *Current Protocols in Pharmacology*, *73*(1), A.3A.1-A.3A.32. https://doi.org/10.1002/cpph.3

Oma, Y., & Harata, M. (2011). Actin-related proteins localized in the nucleus: From discovery to novel roles in nuclear organization. *Nucleus*, *2*(1), 38–46. https://doi.org/10.4161/nucl.2.1.14510

Orjalo, A. V., Arnaoutov, A., Shen, Z., Boyarchuk, Y., Zeitlin, S. G., Fontoura, B., Briggs, S., Dasso, M., & Forbes, D. J. (2006). The Nup107-160 Nucleoporin Complex Is Required for Correct Bipolar Spindle Assembly. *Molecular Biology of the Cell*, *17*(9), 3806–3818. https://doi.org/10.1091/mbc.e05-11-1061

Osborne, C. S., Chakalova, L., Mitchell, J. A., Horton, A., Wood, A. L., Bolland, D. J., Corcoran, A. E., & Fraser, P. (2007). Myc dynamically and preferentially relocates to a transcription factory occupied by Igh. *PLoS Biology*, *5*(8), 1763–1772. https://doi.org/10.1371/journal.pbio.0050192

Otsuka, S., & Ellenberg, J. (2018). Mechanisms of nuclear pore complex assembly – two different ways of building one molecular machine. *FEBS Letters*, *592*(4), 475–488. https://doi.org/10.1002/1873-3468.12905

Otsuka, S., Steyer, A. M., Schorb, M., Hériché, J.-K., Hossain, M. J., Sethi, S., Kueblbeck, M., Schwab, Y., Beck, M., & Ellenberg, J. (2018). Postmitotic nuclear pore assembly proceeds by radial dilation of small membrane openings. *Nature Structural & Molecular Biology*, *25*(1), 21–28. https://doi.org/10.1038/s41594-017-0001-9

Paddy, M. R. (1998). The Tpr Protein: Linking Structure and Function in the Nuclear Interior? *The American Journal of Human Genetics*, *63*(2), 305–310. https://doi.org/10.1086/301989

Palozola, K. C., Lerner, J., & Zaret, K. S. (2019). A changing paradigm of transcriptional memory propagation through mitosis. *Nature Reviews Molecular Cell Biology*, *20*(1), 55–64. https://doi.org/10.1038/s41580-018-0077-z

Parbin, S., Kar, S., Shilpi, A., Sengupta, D., Deb, M., Rath, S. K., & Patra, S. K. (2014). Histone Deacetylases: A Saga of Perturbed Acetylation Homeostasis in Cancer. *Journal*

of Histochemistry & Cytochemistry, *62*(1), 11–33. https://doi.org/10.1369/0022155413506582

Pascual-Garcia, P., & Capelson, M. (2019). Nuclear pores in genome architecture and enhancer function. *Current Opinion in Cell Biology*, *58*, 126–133. https://doi.org/10.1016/j.ceb.2019.04.001

Pascual-Garcia, P., Debo, B., Aleman, J. R., Talamas, J. A., Lan, Y., Nguyen, N. H., Won, K. J., & Capelson, M. (2017). Metazoan Nuclear Pores Provide a Scaffold for Poised Genes and Mediate Induced Enhancer-Promoter Contacts. *Molecular Cell*, *66*(1), 63-76.e6. https://doi.org/10.1016/j.molcel.2017.02.020

Pascual-Garcia, P., Jeong, J., & Capelson, M. (2014). Nucleoporin Nup98 Associates with Trx/MLL and NSL Histone-Modifying Complexes and Regulates Hox Gene Expression. *Cell Reports*, *9*(2), 433–442. https://doi.org/10.1016/j.celrep.2014.09.002

Pederson, T. (2011). The nucleolus. *Cold Spring Harbor Perspectives in Biology*, *3*(3), a000638. https://doi.org/10.1101/cshperspect.a000638

Percipalle, P., Fomproix, N., Cavellán, E., Voit, R., Reimer, G., Krüger, T., Thyberg, J., Scheer, U., Grummt, I., & Östlund Farrants, A. K. (2006). The chromatin remodelling complex WSTF-SNF2h interacts with nuclear myosin 1 and has a role in RNA polymerase I transcription. *EMBO Reports*, *7*(5), 525–530. https://doi.org/10.1038/sj.embor.7400657

Peric-Hupkes, D., Meuleman, W., Pagie, L., Bruggeman, S. W. M., Solovei, I., Brugman, W., Gräf, S., Flicek, P., Kerkhoven, R. M., van Lohuizen, M., Reinders, M., Wessels, L., & van Steensel, B. (2010). Molecular Maps of the Reorganization of Genome-Nuclear Lamina Interactions during Differentiation. *Molecular Cell*, *38*(4), 603–613. https://doi.org/10.1016/j.molcel.2010.03.016

Phelan, K., & May, K. M. (2017). Mammalian Cell Tissue Culture Techniques. *Current Protocols in Molecular Biology*, *117*(1), A.3F.1-A.3F.23. https://doi.org/10.1002/cpmb.31

Pirrotta, V., & Li, H. B. (2012). A view of nuclear Polycomb bodies. *Current Opinion in Genetics and Development*, *22*(2), 101–109. https://doi.org/10.1016/j.gde.2011.11.004

Prakash, K. (2017). Chromatin Architecture Advances from High-Resolution Single Molecule DNA Imaging. In *Springer Theses*. Springer Cham. https://doi.org/10.1007/978-3-319-52183-1

Prakash, K., & Fournier, D. (2018). Evidence for the implication of the histone code in building the genome structure. *BioSystems*, *164*, 49–59. https://doi.org/10.1016/j.biosystems.2017.11.005

Rabut, G., Doye, V., & Ellenberg, J. (2004). Mapping the dynamic organization of the nuclear pore complex inside single living cells. *Nature Cell Biology*, *6*(11), 1114–1121. https://doi.org/10.1038/ncb1184

Radulescu, A. E., & Cleveland, D. W. (2010). NuMA after 30 years: The matrix revisited. *Trends in Cell Biology*, *20*(4), 214–222. https://doi.org/10.1016/j.tcb.2010.01.003

Rajanala, K., & Nandicoori, V. K. (2012). Localization of Nucleoporin Tpr to the Nuclear Pore Complex Is Essential for Tpr Mediated Regulation of the Export of Unspliced RNA. *PLoS ONE*, *7*(1), e29921. https://doi.org/10.1371/journal.pone.0029921

Rajanala, K., Sarkar, A., Jhingan, G. D., Priyadarshini, R., Jalan, M., Sengupta, S., & Nandicoori, V. K. (2014). Phosphorylation of nucleoporin Tpr governs its differential localization and is required for its mitotic function. *Journal of Cell Science*, *127*(Pt 16), 3505–3520. https://doi.org/10.1242/jcs.149112

Ranade, D., Pradhan, R., Jayakrishnan, M., Hegde, S., & Sengupta, K. (2019). Lamin A/C and Emerin depletion impacts chromatin organization and dynamics in the interphase nucleus. *BMC Molecular and Cell Biology*, *20*(1), 1–20. https://doi.org/10.1186/s12860-019-0192-5

Rao, S. S. P., Huntley, M. H., Durand, N. C., Stamenova, E. K., Bochkov, I. D., Robinson, J. T., Sanborn, A. L., Machol, I., Omer, A. D., Lander, E. S., & Aiden, E. L. (2014). A 3D map of the human genome at kilobase resolution reveals principles of chromatin looping. *Cell*, *159*(7), 1665–1680. https://doi.org/10.1016/j.cell.2014.11.021

Rasala, B. A., Ramos, C., Harel, A., & Forbes, D. J. (2008). Capture of AT-rich Chromatin by ELYS Recruits POM121 and NDC1 to Initiate Nuclear Pore Assembly. *Molecular Biology of the Cell*, *19*(9), 3982–3996. https://doi.org/10.1091/mbc.e08-01-0012

Razin, S. V., Iarovaia, O. V., & Vassetzky, Y. S. (2014). A requiem to the nuclear matrix: From a controversial concept to 3D organization of the nucleus. *Chromosoma*, *123*(3), 217–224. https://doi.org/10.1007/s00412-014-0459-8

Reichelt, M., Wang, L., Sommer, M., Perrino, J., Nour, A. M., Sen, N., Baiker, A., Zerboni, L., & Arvin, A. M. (2011). Entrapment of Viral Capsids in Nuclear PML Cages Is an Intrinsic Antiviral Host Defense against Varicella-Zoster Virus. *PLoS Pathogens*, *7*(2), e1001266. https://doi.org/10.1371/journal.ppat.1001266

Ren, Y., Seo, H.-S., Blobel, G., & Hoelz, A. (2010). Structural and functional analysis of the interaction between the nucleoporin Nup98 and the mRNA export factor Rae1. *Proceedings of the National Academy of Sciences*, *107*(23), 10406–10411. https://doi.org/10.1073/pnas.1005389107

Reynolds, C. P., Biedler, J. L., Spengler, B. A., Reynolds, D. A., Ross, R. A., Frenkel, E. P., & Smith, R. G. (1986). Characterization of human neuroblastoma cell lines established

before and after therapy. *Journal of the National Cancer Institute*, *76*(3), 375–387. http://www.ncbi.nlm.nih.gov/pubmed/3456456

Ribbeck, K. (1998). NTF2 mediates nuclear import of Ran. *The EMBO Journal*, *17*(22), 6587–6598. https://doi.org/10.1093/emboj/17.22.6587

Rieder, D., Trajanoski, Z., & McNally, J. G. (2012). Transcription factories. *Frontiers in Genetics*, *3*, 221. https://doi.org/10.3389/fgene.2012.00221

Rikiishi, H. (2011). Autophagic and Apoptotic Effects of HDAC Inhibitors on Cancer Cells. *Journal of Biomedicine and Biotechnology*, *2011*, 1–9. https://doi.org/10.1155/2011/830260

Ris, H. (1997). High-resolution field-emission scanning electron microscopy of nuclear pore complex. *Scanning*, *19*(5), 368–375. https://doi.org/10.1002/sca.4950190504

Rodriguez, M. S., Dargemont, C., & Stutz, F. (2004). Nuclear export of RNA. *Biology of the Cell*, *96*(8), 639–655. https://doi.org/10.1016/j.biolcel.2004.04.014

Ryabichk, S. S., Ibragimo, A. N., Lebedev, L. A., Kozlov, E. N., & Shidlovskii, Y. V. (2017). Super-resolution microscopy in studying the structure and function of the cell nucleus. *Acta Naturae*, *9*(4), 42–51. https://doi.org/10.32607/2075851-2017-9-4-42-51

Sasse, J., & Gallagher, S. R. (2009). Staining Proteins in Gels. *Current Protocols in Molecular Biology*, *85*(1), 10.6.1-10.6.27. https://doi.org/10.1002/0471142727.mb1006s85

Saunders, L. R., & Verdin, E. (2007). Sirtuins: critical regulators at the crossroads between cancer and aging. *Oncogene*, *26*(37), 5489–5504. https://doi.org/10.1038/sj.onc.1210616

Schlaitz, A.-L. L., Thompson, J., Wong, C. C. L., Yates, J. R., & Heald, R. (2013). REEP3/4 ensure endoplasmic reticulum clearance from metaphase chromatin and proper nuclear envelope architecture. *Developmental Cell*, *26*(3), 315–323. https://doi.org/10.1016/j.devcel.2013.06.016

Schmidt, H. B., & Görlich, D. (2016). Transport Selectivity of Nuclear Pores, Phase Separation, and Membraneless Organelles. *Trends in Biochemical Sciences*, *41*(1), 46–61. https://doi.org/10.1016/j.tibs.2015.11.001

Schoen, I., Aires, L., Ries, J., & Vogel, V. (2017). Nanoscale invaginations of the nuclear envelope: Shedding new light on wormholes with elusive function. *Nucleus*, *0*(0), 1–9. https://doi.org/10.1080/19491034.2017.1337621

Schwartz, T. U. (2016). The Structure Inventory of the Nuclear Pore Complex. *Journal of Molecular Biology*, *428*(10), 1986–2000. https://doi.org/10.1016/j.jmb.2016.03.015

Schweizer, N., Ferrás, C., Kern, D. M., Logarinho, E., Cheeseman, I. M., & Maiato, H. (2013). Spindle assembly checkpoint robustness requires Tpr-mediated regulation of Mad1/Mad2 proteostasis. *The Journal of Cell Biology*, *203*(6), 883–893. https://doi.org/10.1083/jcb.201309076

See, K., Lan, Y., Rhoades, J., Jain, R., Smith, C. L., & Epstein, J. A. (2019). Lineage-specific reorganization of nuclear peripheral heterochromatin and H3K9Me2 domains. *Development (Cambridge)*, *146*(3). https://doi.org/10.1242/dev.174078

Seto, E., & Yoshida, M. (2014). Erasers of Histone Acetylation: The Histone Deacetylase Enzymes. *Cold Spring Harbor Perspectives in Biology*, *6*(4), a018713–a018713. https://doi.org/10.1101/cshperspect.a018713

Shimi, T., Pfleghaar, K., Kojima, S. I., Pack, C. G., Solovei, I., Goldman, A. E., Adam, S. A., Shumaker, D. K., Kinjo, M., Cremer, T., & Goldman, R. D. (2008). The A- and B-type nuclear lamin networks: Microdomains involved in chromatin organization and transcription. *Genes and Development*, *22*(24), 3409–3421. https://doi.org/10.1101/gad.1735208

Shumaker, D. K., Solimando, L., Sengupta, K., Shimi, T., Adam, S. A., Grunwald, A., Strelkov, S. V., Aebi, U., Cardoso, M. C., & Goldman, R. D. (2008). The highly conserved nuclear lamin Ig-fold binds to PCNA: Its role in DNA replication. *Journal of Cell Biology*, *181*(2), 269–280. https://doi.org/10.1083/jcb.200708155

Simon, D. N., & Wilson, K. L. (2011). The nucleoskeleton as a genome-associated dynamic "network of networks". *Nature Reviews. Molecular Cell Biology*, *12*(11), 695–708. https://doi.org/10.1038/nrm3207

Sloan, K. E., Gleizes, P.-E., & Bohnsack, M. T. (2016). Nucleocytoplasmic Transport of RNAs and RNA–Protein Complexes. *Journal of Molecular Biology*, *428*(10), 2040–2059. https://doi.org/10.1016/j.jmb.2015.09.023

Smallwood, A., Estève, P. O., Pradhan, S., & Carey, M. (2007). Functional cooperation between HP1 and DNMT1 mediates gene silencing. *Genes and Development*, *21*(10), 1169–1178. https://doi.org/10.1101/gad.1536807

Smeets, D., Markaki, Y., Schmid, V. J., Kraus, F., Tattermusch, A., Cerase, A., Sterr, M., Fiedler, S., Demmerle, J., Popken, J., Leonhardt, H., Brockdorff, N., Cremer, T., Schermelleh, L., & Cremer, M. (2014). Three-dimensional super-resolution microscopy of the inactive X chromosome territory reveals a collapse of its active nuclear compartment harboring distinct Xist RNA foci. *Epigenetics and Chromatin*, *7*(1), 1–27. https://doi.org/10.1186/1756-8935-7-8

Smith, A., Brownawell, A., & Macara, I. G. (1998). Nuclear import of Ran is mediated by the transport factor NTF2. *Current Biology*, *8*(25), 1403-S1. https://doi.org/10.1016/S0960-9822(98)00023-2

Smyth, J. T., Beg, A. M., Wu, S., Putney, J. W., & Rusan, N. M. (2012). Phosphoregulation of STIM1 Leads to Exclusion of the Endoplasmic Reticulum from the Mitotic Spindle. *Current Biology*, *22*(16), 1487–1493. https://doi.org/10.1016/j.cub.2012.05.057

Smythe, C., Jenkins, H. E., & Hutchison, C. J. (2000). Incorporation of the nuclear pore basket protein nup153 into nuclear pore structures is dependent upon lamina assembly: evidence from cell-free extracts of Xenopus eggs. *The EMBO Journal*, *19*, 3918–3931. https://doi.org/10.1093/emboj/19.15.3918

Soop, T., Ivarsson, B., Björkroth, B., Fomproix, N., Masich, S., Cordes, V. C., & Daneholt, B. (2005). Nup153 Affects Entry of Messenger and Ribosomal Ribonucleoproteins into the Nuclear Basket during Export. *Molecular Biology of the Cell*, *16*(12), 5610–5620. https://doi.org/10.1091/mbc.e05-08-0715

Souquet, B., Freed, E., Berto, A., Andric, V., Audugé, N., Reina-San-Martin, B., Lacy, E., & Doye, V. (2018). Nup133 Is Required for Proper Nuclear Pore Basket Assembly and Dynamics in Embryonic Stem Cells. *Cell Reports*, 2443–2454. https://doi.org/10.1016/j.celrep.2018.04.070

Spange, S., Wagner, T., Heinzel, T., & Krämer, O. H. (2009). Acetylation of non-histone proteins modulates cellular signalling at multiple levels. *The International Journal of Biochemistry & Cell Biology*, *41*(1), 185–198. https://doi.org/10.1016/j.biocel.2008.08.027

Spector, D. L., & Lamond, A. I. (2011). Nuclear speckles. *Cold Spring Harbor Perspectives in Biology*, *3*(a000646). https://doi.org/10.1101/cshperspect.a000646

Sridharan, D. M., McMahon, L. W., & Lambert, M. W. (2006). αII-Spectrin interacts with five groups of functionally important proteins in the nucleus. *Cell Biology International*, *30*(11), 866–878. https://doi.org/10.1016/j.cellbi.2006.06.005

Srivastava, R. K., Kurzrock, R., & Shankar, S. (2010). MS-275 sensitizes TRAIL-resistant breast cancer cells, inhibits angiogenesis and metastasis, and reverses epithelial-mesenchymal transition in vivo. *Molecular Cancer Therapeutics*. https://doi.org/10.1158/1535-7163.MCT-10-0582

Staněk, D. (2017). Cajal bodies and snRNPs - friends with benefits. *RNA Biology*, *14*(6), 671–679. https://doi.org/10.1080/15476286.2016.1231359

Staněk, D., & Fox, A. (2017). Nuclear bodies: news insights into structure and function. *Current Opinion in Cell Biology*, *46*, 94–101. https://doi.org/10.1016/j.ceb.2017.05.001

Stick, R., & Peter, A. (2017). Evolutionary changes in lamin expression in the vertebrate lineage. *Nucleus*, *8*(4), 392–403. https://doi.org/10.1080/19491034.2017.1303592

Storch, K. N., Taatjes, D. J., Bouffard, N. a, Locknar, S., Bishop, N. M., & Langevin, H. M. (2007). Alpha smooth muscle actin distribution in cytoplasm and nuclear invaginations of connective tissue fibroblasts. *Histochemistry and Cell Biology*, *127*(5), 523–530. https://doi.org/10.1007/s00418-007-0275-9

Strahl, B. D., & Allis, C. D. (2000). The language of covalent histone modi®cations. *Nature*, *403*(January), 41–45. https://doi.org/10.1038/47412

Strom, A. R., & Brangwynne, C. P. (2019). CELL SCIENCE AT A GLANCE The liquid nucleome – phase transitions in the nucleus at a glance. *Journal of Cell Science*, *132*, 1–7. https://doi.org/10.1242/jcs.235093

Stuwe, T., Schada von Borzyskowski, L., Davenport, A. M., & Hoelz, A. (2012). Molecular Basis for the Anchoring of Proto-Oncoprotein Nup98 to the Cytoplasmic Face of the Nuclear Pore Complex. *Journal of Molecular Biology*, *419*(5), 330–346. https://doi.org/10.1016/j.jmb.2012.03.024

Sun, Q., Hao, Q., & Prasanth, K. V. (2018). Nuclear Long Noncoding RNAs: Key Regulators of Gene Expression. *Trends in Genetics*, *34*(2), 142–157. https://doi.org/10.1016/j.tig.2017.11.005

Sutherland, H., & Bickmore, W. A. (2009). Transcription factories: gene expression in unions? *Nature Reviews Genetics*, *10*(7), 457–466. https://doi.org/10.1038/nrg2592

Talamas, J. A., & Hetzer, M. W. (2011). POM121 and sun1 play a role in early steps of interphase NPC assembly. *Journal of Cell Biology*, *194*(1), 27–37. https://doi.org/10.1083/jcb.201012154

Tatomer, D. C., Terzo, E., Curry, K. P., Salzler, H., Sabath, I., Zapotoczny, G., McKay, D. J., Dominski, Z., Marzluff, W. F., & Duronio, R. J. (2016). Concentrating pre-mRNA processing factors in the histone locus body facilitates efficient histone mRNA biogenesis. *Journal of Cell Biology*, *213*(5), 557–570. https://doi.org/10.1083/jcb.201504043

Teif, V. B., Mallm, J. P., Sharma, T., Mark Welch, D. B., Rippe, K., Eils, R., Langowski, J., Olins, A. L., & Olins, D. E. (2017). Nucleosome repositioning during differentiation of a human myeloid leukemia cell line. *Nucleus*, *8*(2), 188–204. https://doi.org/10.1080/19491034.2017.1295201

Toda, T., Hsu, J. Y., Linker, S. B., Hu, L., Schafer, S. T., Mertens, J., Jacinto, F. V., Hetzer, M. W., & Gage, F. H. (2017). Nup153 Interacts with Sox2 to Enable Bimodal Gene Regulation and Maintenance of Neural Progenitor Cells. *Cell Stem Cell*, *21*(5), 618-634.e7. https://doi.org/10.1016/j.stem.2017.08.012

Tolhuis, B., Blom, M., Kerkhoven, R. M., Pagie, L., Teunissen, H., Nieuwland, M., Simonis, M., de Laat, W., van Lohuizen, M., & van Steensel, B. (2011). Interactions among Polycomb Domains Are Guided by Chromosome Architecture. *PLoS Genetics*, *7*(3), e1001343. https://doi.org/10.1371/journal.pgen.1001343

Troeberg, L., & Nagase, H. (2003). Zymography of Metalloproteinases. *Current Protocols in Protein Science*, *33*, 21.15.1-21.15.12. https://doi.org/10.1002/0471140864.ps2115s33

Umlauf, D., Bonnet, J., Waharte, F., Fournier, M., Stierle, M., Fischer, B., Brino, L., Devys, D., & Tora, L. (2013). The human TREX-2 complex is stably associated with the nuclear pore basket. *Journal of Cell Science*, *126*(12), 2656–2667. https://doi.org/10.1242/jcs.118000

Ungricht, R., & Kutay, U. (2017). Mechanisms and functions of nuclear envelope remodelling. *Nature Reviews Molecular Cell Biology*, *18*(4), 229–245. https://doi.org/10.1038/nrm.2016.153

Vaquerizas, J. M., Suyama, R., Kind, J., Miura, K., Luscombe, N. M., & Akhtar, A. (2010). Nuclear Pore Proteins Nup153 and Megator Define Transcriptionally Active Regions in the Drosophila Genome. *PLoS Genetics*, *6*(2), e1000846. https://doi.org/10.1371/journal.pgen.1000846

Vollmer, B., & Antonin, W. (2014). The diverse roles of the Nup93/Nic96 complex proteins – structural scaffolds of the nuclear pore complex with additional cellular functions. *Biological Chemistry*, *395*(5), 515–528. https://doi.org/10.1515/hsz-2013-0285

Vollmer, B., Lorenz, M., Moreno-Andrés, D., Bodenhöfer, M., De Magistris, P., Astrinidis, S. A., Schooley, A., Flötenmeyer, M., Leptihn, S., & Antonin, W. (2015). Nup153 Recruits the Nup107-160 Complex to the Inner Nuclear Membrane for Interphasic Nuclear Pore Complex Assembly. *Developmental Cell*, *33*(6), 717–728. https://doi.org/10.1016/j.devcel.2015.04.027

von Appen, A., Kosinski, J., Sparks, L., Ori, A., DiGuilio, A. L., Vollmer, B., Mackmull, M.-T., Banterle, N., Parca, L., Kastritis, P., Buczak, K., Mosalaganti, S., Hagen, W., Andres-Pons, A., Lemke, E. A., Bork, P., Antonin, W., Glavy, J. S., Bui, K. H., & Beck, M. (2015). In situ structural analysis of the human nuclear pore complex. *Nature*, *526*(7571), 140–143. https://doi.org/10.1038/nature15381

Wanczyk, M. (2011). HDACi - going through the mechanisms. *Frontiers in Bioscience*, *16*(1), 340. https://doi.org/10.2741/3691

Weber, J. D., Taylor, L. J., Roussel, M. F., Sherr, C. J., & Bar-Sagi, D. (1999). Nucleolar Arf sequesters Mdm2 and activates p53. *Nature Cell Biology*, *1*(1), 20–26. https://doi.org/10.1038/8991

Weberruss, M., & Antonin, W. (2016). Perforating the nuclear boundary – how nuclear pore complexes assemble. *Journal of Cell Science*, *129*(24), 4439–4447. https://doi.org/10.1242/jcs.194753

Wilson, K. L., & Berk, J. M. (2010). The nuclear envelope at a glance. *Journal of Cell Science*, *123*(Pt 12), 1973–1978. https://doi.org/10.1242/jcs.019042

Wong, R. W., Blobel, G., & Coutavas, E. (2006). Rae1 interaction with NuMA is required for bipolar spindle formation. *Proceedings of the National Academy of Sciences*, *103*(52), 19783–19787. https://doi.org/10.1073/pnas.0609582104

Xie, X., & Percipalle, P. (2018). An actin-based nucleoskeleton involved in gene regulation and genome organization. *Biochemical and Biophysical Research Communications*, *506*(2), 378–386. https://doi.org/10.1016/j.bbrc.2017.11.206

Xu, W. S., Parmigiani, R. B., & Marks, P. A. (2007). Histone deacetylase inhibitors: molecular mechanisms of action. *Oncogene*, *26*(37), 5541–5552. https://doi.org/10.1038/sj.onc.1210620

Yokoyama, W. M., Christensen, M., Santos, G. Dos, Miller, D., Ho, J., Wu, T., Dziegelewski, M., & Neethling, F. A. (2013). Production of monoclonal antibodies. *Current Protocols in Immunology*, *SUPPL.102*, 2.5.1-2.5.29. https://doi.org/10.1002/0471142735.im0205s102

Yoneda, Y., Hieda, M., Nagoshi, E., & Miyamoto, Y. (1999). Nucleocytoplasmic Protein Transport and Recycling of Ran. *Cell Structure and Function*, *24*(6), 425–433. https://doi.org/10.1247/csf.24.425

Zastrow, M. S., Flaherty, D. B., Benian, G. M., & Wilson, K. L. (2006). Nuclear titin interacts with A- and B-type lamins in vitro and in vivo. *Journal of Cell Science*, *119*(2), 239–249. https://doi.org/10.1242/jcs.02728

Zhou, L., & Panté, N. (2010). The nucleoporin Nup153 maintains nuclear envelope architecture and is required for cell migration in tumor cells. *FEBS Letters*, *584*(14), 3013–3020. https://doi.org/10.1016/j.febslet.2010.05.038

Zimowska, G, Aris, J. P., & Paddy, M. R. (1997). A Drosophila Tpr protein homolog is localized both in the extrachromosomal channel network and to nuclear pore complexes. *Journal of Cell Science*, *110 (Pt 8*, 927–944. https://jcs.biologists.org/content/110/8/927.long

Zimowska, Grazyna, & Paddy, M. R. (2002). Structures and Dynamics of Drosophila Tpr Inconsistent with a Static, Filamentous Structure. *Experimental Cell Research*, *276*(2), 223–232. https://doi.org/10.1006/excr.2002.5525